

UC Irvine

UC Irvine Electronic Theses and Dissertations

Title

Development and Design of Transition Metal-Catalyzed Transformations in Macrocyclizations and Carbon–Carbon Bond Formations

Permalink

<https://escholarship.org/uc/item/0303b33k>

Author

Riedel, Jan Christian

Publication Date

2019

Supplemental Material

<https://escholarship.org/uc/item/0303b33k#supplemental>

Peer reviewed|Thesis/dissertation

UNIVERSITY OF CALIFORNIA,
IRVINE

Development and Design of Transition Metal-Catalyzed Transformations in
Macrocyclizations and Carbon–Carbon Bond Formations

DISSERTATION

submitted in partial satisfaction of the requirements
for the degree of

DOCTOR OF PHILOSOPHY

in Chemistry

by

Jan Riedel

Dissertation Committee:
Professor Vy M. Dong, Chair
Professor Philipp Furche
Professor Rachel W. Martin

2019

Chapter 1 © 2017 American Chemical Society
Portion of Chapter 2 © 2017 American Chemical Society
Chapter 4 © 2017 John Wiley & Sons, Inc.
All other materials © 2019 Jan Riedel

TABLE OF CONTENTS

	Page
LIST OF FIGURES	iv
LIST OF TABLES	vi
ACKNOWLEDGMENTS	vii
CURRICULUM VITAE	ix
ABSTRACT OF THE DISSERTATION	xi
1 Dehydro Amino Acids as Turn-Inducer in the Cyclization of Peptides	1
1.1 Total Synthesis of Dichotomin E	2
1.1.1 Introduction	2
1.1.2 Results and Discussion	3
1.2 Experimental Data	10
1.2.1 Experimental Details	10
1.2.2 2D NOESY Spectroscopy	21
1.2.3 Molecular modeling using Maestro	22
2 Cobalt-Catalyzed Hydroacylation	26
2.1 Enantioselective Cyclobutanone Synthesis	27
2.1.1 Introduction	27
2.1.2 Results and Discussion	29
2.2 Selective Synthesis of <i>trans</i> -Hydrindanones	35
2.2.1 Introduction	35
2.2.2 Results and Discussion	36
2.2.3 Conclusion and Future Work	40
2.3 Experimental Data	40
2.3.1 Experimental Details for Enantioselective Cyclobutanone Synthesis . .	41
2.3.2 Experimental Details for Selective Synthesis of <i>trans</i> -Hydrindanones .	53
3 Mechanistic DFT Studies and <i>In-Silico</i> Catalyst Design	58
3.1 Mechanistic DFT Studies of Rh-Catalyzed Cycloisomerizations	59
3.1.1 Introduction	59
3.1.2 Results and Discussion	61

3.1.3	Conclusion and Future Work	67
3.2	<i>In-Silico</i> Catalyst Design and Synthesis of a New Class of Ligand	68
3.2.1	Introduction	68
3.2.2	Results and Discussion	70
3.2.3	Conclusion and Future Work	76
3.3	Experimental and Computational Data	76
3.3.1	Computational Details	76
3.3.2	Experimental Details	79
4	Copper Catalyzed Synthesis of γ, δ-Unsaturated Nitriles	83
4.1	Introduction	84
4.2	Results and Discussion	85
4.3	Experimental Data	91
4.3.1	Experimental Details	91
Appendix A	Supporting Information for Chapter 1	114
A.1	NMR Spectra	114
Appendix B	Supporting Information for Chapter 2.1	126
B.1	NMR Spectra	126
Appendix C	Supporting Information for Chapter 2.2	149
C.1	NMR Spectra	149
Appendix D	Supporting Information for Chapter 3	156
D.1	NMR Spectra	156
Appendix E	Supporting Information for Chapter 4	161
E.1	NMR Spectra	161

LIST OF FIGURES

	Page
Figure 1.1 Retrosynthetic Analysis	4
Figure 1.2 Synthesis of Unsaturated Pentapeptide 3	5
Figure 1.3 Hydrogenation Yielding Epimer of Dichotomin E	5
Figure 1.4 Asymmetric Hydrogenation to Yield Dichotomin E	7
Figure 1.5 CD spectra of pentapeptides 12 , 3 , and 2	7
Figure 1.6 Minimized-energy conformation 17 of unsaturated peptide 3	8
Figure 2.1 Inspiration for cobalt-based cyclase mimic	27
Figure 2.2 Challenges and literature precedents	28
Figure 2.3 Proposed mechanism	30
Figure 2.4 Reaction evaluation of dienyl aldehyde	33
Figure 2.5 Derivatization of cyclobutanone 24a	33
Figure 2.6 Chemical space from the desymmetrization of cyclohexenaldehydes	35
Figure 2.7 Natural motifs containing hydrindane skeleton	36
Figure 2.8 Substrate synthesis	37
Figure 2.9 Initial hit	37
Figure 2.10 Proposed reaction mechanism	38
Figure 2.11 Proposed total synthesis of Seiricardine A	40
Figure 3.1 Cycloisomerizations in nature and transition metal catalysis	59
Figure 3.2 Conformational selection and induced-fit	60
Figure 3.3 Ligand controls regiochemical outcome	61
Figure 3.4 Ligand controls regiochemical outcome	63
Figure 3.5 Analysis of the transition state geometries	64
Figure 3.6 Distortion-interaction energies	66
Figure 3.7 Distortion-interaction energies for ligand and substrate fragments	67
Figure 3.8 Distortion-interaction energies for ligand and substrate fragments	68
Figure 3.9 Studied reaction	69
Figure 3.10 CH- π interaction between ligand and substrate	69
Figure 3.11 Predicted <i>rr</i> of <i>in-silico</i> designed SDP-variants	70
Figure 3.12 Proposed ligand design	71
Figure 3.13 Isosteric relationship between <i>ortho,meta</i> and <i>metaxy</i> substitution	72
Figure 3.14 Synthesis of bromo-hydrindacene 78	73
Figure 3.15 Attempted coupling of phosphine oxide 79 to SDP backbone	74
Figure 3.16 Dispersion interaction density plot with 72w and 72z	74

Figure 3.17	Distortion-Interaction analysis for new SDP-ligands	75
Figure 3.18	Coupling of 80 to the SDP backbone	76
Figure 3.19	Fragmentation of substrate and ligand fragment	78
Figure 4.1	Allylic cyanoalkylation	84
Figure 4.2	Allylic cyanoalkylation of terminal olefins	87
Figure 4.3	Application of the γ,δ -unsaturated nitriles	88
Figure 4.4	Allylic cyanoalkylation of internal olefins	89
Figure 4.5	Proposed mechanism and rationale for the regioselectivity	90
Figure 4.6	Intermediate-trapping and radical-clock experiment	91

LIST OF TABLES

	Page
Table 1.1 Effect of Dehydroamino Acid on Macrocyclization	6
Table 2.1 Identifying catalyst for cyclobutanones	29
Table 2.2 Synthesis of enantioenriched cyclobutanones	31
Table 2.3 Optimization of precatalyst and reductant	38
Table 2.4 Enantioselective conditions	39
Table 3.1 Experimental and computational agreement	62
Table 3.2 Predicted rr for ligands with metaxy-isosteric benzenes	73
Table 3.3 Predicted rr for P-chiral ligand designs	74
Table 4.1 Counter effects on Cu-catalyzed allylic cyanoalkylation	86

ACKNOWLEDGMENTS

I'm sitting on the shoulders of giants and only am able to do what I do due to the numerous contributions to science and society of generations before me. But I'm more so sitting on the shoulders of my Adviser, committee members, colleagues and collaborators.

I want to start out by thanking my adviser Professor Vy Dong. I remember seeing you give a talk at the Max-Planck Institut für Kohleforschung and being really impressed by the work of your group and coming up to you after the talk asking nervously for an internship opportunity. I enjoyed my time in the group so much that it was almost a no-brainer for me to come back and join your group for graduate studies. I appreciate you for seeing potential in me and supporting me by giving me the freedom to be creative with my research and ideas. I want to also thank Wilmer, I appreciate all the work you're doing to help us reach our goals and for caring about every single one of us. I vividly remember you giving me a ride back home from LAX after coming back from Germany. Initially, I was very grateful that you took the time to pick me up from LAX, but that was before I realized that you would take the Corvette and drive 120 mph on the freeway. Although having driven at this speed myself in Germany, I thought it was insane to do it on the 405 with unpredictable people around you. I was certain I would die in your car. I tried to play it cool but that probably encouraged you to drive even faster. Anyways, I'm thankful for all the things you did for me, and I'm glad you're not driving the Corvette anymore.

I also want to thank my committee members, Professors Rachel Martin and Filipp Furche for serving on my committee and for their time. I'm grateful for the help and mentorship of Mikko Muuronen, I will be always grateful for your friendship, cheerful attitude, and the incredible amount of time that you have spent to mentor me. I'm thankful for Matt Beaver and the people at Amgen who had a big part in my development as a researcher.

My labmates and collaborators deserve a lot of appreciation for their support, contributions and insightful discussions. I want to especially thank Boni Kim for being a friend, mentor, travel buddy, and role model. I'm thankful for the mentor- and friendship during my internship and without you showing me the spirit of the group, I would've not returned. Stephen Murphy, for introducing me to my passion of rock climbing, being another role model and your friendship. Your Canadian sense of humor is much missed in the lab. Daniel Kim, for being a good friend, climbing partner, and desk neighbor. I always enjoyed talking about chemistry with you and working together with you on the cobalt hydroacylation project. Jihye Park, for joining me on the hydroacylation to form hydrindanones. You've been a very valuable addition to the team and I appreciate all the contributions you made and where the project is now. Shaozhen, for being excited about my research and joining me to push it to the finish line. Without your contribution and expertise in phosphine chemistry, the project would've died a while ago. I'm excited for you to finish the ligand synthesis and further build on it in the future. I also want to thank Diane Le, Natalia Kozlyuk, Professor Rachel Martin, Raphael Kim, Xuesong Wu, and Anna Zhou.

I'm grateful for the world-class facilities at UCI that made my research possible. I want to

especially thank the directors John Greaves (Mass Spec), Felix Grun (Mass Spec), Dmitry Fishman (Laser Spec), Phil Dennison (NMR Spec), Nate Crawford (Cluster) and Joe Ziller (X-Ray Cryst).

I would also like to thank the American Chemical Society, and John Wiley and Sons for permission to include portions of Chapters 1, 2 and 4 in my dissertation.

My family and friends for being supportive of me and my plans, and for being there for me.

And lastly, I want to thank Jo, for your support, your love, your encouragement, and for believing in me and being my biggest fan, my best friend and my love. You took a big part in this work, and you've helped me to keep a positive attitude through difficult times. I'm thankful for all the time and adventures we have shared together, and I'm excited for the adventures that the future holds for us. I also appreciate you for introducing me to both kinds of Mochi: the sweet and fluffy kind and the rice cake.

CURRICULUM VITAE

Jan Riedel

EDUCATION

Doctor of Philosophy in Chemistry University of California, Irvine	2014-2019 <i>Irvine, California</i>
Master of Science in Chemistry Technische Universität Dortmund	2011-2014 <i>Dortmund, Germany</i>
Bachelor of Science in Chemistry Technische Universität Dortmund	2008-2011 <i>Dortmund, Germany</i>

RESEARCH EXPERIENCE

Ph.D. Organic Chemistry University of California, Irvine Research Advisor: Prof. Vy M. Dong, Method development, and DFT-guided catalyst design	2014-2019 <i>Irvine, California</i>
Industry Internship University of California, Irvine Research Advisor: Dr. Matt Beaver, Process improvement and methodology development	2015 <i>Cambridge, Massachusetts</i>
Visiting Researcher University of California, Irvine Research Advisor: Prof. Vy M. Dong, Synthesis and conformational analysis of cyclic peptides	2013 <i>Irvine, California</i>
Scientific Assistant Max-Planck-Institut Research Advisor: Prof. Christian Hedberg, Natural Product isolation and derivatization	2012-2013 <i>Dortmund, Germany</i>
Undergraduate Research Technische Universität Dortmund Research Advisor: Prof. Martin Hiersemann and Prof. Herbert Waldmann, Natural product and nucleotide synthesis	2008-2011 <i>Dortmund, Germany</i>

TEACHING EXPERIENCE

Teaching Assistant

University of California, Irvine
CHEM51A, Organic Chemistry
CHEM160L, Organic Chemistry Laboratory
CHEM51C, Organic Chemistry
CHEM203, Organic Spectroscopy

2014–2019
Irvine, California

PUBLICATIONS

Wu, **Riedel**, et al. *Angew. Chem. Int. Ed.* **2017**, *56*, 11589.
Kim, **Riedel**, et al. *J. Am. Chem. Soc.* **2017**, *139*, 10208.
Le, **Riedel**, et al. *Org. Lett.* **2017**, *19*, 114.

CONFERENCES

257th ACS National Meeting, Orlando, Florida **2019**
Complexity through Simplicity:
Design Principles in Catalysis (oral)

Stereochemistry Gordon Conference, Newport, Rhode Island **2018**
Design Principles in Catalysis:
Cobalt-Catalyzed Cycloisomerizations and In-Silico Catalyst Design (poster)

UCCS 2017 Meeting, Lake Arrowhead, California **2017**
Cobalt Catalysis for Enantioselective Cyclobutanone Construction (oral)

Orchem 2016, Weimar, Germany **2016**
Cobalt-Catalyzed Hydroacylation:
Desymmetrization of Quaternary Centers to afford Cyclobutanones (poster)

UCCS 2016 Meeting, Lake Arrowhead, California **2016**
Overcoming Obstacles in Ring-Closing
From Macrocycles to Cyclobutanones (oral)

249th ACS National Meeting, Indianapolis, Indiana **2013**
Bending Peptides out of Shape
Molecular Dynamic Studies and Progress Towards
the Synthesis of Cyclic Peptides (poster)

ABSTRACT OF THE DISSERTATION

Development and Design of Transition Metal-Catalyzed Transformations in
Macrocyclizations and Carbon–Carbon Bond Formations

By

Jan Riedel

Doctor of Philosophy in Chemistry

University of California, Irvine, 2019

Professor Vy M. Dong, Chair

Cyclic peptides have been recognized for their potential to mimic protein-protein interactions. Traditionally, cyclizations are carried out at high dilution to suppress competitive intermolecular reactions, which makes these cyclizations economically inefficient and hard to perform at scale. We developed the use of dehydro amino acids as traceless turn-inducers to enable macrocyclizations at high concentrations. We demonstrated our strategy in the total synthesis of dichotomin E at cyclization concentrations as high as 0.1 M. In collaboration with Prof. Rachel Martin, we studied the origin of the turn-inducing effect by CD-spectroscopy, NMR and molecular mechanics simulations.

Inspired by nature's ability to take a common precursor like geranyl pyrophosphate and cyclize it into an array of natural products (e.g., sabinene, limonene, camphene, and pinene), we expanded the cycloisomerization chemistry of 2-allyl-4-pentenal derivatives. We found that cobalt is a competent catalyst in the synthesis of cyclobutanones over cyclopentanones. We propose a Co(0) active catalyst. Building on this chemistry, we extended our methodology by making bicyclic systems. From a symmetrical starting material we affect a desymmetrization and build *trans*-fused hydrindanones selectively.

Using DFT, we studied the mechanism of a rhodium catalyzed cycloisomerization to under-

stand the structure-selectivity relationship between ligand and reaction outcome. A unprecedented induced-fit mechanism has been found operable, and the insights of these studies led to the design and synthesis of new ligands to access new pathways.

Simple unsaturated nitriles play an important role as flavoring agents and precursors for fine chemicals and polymers. Traditional synthesis would involve the use of halides and toxic cyanides. We developed a method that improves previous approaches by using a Cu(II) catalyst and di-tert-butyl peroxide to generate alkyl radicals from alkylnitriles. We used unactivated olefins and simple alkylnitriles in a broad reaction scope through double sp^3 C–H activation. Internal as well as terminal olefins are competent coupling partners. We hypothesize, that the high chemo- and regioselectivity comes from a directing group effect of the nitrile to the copper catalyst.

Chapter 1

Dehydro Amino Acids as Turn-Inducer in the Cyclization of Peptides: Total Synthesis of Dichotomin E*

Reproduced in part with permission from Le, D. N.; Riedel, J.*; Kozlyuk, N.; Martin, R. W.; Dong, V. M. *Org. Lett.* **2017**, *19*, 114. Copyright 2017 American Chemical Society

1.1 Total Synthesis of Dichotomin E

1.1.1 Introduction

Naturally occurring cyclic peptides have inspired the invention of strategies¹⁻⁵ for organic synthesis and therapeutics for use as antibiotics⁶⁻⁸ and immunosuppressants.⁹ In comparison with their linear counterparts, these cyclic structures show enhanced metabolic stability,¹⁰ conformational rigidity,¹¹ and potential to mimic protein-protein interactions.¹² While significant progress has been made in the construction of relatively large cyclic peptides, the construction of smaller peptides (i.e., those containing five or fewer amino acids) remains a challenge.¹³⁻¹⁷ In addition, cyclizing peptides at high concentrations on an industrial scale is important, and thus, a turn-inducer is desirable to ensure an efficient and economically feasible process.^{18,19} Specific amino acids (e.g., proline, pseudoproline, D-amino acids, and N-methylated amino acids) have been identified as turninducers that can be incorporated into a linear precursor to facilitate macrocyclizations.²⁰⁻²² Ring closing of small peptides without such turn-inducers is plagued by competitive dimerization and epimerization.^{23,24} Toward a more general solution to this challenge, we propose the use of dehydroamino acids as traceless turn-inducers.

Dehydroamino acids modulate backbone conformations and produce folded structures.²⁵⁻²⁸ The impact of dehydrophenylalanine on the conformation of small peptides has been studied extensively over the past decade.²⁹⁻³³ For example, Singh has shown that dehydrophenylalanines can induce β -turns in a linear tetrapeptide on the basis of X-ray crystallography studies (Figure 1a).³⁴ The ability of dehydroamino acids to impart folded conformations has yet to be exploited to achieve efficient ring closings in order to gain access to various cyclic peptides. We envisioned that this unsaturated moiety could serve as a versatile functional handle for further elaboration in the late-stage preparation of natural product derivatives.³⁵ Moreover, these unsaturated derivatives could serve as analogues in structure- activity rela-

tionship (SAR) studies or serve as potential epitope mimetics.^{36,37} Here we report the first use of dehydrophenylalanine as a traceless turn-inducer via its application in the synthesis of *dichotomin E* (**1**).

1.1.2 Results and Discussion

Isolated from the chickweed plant, *Stellaria dichotoma*, **1** is a cyclic peptide containing five amino acids with cell growth inhibitory activity against leukemia cells.³⁸ Our retrosynthetic analysis for construction of this small cyclic peptide is summarized in Figure 1.1. First, we imagined that the natural product could be obtained from cyclic peptide **2**, containing a (*Z*)-dehydrophenylalanine,³⁹ by catalytic hydrogenation. In contrast to the incorporation of other turn-inducers, the dehydrophenylalanine can be easily unveiled to the L- or D-amino acid. Next, we chose to disconnect the glycine-alanine peptide bond to reveal the linear and unsaturated peptide **3**. We chose this disconnection to help favor an effective macrocyclization by placing the dehydrophenylalanine at the $i + 2$ position, where it was previously reported to induce a β -turn.⁴⁰ A similar disconnection was used in the previous synthesis of **1** by Tam.⁴¹ In general, macrocyclizations are more favorable using glycine because it is a relatively unhindered nucleophile.⁴²

With this retrosynthetic analysis in mind, we prepared unsaturated pentapeptide **3** as shown in Figure 1.2. Boc-L-alanine (**6**) was coupled to DL-(β -OH)-Phe-OMe (**7**) to afford the corresponding dipeptide in 76% yield. Treatment with Boc anhydride and tetramethylguanidine afforded unsaturated dipeptide **8** in 91% yield.⁴³ Subjecting **8** to hydrolysis, peptide coupling, and deprotection gave tripeptide **4** in 63% yield. **4** was then coupled to dipeptide **5** in 61% yield to afford the corresponding pentapeptide. After hydrolysis and deprotection, unsaturated pentapeptide **3** was obtained in 97% yield. For comparison, we also prepared saturated linear peptide **12** in 64% yield using solid-phase peptide synthesis (SPPS) (see the

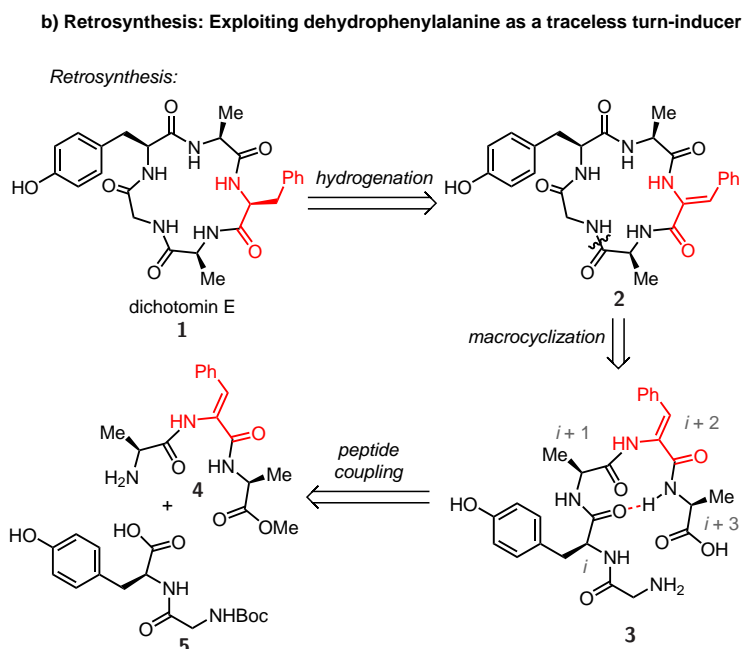


Figure 1.1. Retrosynthetic Analysis

Supporting Information (SI)).

When saturated linear pentapeptide **12** was subjected to macrocyclization at 0.1 M, only a 15% yield of **1** was obtained, with 1.5:1 selectivity for the desired monomer over the cyclodimer (Table 1.1). In stark contrast, treatment of unsaturated pentapeptide **3** under the same conditions resulted in the formation of cyclic pentapeptide **2** in 74% yield, and the selectivity improved to 20:1 for the monomer versus the cyclodimer. Subsequently, cyclic pentapeptide **2** was isolated in 81% yield with 39:1 selectivity for the desired monomer over cyclodimer at 0.05 M. In comparison to Tam's method, where a silver-ion-assisted orthogonal cyclization at 0.001 M concentration afforded the macrolactam in 87% yield, our approach circumvents the need for high dilution by using 100 times less solvent in the macrocyclization.

Next, we prepared pentapeptide **13** bearing two dehydroamino acids (see the SI) and subjected this linear precursor to ring closing. Under the same cyclization conditions at 0.1 M concentration, cyclic pentapeptide **14** was isolated in 84% yield with improved 26:1 se-

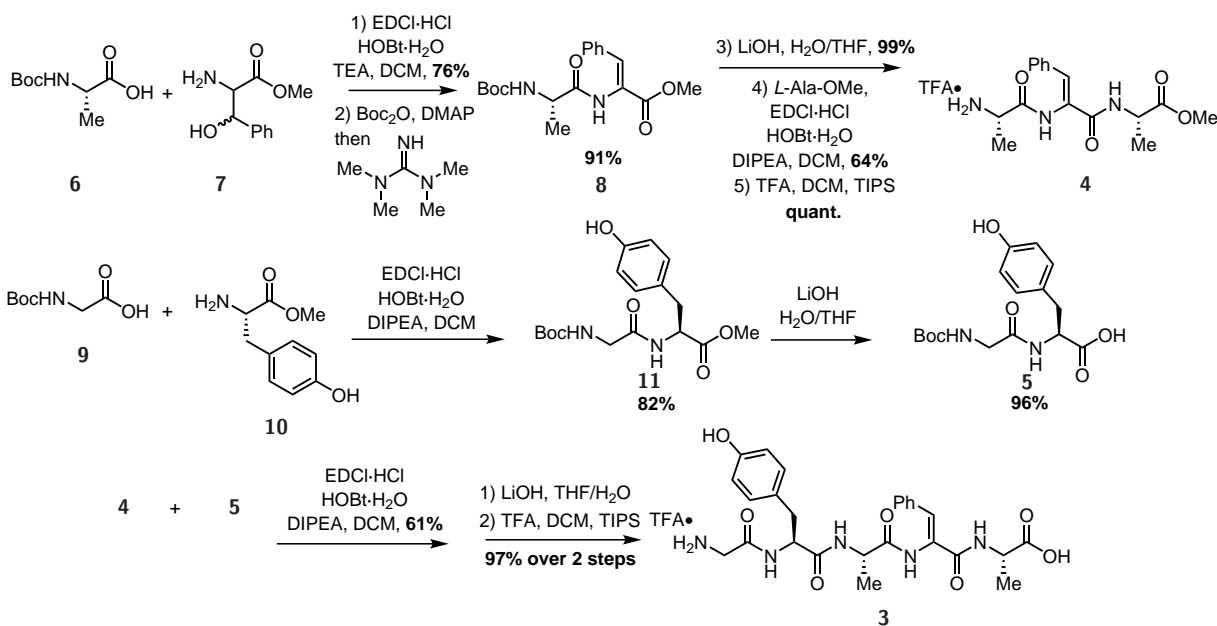


Figure 1.2. Synthesis of Unsaturated Pentapeptide **3**

lectivity for the monomer over the cyclodimer (cf. Table 1.1).^{*} Together, these results demonstrate that dehydrophenylalanines act as turn-inducers that greatly favor macrocyclization even at high concentrations. With unsaturated cyclic peptides **2** and **14** in hand, we applied hydrogenation to install the final stereocenters. Hydrogenation of cyclic peptide **2** using $\text{Rh}(\text{cod})_2\text{BF}_4$ and the achiral dppp ligand resulted in the formation of an 8:1 mixture favoring epimer **15** of dichotomin E (Figure 1.3).

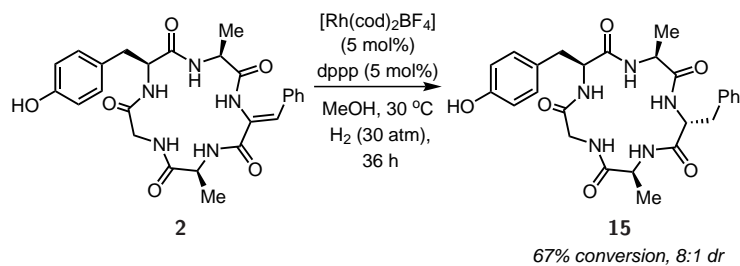
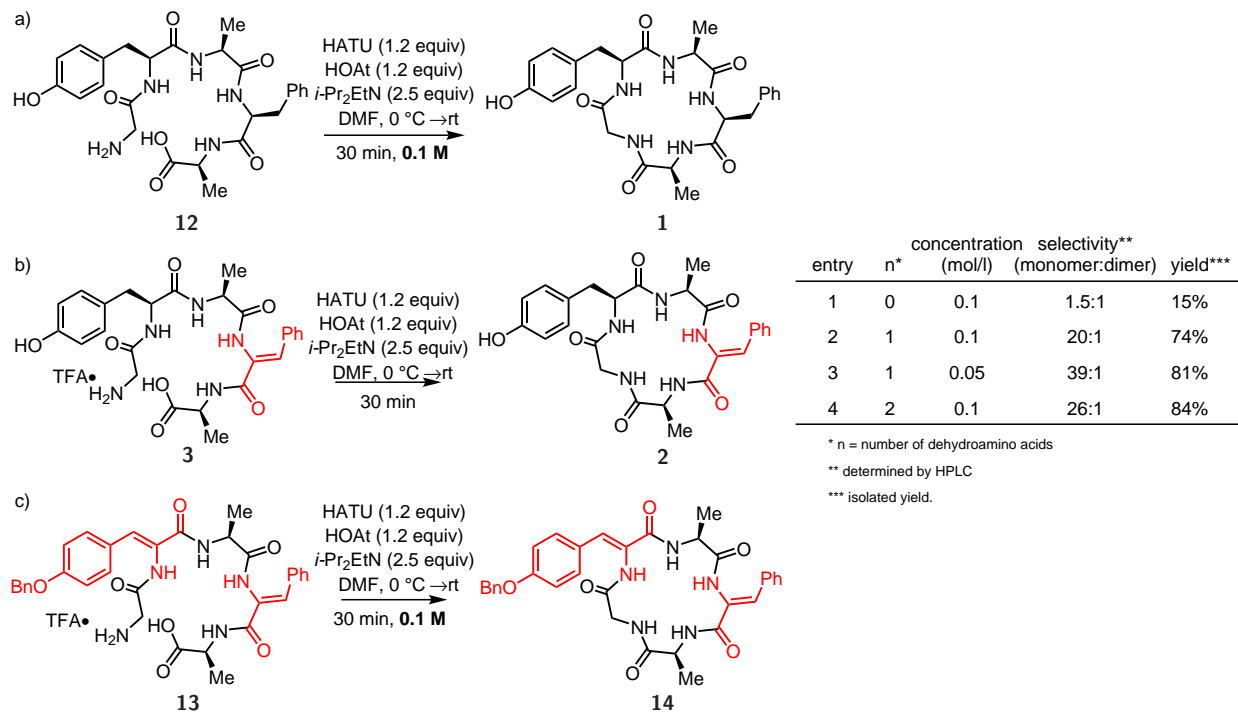


Figure 1.3. Hydrogenation Yielding Epimer of Dichotomin E

To overcome the inherent substrate bias, we turned to asymmetric hydrogenation, which is commonly used in the synthesis of medicines in industry.⁴⁴ Liu and Zhang⁴⁵ previously

^{*}Additionally, when we switched the position of the dehydroamino acid to tyrosine, we saw predominant dimer formation over monomer formation (see the SI)

Table 1.1. Effect of Dehydroamino Acid on Macrocyclization

reported the asymmetric hydrogenation of enamides using Rh(I) with Duanphos as the ligand to afford the corresponding amide with 99% ee. By using 5 mol% Rh(cod)₂BF₄ and 5 mol% (*S,S',R,R'*)-Duanphos in THF under 30 atm hydrogen, we were able to hydrogenate peptide **2** and obtain dichotomin E (**1**) in 96% yield with >95:5 *dr* (Figure 1.4). It is worthy of note that reduction of cyclic peptide **2** using (*R,R',S,S'*)-Duanphos affords the epimer **15** in 82% yield with >95:5 *dr*. Cyclic peptide **14** bearing two enamides can also be transformed to dichotomin E by tandem asymmetric reduction followed by debenzoylation (Figure 1.4).

To better understand the mechanism of macrocyclization, we performed CD-spectroscopy experiments on pentapeptides **12**, **3**, and **2** in MeOH (298 K) to investigate the presence of secondary structure (Figure 1.5).⁴⁶ Uncyclized dehydropeptide **3** showed absorption patterns consistent with a cyclized structure, similar to cyclic dehydropeptide **2**. In contrast, uncyclized, saturated pentapeptide **12** showed no absorption patterns indicative of any secondary structural motif. The CD spectrum supports the pronounced effect of the presence of dehydrophenylalanine on the secondary structure of uncyclized dehydropeptide **3**, which

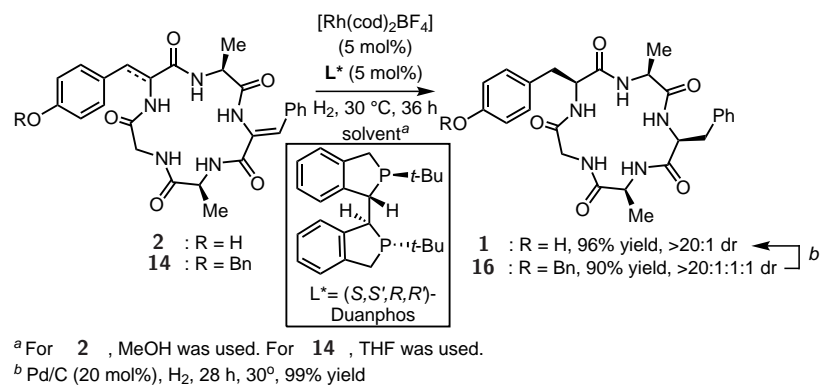


Figure 1.4. Asymmetric Hydrogenation to Yield Dichotomin E

helps to facilitate macrocyclization.

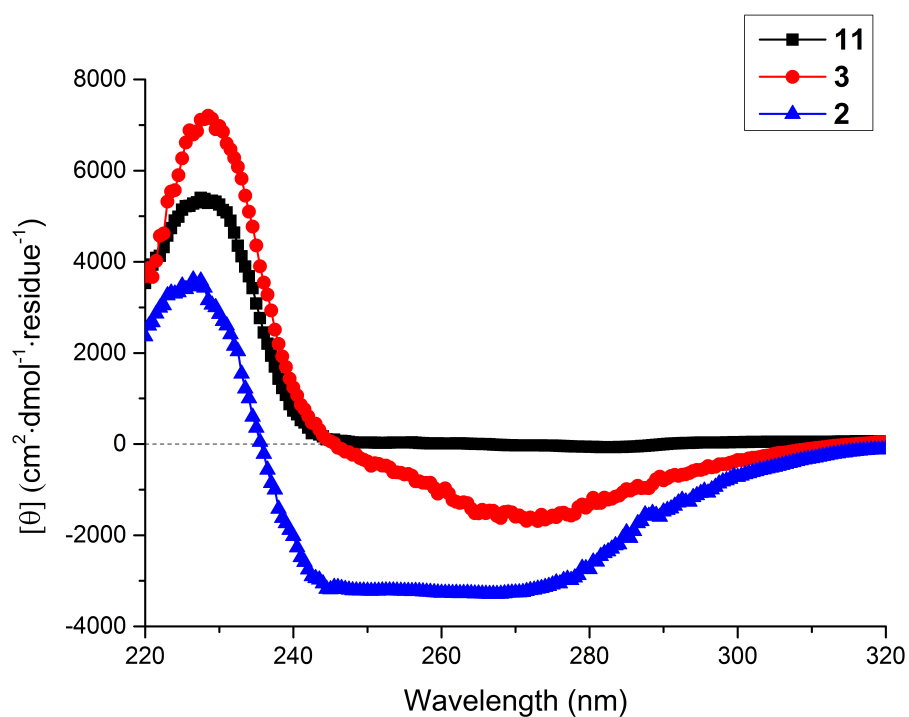


Figure 1.5. CD spectra of pentapeptides **11**, **3**, and **2**

We used solution-state NMR spectroscopy and molecular modeling to elucidate the structure of unsaturated pentapeptide **3**. The 3J couplings for the Tyr residue and the two Ala residues were obtained from 2D J-resolved 1H NMR spectra.⁴⁷ These couplings were used to calculate $H_N H_\alpha \Phi$ dihedral angles via the Karplus relation.⁴⁸ Using these dihedral angle and

2D NOESY restraints, we performed molecular modeling studies with Maestro* to obtain 20 low-energy conformations that were consistent with our experimental observations (see the SI). These calculations support the lowest-energy structure **17** containing a left-handed α -turn, which is preorganized toward macrocyclization (Figure 1.6). Intramolecular H-bonding was also investigated using the temperature coefficients of the N-H chemical shifts ($\Delta\delta/\Delta T$), which can be used as an indicator of intramolecular H-bonding as opposed to H-bonds to solvent.^{49,50} A value of -0.0039 ppm/K was obtained for the internal alanine N-H in dehydropeptide **3**, in contrast to the value of -0.0052 ppm/K observed for saturated pentapeptide **12** (see the SI). This difference suggests that there is dynamic intramolecular H-bonding in dehydropeptide **3** but not in saturated pentapeptide **12**, consistent with the ensemble of structures predicted by the molecular modeling. Together, these results demonstrate that a single dehydrophenylalanine residue can induce a left-handed α -turn.

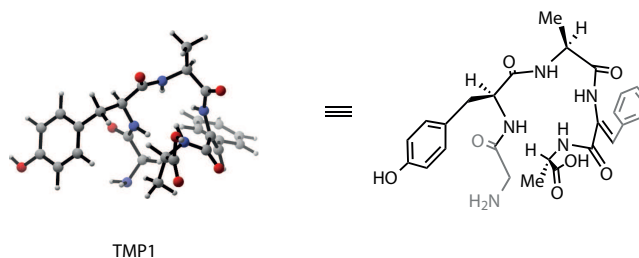


Figure 1.6. Minimised-energy conformation **17** of unsaturated peptide **3**

When we replaced the phenyl substituent with a cyclohexyl substituent in **3**, cyclic monomer formation was observed in a promising yet less efficient 54% yield by ¹H NMR analysis (see the SI). This result suggests that the steric impact of the substituent influences the cyclization. In view of the higher-yielding macrocyclizations we observed in Table 1.1, conjugation between the phenyl substituent and the alkene helps promote ring closing by increasing the steric impact of the phenyl group. Weiss, Lawrence, and co-workers used dehydrophenylalanine as a β - breaker to study insulin and showed that extended conjugation of the aromatic π electrons with the neighboring C=C and C=O electrons enforces near-planarity.⁵¹ The

*Schrödinger, release 2015-2: Maestro, version 10.2; Schrödinger, LLC: New York, 2015.

near-planar conformation of dehydrophenylalanine results in a greater steric interaction between the phenyl group and the adjacent amide group, as shown in **17**, which ultimately restricts the Φ angle of the dehydroamino acid.³³ This restriction, through the increased $A_{1,3}$ strain, biases the N- and C-termini toward cyclization. Interestingly, a peptide containing three consecutive dehydroalanine units has been shown to adopt an extended conformation in which all of the amide groups show near-planarity.⁵² This example suggests that the steric interactions of the group at the β - carbon of the dehydroamino acid are correlated to its ability to induce a turn. In conclusion, we have demonstrated dehydrophenylalanine as an effective and traceless turn-inducer in the synthesis of dichotomin E. NMR analysis revealed that unsaturated pentapeptide **3** adopts a cyclic, preorganized structure. The enamide serves as a turn-inducer to facilitate ring closing without the need for high dilution. Moreover, it is a convenient functional handle for the late-stage construction of natural products and their derivatives. In SPPS, the overall yield is typically exceptional because each step in this linear approach is driven by exploiting excess reagents.⁵³ Combined with the need for dilute solvent conditions, the amount of waste generated in this traditional approach to cyclic peptide construction is significant. Our approach aims for a more efficient synthesis of cyclic peptides, especially on a large scale, while SPPS enables the rapid synthesis of peptide libraries on a small scale. Future studies in our laboratory will be focused on better understanding (1) the scope and limitations of dehydroamino acids as turn-inducers for macrocyclization* and (2) the mechanism of tandem hydrogenations in cyclic enamides. We expect that our simple yet effective strategy for ring closing will be of use to chemists interested in accessing cyclic pentapeptides for use as biological probes and therapeutics.

*Our method is currently limited to the synthesis of cyclic pentapeptides. When we cyclized the linear tetrapeptide (HO-Ala- Δ Phe-Ala-Gly-NH₂) at 0.01 M, we observed the formation of the cyclooctamer via LC-MS analysis.

1.2 Experimental Data

The details of the studies described in this chapter can be found in the Supporting Information of the published manuscript.⁵⁴ My contributions to the project are detailed in this section.

1.2.1 Experimental Details

Representative peptide coupling with EDCI (Method A)

To a round bottom flask equipped with a stir bar was added Boc-L-alanine (5.00 g, 26.4 mmol), DL-(β -OH)-Phe-OMe (6.13 g, 26.4 mmol), HOBT·H₂O (4.29 g, 31.7 mmol), and DCM (100 mL). The mixture was cooled to 0 °C and Et₃N (9.16 mL, 66.1 mmol) was subsequently added. EDCI·HCl (6.08 g, 31.7 mmol) was added in portions and the reaction gradually warmed to rt and stirred for 22 h. The reaction mixture was transferred to a separatory funnel and was washed with 100 mL sat. NaHCO₃ (aq), 100 mL 10% KHSO₄ (aq), and 100 mL brine. The organic phase was dried over Na₂SO₄, filtered, and concentrated under reduced pressure. The unpurified reaction mixture was then purified by column chromatography (eluting with 20:1 DCM/MeOH) to afford the corresponding dipeptide as a white solid (7.4 g, 76%).

Representative elimination to form dehydroamino acid (Method B)

The procedure was adapted from Suárez.* To a round bottom flask equipped with a stir bar was added methyl 2-((*S*)-2-((*tert*-butoxycarbonyl)amino)propanamido)-3-hydroxy-3-phenylpropanoate (7.40 g, 20.2 mmol), DMAP (244 mg, 2.00 mmol) and MeCN (60 mL).

*Monteiro, L. S.; Andrade, J. J.; Suárez, A. C. *Eur. J. Org. Chem.* **2011**, 2011, 6764.

The mixture was cooled to 0 °C and Boc₂O (4.63 g, 21.2 mmol) was quickly added. After disappearance of starting material analyzed via LC-MS, tetramethylguanidine (0.77 mL, 6.1 mmol) was added. After 12 h, the reaction mixture was concentrated under reduced pressure and then purified by column chromatography (eluting with 20:1 DCM/MeOH) to afford the unsaturated dipeptide **8** as a white solid (6.4 g, 91%, 2 steps).

Representative hydrolysis procedure (Method C)

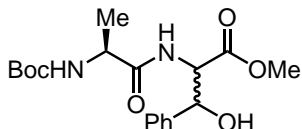
To a round bottom flask equipped with a stir bar was added methyl ester **8** (6.40 g, 18.4 mmol), THF (90 mL), and H₂O (90 mL). The mixture was cooled to 0 °C and 1M LiOH (aq) (19 mL, 19 mmol) was subsequently added. The reaction gradually warmed to rt and stirred for 14 h. The reaction mixture was acidified with 10% KHSO₄ (aq), and the THF was concentrated under reduced pressure. The reaction mixture was transferred to a separatory funnel where it was extracted with ethyl acetate (3 x 100 mL). The organic layer was washed with 100 mL brine, dried over Na₂SO₄, filtered, and concentrated under reduced pressure to afford the corresponding carboxylic acid as a colorless oil (6.1 g, 99%).

Representative Boc deprotection (Method D)

To a round bottom flask equipped with a stir bar was added (*Z*)-2-((*S*)-2-((*tert*-butoxycarbonyl)amino)propanamido)-3-phenylacryloyl)-L-alaninate (638 mg, 1.52 mmol), triisopropylsilane (0.33 mL, 1.6 mmol), and DCM (15 mL). The reaction mixture was cooled to 0 °C and TFA (1.17 mL, 15.2 mmol) was slowly added. The reaction slowly warmed to rt and stirred for 24 h. The DCM was concentrated under reduced pressure and to the mixture was added toluene to form a TFA azeotrope, which was subsequently concentrated under reduced pressure. The reaction mixture was further dried on the high vacuum and subsequently triturated with Et₂O to afford the corresponding amine in quantitative yield which

was used without further purification.

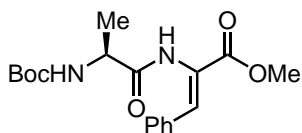
Methyl 2-((*S*)-2-((*tert*-butoxycarbonyl)amino)propanamido)-3-hydroxy-3-phenylpropanoate



The product was prepared by method A using Boc alanine **6** (5.00 g, 26.4 mmol) and purified by column chromatography (eluting with 90:10 DCM/MeOH) to afford a white solid (7.4 g, 61%, 1:1 dr). ¹H-NMR: δ (499 MHz, DMSO) 7.89 (d, $J = 9.1$ Hz, 1H),

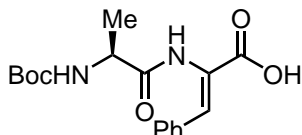
7.76 (d, $J = 8.9$ Hz, 1H), 7.45 – 7.32 (m, 4H), 7.31 – 7.24 (m, 4H), 7.25 – 7.19 (m, 2H), 7.00 (d, $J = 8.0$ Hz, 1H), 6.86 (d, $J = 8.0$ Hz, 1H), 5.92 (d, $J = 4.8$ Hz, 2H), 5.14 (dd, $J = 4.9, 3.2$ Hz, 1H), 5.12 – 5.06 (m, 1H), 4.55 (ddd, $J = 12.7, 9.0, 3.2$ Hz, 2H), 4.10 – 3.84 (m, 2H), 3.65 (s, 3H), 3.61 (s, 3H), 1.39 (s, 9H), 1.38 (s, 9H), 1.02 (d, $J = 7.2$ Hz, 3H), 0.94 (d, $J = 7.2$ Hz, 3H). ¹³C-NMR: δ (126 MHz, DMSO) 172.96, 172.91, 170.61, 154.88, 154.82, 141.57, 141.47, 127.76, 127.73, 127.25, 127.16, 126.38, 126.14, 109.52, 78.15, 77.97, 72.22, 72.11, 58.05, 52.02, 51.99, 49.78, 49.29, 28.21, 18.30, 17.96. IR (ATR): 3337, 3013, 2978, 1660, 1498, 1365, 1168 cm^{-1} . HRMS (ESI-TOF) m/z calculated for $\text{C}_{18}\text{H}_{26}\text{N}_2\text{O}_6\text{Na}[\text{M}+\text{Na}]^+$: 389.1689, found: 389.1687.

Methyl (*S,Z*)-2-(2-((*tert*-butoxycarbonyl)amino)propanamido)-3-phenylacrylate
(8)



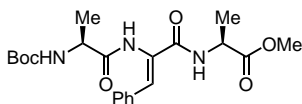
The product was prepared by method B using the previously prepared methyl ester (7.40 g, 20.2 mmol) and purified by column chromatography (eluting with 93:7 DCM/MeOH) to afford the product as a white solid (6.4 g, 91%, 2 steps). $^1\text{H-NMR}$: δ (400 MHz, DMSO) 9.56 (s, 1H), 7.77 – 7.64 (m, 2H), 7.43 – 7.30 (m, 3H), 7.26 (s, 1H), 7.03 (d, $J = 7.2$ Hz, 1H), 4.21 – 4.05 (m, 1H), 3.70 (d, $J = 1.4$ Hz, 3H), 1.41 (s, 9H), 1.26 (d, $J = 7.2$ Hz, 3H). $^{13}\text{C-NMR}$: δ (126 MHz, DMSO) 173.13, 165.41, 155.23, 133.31, 132.11, 130.23, 129.47, 128.49, 125.92, 78.05, 52.16, 49.82, 28.24, 17.40. IR (ATR): 3291, 3005, 2979, 1673, 1490, 1249, 1162 cm^{-1} . HRMS (ESI-TOF) m/z calculated for $\text{C}_{18}\text{H}_{24}\text{N}_2\text{O}_5\text{Na}$ $[\text{M}+\text{Na}]^+$: 371.1583, found: 371.1588. $[\alpha]_D^{24} +66$ ($c = 0.46$, MeOH).

(*S,Z*)-2-(2-((*tert*-butoxycarbonyl)amino)propanamido)-3-phenylacrylic acid



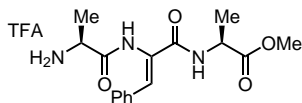
The product was prepared by method C using unsaturated dipeptide **8** (6.40 g, 18.4 mmol) and obtained as a white solid (6.0 g, 99%). $^1\text{H-NMR}$: δ (500 MHz, DMSO) 12.68 (s, 1H), 9.39 (s, 1H), 7.76 – 7.55 (m, 2H), 7.42 – 7.32 (m, 3H), 7.28 (s, 1H), 7.02 (d, $J = 7.3$ Hz, 1H), 4.21 – 4.05 (m, 1H), 1.40 (s, 9H), 1.25 (d, $J = 7.2$ Hz, 3H). $^{13}\text{C-NMR}$: δ (126 MHz, CDCl_3) 172.66, 166.30, 155.21, 133.68, 131.83, 130.14, 129.19, 128.39, 126.52, 78.03, 49.83, 28.25, 17.52. IR (ATR): 3281, 2980, 1685, 1539, 1162 cm^{-1} HRMS (ESI-TOF) m/z calculated for $\text{C}_{17}\text{H}_{22}\text{N}_2\text{O}_5\text{Na}$ $[\text{M}+\text{Na}]^+$: 357.1426, found: 357.1419. $[\alpha]_D^{25} +70$ ($c = 0.25$, MeOH).

Methyl ((*Z*)-2-((*S*)-2-((*tert*-butoxycarbonyl)amino)propanamido)-3-phenylacryloyl)-L-alaninate



The product was prepared by method A using the previously prepared carboxylic acid (3.80 g, 11.4 mmol), L-alanine methyl ester (1.60 g, 11.4 mmol), and *i*-Pr₂EtN (7.90 mL, 45.6 mmol) and purified by column chromatography (eluting with 85:15 DCM/Acetone) to afford the product as a white solid (3.0 g, 64%). ¹H-NMR: δ (499 MHz, DMSO) 9.57 (s, 1H), 7.93 (d, $J = 6.8$ Hz, 1H), 7.65 – 7.49 (m, 2H), 7.42 – 7.31 (m, 3H), 7.25 (s, 1H), 7.21 (m, 1H), 4.44 – 4.34 (m, 1H), 4.08 – 3.99 (m, 1H), 3.64 (s, 3H), 1.39 (s, 9H), 1.34 (d, $J = 7.2$ Hz, 3H), 1.23 (d, $J = 7.1$ Hz, 3H). ¹³C-NMR: δ (126 MHz, DMSO) 172.75, 172.71, 164.34, 155.71, 133.83, 130.04, 129.58, 128.84, 128.47, 128.39, 78.35, 51.86, 50.06, 48.23, 28.19, 16.93, 16.71. IR (ATR): 3291, 3017, 2981, 1751, 1685, 1530, 1163 cm⁻¹. HRMS (ESI-TOF) m/z calculated for C₂₁H₂₉N₃O₆Na [M+Na]⁺: 442.1954, found: 442.1946. $[\alpha]_D^{25}$ -41 (c = 0.25, MeOH).

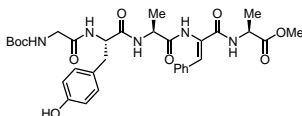
Methyl ((*Z*)-2-((*S*)-2-aminopropanamido)-3-phenylacryloyl)-L-alaninate 4



The product was prepared by method D using the previously prepared tripeptide (5.60 g, 13.3 mmol) and obtained as a white solid in quantitative yield. ¹H-NMR: δ (499 MHz, DMSO) 9.95 (s, 1H), 8.46 (d, $J = 7.1$ Hz, 1H), 8.22 – 8.14 (m, 2H), 7.60 – 7.52 (m, 2H), 7.49 – 7.39 (m, 2H), 7.38 – 7.33 (m, 1H), 7.16 (s, 1H), 4.41 (p, $J = 7.2$ Hz, 1H), 4.11 – 4.01 (m, 1H), 3.65 (s, 3H), 1.44 (d, $J = 7.0$ Hz, 3H), 1.35 (d, $J = 7.3$ Hz, 3H). ¹³C-NMR: δ (126 MHz, DMSO) 172.95, 169.08, 164.31, 133.67, 129.40, 129.08, 128.91, 128.55, 128.34, 51.91, 48.47, 48.12, 16.87, 16.42. IR (ATR): 2996, 1740, 1660, 1519, 1137 cm⁻¹. HRMS (ESI-TOF) m/z calculated for C₁₆H₂₁N₃O₄H [M+H]⁺: 320.1610, found: 320.1620. $[\alpha]_D^{26}$

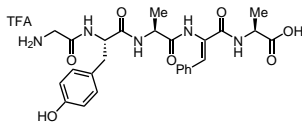
+90 (c = 0.31, MeOH).

Methyl ((Z)-2-((S)-2-((S)-2-(2-((tert-butoxycarbonyl)amino)acetamido)-3-(4-hydroxyphenyl)propanamido)propanamido)-3-phenylacryloyl)-L-alaninate



To a round bottom flask equipped with a stir bar was added (*tert*-butoxycarbonyl)glycyl-L-tyrosine (4.10 g, 12.2 mmol), amine **4** (4.80 g, 11.1 mmol), HATU (5.00 g, 13.3 mmol), HOAt (0.452 g, 3.32 mmol) and DMF (42 mL). The reaction mixture was cooled to 0 °C and 2,4,6-collidine (3.70 mL, 27.7 mmol) was added. The reaction warmed to rt and stirred for 24 h. The solvent was removed under reduced pressure and the product was purified by column chromatography (eluting with 90:10 DCM/MeOH, increasing in 0.5% increments) to afford the product as a white solid (4.32 g, 61%). ¹H-NMR: δ (500 MHz, DMSO) 9.66 (s, 1H), 9.16 (s, 1H), 8.47 (d, *J* = 5.1 Hz, 1H), 8.00 (d, *J* = 6.3 Hz, 1H), 7.65 (d, *J* = 8.2 Hz, 1H), 7.61 – 7.53 (m, 2H), 7.44 – 7.37 (m, 2H), 7.38 – 7.32 (m, 1H), 7.27 (s, 1H), 6.98 (d, *J* = 8.2 Hz, 2H), 6.94 (*t*, *J* = 6.2 Hz, 1H), 6.60 (d, *J* = 8.4 Hz, 2H), 4.48 (td, *J* = 8.4, 4.3 Hz, 1H), 4.40 – 4.18 (m, 2H), 3.64 (s, 3H), 3.54 (dd, *J* = 16.8, 6.1 Hz, 1H), 3.43 (dd, *J* = 16.8, 6.0 Hz, 1H), 2.88 (dd, *J* = 14.1, 4.3 Hz, 1H), 2.67 (dd, *J* = 14.1, 8.6 Hz, 1H), 1.36 (s, 9H), 1.31 (d, *J* = 7.1 Hz, 3H), 1.26 (d, *J* = 7.3 Hz, 3H). ¹³C-NMR: δ (126 MHz, DMSO) 173.10, 172.16, 171.74, 169.06, 164.27, 155.84, 155.80, 133.82, 130.25, 130.22, 129.58, 128.94, 128.51, 128.40, 127.33, 114.84, 78.15, 53.39, 51.86, 49.24, 48.52, 43.26, 36.74, 28.17, 16.66, 16.49. IR (ATR): 3305, 2974, 1656, 1514, 1160 cm⁻¹. HRMS (ESI-TOF) *m/z* calculated for C₃₂H₄₁N₅O₉Na [M+Na]⁺: 662.2802, found: 662.2817. [α]_D²⁶ -82 (c = 0.25, MeOH).

((Z)-2-((S)-2-((S)-2-(2-aminoacetamido)-3-(4-hydroxyphenyl)propanamido)propanamido)-3-phenylacryloyl)-L-alanine 3

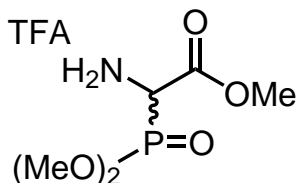


To a round bottom flask equipped with a stir bar was added the previously prepared methyl ester (4.20 g, 6.60 mmol), THF (30 mL), and H₂O (30 mL). The mixture was cooled to 0 °C and 1M LiOH (aq) (7.26 mL, 7.26 mmol) was subsequently added.

The reaction gradually warmed to rt and stirred for 48 h. The reaction mixture was acidified with 10% KHSO₄ (aq) and the THF was concentrated under reduced pressure. The reaction mixture was transferred to a separatory funnel where it was extracted with ethyl acetate (3 x 100 mL). The organic layer was washed with 100 mL brine, dried over Na₂SO₄, filtered, and concentrated under reduced pressure to afford the corresponding carboxylic acid which was used in the next step without further purification. To a round bottom flask equipped with a stir bar was added the previously prepared carboxylic acid (6.60 mmol), and DCM (60 mL). The reaction mixture was cooled to 0 °C and TFA (5.1 mL, 66 mmol) was slowly added. The reaction slowly warmed to rt and stirred for 14 h. The DCM was concentrated under reduced pressure and to the mixture was added toluene to form a TFA azeotrope, which was subsequently concentrated under reduced pressure. The reaction mixture was further dried on the high vacuum and subsequently triturated with Et₂O to afford unsaturated peptide **3** (4.0 g, 97% 2 steps). ¹H-NMR: δ (500 MHz, DMSO) 9.62 (s, 1H), 9.22 (s, 1H), 8.56 (d, *J* = 5.7 Hz, 1H, N-H_{Ala(term)}), 8.52 (d, *J* = 8.4 Hz, 1H, N-H_{Tyr}), 7.91 (d, *J* = 6.9 Hz, 3H, N-H_{Ala(int)+Gly}), 7.57 (d, *J* = 7.7 Hz, 2H), 7.42 – 7.30 (m, 3H), 7.22 (s, 1H), 7.04 (d, *J* = 8.1 Hz, 2H), 6.64 (d, *J* = 8.0 Hz, 2H), 4.56 (td, *J* = 9.2, 3.7 Hz, 1H), 4.39 – 4.22 (m, 2H), 3.55 (d, *J* = 16.2 Hz, 1H), 3.43 (d, *J* = 16.2 Hz, 1H), 2.93 (dd, *J* = 14.2, 3.8 Hz, 1H), 2.59 (dd, *J* = 14.1, 10.1 Hz, 1H), 1.36 (d, *J* = 7.3 Hz, 3H), 1.31 (d, *J* = 7.1 Hz, 3H). ¹³C-NMR: δ (126 MHz, DMSO) 174.22, 172.30, 171.59, 165.91, 164.30, 156.09, 134.02, 130.22, 129.90, 129.71, 129.02, 128.81, 128.64, 127.69, 115.13, 54.36, 49.29, 48.38, 40.19, 36.94, 17.25, 16.84.

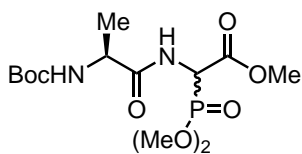
IR (ATR): 3270, 1656, 1515, 1172 cm^{-1} . HRMS (ESI-TOF) m/z calculated for $\text{C}_{26}\text{H}_{31}\text{N}_5\text{O}_7\text{H}$ $[\text{M}+\text{H}]^+$: 526.2302, found: 526.2303. $[\alpha]_D^{26}$ -20 ($c = 0.23$, MeOH).

Methyl 2-amino-2-(dimethoxyphosphoryl)acetate



To a round bottom flask equipped with a stir bar was added methyl 2-((tert-butoxycarbonyl)amino)-2-(dimethoxyphosphoryl)acetate (10 g, 32 mmol) and DCM (340 mL). The reaction cooled to 0 °C and TFA was subsequently added dropwise. The reaction warmed to rt and stirred for 16 h. The DCM was concentrated under reduced pressure and toluene was added to form a TFA azeotrope, which was subsequently concentrated under reduced pressure. The unpurified reaction mixture was further dried on the high vacuum and subsequently triturated with Et_2O to afford the product in quantitative yield which was used without further purification. $^1\text{H-NMR}$: δ (500 MHz, DMSO) 9.04 (s, 2H), 5.04 (d, $J = 20.5$ Hz, 1H), 3.83 – 3.73 (m, 9H). $^{13}\text{C-NMR}$: δ (126 MHz, DMSO) 165.20 (d, $J = 3.7$ Hz), 54.58 (d, $J = 6.5$ Hz), 54.39 (d, $J = 6.4$ Hz), 53.63, 49.18 (d, $J = 140.8$ Hz). IR (ATR): 2975, 2869, 1761, 1218, 1140 cm^{-1} . HRMS (ESI-TOF) m/z calculated for $\text{C}_5\text{H}_{12}\text{NO}_5\text{PNa}$ $[\text{M}+\text{Na}]^+$: 220.0351, found: 220.0355.

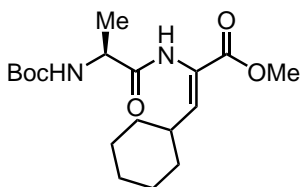
Methyl 2-((S)-2-((tert-butoxycarbonyl)amino)propanamido)-2-(dimethoxyphosphoryl)acetate



The herein described dipeptide was prepared according to method A using the previously prepared amine (6.3 g, 32 mmol), and Boc-L-Ala-OH (6.36 g, 33.6 mmol) and purified by column chromatography to afford the product as a white solid (8.1 g, 69%, 1:1 *dr*). $^1\text{H-NMR}$: δ (500 MHz, DMSO) 8.67 – 8.54 (m, 1H), 7.02 (dd, $J = 13.1, 7.9$ Hz,

1H), 5.27 – 4.80 (m, 1H), 4.26 – 3.95 (m, 1H), 3.83 – 3.50 (m, 9H), 1.37 (s, 9H), 1.17 (dd, $J = 7.3, 3.1$ Hz, 3H). ^{13}C -NMR: δ (126 MHz, DMSO) 173.43 , 173.37 , 173.17 , 173.12 , 167.03 (d, $J = 2.7$ Hz), 166.92 (d, $J = 3.0$ Hz), 155.06 , 155.00 , 78.08 , 78.05 , 54.04 (d, $J = 6.6$ Hz), 53.81 (d, $J = 5.8$ Hz), 53.78 (d, $J = 6.8$ Hz), 53.75 (d, $J = 5.5$ Hz), 52.88 , 52.86 , 49.66 (d, $J = 147.2$ Hz), 49.64 (d, $J = 146.3$ Hz), 49.32 , 28.19 , 18.08 , 17.86. IR (ATR): 3005, 2970, 2935, 1749, 1674, 1506, 1249, 1163, 1075 cm^{-1} . HRMS (ESI-TOF) m/z calculated for $\text{C}_{13}\text{H}_{25}\text{N}_2\text{O}_8\text{PNa}$ $[\text{M}+\text{Na}]^+$: 391.1246, found: 391.1248.

Methyl (*S,Z*)-2-(2-((*tert*-butoxycarbonyl)amino)propanamido)-3-cyclohexylacrylate



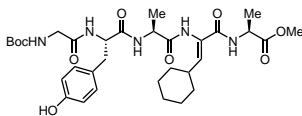
The Horner-Wadsworths-Emmons product was prepared according to an adapted procedure reported by Schmidt.*† To a solution of the previously prepared dipeptide (8.1 g, 22 mmol) in DCM (73 mL) at 0 °C was added DBU (4.0 mL, 26 mmol). After 10 min, cyclohexanecarbaldehyde (3 g, 26.7 mmol) was added and the reaction mixture stirred at rt for 24 h. The reaction mixture was transferred to a separatory funnel and washed with 100 mL sat. NaHCO_3 (aq), 100 mL 10% KHSO_4 , and 100 mL brine. The organic phase was dried over Na_2SO_4 , filtered, and concentrated under reduced pressure. The reaction mixture was then purified by column chromatography (eluting with 3:7 hexanes/ethyl acetate) to afford the product as a white solid (7.2 g, 92%). ^1H -NMR: δ (500 MHz, DMSO) 9.08 (s, 1H), 6.93 (d, $J = 7.4$ Hz, 1H), 6.27 (d, $J = 10.0$ Hz, 1H), 4.10 – 3.98 (m, 1H), 3.62 (s, 3H), 2.38 – 2.24 (m, 1H), 1.70 – 1.52 (m, 5H), 1.38 (s, 9H), 1.22 (d, $J = 7.3$ Hz, 4H), 1.19 – 1.02 (m, 4H). ^{13}C -NMR: δ (126 MHz, DMSO) 172.50, 164.85, 155.04, 142.22, 125.30, 77.95, 51.80, 49.62, 35.98, 31.06, 30.96, 28.20, 25.32, 25.04, 24.99, 17.90.

*Schmidt, U.; Griesser, H.; Leitenberger, V.; Liebenknecht, A.; Mangold, R.; Meyer, R.; Reidl, B. *Synthesis* **1992**, 487.

†Burk, M. J.; Johnson, N. B.; Lee, J. R. *Tetrahedron Lett.* **1990**, 40, 6685.

IR (ATR): 2984, 2929, 2850, 1719, 1674, 1506, 1258, 1225, 1162 cm^{-1} . HRMS (ESI-TOF) m/z calculated for $\text{C}_{18}\text{H}_{30}\text{N}_2\text{O}_5\text{Na}$ $[\text{M}+\text{Na}]^+$: 377.2052, found: 377.2048. $[\alpha]_D^{25}$ -5 (c = 0.55, MeOH).

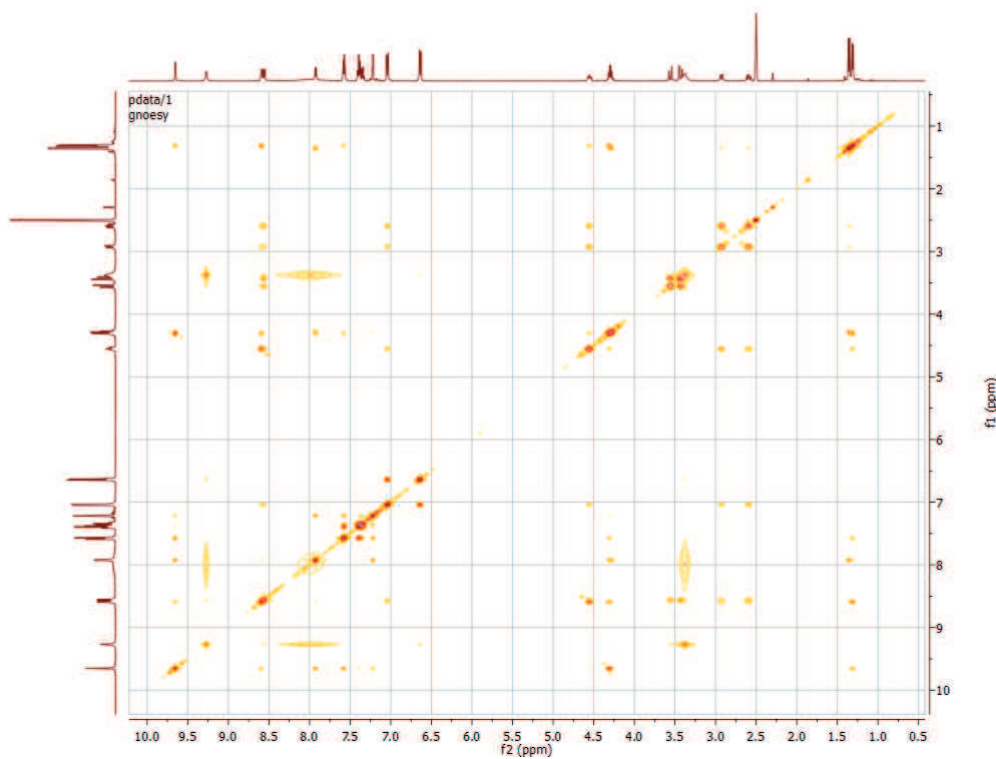
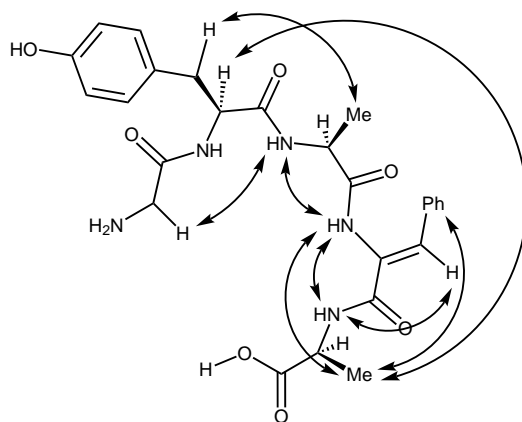
Methyl ((*Z*)-2-((2*S*)-2-(2-(2-((*tert*-butoxycarbonyl)amino)acetamido)-3-(4-hydroxyphenyl)propanamido)propanamido)-3-cyclohexylacryloyl)-L-alaninate



The previously prepared tripeptide (6.2 g, 15 mmol) was deprotected according to general procedure D to afford the corresponding amine in quantitative yield which was used without further purification. To a round bottom flask equipped with a stir bar was added (*tert*-butoxycarbonyl)glycyl-L-tyrosine (4.7 g, 14 mmol), the previously prepared amine (15 mmol), HATU (5.3 g, 14 mmol), HOAt (0.50 g, 4.0 mmol) and DCM (49 mL). The reaction mixture was cooled to 0 °C and *i*Pr₂EtN (5.5 mL, 32 mmol) was added. The reaction was warmed to rt and stirred for 24 h. The solvent was removed under reduced pressure and the product was purified by column chromatography (eluting with 95:5 ethyl acetate/acetone) to afford the product as a white solid (1.8 g, 22%). ¹H-NMR: δ (400 MHz, DMSO) 9.19 – 8.97 (m, 2H), 8.36 (d, *J* = 5.5 Hz, 1H), 7.73 (d, *J* = 6.6 Hz, 1H), 7.66 (d, *J* = 8.2 Hz, 1H), 6.98 (d, *J* = 8.0 Hz, 2H), 6.60 (d, *J* = 7.4 Hz, 2H), 6.29 (d, *J* = 8.3 Hz, 1H), 4.59 – 4.39 (m, 1H), 4.33 – 4.17 (m, 2H), 3.61 (s, 3H), 3.56 – 3.48 (m, 1H), 3.48 – 3.37 (m, 1H), 3.38 – 3.33 (m, 1H), 2.93 – 2.84 (m, 1H), 2.75 – 2.61 (m, 1H), 2.22 (d, *J* = 11.3 Hz, 1H), 1.74 – 1.53 (m, 5H), 1.36 (s, 9H), 1.28 (d, *J* = 6.6 Hz, 3H), 1.23 (d, *J* = 7.2 Hz, 4H), 1.20 – 1.03 (m, 4H). ¹³C-NMR: δ (126 MHz, DMSO) 173.12, 171.98, 171.52, 169.07, 163.85, 155.82, 155.79, 139.61, 130.21, 127.41, 127.37, 114.84, 78.14, 59.79, 53.49, 51.83, 49.06, 48.19, 43.25, 36.06, 31.24, 28.16, 25.41, 25.15, 20.79, 17.25, 16.73, 14.12. IR (ATR): 3003, 2984, 2929, 2850, 1751, 1686, 1510, 1150 cm⁻¹. HRMS (ESI-TOF) *m/z* calculated for C₃₂H₄₇N₅O₉Na [M+Na]⁺: 668.3271, found: 668.3270. [α]_D²⁵ -33 (c = 0.25, MeOH).

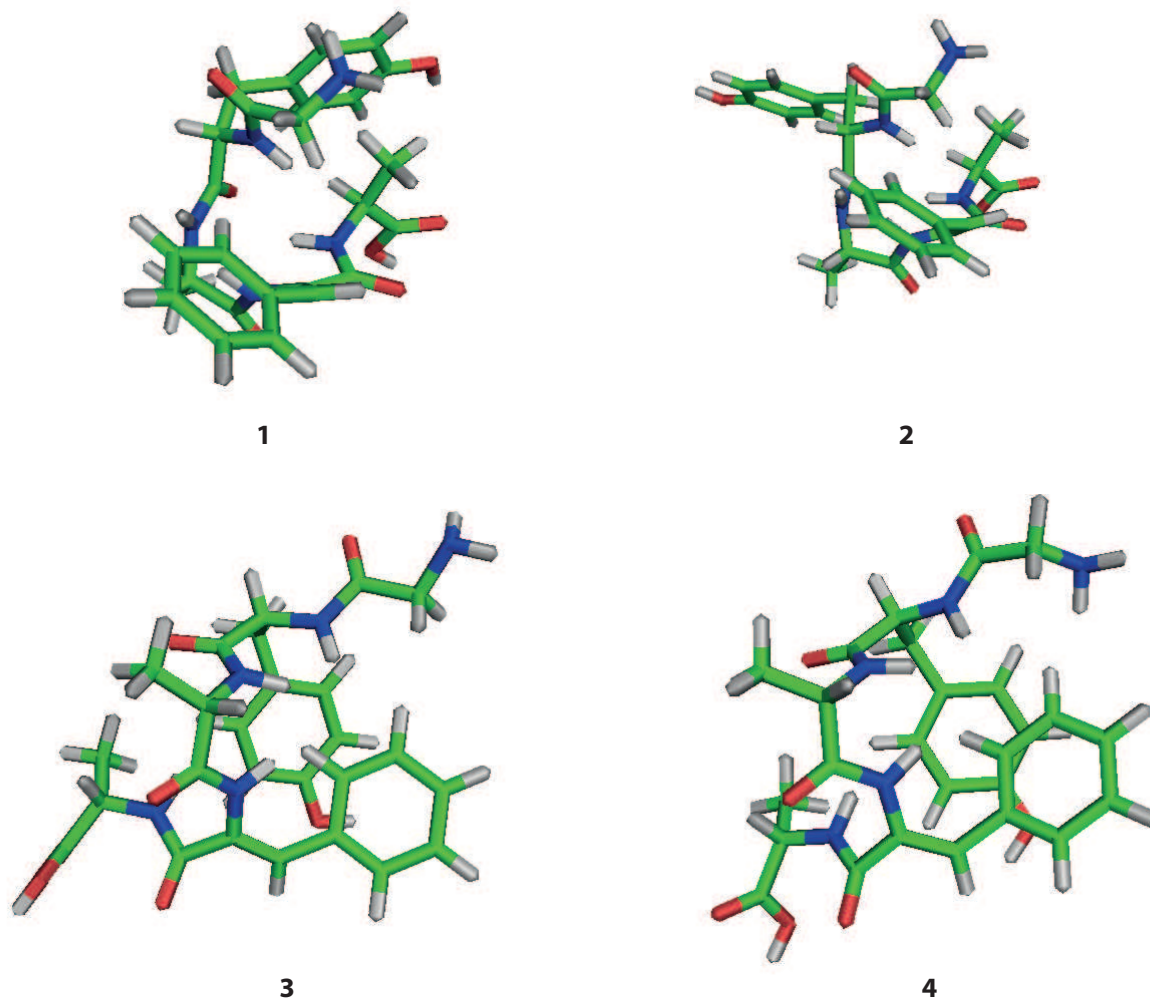
1.2.2 2D NOESY Spectroscopy

2D NOESY experiments were performed on a 500 MHz Bruker DRX500 spectrometer with a TCI cryoprobe with 2 number of scans, 800 ms mixing time, 2 s relaxation delay, and a spectral width of 8012.8 Hz.

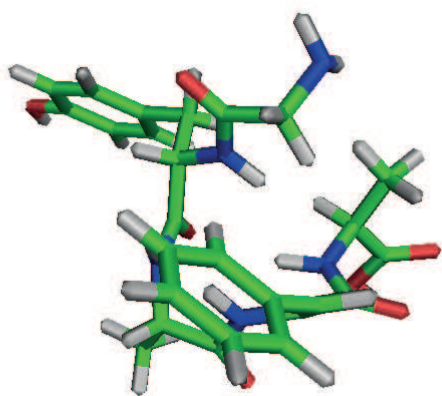


1.2.3 Molecular modeling using Maestro

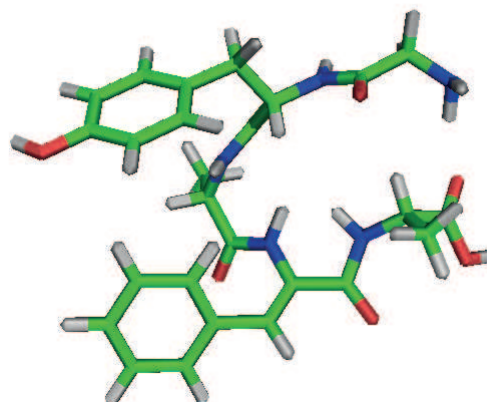
Structures with all experimentally feasible combinations of $H_N H_\alpha \phi$ dihedral angles for Tyr, Ala (internal) and Ala (terminal) were simulated in no solvent but with a dielectric constant corresponding to that of DMSO (47.6) using Maestro (Schrodinger, Inc.).* An error of $\pm 40^\circ$ was added to every structure. Only weak and very weak distance restraints found from NOESY spectrum using a mixing time of 800 ms were also included in the simulations. The cross-peak volumes were classified as weak (upper distance constraint ≤ 5) and very weak (upper distance constraint ≤ 6). The 19 lowest-energy structures are displayed.



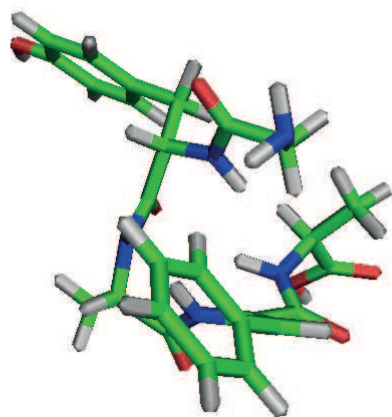
*Schrödinger Release 2015-2: Maestro, version 10.2, Schrödinger, LLC, new York, NY, 2015



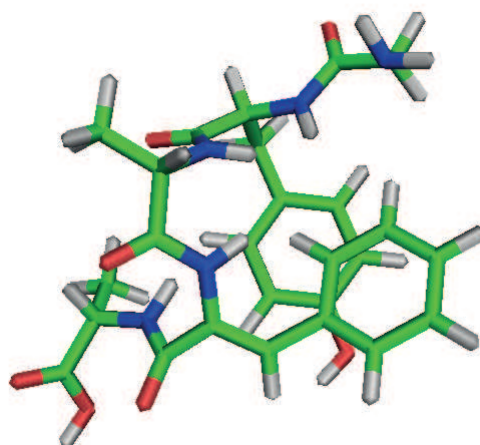
5



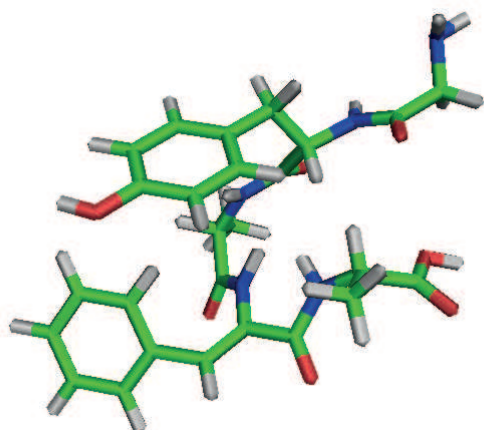
6



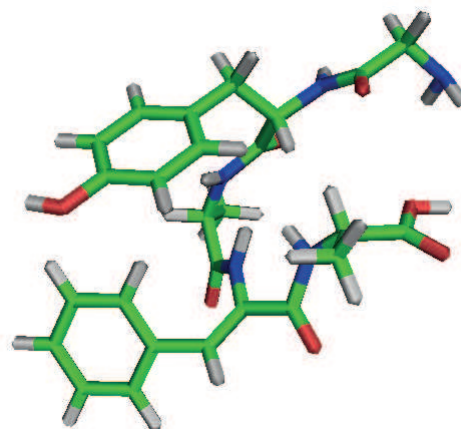
7



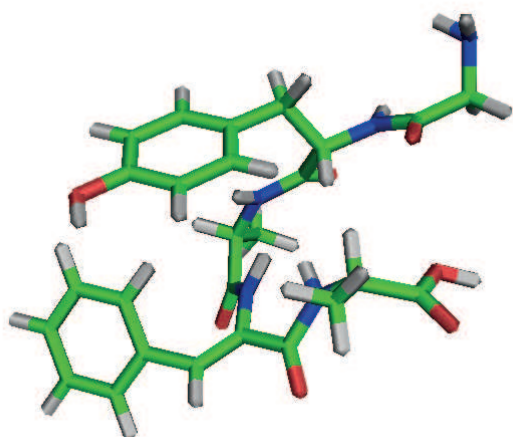
8



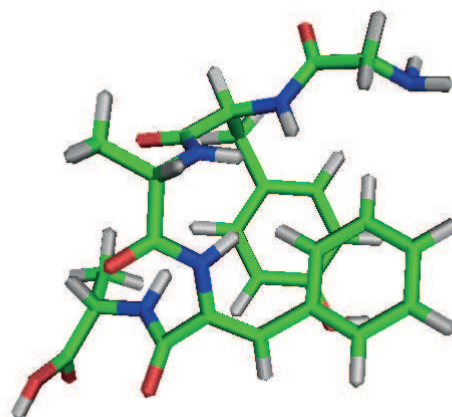
9



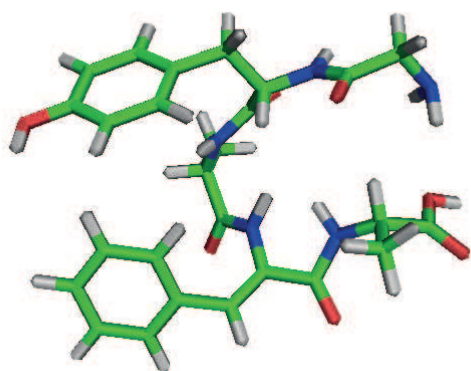
10



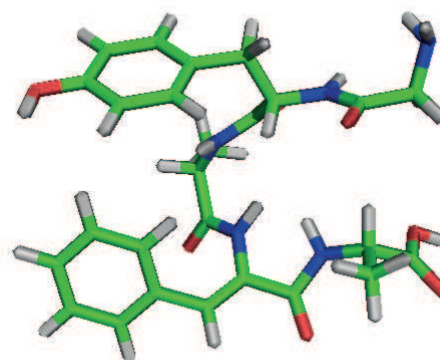
11



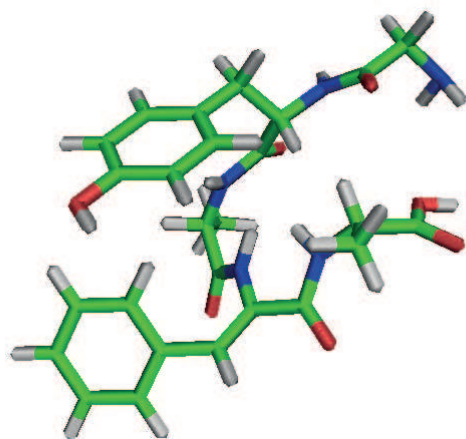
12



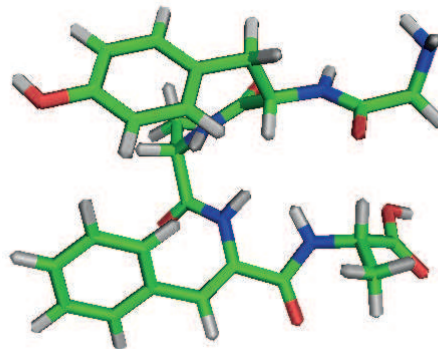
13



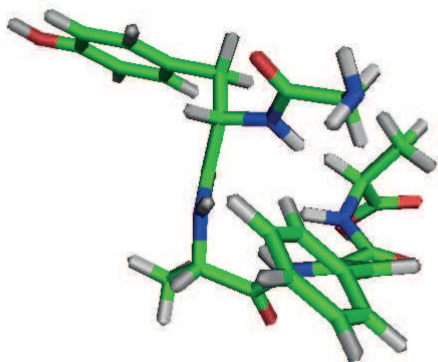
14



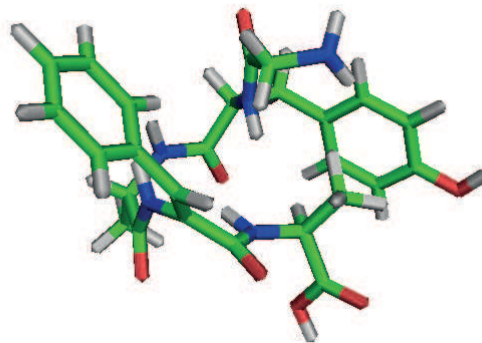
15



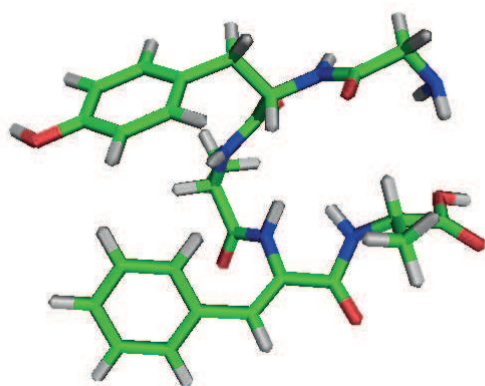
16



17



18



19

Chapter 2

Cobalt-Catalyzed Hydroacylation to from Thermodynamically Unfavored Motifs*

*Reproduced in part with permission from Kim, D. D.; Riedel, J.; Kim, R., S.; Dong, V. M. *J. Am. Chem. Soc.* **2017**, *139*, 10208. Copyright 2017 American Chemical Society

2.1 Enantioselective Cyclobutanone Synthesis

2.1.1 Introduction

Metalloenzymes can transform simple olefins into a diverse array of cyclic natural products.⁵⁵ For example, an achiral building block such as geranyl pyrophosphate undergoes ring-closing to generate a range of enantiopure terpenoids (e.g., sabinene, limonene, camphene, and pinene) (Figure 2.1). Considering Nature's ability to construct various rings via cyclases,⁵⁶ we aim to diversify common building blocks into different cyclic isomers, with high enantioselectivity via synthetic catalysts.^{57,58} As an analogue to geranyl pyrophosphate, we designed a simple model, dienyl aldehyde (**19**), that can be accessed in one step from commercial materials.⁵⁹ When using Rh-catalysis, we can transform this achiral aldehyde into the corresponding cyclopentanone (**23**), bicycloheptanone (**21**), or cyclohexenal (**22**) scaffold, by tuning the ligand scaffold (Figure 2.1).^{57,58} Herein, we report a cobalt catalyst that enables ring closing to generate the four-membered ring (**24**) via enantioselective hydroacylation.

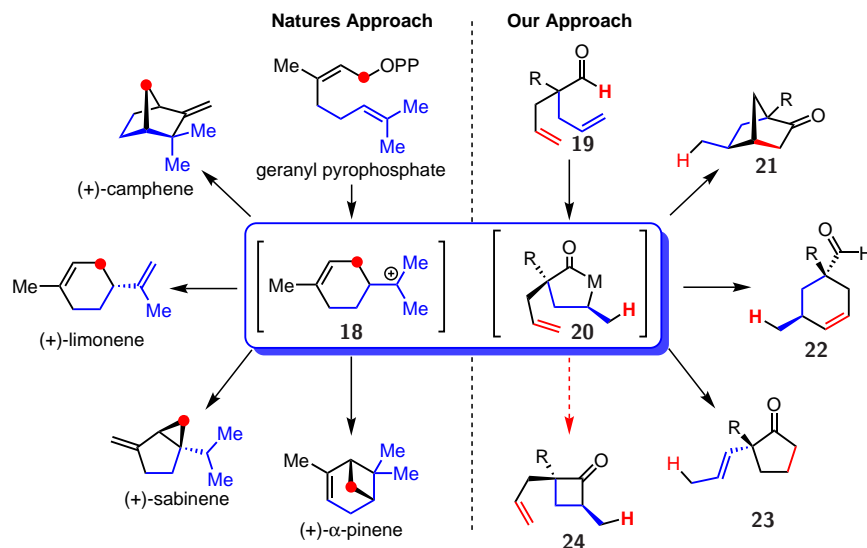


Figure 2.1. Inspiration for cobalt-based cyclase mimic

Hydroacylation⁶⁰ (the addition of an aldehyde C–H bond across an olefin or alkyne) enables C–C bond formation with excellent atom economy.^{61,62} Most intramolecular variants provide

exclusive access to cyclopentanones in preference to cyclobutanones.⁶⁰ However, there are two exceptions, both of which use substrates bearing a methoxy-directing group under Rh-catalysis.⁶³ Fu's method achieves an enantioenriched mixture of four- and five-membered ketones via a parallel kinetic resolution. Aïssa observed a 12% yield of the four-membered ketone when performing a similar parallel kinetic resolution. Rather than relying on a precious metal or a kinetic resolution, we propose using a base-metal (Co) to overturn the usual regioselectivity of hydroacylation to favor the more strained ring.

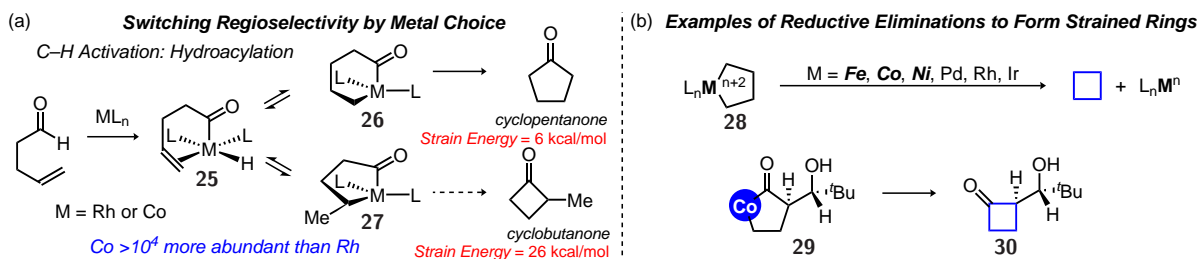


Figure 2.2. Challenges and literature precedents

Both Rh and Co are known to activate aldehyde C–H bonds through oxidative addition to form an acyl-metal-hydride intermediate **25** (Figure 2.2).^{60,64–68} From this intermediate, olefin insertion results in an equilibrium mixture of the six- (**26**) and five-membered (**27**) metallacycles. In general, reductive elimination from **26** is thermodynamically and kinetically favored to generate the less strained cyclopentanone product.⁶⁹ Moreover, achieving reductive elimination from a five-membered metallacycle (**27**) is challenging due to competitive endocyclic β -hydride elimination.^{70,71} By using first-row metals, however, C–C bond forming reductive eliminations from **28** to make small strained rings have been observed (Figure 2.2).^{70–86} Most relevant to our study, Bergman characterized a cobaltacycle (**29**), that upon treatment with stoichiometric FeCl₃ undergoes reductive elimination to form cyclobutanone (**30**).⁷³ Encouraged by these breakthroughs, we set out to identify the first cobalt-catalyst capable of generating cyclobutanones.

2.1.2 Results and Discussion

In our initial study, we found that commercially available Co^I-catalysts, such as Co(PPh₃)₃Cl, result in no conversion to the desired cyclobutanone (Table 2.1). However, with Co(PPh₃)₃Cl, in the presence of a zinc reductant, we observe a 5% yield and 6:1 regioisomeric ratio (*rr*) of **24a**:**31a**. We postulate that the reductant transforms the Co^I-complex into a Co⁰-catalyst critical for reactivity.

Table 2.1. Identifying catalyst for cyclobutanones

entry	Co ⁿ -catalyst	reductant	yield 24a	selectivity
1	(PPh ₃) ₃ Co ^I Cl (5 mol%) + BDPP (5 mol%)	none	0%	<i>rr</i> n.d. <i>dr</i> n.d.
2	(PPh ₃) ₃ Co ^I Cl (5 mol%) + BDPP (5 mol%)	Zn (10 mol%)	5%	6:1 <i>rr</i> >20:1 <i>dr</i>
3	(PMe ₃) ₄ Co ⁰ (5 mol%)	none	10%	1:1 <i>rr</i> 1:1 <i>dr</i>
4	(BDPP)Co ^{II} Cl ₂ (10 mol%)	Et ₂ Zn (50 mol%)	89%	10:1 <i>rr</i> 10:1 <i>dr</i>
5	(BDPP)Co ^{II} Cl ₂ (2 mol%)	Zn (10 mol%)	92% <i>ee</i> 93%	>20:1 <i>rr</i> >20:1 <i>dr</i>

Indeed, using a well-characterized and isolable Co(PMe₃)₄ (synthesized from CoCl₂, sodium naphthalenide, and trimethylphosphine) results in a mixture of **24a** and **31a** in 1:1 *rr* in 10% yield. Switching to a CoCl₂/reductant system,^{87,88} as a precursor for Co⁰, enabled rapid evaluation of a range of chiral phosphine ligands.* Under these conditions, we identified a chiral ligand, (*S,S*)-2,4-bis(diphenylphosphino)-pentane (BDPP), that promotes the formation of **24a** in preference to **31a**. A catalyst loading of 10 mol% using diethyl zinc as the reducing agent gave promising selectivities (10:1 *dr*, 10:1 *rr*). Moreover, by desymmetrization, we access these motifs with 92% *ee* using this chiral bidentate phosphine ligand. On the basis of ¹H NMR studies, we observe evolution of ethylene and ethane gas when using diethyl zinc. This observation is consistent with formation of a Co⁰-species. For a proposed

*For a comprehensive list of ligands evaluated, see SI. For synthesis of [(*S,S*)-BDPP]CoCl₂ see Sharma, R. S.; RajanBabu, T. V. *J. Am. Chem. Soc.* **2010**, *132*, 3295.

mechanism, ^1H NMR, and UV/vis absorption spectra data for the formation of Co^0 -species using diethyl zinc (see SI). The catalyst loading can be lowered to 2 mol% when switching to activated zinc metal as a stronger reducing agent. The use of activated zinc improves reactivity (from 24 to 4 h) and selectivity (from 10:1 *dr* and *rr* to >20:1 *dr* and *rr*) when using 10 mol% of the catalyst.

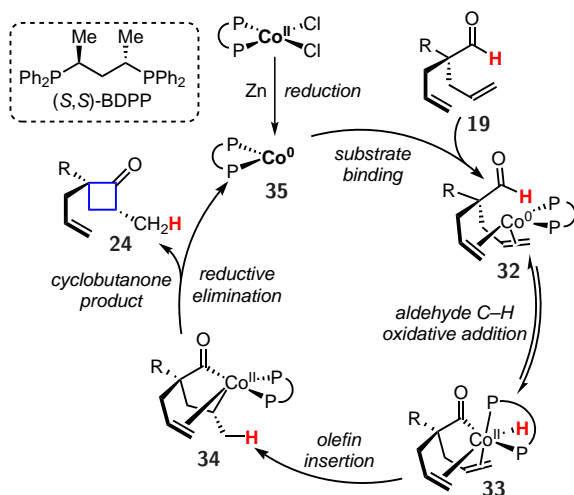


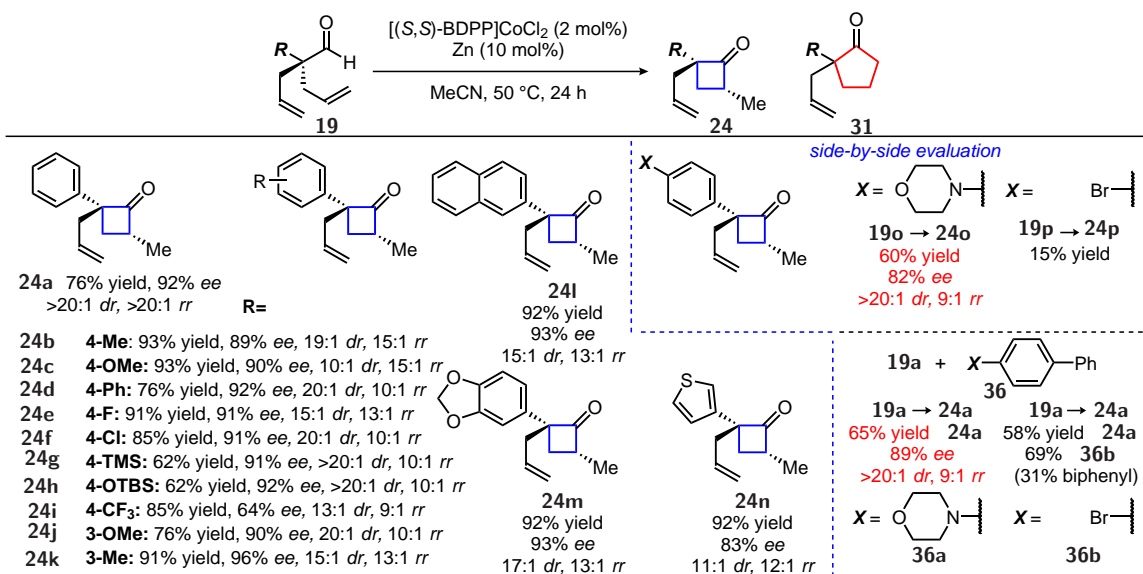
Figure 2.3. Proposed mechanism

Related protocols for Co-hydroacylation have been proposed to occur through $\text{Co}^0/\text{Co}^{\text{II}}$ and $\text{Co}^{\text{I}}/\text{Co}^{\text{III}}$ catalytic cycles.^{64,66-68} Although both are feasible, on the basis of our results, we propose this cyclization occurs by initial reduction of Co^{II} -chloride to a Co^0 -complex (**35**), with activated zinc or diethyl zinc (Figure 2.3). The Co^0 -catalyst then binds to the substrate (**19**) to form complex (**32**) prior to aldehyde C-H bond activation by oxidative addition. The acyl-Co-hydride intermediate (**33**) can isomerize by olefin insertion into the metal-hydride bond to forge the five-membered metallacycle (**35**). From here, reductive elimination forms the C-C bond to construct the strained ring (**24**).

Under these mild conditions, a variety of α -aryl dienyl aldehydes undergo isomerization to the corresponding cyclobutanones (Table 2.2). Dienyl aldehydes bearing electron-rich α -aromatic groups (alkyls, ethers, acetals, and alcohols) ring close in good yields and selectivities (76-93% yields, >89% *ee*, >10:1 *dr*, >10:1 *rr*). Substrates with electron-poor α -aromatic

groups (F, Cl, and CF₃) also cyclize (91-85% yield, >64% *ee*, >13:1 *dr*, and >9:1 *rr*) albeit with lower enantioselectivities. Heteroaryl thiophene, silylated phenol, and amine substrates are well tolerated (60-92% yield, 82-95% *ee*, >11:1 *dr*, >9:1 *rr*). Of note, cyclobutanone **24a** was generated on gram scale without impact on selectivity.

Table 2.2. Synthesis of enantioenriched cyclobutanones



We imagined that an aryl group bearing a range of functional groups could be tolerated in this transformation. To probe this idea, we performed a functional group compatibility test.⁸⁹⁻⁹¹ We added an equivalent amount of various additives (e.g., pyridine, phenol, amines, etc.) with aldehyde (**19a**) under otherwise standard conditions.* The cyclization to cyclobutanone (**24a**) occurs smoothly in the presence of heterocycles such as pyridines and indoles. Additives containing polar protic functional groups such as phenols, anilines, and amides as well as other carbonyl-containing additives such as aldehydes, ketones, esters, and amides had little effect on the transformation.

The robustness screen provides a general guideline to the selectivities and to the types of functional groups tolerated in our reaction,⁸⁹⁻⁹¹ although selectivities can vary depending on

*For a comprehensive list of functional groups evaluated and reaction outcomes under standard reaction conditions with **19a**, see SI

where the functional group is attached. For example, we found that the addition of morpholine additive (**36a**) yielded **24a** in 65% yield and 89% *ee*. We prepared the analogous morpholine containing substrate (**19o**) and performed the cyclization to provide cyclobutanone (**24o**) in similar yield but slightly lower *ee*.⁹²⁻⁹⁴ In contrast, an aryl-bromide containing additive (**36b**) and 4-bromophenyldienyl aldehyde (**19p**) both underwent debromination to form biphenyl and **19a**, respectively. Our cyclization proceeds well in the presence of known radical inhibitors such as butylated hydroxytoluene (BHT),⁹⁵ 9,10-dihydroanthracene (DHA),⁹⁶ and 1,1-diphenylethylene (DPE) (84% yield, 93% *ee*, >20:1 *dr*, 7:1 *rr*, with 94% additive recovered). The use of TEMPO as an additive inhibited reactivity presumably acting as an oxidant as well as a ligand on Co.⁹⁷

When using deuterium-labeled aldehyde **19a-D**, we observe full incorporation of the deuteride into the α -methyl position of the cyclobutanone product **24a-D** (Figure 2.4). This isotopic labeling study provides results consistent with our proposed mechanism (Figure 2.3). When comparing the measured initial rates of two parallel reactions between the protio-aldehyde (**19a**) and deuterio-aldehyde (**19a-D**), we observe a primary kinetic isotope effect of 2.7 (KIE = 2.7). When monitoring the reaction with **19a-D** as the substrate, no deuterium scrambling in the product or the starting material was observed. The primary KIE alongside a lack of deuterium scrambling likely points to aldehyde C-H bond activation or olefin insertion into the Co-H bond as the turnover-limiting step.

By studying the scope of this cyclization, we found that regioisomeric ratio (*rr*) of 5:6 is influenced by the α -position of the aldehyde (Figure 2.4). Higher selectivity for the four-membered versus five-membered ketone is observed with increasing size of the α -substituent (R in Figure 2.4). The highest selectivity is observed with phenyldienyl aldehyde **19a** (>20:1 *rr*, A-value = 3.0 for R = Ph) and the lowest selectivity is observed with dienyl aldehyde **19r** (1:2 *rr*, A-value = 0.0 for R = H).⁹⁸ We reason that the increased steric crowding around the metal center promotes formation of the five-membered metallacycle **27** over the

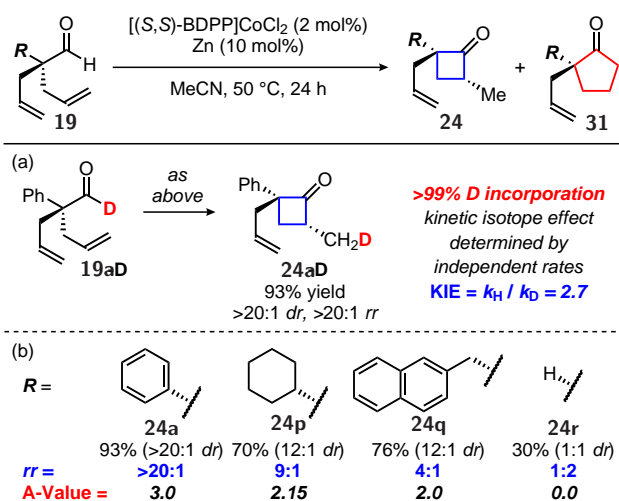


Figure 2.4. Reaction evaluation of diene aldehyde

six-membered metallacycle **26**.⁹⁹ This is due to bond-angle compression, making the five-membered metallacycle **27** more thermodynamically stable and kinetically accessible. Thus, despite ring-strain, reductive elimination to form the four-membered ring is not turnover-limiting. Therefore, we propose that olefin insertion is turnover-limiting and favors formation of the five-membered metallacycle.

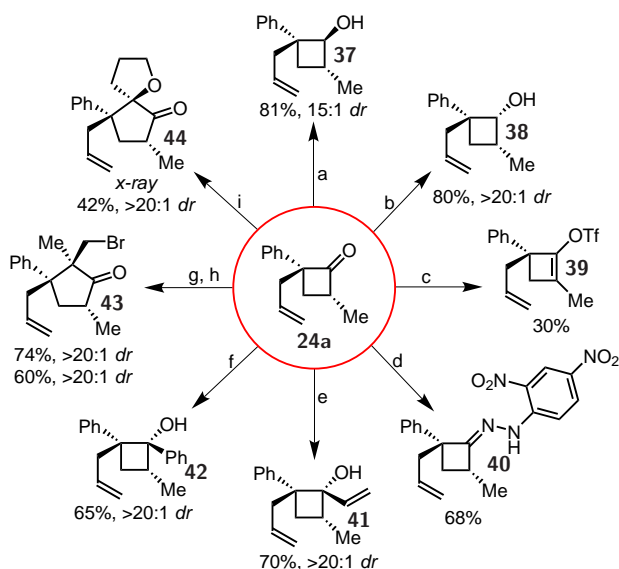


Figure 2.5. Derivatization of cyclobutanone **24a**

The newly formed stereocenters in our cyclobutanone scaffold can be put to use in a number of stereoselective reactions to build different structures (Figure 2.5). The reduction to the

secondary alcohol can be controlled depending on choice of the reductant. DIBAL-H adds from the more sterically hindered face (a), whereas L-selectride adds from the less hindered face (b). This strained ketone can be converted to an enol-triflate suitable for cross-coupling reactions (c). A strained ketimine can be prepared by condensation with 2,4- dinitrohydrazine (d). New C-C bonds can be generated in a highly diastereoselective fashion (>20:1) by using vinyl- (e) or phenyl-Grignard (f) addition to generate the tertiary cyclobutanols. Taking advantage of the ring-strain,¹⁰⁰ the cyclobutanones can undergo ring-expansion to enantioenriched cyclopentanones with vicinal all-carbon quaternary centers by addition of isopropenylmagnesium bromide (g) followed by electrophilic bromination (h). Similarly, the addition of a lithiated-dihydrofuran followed by treatment with mild acid results in a one-carbon ring expansion to form a cyclopentanone (i). This spirocyclopentanone was crystallized and a molecular structure was unambiguously determined by X-ray crystallography along with assignment of the absolute stereochemistry of the cyclobutanone products **24a-o** by analogy.

Although it is not depicted, the unreacted allyl-moiety could also be used as an additional functional handle. Although cycloadditions are typically used to make four-membered rings, cyclobutanones bearing α -quaternary carbons are challenging to access, especially with high enantiocontrol.¹⁰¹⁻¹⁰⁴ Our approach features a Co-catalyst that can isomerize a simple, prochiral dienyl aldehyde into cyclobutanones bearing chiral α -quaternary carbon centers, with excellent diastereo-, regio-, and enantiocontrol. Mechanistic studies suggest a pathway involving a $\text{Co}^0/\text{Co}^{\text{II}}$ cycle that is triggered by C-H bond activation. A switch from a precious metal to an abundant base-metal enables a shift in the construction of strained rings.

2.2 Selective Synthesis of *trans*-Hydrindanones

2.2.1 Introduction

Academia and industry are targeting increasingly complex molecular architectures, while trying to uphold high standards in efficiency.⁶² One emerging strategy to build up complexity is the breakage of symmetry¹⁰⁵ in molecules, it is believed that the homochirality of biomolecules resulted from such a symmetry breaking event.¹⁰⁶ In a synthetic setting, the breakage of symmetry can be achieved by the use of chiral catalysts that can differentiate two faces of a prochiral molecule and selectively let only one face of molecule undergo a reaction.¹⁰⁷⁻¹¹⁴ This strategy has been applied in the total synthesis of (-)-cyanthiwigin F by the Stoltz group.¹¹⁵

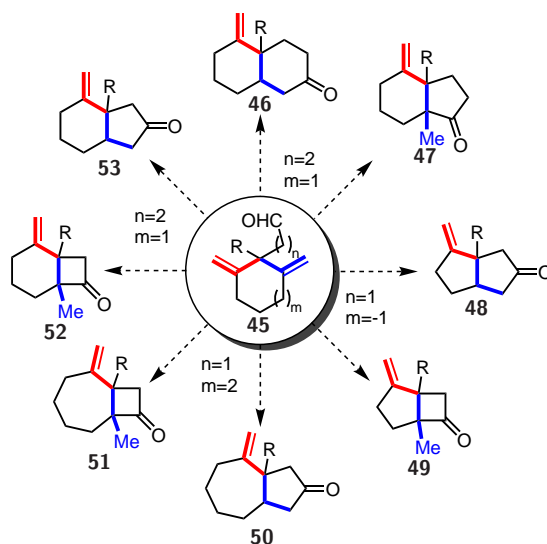


Figure 2.6. Chemical space from the desymmetrization of cyclohexenaldehydes

Another important aspect of efficient synthesis is the minimization of waste- and byproducts.^{116,117} The ideal process would be a catalyst enabled isomerization reaction, where all the atoms of the starting material end up in the product.⁶¹ Combining the idea of an economical isomerization and a complexity-introducing desymmetrization, a variety of different complex motifs can be built up quickly.^{57,58,118} I focused on a class of cyclohexenals

(**45**). Depending on the ring size and the linkage between the ring and the aldehyde, a variety of different motifs could be realized through metal catalyzed cycloisomerizations (Figure 2.6). Of special interest is hydrindanone **53**. Hydrindane cores are prevalent motifs in bioactive molecules and important intermediates in total syntheses.^{119–125} Traditionally, they have been accessed in numerous total syntheses through the Hajos-Parrish ketone (Figure 2.7).^{126–132} The *cis*-hydrindanone can be easily accessed through a desymmetrization of a α,α -disubstituted 1,3-cyclohexanedione.^{133–135} Methods to make the corresponding *trans*-hydrindanone are scarce (also Nagata hydrocyanation)^{136–141} although there are several families of natural products containing this fused ring system.^{142,143} Asymmetric cobalt catalyzed hydroacylation can provide an attractive solution to access these motifs.¹¹⁸

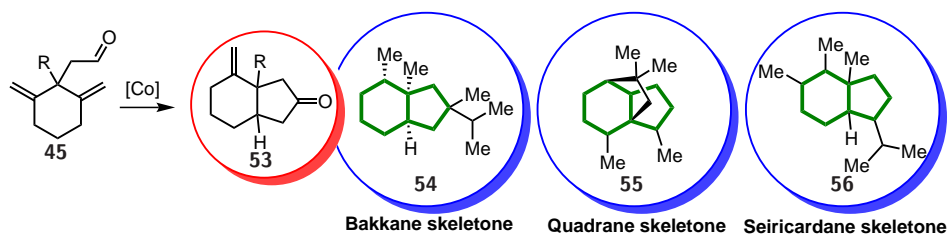


Figure 2.7. Natural motifs containing hydrindane skeleton

We envisioned that a cobalt catalyst could be able to take cyclohexenal **45** form a C-C bond through intramolecular hydroacylation, resulting in hydrindanone **53** or the isomeric four-membered fused ring system **52**.

2.2.2 Results and Discussion

To test our hypothesis, cyclohexenal **53a** was prepared by using 1,3-cyclohexandione **6** and doing a Knoevenagel-condensation with benzaldehyde, followed by a Hantzsch-ester reduction in one pot, giving benzylated 1,3-cyclohexandione **7**.¹⁴⁴ Initially, intermediate **7** was alkylated with methyl bromoacetate, but the following olefination proved to be challenging (see SI). Next, intermediate **7** was allylated with allyl bromide to afford the disubstituted

1,3-cyclohexandione **6**. Although bearing an α quaternary center, the ketones could be converted into the corresponding olefins, using standard Wittig olefination conditions, giving cyclohexene **9**. From there, a sequence of dihydroxylation with OsO_4 and oxidative cleavage with NaIO_4 afforded the desired cyclohexenal **53a**.

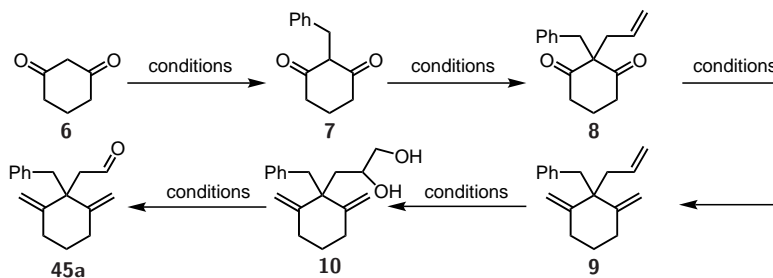


Figure 2.8. Substrate synthesis

With cyclohexenal **53a** in hand, I tested the key reaction as shown in Figure 2.9. When using CoCl_2 as precatalyst, zinc as reductant and dppe as the ligand, hydrindanone **53a** can be obtained in 58% isolated yield with $>20:1$ *dr* for the *trans*-fused ring system. The corresponding four-membered fused ring system **52a** was not observed. The selective formation of *trans*-fused diastereomer can be explained when taking a look at the mechanism (Figure 2.10).

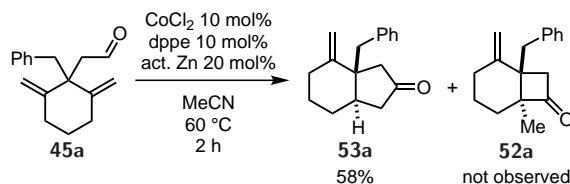


Figure 2.9. Initial hit

In analogy to our previous chemistry, we propose the initial reduction of Co^{II} to Co^0 followed by oxidative addition into the aldehyde C–H bond of the cyclohexenal **53a** to form cobalt acylhydride intermediate **57**. Insertion of the olefin into the cobalt-hydride bond will form the acyl cobaltacycle **58**. This step is inherently *trans*-selective, since the face from which the hydride migrates is dictated by the acyl group as shown in Figure 2.10. Reductive elimination of acyl cobaltacycle **58** will then form the final hydrindanone product **53**.

With this initial hit in hand, the reaction conditions were optimized by first looking at

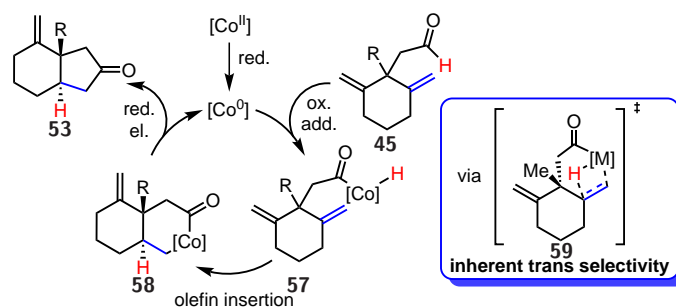


Figure 2.10. Proposed reaction mechanism

different Co^{II} precatalysts (Table 2.3). There is an increase in reactivity moving in the Co^{II} -halide series from CoF_2 to CoI_2 , with CoI_2 showing the best reactivity. Interestingly, when using $\text{Co}(\text{OAc})_2$ and $\text{Co}(\text{BF}_4)_2$ hexahydrate, isomerization and reduction of the aldehyde are the predominant pathways. Next, different reductants and their effect on the reactivity were investigated. A range of different metals and metal complexes are competent reductants in this reaction, with Rieke zinc standing out, showing the best reactivity. Hydroacylations on related motifs have been reported before.¹⁴⁵

Table 2.3. Optimization of precatalyst and reductant

entry	Precatalyst	conv.	yield
1	CoF_2	32%	13%
2	CoCl_2	81%	58%
3	CoBr_2	92%	68%
4	CoI_2	full conv.	73%
5*	$\text{Co}(\text{OAc})_2$	72%	-
6**	$\text{Co}(\text{BF}_4)_2 \cdot 6 \text{H}_2\text{O}$	92%	2%

entry	reductant	conv.	yield
1	Zn dust	31%	6%
2	ZnEt_2	72%	63%
3	Rieke Mg	97%	64%
4	Rieke Co	n.r.	n.d.
5	In	6%	n.d.
6	Mn	59%	53%
7	Rieke Zn	full conv.	73%

* reduction and isomerization observed

** reaction time was 6 h.

In 2015, our group published the isomerization/hydroacylation of 2-allyl-4-pentenals derivatives using a $\text{Rh}^{\text{I/III}}$ catalytic system.⁵⁷ We proposed a mechanism similar to the cobalt catalyzed hydroacylation. When using the conditions from the rhodium catalyzed hydroacylation with **45a**, no reaction was observed (see SI). In 2000 Tanaka reported the hydroa-

cylation of 4-methyl-3-(prop-1-en-2-yl)pent-4-enal, which are closely related to cyclohexenal 45.¹⁴⁵ Yet, when employing his conditions using again a rhodium catalyst system, no reaction was observed. Interestingly, the developed cobalt catalyst is complementary to previously developed catalyst systems and expands the general substrate scope of intramolecular hydroacylations.

Table 2.4. Enantioselective conditions

entry	ligand	conv.	yield	ee
1	dppe	full conv.	79%	n.d.
2	dppf	n.r.	n.d.	n.d.
3	(<i>R</i>)-ProPhos	32%	29%	n.d.
4**	(<i>R,R</i>)-DIPAMP	full conv.	46%	12%
5	(<i>S,S</i>)-BDPP	full conv.	79%	19%
6**	(<i>R,R</i>)- <i>i</i> -Pr-DuPhos	full conv.	46%	22%
7**	(<i>S,S,R,R</i>)-DuanPhos	full conv.	46%	24%
8**	(<i>S,S</i>)-NorPhos	full conv.	46%	33%
9*	(<i>S,S</i>)-ChiraPhos	full conv.	99%	43%
10**	(<i>S,S</i>)- <i>i</i> -Pr-BPE	full conv.	46%	46%
11**	(<i>S,S</i>)-Ph-BPE	full conv.	46%	51%
12**	(<i>S,S</i>)-QuinoxP*	full conv.	46%	56%
13***	(<i>R,R</i>)-JoSPOphos	full conv.	99%	99%

ProPhos

DIPAMP

ChiraPhos

BPE

JoSPOphos

NorPhos

DuanPhos

DuPhos

QuinoxP*

* 34% conv., 8% yield, 39% ee at 40 °C after 6 h.
 ** Aldehyde prepared through DMP oxidation and presumably of low purity
 *** with 10 mol% AgPF₆

A variety of chiral bidentate phosphine ligands have been tested to render this transformation enantioselective. Based on previously reported cobalt catalyzed hydroacylations and experience from our group.^{64,118,146–150} We initially focused on chiral bidentate bis-phosphine ligands. Given that we saw good reactivity with dppe, an achiral bidentate bis-phosphine ligand, we initially focused on chiral ligands, that have a ethane linkage between the phosphines. Interestingly, (*R*)-ProPhos is structurally very similar so dppe, yet when employing this ligand in the reaction, we saw dampened reactivity. On the other (*S,S*)-ChiraPhos, which bears an extra methyl group in the ethane backbone, shows excellent reactivity and a promising enantioselectivity of 43% *ee*. Only (*S,S*)-QuinoxP* was able to give a higher selectivity of 56% *ee*. JoSPOphos proved to be the best ligand for this transformation giving

both, high reactivity as well as selectivity.

2.2.3 Conclusion and Future Work

Future studies will focus on the substrate evaluation. Furthermore, an interesting application could involve the total synthesis of seiricardine A **63** (Figure 2.11).¹⁴² This molecule is a sesquiterpinoid natural product, that shows phytotoxic activity and has never been synthesized before.¹⁵¹ Starting from hydrindanone **53b**, allylic oxidation and hydrogenation of the olefin would give alcohol **60**. Formation of the enol triflate, followed by reduction would give alkene **61**. The isopropenyl group can be introduced through a sequence of epoxidation and epoxide ring opening to give ketone **62**. Finally, olefination of the ketone, followed by subsequent epoxidation and epoxide ring opening would furnish seiricardine A **63**.

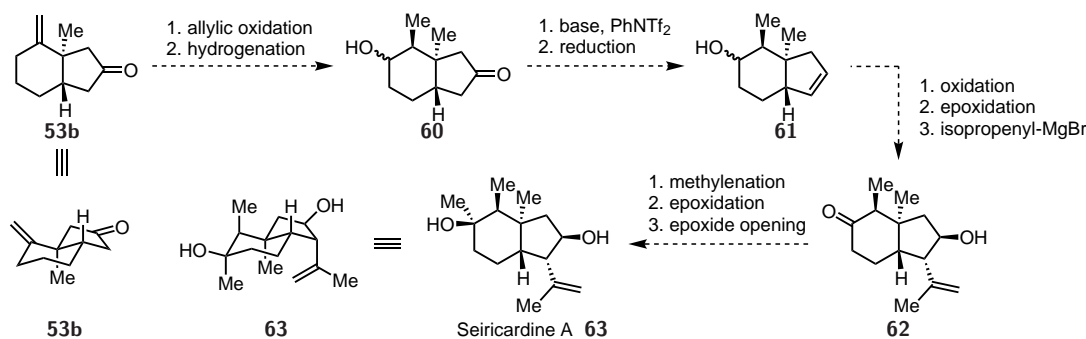


Figure 2.11. Proposed total synthesis of Seiricardine A

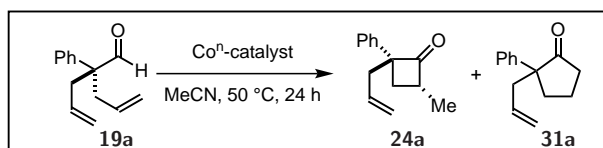
2.3 Experimental Data

The details of the studies described in this chapter can be found in the Supporting Information of the published manuscript.¹¹⁸ My contributions to the project are detailed in this section.

2.3.1 Experimental Details for Enantioselective Cyclobutanone Synthesis

Evaluation of Cobalt Catalysts

The evaluation of cobalt catalysts was done together with Daniel K. Kim.



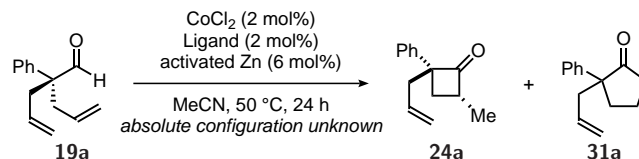
<i>Coⁿ-catalyst</i>	<i>reductant</i>	<i>yield (5a)</i>	<i>selectivity</i>
(PPh ₃) ₃ Co ^I Cl (5 mol%) + BDPP (5 mol%)	none	0%	<i>rr n.d.</i> <i>dr n.d.</i>
(PPh ₃) ₃ Co ^I Cl (5 mol%) + BDPP (5 mol%)	Zn (10 mol%)	5% <i>ee n.d.</i>	6:1 <i>rr</i> >20:1 <i>dr</i>
(PMe ₃) ₄ Co ⁰ (5 mol%)	none	10% <i>ee n.d.</i>	1:1 <i>rr</i> 1:1 <i>dr</i>
(BDPP)Co ^{II} Cl ₂ (10 mol%)	Et ₂ Zn (50 mol%)	89% 93% <i>ee</i>	10:1 <i>rr</i> 10:1 <i>dr</i>
(BDPP)Co ^{II} Cl ₂ (2 mol%)	Zn (10 mol%)	93% 93% <i>ee</i>	>20:1 <i>rr</i> >20:1 <i>dr</i>

Evaluation of Ligands

The evaluation of ligands was done together with Daniel K. Kim.

All cobalt-catalyzed reactions were set up inside of a nitrogen-filled glovebox. To a 1-dram vial was added a stirbar and CoCl₂ (0.002 mmol, 2 mol%) and ligand (0.002 mmol, 2 mol%) in MeCN (0.50 mL, 0.2 M). The catalyst mixture was stirred for 5 minutes at room temperature. To the catalyst mixture was added aldehyde **19a** (20.0 mg, 0.10 mmol, 1 equiv), followed by the addition of the indicated amount of activated zinc (0.006 mmol, 6 mol%). The heterogeneous mixture was sealed with a Teflon-lined screw cap and heated the indicated temperature and time. Note: While heating the reaction mixture, the blue mixture turns green and then yellow before finally turning dark brown in color over 15–30 minutes.

Chemo- and regioselectivity were determined from analysis of the reaction mixture by GC-FID analysis. Yields and selectivities were determined by GC-FID using a standard curve. Enantiomeric excess were not determined.



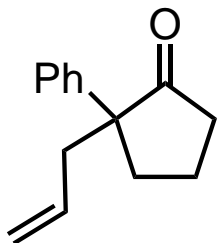
entry	ligand	conv.	yield	<i>dr</i>	<i>rr</i>
1	dppm	5%	0%	n.d.	n.d.
2	dppe	99%	88%	>20:1	>20:1
3	dppp	85%	40%	10:1	2:1
4	dppb	68%	3%	n.d.	1:1
5	dppf	12%	0%	n.d.	n.d.
6	PPh_3 (4 mol%)	70%	2%	10:1	2:1
7	(<i>R,R</i>)- <i>i</i> -Pr-BPE	78%	10%	4:1	1:8
8	(<i>R,R</i>)- <i>i</i> -Pr-DuPhos	64%	5%	2:1	1:22
9	(<i>S,S</i>)-BenzP*	57%	10%	15:1	1:7
10	(<i>R</i>)-Binap	12%	5%	n.d.	1:1
11	JosiPhos (SL-J008-1)	89%	70%	11:1	8:1
12	(<i>S,S</i>)-ChiraPhos	20%	16%	>20:1	2:1
13	(<i>S</i>)-ProPhos	20%	17%	>20:1	2:1
14	(<i>R</i>)-Ph-MeOBIPHEP	40%	5%	>20:1	1:11
15	(<i>S,S</i>)-Ph-MeOBIPHEP	99%	96%	>20:1	>20:1

Synthesis of Activated Zinc (Modified Synthesis for Rieke Zinc)

In a 250 mL schlenk flask was added zinc chloride (3.0 g, 22.01 mmol, 1 equiv) and 1 mL of thionyl chloride to dry the zinc chloride. The mixture was heated under vacuum with a bunsen burner until zinc chloride melted. The salt was allowed to cool to room temperature under nitrogen gas. To the cooled mixture was added THF (70.5 mL, 0.31 M) to form a colorless solution. In a separate 500 mL schlenk flask was added a stirbar, benzo[b]thiophene (0.107 g, 0.800 mmol, 3.6 mol%), naphthalene (5.77 g, 45.0 mmol, 2.04 equiv), and lithium metal (0.306 g, 44.0 mmol, 2 equiv) in THF (70.5 mL, 0.62 M) to give a colorless suspension. To help the lithium dissolve, the mixture was sonicated for 3 minutes. During this time the solution turned dark green, indicative of lithium naphthalide formation. The zinc chloride

solution was transferred via cannula addition. The pressure was adjusted to allow for dropwise addition of zinc chloride into the lithium naphthalide solution. The reaction was stirred for 1 hour. After 1 hour, the stirring was stopped to allow a black solid to settle to the bottom of the flask. Most of the solvent was then removed via cannula transfer and discarded after careful quenching. Fresh THF (20 mL) was added to the black solid and stirred vigorously for a few minutes. After vigorous mixing, the stirring was stopped to allow the black solid to settle at the bottom and most of the solvent removed via cannula transfer. This procedure was repeated three more times to remove most of the lithium naphthalide and benzo[b]thiophene. Finally, the residual THF was removed in vacuo. A black shiny solid was isolated (608 mg, 46% yield) and stored in a nitrogen-rich glovebox. Any unreacted lithium pellets that were still present were removed and quenched.

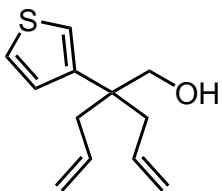
2-allyl-2-phenylcyclopentan-1-one **31a**



Inside a nitrogen-filled glovebox, to a 100 ml round-bottom flask was added a stirbar and $\text{Co}[(S,S)\text{-BDPP}]\text{Cl}_2$ (30 mg, 0.3 mmol, 3 mol%) in MeCN. The catalyst mixture was stirred for 5 minutes at room temperature. To the catalyst mixture was added aldehyde **19n** (2 g, 10 mmol, 1 equiv) and activated zinc (98 mg, 1.5 mmol, 15 mol%). The heterogeneous mixture was heated to 60 °C for 24 h. The selectivities were determined by GC-FID and ^1H NMR analysis (20 second relaxation delay). The crude reaction was filtered through a 10 ml syringe filled with silica and eluted with diethyl ether. The pure ketone **24n** was isolated by column chromatography (1.5% EtOAc/Hexanes) in 46 mg as a colorless oil, 2% yield. ^1H -NMR: δ (500 MHz, CDCl_3) 7.43 – 7.38 (m, 2H), 7.36 – 7.30 (m, 2H), 7.29 – 7.14 (m, 1H), 5.58 – 5.43 (m, 1H), 5.03 – 4.93 (m, 2H), 2.64 – 2.50 (m, 2H), 2.48 – 2.40 (m, 1H), 2.37 – 2.20 (m, 2H), 2.15 – 2.04 (m, 1H), 1.99 – 1.89 (m, 1H), 1.89 – 1.77 (m, 1H). ^{13}C -NMR: δ (126 MHz, CDCl_3) 219.28, 139.69, 134.12, 128.65,

126.97, 126.95, 118.15, 56.62, 43.44, 37.81, 33.38, 18.69. HRMS (ESI-TOF) m/z calculated for $C_{14}H_{16}O$ $[M+Na]^+$: 223.1099, found 223.1098. IR (ATR): 2963, 1732, 1495, 1445, 1153, 1001, 916, 754, 698 cm^{-1} . $[\alpha]_D^{25} +245.0^\circ$ ($c=0.05$, $CHCl_3$).

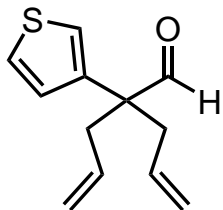
2-allyl-2-(thiophen-3-yl)pent-4-en-1-ol



In a round-bottom flask was a THF (0.2 M) solution of methyl 2-(thiophen-3-yl)acetate (1 equiv) in an acetone/dry ice bath at $-78^\circ C$. Sodium bis(trimethylsilyl)amide (NaHMDS) in THF (2.5 equiv) was added. The solution was stirred for 30 minutes. Then, allyl bromide (2.5 equiv) was added dropwise to the reaction mixture. The solution was warmed to room temperature and stirred for 1–4 hours, monitoring by TLC. The reaction mixture was quenched with aqueous NH_4Cl solution and washed with aqueous 2 M HCl solution (to remove amine salts). The aqueous layer was extracted with ethyl acetate three times. The organic layers were combined and dried over Na_2SO_4 , filtered, and concentrated. The resulting dienylester was used without further purification. $LiAlH_4$ (2.5 equiv) was added slowly to a stirring solution of dienylester (1 equiv) in 25 mL THF (0.2 M) in a $^\circ C$ ice/water bath. After addition of $LiAlH_4$, the ice bath was removed and the reaction mixture was allowed to stir at room temperature for 20 minutes to 4 hours, monitoring by TLC. The reaction mixture was quenched by careful dropwise addition of 1 M HCl solution at $0^\circ C$. The mixture was separated by separatory funnel and the aqueous layer was extracted three times with ethyl acetate. The organic layer was dried over Na_2SO_4 , filtered, and concentrated. The resulting alcohol was then purified by flash column chromatography, giving 1.03 g as a colorless oil, 77% yield. 1H -NMR: δ (499 MHz, $CDCl_3$) 7.33 (dd, $J = 5.0, 2.9$ Hz, 1H), 7.12 – 6.95 (m, 2H), 5.67 (ddt, $J = 17.3, 10.1, 7.3$ Hz, 2H), 5.15 – 4.93 (m, 4H), 3.71 (s, 2H), 2.47 (qd, $J = 13.9, 7.3$ Hz, 4H), 1.36 (s, 1H). ^{13}C -NMR: δ (126 MHz, $CDCl_3$) 145.44, 134.28, 126.37, 125.86, 121.14, 118.13, 68.14, 45.17, 39.81. HRMS (ESI-TOF) m/z calculated for

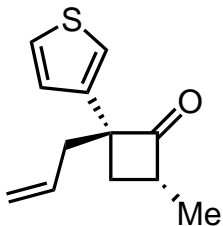
C₁₂H₁₆OS [M+Na]⁺: 231.0820, found 231.0827. IR (ATR): 3408, 3073, 2923, 1638, 1047, 912, 780 cm⁻¹.

2-allyl-2-(thiophen-3-yl)pent-4-enal (**19n**)



To a round-bottom flask was added dropwise dimethylsulfoxide (DMSO)(3 equiv) to a solution of oxalyl chloride (1.3 equiv) in DCM (0.2 M) at -78 °C in an acetone/dry ice bath, and then stirred for 30 minutes. A solution of dienylalcohol (1 equiv) in DCM was added dropwise at -78 °C and stirred for 30 minutes. After stirring the reaction for 30 minutes, triethylamine (5 equiv) was added dropwise at -78 °C. The reaction mixture was then warmed to room temperature and stirred for an additional 30 minutes. The reaction was quenched with water and extracted with DCM. The organic layer was washed with water, dried over Na₂SO₄, filtered, and concentrated in vacuo. The crude residue was purified by silica gel column chromatography, giving 360 mg of **19n**) as a colorless oil, 48% yield. ¹H-NMR: δ (500 MHz, CDCl₃) 9.50 (s, 1H), 7.40 – 7.30 (m, 1H), 7.20 – 7.05 (m, 1H), 7.04 – 6.83 (m, 1H), 5.58 (dq, *J* = 17.2, 8.7, 8.1 Hz, 2H), 5.25 – 4.62 (m, 4H), 2.70 (d, *J* = 7.3 Hz, 4H). ¹³C-NMR: δ (126 MHz, CDCl₃) 201.11, 139.50, 132.70, 126.72, 126.51, 122.69, 119.10, 55.30, 37.18. HRMS (ESI-TOF) *m/z* calculated for C₂₃H₁₄OS [M+Na]⁺: 224.1109, found 224.1110. IR (ATR): 3077, 2978, 2917, 2805, 2710, 1722, 1441, 994, 916, 862, 778, 664 cm⁻¹.

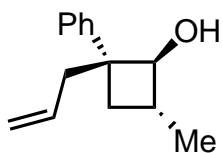
(2*R*,4*R*)-2-allyl-4-methyl-2-(thiophen-3-yl)cyclobutan-1-one (**24n**)



Inside a nitrogen-filled glovebox, to a 1-dram vial was added a stirbar and Co[(*S,S*)-BDPP)]Cl₂(1.1 mg, 0.002 mmol, 2 mol%) in MeCN. The catalyst mixture was stirred for 5 minutes at room temperature. To

the catalyst mixture was added aldehyde **19n** (20.6 mg, 0.1 mmol, 1 equiv) and activated zinc (0.6 – 0.7 mg, 0.010 mmol, 10 mol%). The heterogeneous mixture was sealed with a Teflon-lined screw cap and heated to 50 °C for 24 h. The selectivities were determined by GC-FID and ¹H NMR analysis (20 second relaxation delay). The pure ketone **24n** was isolated by preparative TLC (10% EtOAc/Hexanes) as a colorless oil (18.9 mg, 92% isolated yield, 83% *ee*, 11:1 *dr*, 12:1 *rr*). ¹H-NMR: δ (499 MHz, CDCl₃) 7.31 – 7.27 (m, 1H), 7.15 – 7.12 (m, 1H), 7.09 – 7.00 (m, 1H), 5.63 (ddt, *J* = 17.3, 10.4, 7.2 Hz, 1H), 5.33 – 4.90 (m, 2H), 3.48 – 3.25 (m, 1H), 2.66 – 2.44 (m, 3H), 1.93 (dd, *J* = 11.3, 7.6 Hz, 1H), 1.17 (d, *J* = 7.4 Hz, 3H). ¹³C-NMR: δ (500 MHz CRYO, CDCl₃) 213.73, 141.64, 133.19, 126.27, 125.87, 120.24, 118.81, 66.48, 50.19, 42.86, 31.81, 14.50. IR(ATR): 2965, 1769, 1373, 991, 919, 784, 645 cm⁻¹. HRMS (ESI-TOF) *m/z* calculated for C₁₂H₁₄OS [M+Na]⁺: 229.0663, found 229.0673. Chiral SFC (Regis Technologies, Whelk-O column, 220 nm, 2% 2-propanol in CO₂, 2.0 mL/min, 30 °C): 3.19 minutes, 3.61 minutes (back peak is major enantiomer).

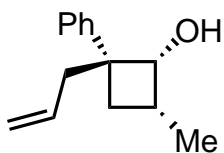
(1*S*,2*R*,4*R*)-2-allyl-4-methyl-2-phenylcyclobutan-1-ol (37)



To a vial equipped with a stir bar was added ketone **24a** (25 mg, 0.13 mmol) and Diisobutylaluminium hydride (137 μ l, 1M in THF, 0.14 mmol) in THF (0.3 ml). The reaction was stirred at 0 °C for 1 h. A few drops of AcOH were added until gas evolution stopped. 3 ml of sat. NH₄Cl (aq) were added and the layers separated. The aq. layer extracted with 2 ml of EtOAc three times. The organic phase was washed with 5 ml of sat. NaCl (aq), dried over MgSO₄, filtered, and concentrated under reduced pressure. The unpurified reaction mixture was then purified by PTLC (10% EtOAc/Hexanes) to afford 25 mg of **(37)** as a colorless oil, 80% yield, 15:1 *dr*. ¹H-NMR: δ (499 MHz, CDCl₃) 7.34 – 7.24 (m, 2H), 7.24 – 7.13 (m, 3H), 5.82 – 5.44 (m, 1H), 5.35 – 4.61 (m, 2H), 3.92 (d, *J* = 7.8 Hz, 1H), 2.63 – 2.45

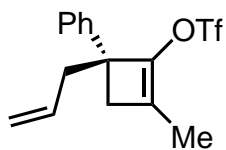
(m, 2H), 2.40 – 2.27 (m, 1H), 2.26 – 2.16 (m, 1H), 2.09 (s, 1H), 1.41 (t, $J = 10.3$ Hz, 1H), 1.13 (d, $J = 6.5$ Hz, 3H). ^{13}C -NMR: δ (126 MHz, CDCl_3) 149.37, 135.17, 128.19, 126.00, 125.86, 117.35, 81.91, 50.03, 40.26, 37.05, 30.96, 18.77. HRMS (ESI-TOF) m/z calculated for $\text{C}_{14}\text{H}_{18}\text{O}$ $[\text{M}+\text{Na}]^+$: 225.1255, found 225.1263. IR (ATR): 3332, 2951, 1445, 1071, 1071, 912, 701 cm^{-1} . $[\alpha]_D^{25} +30.6^\circ$ ($c=0.75$, CHCl_3).

(1*R*,2*R*,4*R*)-2-allyl-4-methyl-2-phenylcyclobutan-1-ol (38)



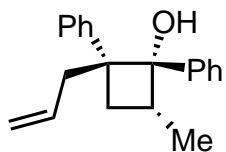
To a vial equipped with a stir bar was added ketone **24a** (10 mg, 0.05 mmol) and L-Selectride (55 μl , 1M in THF, 0.06 mmol) in THF (0.3 ml). The reaction was stirred at 0 $^\circ\text{C}$ for 1 h. A few drops of AcOH were added until gas evolution stopped. 3 ml of sat. NH_4Cl (aq) were added and the layers separated. The aq. layer extracted with 2 ml of EtOAc three times. The organic phase was washed with 5 ml of sat. NaCl (aq), dried over MgSO_4 , filtered, and concentrated under reduced pressure. The unpurified reaction mixture was then purified by PTLC (10% EtOAc/Hexanes) to afford 10 mg of **38** as a colorless oil, 81% yield, >20:1 *dr*. ^1H -NMR: δ (500 MHz, CDCl_3) 7.39 – 7.30 (m, 2H), 7.24 – 7.18 (m, 1H), 7.17 – 7.11 (m, 2H), 5.55 – 5.29 (m, 1H), 5.05 – 4.77 (m, 2H), 4.22 (s, 1H), 2.80 – 2.58 (m, 1H), 2.58 – 2.38 (m, 2H), 2.30 – 2.16 (m, 1H), 2.16 – 2.04 (m, 1H), 1.34 (s, 1H), 0.98 (d, $J = 7.1$ Hz, 3H). ^{13}C -NMR: δ (126 MHz, CDCl_3) 142.68, 134.57, 128.47, 127.83, 126.24, 117.40, 76.16, 50.03, 46.42, 33.75, 29.66, 13.94. HRMS (ESI-TOF) m/z calculated for $\text{C}_{14}\text{H}_{18}\text{O}$ $[\text{M}+\text{Na}]^+$: 255.1255, found 225.1261. IR (ATR): 3426, 2925, 1444, 1104, 989, 912, 767, 701 cm^{-1} . $[\alpha]_D^{25} -5.53^\circ$ ($c=0.041$, CHCl_3).

(*R*)-4-allyl-2-methyl-4-phenylcyclobut-1-en-1-yl trifluoromethanesulfonate (39)



In a 100 ml schlenk flask equipped with a stir bar was LiHMDS (134 mg, 0.80 mmol) in THF (1.5 ml) to give a yellow solution. Ketone **24a** (100 mg, 0.50 mmol) in THF (1.5 ml) was added to the LiHMDS solution and the resulting reaction mixture cooled to $-30\text{ }^{\circ}\text{C}$. Comin's reagent in THF (1.5 ml) was added to the reaction and stirred at rt for 2 h. 3 ml of sat. NaCl (aq) and 3 ml of EtOAc were added to the reaction and the layers separated in a separatory funnel. The organic phase was washed with 5 ml of sat. NaCl (aq), dried over MgSO_4 , filtered, and concentrated under reduced pressure. The unpurified reaction mixture was then purified by column chromatography (0.5% EtOAc and 0.5% Et_3N in Hexanes) to afford 50 mg of **39** as a colorless oil, 30% yield. $^1\text{H-NMR}$: δ (500 MHz, CDCl_3) 7.45 – 7.06 (m, 5H), 5.68 (ddt, $J = 17.1, 10.0, 7.1$ Hz, 1H), 5.27 – 4.87 (m, 2H), 2.64 (d, $J = 7.2$ Hz, 2H), 2.37 (q, $J = 11.0$ Hz, 2H), 1.80 (s, 3H). $^{13}\text{C-NMR}$: δ (126 MHz, CDCl_3) 143.29, 142.01, 135.87, 133.80, 128.49, 127.34, 126.93, 126.64, 118.39, 56.81, 42.22, 38.57, 12.62. HRMS (ESI-TOF) m/z calculated for $\text{C}_{15}\text{H}_{15}\text{F}_3\text{O}_3\text{S}$ $[\text{M}+\text{Na}]^+$: 355.0592, found 355.0604. IR (ATR): 2922, 1417, 1208, 1139, 1063, 857, 697, 611 cm^{-1} . $[\alpha]_D^{25} +27.8^{\circ}$ ($c=0.3$, CHCl_3).

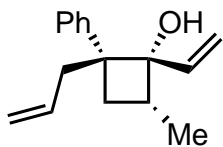
(1*S*,2*R*,4*R*)-2-allyl-4-methyl-1,2-diphenylcyclobutan-1-ol (42)



In a 50 ml schlenk tube equipped with a stir bar was ketone **24a** (100 mg, 0.5 mmol) in THF (2.5 ml) to give a colorless solution. Phenylmagnesium bromide (0.37 ml, 2.71 M in THF, 1 mmol) was added to the reaction at $0\text{ }^{\circ}\text{C}$. The reaction was stirred at rt for 2 h. 3 ml of sat. KHSO_4 (aq) was added and the reaction mixture transferred to a separatory funnel. The layers were separated and the aq. layer extracted with 5 ml of EtOAc three times. The organic phase was washed with 5 ml of sat. KHSO_4 (aq), 5 ml of sat. NaCl (aq), dried over MgSO_4 , filtered, and concentrated under reduced pressure. The unpurified reaction mixture was then purified by column chromatography (5% EtOAc in Hexanes) to afford 126 mg of

42 as a colorless oil, 91% yield >20:1 *dr*. ¹H-NMR: δ (499 MHz, CDCl₃) 7.69 – 7.57 (m, 2H), 7.53 – 7.37 (m, 5H), 7.36 – 7.25 (m, 3H), 5.31 – 5.14 (m, 1H), 5.00 – 4.84 (m, 2H), 3.34 (dq, $J = 15.9, 8.3, 7.2$ Hz, 1H), 2.47 (dd, $J = 13.8, 8.1$ Hz, 1H), 2.43 – 2.33 (m, 1H), 2.33 – 2.24 (m, 1H), 2.10 (dd, $J = 13.7, 5.4$ Hz, 1H), 1.92 (s, 1H), 1.15 (d, $J = 6.8$ Hz, 3H). ¹³C-NMR: δ (126 MHz, CDCl₃) 142.34, 141.96, 134.81, 128.47, 128.27, 127.91, 127.47, 126.94, 126.70, 117.22, 82.52, 53.71, 42.98, 31.79, 31.61, 12.86. HRMS (ESI-TOF) m/z calculated for C₂₀H₂₂O [M+Na]⁺: 301.1568, found 301.1563. IR (ATR): 3560, 2924, 1494, 1444, 1278, 992, 912, 696 cm⁻¹. $[\alpha]_D^{25} -31.9^\circ$ (c=0.3, CHCl₃).

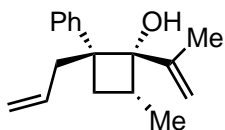
(1*R*,2*R*,4*R*)-2-allyl-4-methyl-2-phenyl-1-vinylcyclobutan-1-ol (41)



In a 100 ml schlenk flask equipped with a stir bar was ketone **24a** (200 mg, 1.0 mmol) in THF (5 ml) to give a colorless solution. Vinylmagnesium bromide (12.48 ml, 0.36 M in THF, 4.5 mmol) was added to the reaction at 0 °C. The reaction was stirred at rt for 2 h. 5 ml of sat. KHSO₄ (aq) was added and the reaction mixture transferred to a separatory funnel. The layers were separated and the aq. layer extracted with 5 ml of EtOAc three times. The organic phase was washed with 5 ml of sat. KHSO₄ (aq), 5 ml of sat. NaCl (aq), dried over MgSO₄, filtered, and concentrated under reduced pressure. The unpurified reaction mixture was then purified by column chromatography (3% EtOAc in hexanes) to afford 159 mg of **(41)** as a colorless oil, 70% yield >20:1 *dr*. ¹H-NMR: δ (499 MHz, CDCl₃) 7.37 – 7.30 (m, 2H), 7.24 – 7.18 (m, 1H), 7.10 – 7.00 (m, 2H), 6.20 (dd, $J = 17.3, 11.1$ Hz, 1H), 5.43 – 5.20 (m, 3H), 4.96 – 4.83 (m, 2H), 2.70 – 2.61 (m, 1H), 2.59 – 2.51 (m, 1H), 2.51 – 2.42 (m, 1H), 2.23 – 2.15 (m, 1H), 2.15 – 2.05 (m, 1H), 1.35 (s, 1H), 0.99 (d, $J = 6.8$ Hz, 3H). ¹³C-NMR: δ (126 MHz, CDCl₃) 143.01, 140.24, 134.86, 128.59, 127.08, 126.51, 117.38, 114.94, 80.80, 53.17, 43.52, 33.61, 32.60, 12.69. HRMS (ESI-TOF) m/z calculated for C₁₆H₂₀O [M+Na]⁺: 251.1412, found 251.1405. IR (ATR): 3565, 2975, 2926, 1445, 979, 912, 700 cm⁻¹. $[\alpha]_D^{25}$

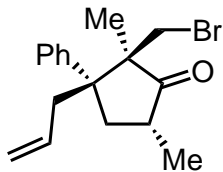
-12.45° (c=0.4, CHCl₃).

(1*S*,2*R*,4*R*)-2-allyl-4-methyl-2-phenyl-1-(prop-1-en-2-yl)cyclobutan-1-ol



In a 25 ml schlenk tube equipped with a stir bar was ketone **24a** (100 mg, 0.50 mmol) in THF (2.5 ml) to give a colorless solution. Isopropenyl magnesium bromide (2 ml, 0.5 M in THF, 1 mmol) was added to the reaction at 0 °C. The reaction was stirred at rt for 2 h. 5 ml of sat. KHSO₄ (aq) was added and the reaction mixture transferred to a separatory funnel. The layers were separated and the aq. layer extracted with 5 ml of EtOAc three times. The organic phase was washed with 5 ml of sat. KHSO₄ (aq), 5 ml of sat. NaCl (aq), dried over MgSO₄, filtered, and concentrated under reduced pressure. The unpurified reaction mixture was then purified by column chromatography (5% EtOAc in hexanes) to afford 90 mg as a colorless oil, 74% yield >20:1 *dr*. ¹H-NMR: δ (499 MHz, CDCl₃) 7.40 – 7.33 (m, 2H), 7.32 – 7.28 (m, 2H), 7.28 – 7.21 (m, 1H), 5.36 – 5.24 (m, 1H), 5.11 (s, 1H), 5.06 (s, 1H), 4.97 – 4.81 (m, 2H), 2.98 – 2.81 (m, 1H), 2.59 – 2.51 (m, 1H), 2.50 – 2.41 (m, 1H), 2.19 – 2.11 (m, 1H), 2.11 – 2.03 (m, 1H), 1.89 (s, 3H), 1.45 (s, 1H), 1.03 (d, *J* = 6.8 Hz, 3H). ¹³C-NMR: δ (126 MHz, CDCl₃) 146.03, 141.42, 135.01, 128.43, 128.40, 126.64, 117.29, 114.08, 83.32, 53.46, 41.57, 31.81, 30.88, 20.42, 13.00. HRMS (ESI-TOF) *m/z* calculated for C₁₇H₂₂O [M+Na]⁺: 265.1568, found 265.1557. IR (ATR): 3568, 2974, 1773, 1638, 1445, 1127, 984, 901, 699 cm⁻¹. [α]_D²⁵ -29.7 (c=0.4, CHCl₃).

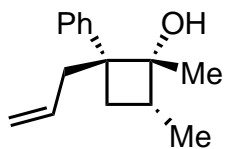
(2*R*,3*R*,5*R*)-3-allyl-2-(bromomethyl)-2,5-dimethyl-3-phenylcyclopentan-1-one (43)



In a 25 ml schlenk tube equipped with a stirbar was *N*-bromosuccinimide (99 mg, 0.56 mmol) in THF (4.6 ml) to give a yellow solution. The previously prepared alcohol (90 mg, 0.37 mmol) was

added to the reaction at 0 °C. The reaction was stirred at 0 °C for 4 h. 5 ml of sat. NaHCO₃ (aq) was added and the reaction mixture transferred to a separatory funnel. The layers were separated and the aq. layer extracted with 5 ml of EtOAc three times. The organic phase was washed with 5 ml of sat. NaCl (aq), dried over MgSO₄, filtered, and concentrated under reduced pressure. The unpurified reaction mixture was then purified by column chromatography (5% EtOAc in hexanes) to afford 72 mg of **43** as a colorless oil, 60% yield >20:1 *dr*. ¹H-NMR: δ (500 MHz, CDCl₃) 7.49 – 7.41 (m, 2H), 7.39 – 7.30 (m, 2H), 7.30 – 7.21 (m, 1H), 5.39 – 5.24 (m, 1H), 5.09 – 4.89 (m, 2H), 3.80 (d, *J* = 11.3 Hz, 1H), 3.69 (d, *J* = 11.3 Hz, 1H), 3.11 – 3.01 (m, 1H), 2.48 – 2.40 (m, 1H), 2.40 – 2.33 (m, 1H), 2.29 (dd, *J* = 14.3, 9.3 Hz, 1H), 2.17 – 2.06 (m, 1H), 1.26 (d, *J* = 6.9 Hz, 3H), 0.78 (s, 3H). ¹³C-NMR: δ (126 MHz, CDCl₃) 220.21, 141.06, 134.40, 128.26, 128.19, 126.94, 118.03, 56.21, 51.49, 40.09, 39.96, 35.35, 34.62, 21.95, 16.24. HRMS (ESI-TOF) *m/z* calculated for C₁₇H₂₁BrO [M+Na]⁺: 343.0674 and 345.0655, found 343.0670 and 345.0654. IR (ATR): 2970, 1735, 1445, 1372, 1295, 1255, 993, 915, 697 cm⁻¹. [α]_D²⁵ -44.9° (c=0.3, CHCl₃).

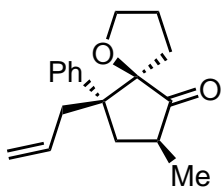
(1*R*,2*R*,4*R*)-2-allyl-1,4-dimethyl-2-phenylcyclobutan-1-ol



In a 25 ml schlenk tube equipped with a stir bar was ketone **24a** (100 mg, 0.50 mmol) in THF (2.5 ml) to give a colorless solution. Methylmagnesium bromide (0.3 ml, 3 M in THF, 1 mmol) was added to the reaction at 0 °C. The reaction was stirred at 0 °C for 1 h. 5 ml of sat. KHSO₄ (aq) was added and the reaction mixture transferred to a separatory funnel. The layers were separated and the aq. layer extracted with 5 ml of EtOAc three times. The organic phase was washed with 5 ml of sat. NaCl (aq), dried over MgSO₄, filtered, and concentrated under reduced pressure. The unpurified reaction mixture was then purified by column chromatography (5% EtOAc in hexanes) to afford 34 mg as a colorless oil, 32%

yield >20:1 *dr*. ¹H-NMR: δ (500 MHz, CDCl₃) 7.38 – 7.30 (m, 2H), 7.24 – 7.20 (m, 1H), 7.15 – 7.05 (m, 2H), 5.39 – 5.25 (m, 1H), 5.05 – 4.81 (m, 2H), 2.61 – 2.53 (m, 1H), 2.53 – 2.45 (m, 1H), 2.41 – 2.31 (m, 1H), 2.17 (dd, $J = 10.9, 8.1$ Hz, 1H), 2.11 – 2.01 (m, 1H), 1.39 (s, 3H), 1.32 (s, 1H), 0.99 (d, $J = 6.8$ Hz, 3H). ¹³C-NMR: δ (126 MHz, CDCl₃) 143.32, 135.07, 128.53, 127.35, 126.40, 117.21, 79.39, 52.18, 43.33, 35.07, 33.03, 23.35, 12.80. HRMS (ESI-TOF) m/z calculated for C₁₅H₂₀O [M+Na]⁺: 239.1412, found 239.1413. IR (ATR): 3577, 2924, 1445, 1178, 911, 699 cm⁻¹. $[\alpha]_D^{25} +6.1$ (c=0.5, CHCl₃).

(5*R*,7*S*,9*R*)-9-allyl-7-methyl-9-phenyl-1-oxaspiro[4.4]nonan-6-one (44)

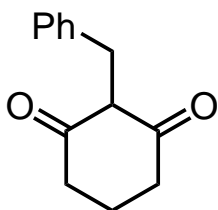


In a 25 ml schlenk tube equipped with a stir bar was 1,2-dihydrofuran (0.1 ml, 1.50 mmol) in THF (2.5 ml) to give a colorless solution. *n*-butyllithium (0.8 ml, 1.6 M in hexane, 1.25 mmol) was added at 0 °C. After 3 h, the reaction was cooled to –78 °C and ketone **24a** (200 mg in 2 ml THF, 1.00 mmol) added dropwise. The reaction was quenched with 5 ml sat. NaHCO₃ (aq) after 3 h and the reaction mixture was transferred to a separatory funnel. The layers were separated and the aq. layer extracted with 5 ml of EtOAc three times. The organic phase was washed with 5 ml of sat. NaCl (aq), dried over MgSO₄, filtered, and concentrated under reduced pressure. The unpurified reaction mixture was then purified by column chromatography (5% EtOAc in hexanes) to afford 114 mg of **44** as a crystalline solid, 42% yield, 15:1 *dr*. ¹H-NMR: δ (600 MHz, CDCl₃) 7.41 – 7.37 (m, 2H), 7.36 – 7.30 (m, 2H), 7.30 – 7.22 (m, 1H), 5.23 (dtd, $J = 17.0, 9.7, 4.8$ Hz, 1H), 4.94 – 4.85 (m, 2H), 4.21 (td, $J = 7.8, 5.7$ Hz, 1H), 4.05 – 3.97 (m, 1H), 2.93 – 2.84 (m, 1H), 2.49 (dd, $J = 12.6, 8.7$ Hz, 1H), 2.36 (ddt, $J = 15.8, 10.6, 7.2$ Hz, 1H), 2.13 (dd, $J = 14.7, 9.4$ Hz, 1H), 1.86 (ddt, $J = 15.0, 12.0, 7.7$ Hz, 1H), 1.73 (ddd, $J = 12.7, 10.9, 1.9$ Hz, 1H), 1.62 – 1.53 (m, 1H), 1.50 (ddd, $J = 12.8, 7.9, 4.9$ Hz, 1H), 1.40 (dt, $J = 12.8, 8.0$ Hz, 1H), 1.24 (d, $J = 7.2$ Hz, 3H). ¹³C-NMR: δ (151 MHz, CDCl₃) 222.17, 142.74, 134.31, 128.32,

127.29, 126.79, 117.48, 94.34, 70.34, 49.86, 40.49, 36.83, 33.23, 31.38, 25.11, 17.32. HRMS (ESI-TOF) m/z calculated for $C_{18}H_{22}O_2$ $[M+NH_4]^+$: 288.1964, found 288.1958. IR (ATR): 2974, 2872, 1745, 1448, 1051, 912, 703 cm^{-1} . $[\alpha]_D^{25}$ -14.5° ($c=0.04$, $CHCl_3$).

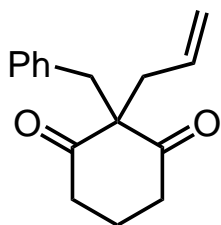
2.3.2 Experimental Details for Selective Synthesis of *trans*-Hydrindanones

2-benzylcyclohexane-1,3-dione **7**



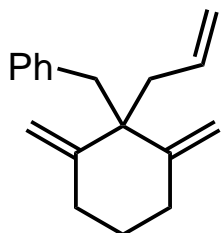
In a 500 ml round-bottom flask was added cyclohexane-1,3-dione (10 g, 89 mmol), benzaldehyde (27.3 ml, 267 mmol) and Hantzsch ester (22.5 g, 89 mmol) in DCM (178 ml) to give a white suspension. L-proline (2.05 g, 1.78 mmol) was added and the reaction stirred for 24 h at room temperature. The reaction was quenched by the addition of 2 M HCl (aq), until the pH was around 3. The reaction mixture was transferred to a separatory funnel. The layers were separated and the aq. layer extracted with 100 ml EtOAc three times. The organic phase was washed with 200 ml of sat. NaCl (aq), dried over $MgSO_4$, filtered, and concentrated under reduced pressure. The unpurified reaction mixture was then recrystallized from EtOAc and a minimum amount of MeOH to afford 16.7 g of **7** as a crystalline solid, 93% yield. 1H -NMR: δ (500 MHz, $CDCl_3$) 7.15 – 7.03 (m, 4H), 7.01 – 6.95 (m, 1H), 2.30 (t, $J = 6.4$ Hz, 4H), 1.83 (p, $J = 6.4$ Hz, 2H). ^{13}C -NMR: δ (126 MHz, $CDCl_3$) 141.56, 128.41, 127.85, 125.25, 115.61, 48.82, 27.36, 20.68. HRMS (ESI-TOF) m/z calculated for $C_{13}H_{14}O_2$ $[M+Na]^+$: 225.0892, found 225.0888. IR (ATR): 3130.05, 1597.59, 1373.48, 1256.93, 1175.24, 1140.38, 1076.19, 1002.01, 759.00, 720.57, 697.25, 597.20 cm^{-1} .

2-allyl-2-benzylcyclohexane-1,3-dione **8**



In a 250 ml round-bottom flask **7** (11.6 g, 57.4 mmol) was added to a solution of NaOH (115 ml, 1 M in H₂O, 115 mmol) at 0 °C. Allyl bromide (9.93 ml, 115 mmol) and TBAI (695 mg, 2.87 mmol) were added. The reaction was stirred for 48 h at room temperature. The reaction was quenched with 500 ml of sat. NaHCO₃ (aq) and the reaction mixture was transferred to a separatory funnel. The layers were separated and the aq. layer extracted with 100 ml EtOAc three times. The organic phase was washed with 200 ml of sat. NaCl (aq), dried over MgSO₄, filtered, and concentrated under reduced pressure. The unpurified reaction mixture was then purified by column chromatography (10% EtOAc in Hexanes) to afford 12.4 g of **8** as a crystalline solid, 89% yield. ¹H-NMR: δ (600 MHz, CDCl₃) 7.24 – 7.14 (m, 3H), 7.03 – 6.92 (m, 2H), 5.57 – 5.46 (m, 1H), 5.08 – 5.00 (m, 2H), 2.64 (d, *J* = 7.6 Hz, 1H), 2.33 (ddd, *J* = 16.9, 8.5, 5.1 Hz, 1H), 2.06 (ddd, *J* = 16.7, 8.3, 5.0 Hz, 1H), 1.69 – 1.56 (m, 1H), 1.15 (ddp, *J* = 13.7, 9.3, 4.9 Hz, 1H). ¹³C-NMR: δ (151 MHz, CDCl₃) 212.24, 136.59, 132.48, 130.00, 128.68, 127.21, 119.70, 69.43, 44.75, 43.06, 41.29, 15.50. HRMS (ESI-TOF) *m/z* calculated for C₁₆H₁₈O₂ [M+Na]⁺: 265.1205, found 265.1208. IR (ATR): 2933.61, 1719.46, 1690.59, 1455.89, 1443.87, 1412.00, 1339.59, 1255.05, 1218.12, 1200.89, 1093.55, 996.18, 929.52, 866.38, 767.23 cm⁻¹.

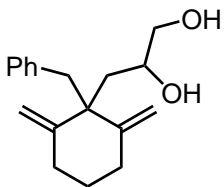
((1-allyl-2,6-dimethylenecyclohexyl)methyl)benzene (**9**)



In a 500 ml schlenk flask was methyltriphenylphosphonium bromide (28.6 g, 103 mmol) in THF (206 ml) to give a white suspension. Potassium *tert*-butoxide (7.54 g, 103 mmol) was added to the reaction and was stirred at room temperature for 30 minutes. A solution of **8** was added (10 ml, 2 M in THF, 20.63 mmol) and the reaction stirred for 3 h. The reaction was quenched with 200 ml of sat. NaHCO₃ (aq) and the reaction mixture was transferred to a separatory funnel. The layers were separated and

the aq. layer extracted with 100 ml EtOAc three times. The organic phase was washed with 200 ml of sat. NaCl (aq), dried over MgSO₄, filtered, and concentrated under reduced pressure. The unpurified reaction mixture was then purified by column chromatography (Hexanes) to afford 4.9 g of **9** as a crystalline solid, 26% yield. ¹H-NMR: δ (500 MHz, CDCl₃) 7.22 (d, *J* = 7.4 Hz, 3H), 7.12 – 7.05 (m, 2H), 5.06 – 4.93 (m, 2H), 4.90 (s, 2H), 4.56 (s, 2H), 2.92 (s, 2H), 2.53 – 2.37 (m, 4H), 2.38 – 2.27 (m, 2H), 1.87 – 1.73 (m, 1H), 1.59 – 1.46 (m, 1H). ¹³C-NMR: δ (126 MHz, CDCl₃) 150.52, 138.25, 136.51, 130.92, 127.45, 126.07, 115.97, 111.04, 50.45, 44.85, 39.20, 33.68, 26.80. HRMS (ESI-TOF) *m/z* calculated for C₁₈H₂₂ [M]⁺: 238.1721, found 238.1726. IR (ATR): 3074.62, 3028.21, 2931.39, 2859.46, 1627.73, 1495.27, 1450.82, 993.02, 894.41, 698.05 cm⁻¹.

3-(1-benzyl-2,6-dimethylenecyclohexyl)propane-1,2-diol (**10**)

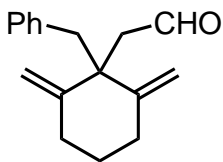


In a 200 ml round-bottom flask was added **9** (1.1 g, 4.61 mmol) in THF (42 ml) and H₂O (4.20 ml) to give a colorless solution. Osmium tetroxide (1.17 ml, 0.19 mmol) and 4-methylmorpholine *N*-oxide (649 mg, 5.54 mmol) were added and the reaction stirred at room temperature.

The reaction was quenched after 24 h with 100 ml of sat. NaSO₃ (aq) and stirred for 1 h. 50 ml of sat. NaHCO₃ (aq) were added and the reaction mixture was transferred to a separatory funnel. The layers were separated and the aq. layer extracted with 100 ml EtOAc three times. The organic phase was washed with 100 ml of sat. NaCl (aq), dried over MgSO₄, filtered, and concentrated under reduced pressure. The unpurified reaction mixture was then purified by column chromatography (40% EtOAc in hexanes) to afford 472 mg of **10** as a colorless oil, 38% yield. ¹H-NMR: δ (499 MHz, CDCl₃) 7.24 – 7.12 (m, 3H), 7.10 – 7.04 (m, 2H), 5.01 (s, 2H), 4.72 (d, *J* = 9.4 Hz, 2H), 4.00 – 3.90 (m, 1H), 3.54 (dd, *J* = 11.1, 3.4 Hz, 1H), 3.41 (dd, *J* = 11.0, 7.6 Hz, 1H), 3.03 – 2.91 (m, 2H), 2.39 – 2.08 (m, 4H), 1.89 (dd, *J* = 15.0, 8.0 Hz, 1H), 1.75 (dd, *J* = 15.0, 2.5 Hz, 1H), 1.69 – 1.57 (m,

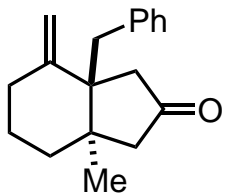
2H). ^{13}C -NMR: δ (151 MHz, CDCl_3) 152.49, 152.35, 137.93, 131.12, 127.51, 126.17, 111.65, 111.18, 69.73, 67.48, 49.83, 45.74, 41.21, 33.05, 24.54. HRMS (ESI-TOF) m/z calculated for $\text{C}_{18}\text{H}_{24}\text{O}_2$ $[\text{M}+\text{Na}]^+$: 295.1674, found 195.1683.

2-(1-benzyl-2,6-dimethylenecyclohexyl)acetaldehyde (**45a**)



In a 50 ml pear shaped flask was added **10** (472 mg, 1.73 mmol) in THF (17.4 ml) and water (4.4 ml) to give a colorless solution. Sodium periodate (741 mg, 3.47 mmol) was added and the reaction stirred for 3 h. The reaction was quenched with 20 ml of sat. NaHCO_3 (aq) and 20 ml of sat. NaCl (aq) and the reaction mixture was transferred to a separatory funnel. The layers were separated and the aq. layer extracted with 20 ml EtOAc three times. The organic phase was washed with 50 ml of sat. NaCl (aq), dried over MgSO_4 , filtered, and concentrated under reduced pressure. The unpurified reaction mixture was then purified by column chromatography (1% EtOAc in hexanes) to afford 309 mg of **45a** as a colorless oil, 74% yield. ^1H -NMR: δ (500 MHz, CDCl_3) 9.58 (t, $J = 2.1$ Hz, 1H), 7.25 – 7.16 (m, 3H), 7.08 – 6.96 (m, 2H), 4.94 (s, 2H), 4.44 (s, 2H), 2.94 (s, 2H), 2.63 (td, $J = 14.1, 4.4$ Hz, 2H), 2.55 (d, $J = 2.3$ Hz, 2H), 2.46 (dt, $J = 14.3, 3.7$ Hz, 2H), 2.03 – 1.79 (m, 1H), 1.66 – 1.43 (m, 1H). ^{13}C -NMR: δ (126 MHz, CDCl_3) 204.36, 150.16, 136.89, 130.69, 127.86, 126.74, 111.51, 48.38, 46.35, 45.54, 33.93, 27.59. HRMS (ESI-TOF) m/z calculated for $\text{C}_{17}\text{H}_{20}\text{O}$ $[\text{M}+\text{H}]^-$: 239.1436, found 239.1445.

3a-benzyl-7a-methyl-4-methyleneoctahydro-2*H*-inden-2-one (**53a**)



Inside a nitrogen-filled glovebox, to a 1-dram vial was added a stirbar, CoI_2 (0.5 mg, 0.004 mmol, 20 mol%) and dppe (1.6 mg, 0.004 mmol) in MeCN (104 μl). The catalyst mixture was stirred for 5 minutes at room temperature. To the catalyst mixture was added aldehyde **45a** (5.0 mg, 0.021 mmol, 1 equiv) and activated zinc (0.6 – 0.7 mg, 0.010 mmol, 60 mol%). The heterogeneous mixture was sealed with a Teflon-lined screw cap and heated to 60 °C for 24 h. The selectivities were determined by GC-FID and ^1H NMR analysis (20 second relaxation delay). The pure ketone **53a** was isolated by preparative TLC (10% EtOAc/Hexanes) as a colorless oil (3.8 mg, 76% isolated yield, >20:1 *dr*). ^1H -NMR: δ (600 MHz, CDCl_3) 7.24 – 7.14 (m, 3H), 6.97 (d, $J = 7.3$ Hz, 2H), 4.74 (s, 1H), 4.14 (s, 1H), 3.17 (d, $J = 13.1$ Hz, 1H), 2.68 (td, $J = 14.3, 5.6$ Hz, 1H), 2.45 – 2.31 (m, 2H), 2.30 – 2.20 (m, 3H), 2.17 – 1.98 (m, 3H), 1.85 – 1.70 (m, 2H), 1.60 (ddt, $J = 18.3, 12.1, 5.7$ Hz, 1H). ^{13}C -NMR: δ (151 MHz, CDCl_3) 217.56, 151.10, 137.51, 130.53, 127.91, 126.42, 108.52, 50.31, 48.32, 47.82, 41.06, 34.32, 31.54, 27.88, 23.98. HRMS (ESI-TOF) m/z calculated for $\text{C}_{17}\text{H}_{20}\text{O}$ $[\text{M}]^+$: 263.1412, found 263.1419. IR (ATR): 2928.38, 2860.80, 1730.72, 1643.80, 1495.78, 1453.55, 1151.54, 1030.15, 892.14, 716.33, 698.86, 603.41 cm^{-1} .

Chapter 3

Mechanistic DFT-Studies and *In-Silico* Catalyst Design

3.1 Mechanistic DFT Studies of Rh-Catalyzed Cycloisomerizations

3.1.1 Introduction

Terpenes are one of the biggest classes of natural products and of great interest to several disciplines in chemistry and biology.¹⁵²⁻¹⁵⁴ The diversity of terpenoid natural products stems from the formation of a common intermediate (i.e. **18**), from where diverse terpene scaffolds can be built up.¹⁵⁵ Simple precursors like farnesyl pyrophosphate and geranyl pyrophosphate are cyclized into a variety of natural products.^{152,156} Their cyclization is carried out by a special class of enzymes, called cyclases.^{155,157,158}

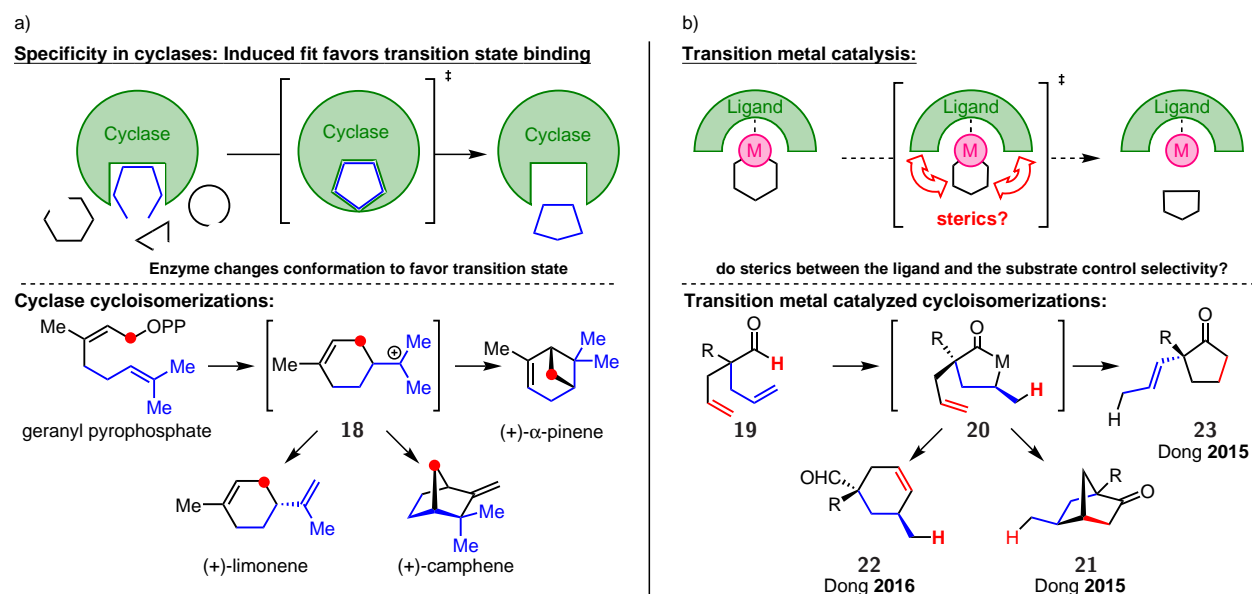


Figure 3.1. Cycloisomerizations in nature and transition metal catalysis

In the case of geranyl pyrophosphate, all the cycloisomerization products derive from a common carbocationic intermediate (**18**). This strategy of product diversification from a common intermediate makes it possible for nature to synthesize a diverse array of natural products through related classes of enzymes (i.e. (+)- α -pinene, (+)-limonene, (+)-camphene,

Figure 3.1).¹⁵⁵ Although there are many mechanistic possibilities from common intermediate **18**, cyclases can perform cycloisomerizations to yield one terpenoid product, selectively.¹⁵⁹ This selectivity arises from the architecture of the active site, that prefers one transition state in particular.¹⁶⁰

The previously developed transition metal catalyzed cycloisomerization of **19** shows many parallels to the cycloisomerization of terpenes (Figure 3.1).^{57,58,118} Also going through a common intermediate (**20**), a variety of cycloisomerization products can be obtained. The selectivity is controlled by an ancillary ligand, coordinated to the transition metal. One common underlying design principle in transition metal catalysis is the use of bulky motifs.^{161–168} A rigid ligand geometry offers a defined binding site for a specific substrate. Steric interactions between the ligand and the substrate, disfavor undesired pathways. Especially, the 3,5-*tert*-benzene is a reappearing motif in bidentate phosphine ligands.^{169–176} This strategy to achieve specificity and selectivity would be analogous to the conformational selection model in enzyme catalysis.

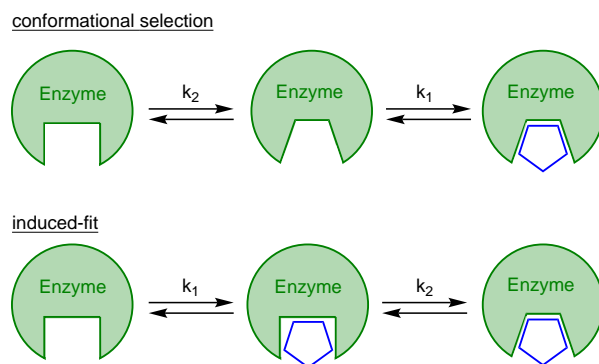


Figure 3.2. Conformational selection and induced-fit

Conformational selection and induced-fit are two common theories to explain the specificity and selectivity of enzymes.^{177–180} In the conformational selection theory, the enzyme is in equilibrium between different conformations, where only one will allow the binding of a given substrate (Figure 3.2). In the induced-fit model, the substrate binds to the enzyme first, which will then undergo a conformational change. Only the correct substrate will undergo

a reaction after the conformational change of the enzyme. Mismatched substrates dissociate quickly before being able to undergo a reaction.¹⁷⁷ While the conformational selection theory can account for substrate specific binding, it can also be used to explain the selectivity in terpene cyclizations from a common intermediate. The induced-fit mechanism has been found operative in class I terpene cyclases.¹⁸¹

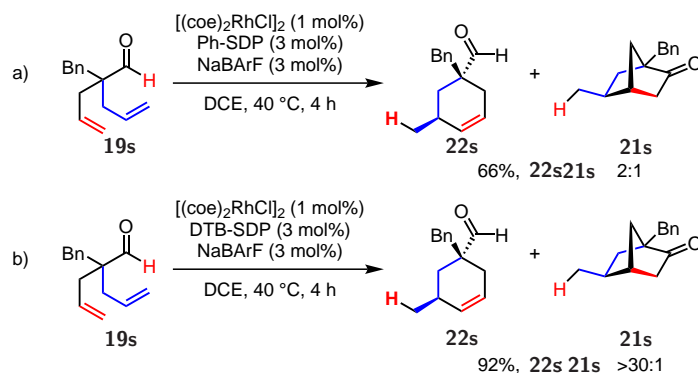


Figure 3.3. Ligand controls regiochemical outcome

Although transition metal catalysis is mainly dominated by a lock-and-key type mechanism, it has been recently suggested that an induced-fit model could also apply to transition metal catalysis.¹⁸² With this study we wanted to investigate if there are other modes that can be operative in transition metal catalysis, besides the lock-and-key model.^{183–188}

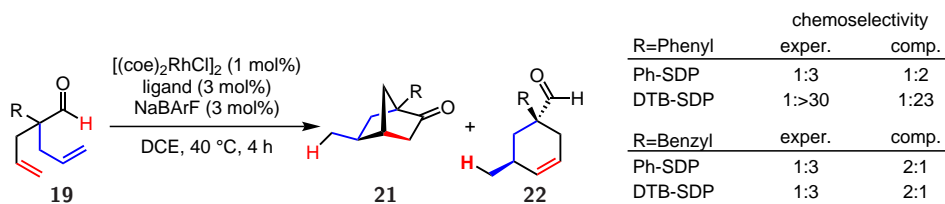
To get a better understanding of the role of bulky motifs in transition metal catalysis, the cycloisomerization of aldehyde **19** to the cyclohexene **22** and bicycle **21** was studied by DFT-calculations. Using Ph-SDP (**72a**) as the ligand, the reaction outcome was a mixture between **22** and **21** (2:1 *rr*, Figure 3.3). When using the bulkier DTB-SDP (**72b**) ligand, the regioselectivity switched and favored now cyclohexene **22** (>30:1 *rr*).¹¹⁸

3.1.2 Results and Discussion

We first started by elucidating the full mechanistic pathway to identify the turnover limiting steps for the reactions shown in Figure 3.3. Based on our substrate design, a variety of

different cycloisomerization products are feasible.^{57,58,118} The full mechanistic pathway is shown in the SI. Figure 3.4 shows the two pathways that lead to either **21** or **22**.

Table 3.1. Experimental and computational agreement



Previous studies on the rhodium catalyzed C–H activation of aldehydes have shown that initial oxidative addition is followed by olefin insertion into the Rh–H bond to form a rhodacycle like **20** as an intermediate.^{69,189–194} From this point, the pending allyl group can intercept this intermediate, leading to pathways other than hydroacylation (Figure 3.4). Following the carboacylation pathway (Figure 3.4, right side), carbometalation of the pending olefin gives bicyclic rhodacycle **70**. Further, reductive elimination regenerates the active catalyst and releases carboacylation product **21**. The carbometalation of the other face of the olefin from rhodacycle **20** leads to the Heck-type pathway (Figure 3.4, left side), giving bicyclic rhodacycle **65** (Figure 3.4). β -hydride elimination is facile from this intermediate, and leads to rhodium hydride **67**. The aldehyde functional group is being regenerated after reductive elimination from rhodium hydride **67**, releasing cyclohexene product **22**. The rate- and regioselectivity-determining step is the carbometallation shown in transition states **69** and **64** (Figure 3.4).

The proposed catalytic cycle was studied by using the cycloisomerization of 2-benzyl-2-allyl-4-pentenal and DTB-SDP as the ligand. Further, the cycloisomerization of 2-benzyl-2-allyl-4-pentenal with Ph-SDP, 2-phenyl-2-allyl-4-pentenal with DTB-SDP and 2-phenyl-2-allyl-4-pentenal with Ph-SDP as the ligand were used to benchmark our computationally obtained results against the experimentally observed regioselectivities.⁵⁸ In all tested cases, we have found good agreement between the computation and the experiment (Table 3.1).

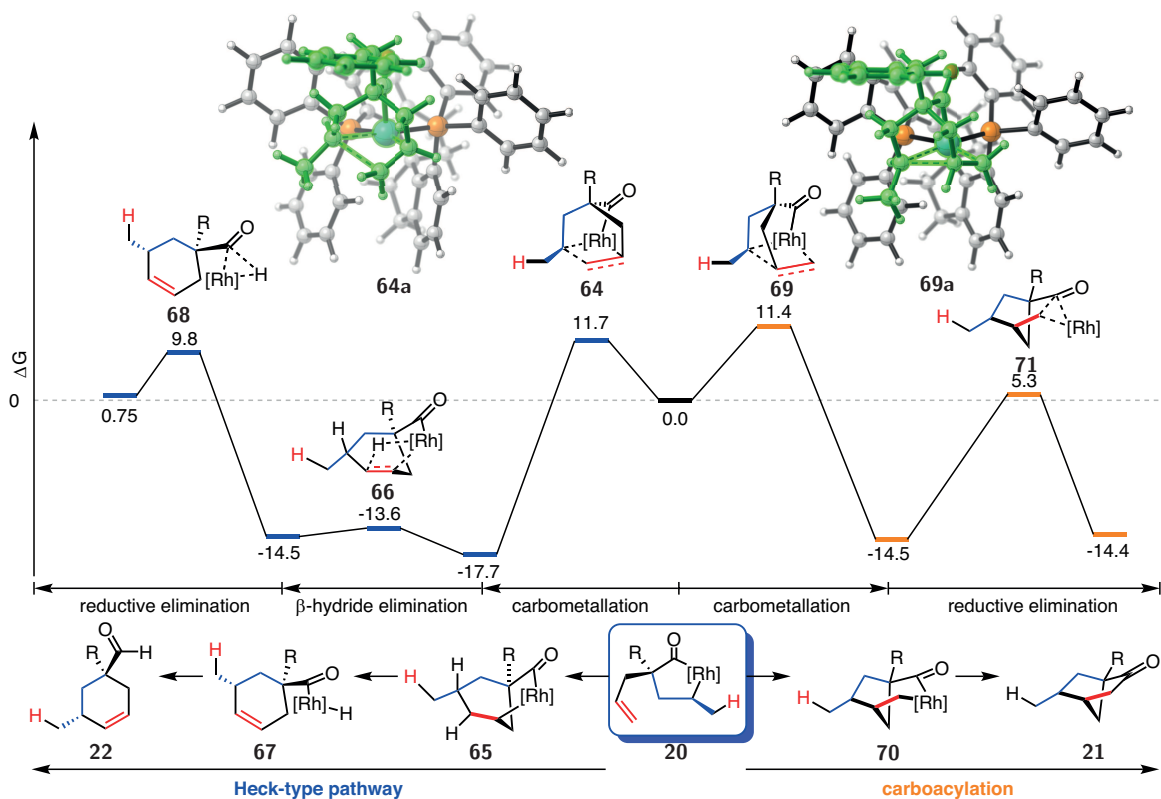


Figure 3.4. Ligand controls regiochemical outcome

Transition states were identified through an initial potential energy surface scan and further optimized. The corresponding product or starting material structures were obtained through dynamic reaction coordinate calculations. After having identified the rate- and selectivity-determining steps, the corresponding transition states **69** and **64** were studied in detail to establish a structure-selectivity relationship. The main focus of the transition state analysis was to investigate the effect of the *t*-Bu groups in the DTB-SDP ligand. One distinctive difference between **69** and **64** is the orientation of the substrate in reference to the ligand (Figure 3.5). In transition state **69a**, the bound substrate (Figure 3.5, highlighted in green) leans more towards the left side of the ligand and has a closer contact with one of the aryl groups. This results in a CH- π interaction (2.37 Å) between the aryl group and one of the methylenes in the substrate (Figure 3.5).^{195–202}

In transition state **64a**, coordination of the other face of the olefin, results in situating the

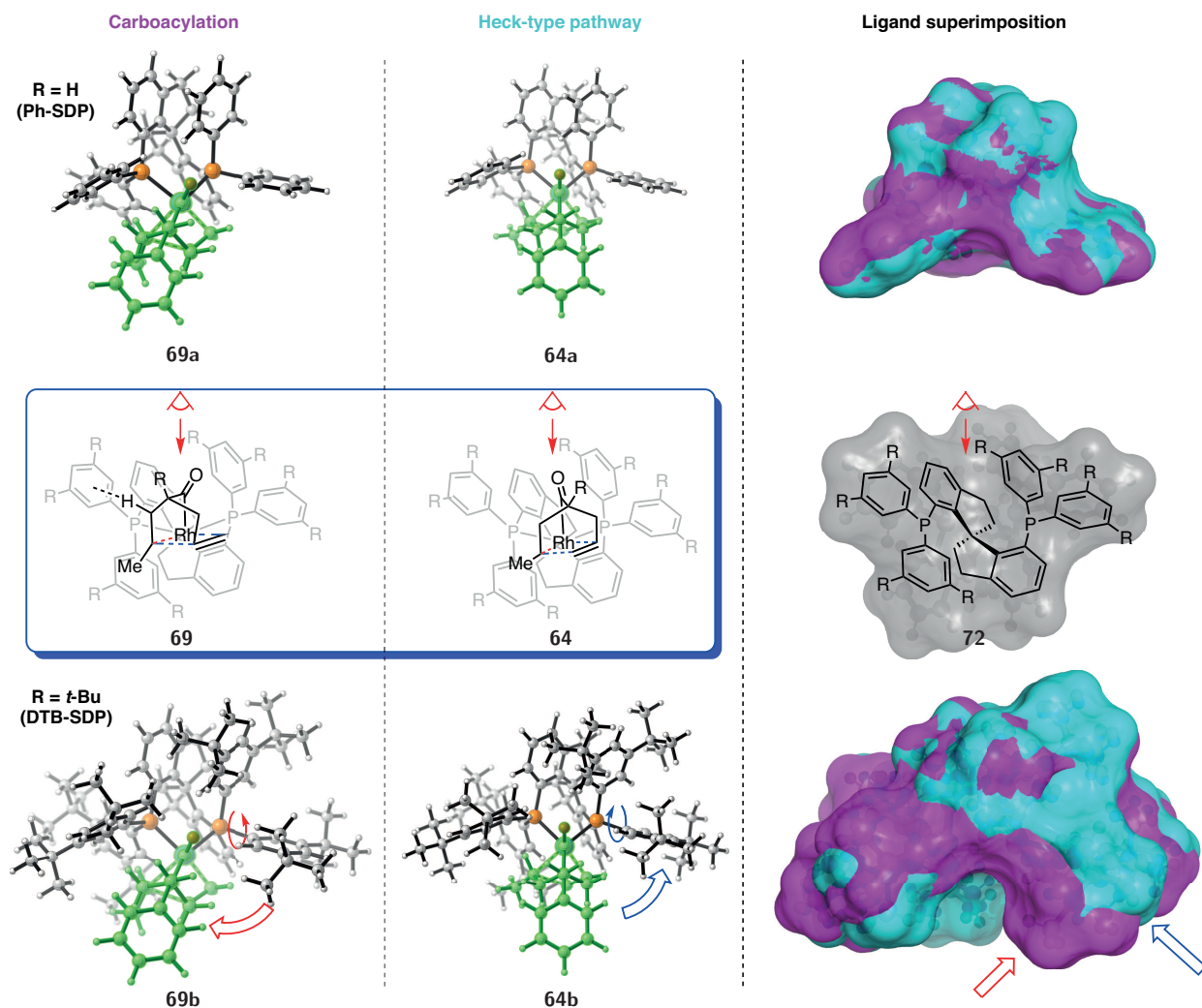


Figure 3.5. Analysis of the transition state geometries

substrate away from the ligand, compared to **69a**. The previously observed CH– π interaction is weakened in **64a** (2.74 Å). In light of these observations, a simple explanation for the experimentally observed selectivities would be the destabilization of transition state **69b**. Steric repulsion between the *t*-Bu groups on the DTB-SDP ligand and the substrate would interrupt any attractive interactions. However, this hypothesis could not be tested. The CH– π interaction (2.37 Å) is still present in **69b**. Comparing the transition state structures obtained with Ph-SDP and DTB-SDP showed, that there was little to no influence on the transition state geometry of the substrates (RMSD <0.02 Å). There is also little change in the conformations of the Ph-SDP ligand in **69a** and **64a**, which can be seen in the

superimposition of both ligands (Figure 3.5, top right, RMSD = 0.1 Å). Going to the DTB-SDP ligand, a change in conformation is apparent when superimposing both structures (Figure 3.5, bottom right, RMSD = 0.6 Å). Most notably, the 3,5-di-*tert*-butyl benzene ring to the right of the substrate rotates inwards in **69b** (Figure 3.5, bottom). This brings one of the *t*-Bu groups closer to the substrate, whereas in **64b** the 3,5-di-*tert*-butyl benzene ring rotates outwards to accommodate the differently situated substrate, moving one of the *t*-Bu away from the substrate.

These different ligand conformations have inherently different stabilities. The experimentally observed selectivities can therefore be dictated by the stabilities of the different ligand conformations.

$$\Delta E^\ddagger = \Delta E_{int} + \Delta E_{dist} \tag{3.1}$$

$$\Delta E_{int} = \Delta E_{int,ligand} + \Delta E_{int,substr} + \Delta E_{int,space/bond} \tag{3.2}$$

$$\Delta E_{dist} = \Delta E_{dist,ligand} + \Delta E_{dist,substr} \tag{3.3}$$

To find further support for this qualitative analysis, the transition states were fragmented into the ligand portion and the substrate portion (containing the Rh metal), and studied using the distortion/interaction-activation strain model.^{203–209} In this model, ΔE^\ddagger is described as the sum of the interaction energy (ΔE_{int}) and the distortion energy (ΔE_{dist}) (Eq. 3.1). ΔE_{int} describes all the interactions within the ligand and substrate fragment, as well as the interaction between those two fragments. While the distortion energy is related to the change in energy, when distorting the geometry of a fragment going towards the transition state structure. This data can be further deconvoluted by describing ΔE_{int} through the sum of the interaction energy within the ligand ($\Delta E_{int,ligand}$), the interaction energy within the substrate ($\Delta E_{int,substr}$) and the interaction energy between the substrate and the ligand

($\Delta E_{int,space/bond}$) (Eq. 3.2). In a similar way, ΔE_{dist} can be seen as the sum between the distortion energy within the ligand ($\Delta E_{dist,ligand}$), and the distortion energy within the substrate ($\Delta E_{dist,substr}$) (Eq. 3.3).

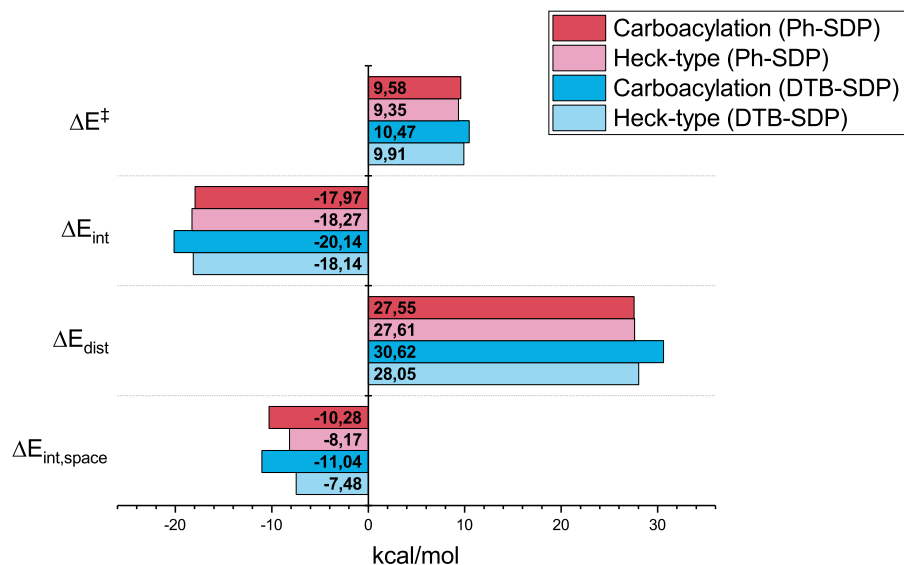


Figure 3.6. Distortion-interaction energies

The results from the distortion/interaction-activation strain model are shown in Figure 3.6. In the case of Ph-SDP (red bars), ΔE_{int} is slightly in favor for the Heck-type pathway, while ΔE_{dist} is almost identical for both pathways. Going to the DTB-SDP cases (blue bars), ΔE_{int} is now more favorable for the carboacylation pathway. It is also apparent from the change of $\Delta E_{int,space/bond}$, when going from Ph-SDP to DTB-SDP, that the experimentally observed selectivities cannot be explained through a change in the interaction between the ligand and the substrate. On the other hand, ΔE_{dist} increases to a greater extent for the carboacylation pathway, than for the Heck-type pathway. To further deconvolute, the same model has been applied to the substrate fragment and the ligand fragment.

The distortion/interaction-activation strain model unveils significant changes in the ligand fragment when going from Ph-SDP to DTB-SDP (Figure 3.7, right side). While the Ph-SDP ligand in the carboacylation pathway adopts a more favorable conformation in the transition

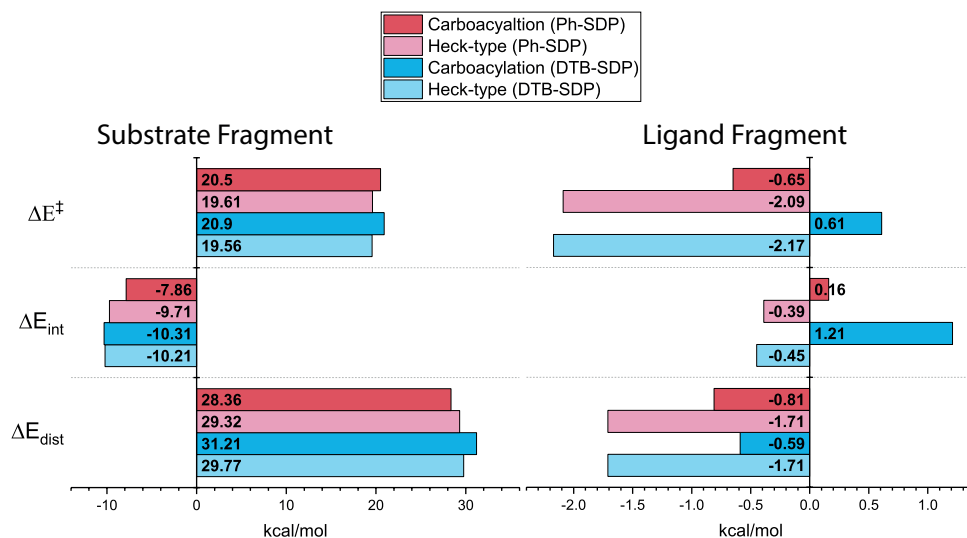


Figure 3.7. Distortion-interaction energies for ligand and substrate fragments

state, the DTB-SDP ligand adopts a less favorable conformation ($\Delta E_{ligand} = -0.65$ kcal/mol and 0.61 kcal/mol, respectively). This difference stems mainly from $\Delta E_{ligand,int}$, showing that the conformational change in DTB-SDP from the ground state to the transition state affects the weak-interaction network within the ligand. Furthermore, $\Delta E_{ligand,dist}$ also increases in the case of DTB-SDP. For the Heck-type pathway, $\Delta E_{ligand}^\ddagger$, $\Delta E_{ligand,int}$, and $\Delta E_{ligand,dist}$ do not differ significantly, when comparing Ph-SDP and DTB-SDP. Same is also true for the substrate fragment. In the carboacylation pathway $\Delta E_{substr}^\ddagger$ is higher for DTB-SDP than for Ph-SDP which stems from a higher $\Delta E_{substr,dist}$. The difference in $\Delta E_{substr}^\ddagger$ is not as pronounced as the difference in $\Delta E_{ligand}^\ddagger$. While both, the change in $\Delta E_{substr}^\ddagger$ and $\Delta E_{ligand}^\ddagger$ contribute to the experimentally observed selectivities, the changes within the ligand weights proportionally stronger.

3.1.3 Conclusion and Future Work

Adding the *t*-Bu groups in DTB-SDP enhances the ligands ability to “sense” the substrate (through weak interactions), resulting in a conformational adaptation of the ligand in accordance to the bound substrate. The conformational change in the ligand is more pronounced

and affects the ligand's weak-interaction network, proportionally. This mode of action allows us to differentiate two very similar transition states and selectively favor one over the other.

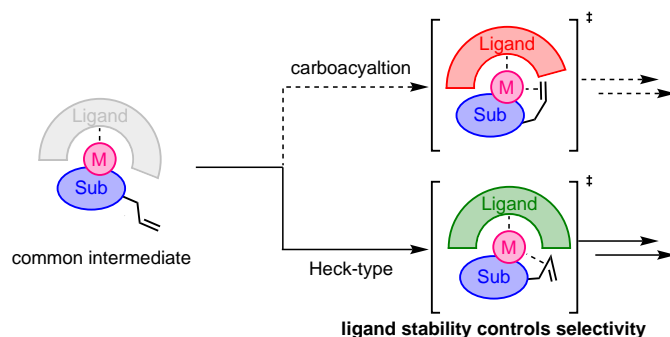


Figure 3.8. Distortion-interaction energies for ligand and substrate fragments

Rather than operating under the common lock and key model in transition metal catalysis, this study unveils an induced-fit-type mechanism. In analogy to the induced-fit mechanism in enzymes, the substrate in this study induces a conformational change in the ligand, which then leads to the selective promotion of one pathway.

After having gained a deep inside into the structure-selectivity relationship, future work focuses on the *in-silico* design of new ligands and catalysts, to selectively enable the carboacylation pathway over the Heck-type pathway.

3.2 *In-Silico* Catalyst Design and Synthesis of a New Class of Ligand

3.2.1 Introduction

Based on the findings from the previous DFT studies, the next goal was to design new catalysts and ligands *in silico* to enable the selective synthesis of **21**, over **22**. Our previous experimental attempts to find a selective catalyst system were unfruitful.

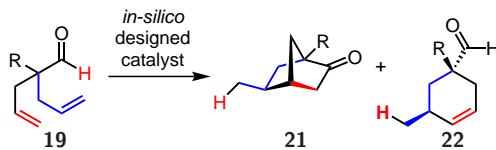


Figure 3.9. Studied reaction

With the insight into the rate-determining step and the transition state geometries in hand, the focus was now on the *in-silico* design of SDP-type ligands. The main difference between transition states **69a** and **64a** is the different spatial relationship between the substrate and the ligand.

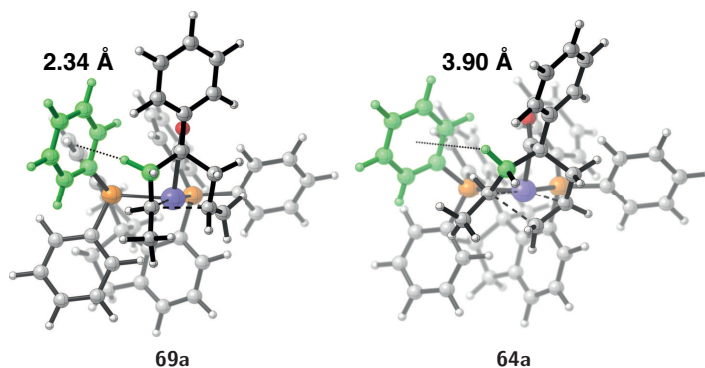


Figure 3.10. CH- π interaction between ligand and substrate

This results in a differentiation of the two transition states through their weak interactions between ligand and substrate ($\Delta E_{int,space/bond}$). Most notable is the CH- π bond in **69a** with an interaction distance of 2.34 Å, while in **64a** this distance is 3.90 Å, for the same methylene (Figure 3.10). Increasing the CH- π interaction could stabilize **69a** over **64a**. Dispersive as well as electrostatic interactions are the main contributors to CH- π bonds. Changing the electronic properties of the aromatic ring can modulate the strength of the CH- π bond.^{197,198,210} We hypothesized that increasing the negative charge on the aromatic ring would strengthen the electrostatic interaction with the positively charged H-atom.^{211,212}

3.2.2 Results and Discussion

All *in-silico* designed ligands are based on the SDP backbone **72**.^{213–215} The aromatic rings that are attached to the phosphines were modulated. To tune the electronic properties, different *para*-substituted benzenes as well as heterocycles have been investigated (Figure 3.11).²¹¹

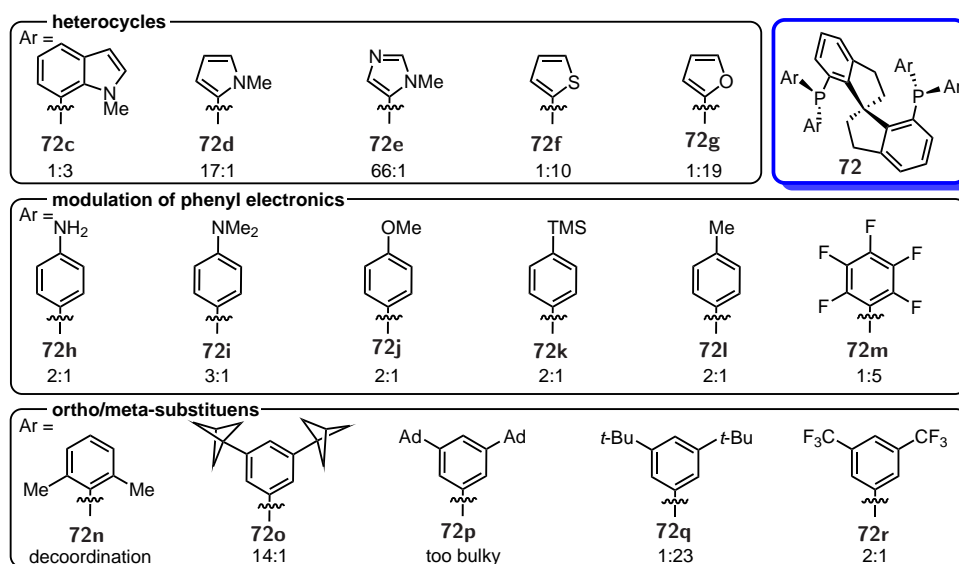


Figure 3.11. Predicted *rr* of *in-silico* designed SDP-variants

Changing the substituent in the *para* position with electron donating groups (i.e. **72h**, **72i**, **72j**, **72k**, **72l**) had little effect and changed the regioselectivity from 1:2 to 2:1. Interestingly, when using ligand **72m** with the electron deficient perfluoro benzenes, the Heck-type pathway becomes more favorable. Inversion of the quadrupole moment of the benzene leads to electrostatic repulsion with the H-atom involved in the CH- π bond, effectively destabilizing transition state **69m**. Overall, the effects on the selectivity when modulating the benzene motif are marginal. Employing heterocycles had a greater effect on the selectivity. Ligand **72d**, containing the electron-rich *N*-methylpyrrole, increased the predicted regioselectivity to 17:1, by strengthening the CH- π (2.27 Å). In a similar way, imidazole containing ligand **72e** switches the regioselectivity towards **21a** with 66:1 *rr*. In this case, there is a further stabilization of transition state **69e**, through coordination of the imidazole nitrogen to Rh. Although also electron rich, indole did not affect the regioselectivity. On the other hand,

when employing electron deficient heterocycles like thiophene (**72f**) and furan (**72g**), the selectivity switches, and favors **22a** (1:10 and 1:10 *rr*, respectively). While modulation of the electrostatic properties had only minor success, increasing the dispersive interactions could have a greater influence on the selectivity. We tested different substituents in the *ortho* and *meta* position of the benzene rings. Substitution at the *ortho* position of the benzenes (**72n**) is not tolerated and leads to decoordination of the ligand *in-silico*, which is in agreement with previous experimental studies.²¹⁶ Interestingly, when using ligand **72o**, bearing bicyclo[1.1.1]pentane substituted benzenes, **21a** is now favored with 14:1 *rr*. This is presumably a result of increased dispersive interactions. Employing substituents with a bigger surface area, to further increase the weak-interactions, was unsuccessful. The adamantyl group in **72p** was too bulky to be attached to the ligand.

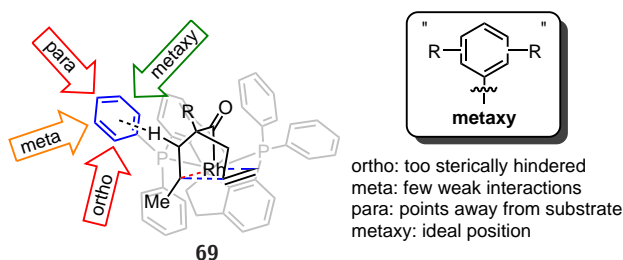


Figure 3.12. Proposed ligand design

Substitution at the *ortho* position of the blue benzene ring in **69** (Figure 3.12) introduces too much steric interaction, while substituents in the *meta* position can have some constructive interactions with the substrate, but the substituents point partly away from the substrate. The ideal substituent would be between (*metaxy*) the *ortho* and the *meta* position. A *metaxy* substituent would decrease steric repulsion with the metal and at the same time increase the surface area that is in contact with the substrate. Formally, a *metaxy* substitution could be realized through a 3-center 2-electron (3c-2e) bond. While there are a few examples of 3c-2e bonds in hydrocarbons (i.e. ethanium and ethenium),^{217–221} they are generally rare and highly reactive species. Motifs that are isosteric to *metaxy* substituents can be realized, though. Rings that are fused at the *ortho* and *meta* positions, and with ring

sizes of cyclopentane or smaller, can be seen as isosteres to *metaxy* substituents due to the compression of the bonding angles.

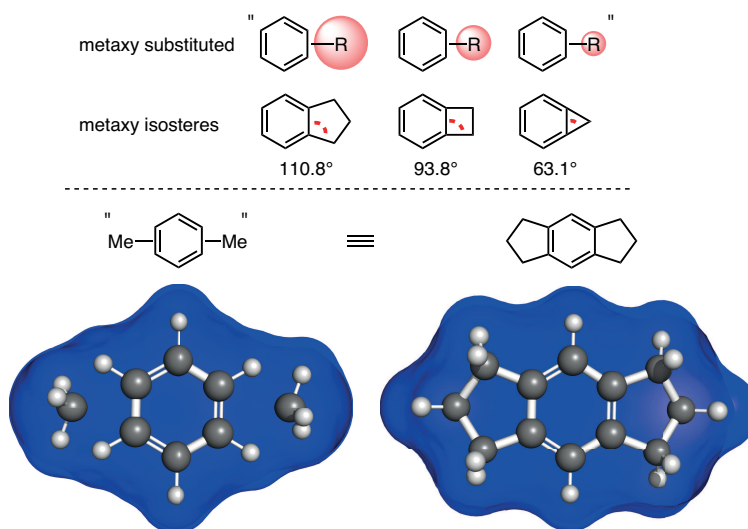
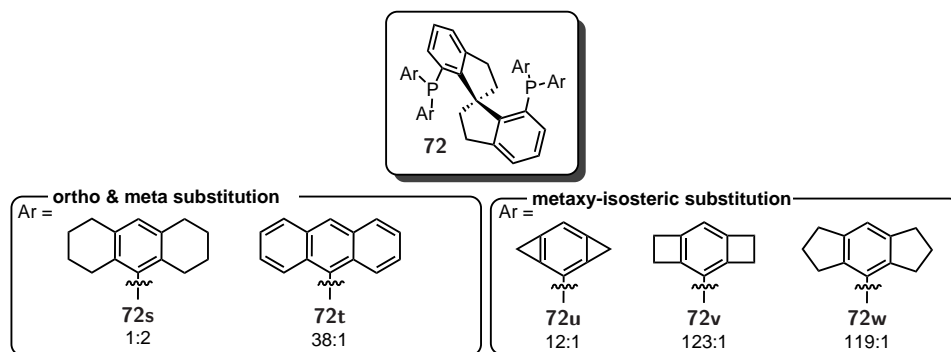


Figure 3.13. Isosteric relationship between *ortho,meta* and *metaxy* substitution

Based on this idea, a series of different ligands have been investigated *in-silico*, bearing either *ortho* and *meta* or *metaxy*-isosteric substitution (Table 3.2). Ligand **72s**, with cyclohexane rings fused to the benzene rings, shows no improvement in the predicted regioselectivity, which is most likely a result of unfavorable steric interactions. Naphthalene substituted ligand **72t** improves the regioselectivity and favors **21a** by 38:1 *rr*. Naphthalene and other extended aromatic systems have been used before in catalysis as dispersion energy donors.^{222–226} Going to the *metaxy* isosteric substituents, ligand **72u** with cyclopropyl-fused benzene rings also starts to favor **21a** with 12:1 *rr*. Interestingly, the introduction of only two methylenes per benzene ring already introduced enough dispersive interactions to favor the carboacylation product **21a**. The cyclobutyl- and cyclopentyl-fused ligand variants **72v** and **72w** show even higher dispersive interactions, with 123:1 *rr* and 119:1 *rr*, respectively.

With these *in-silico* designs in hand, I attempted to synthesize the most promising ligand. Previous attempts in synthesizing cyclopropyl-fused benzene rings like in ligand **72u** were not successful, making this designed ligand combined with the predicted 12:1 *rr* an unappealing target for synthesis.^{227–229} The homologous cyclobutyl-fused benzene ring is known in the

Table 3.2. Predicted *rr* for ligands with metaxy-isosteric benzenes



literature but the precursor synthesis can involve many steps.^{230–235} All attention has been focused on ligand **72w**, where the corresponding hydrindacene can be build up through a series of Friedel-Crafts acylation and alkylation (Figure 3.14).²³⁶

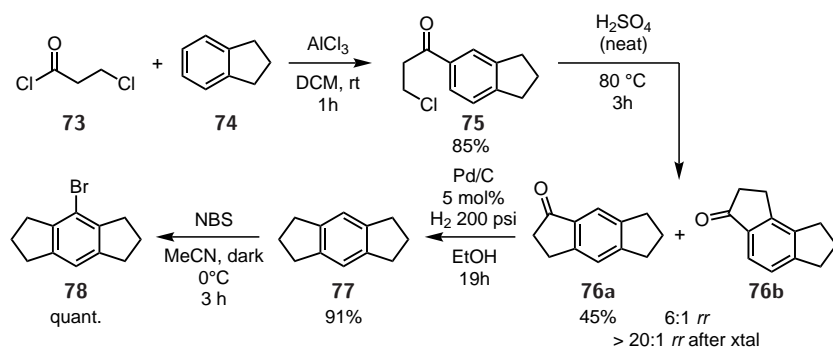


Figure 3.14. Synthesis of bromohydrindacene **78**

Starting from indane (**74**) and 3-chloropropionic acid chloride (**73**) indane **75** was afforded in 85% yield after Friedel-Crafts acylation. In neat H_2SO_4 , the pending alkyl chloride and the indane motif undergo a Friedel-Crafts alkylation, affording a mixture of *s*-hydroindacenone **76a** and *as*-hydroindacenone **76b** in 6:1 *rr*. Although inseparable by column chromatography, the minor regioisomer was removed through recrystallization. Hydrogenation with palladium on carbon reduced *s*-hydroindacenone **76a** to hydrindacene **77** in 91%. In the last step, a mild mono-bromination protocol was applied to give bromohydrindacene **78** in near quantitative yield.²³⁷

With bromohydrindacene **78** in hand, the corresponding Grignard reagent was formed and

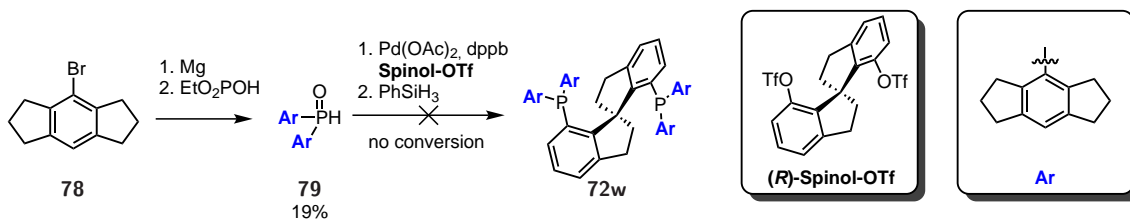


Figure 3.15. Attempted coupling of phosphine oxide **79** to SDP backbone

added to diethyl phosphite to give phosphine oxide **79** in 19% yield (Figure 3.15). The next key step was the cross-coupling of phosphine oxide **79** to (*R*)-spinol-OTf. Under all the tested palladium cross-coupling conditions no product formation was ever observed. This might be due to the steric hindrance of phosphine oxide **79**.^{214,215}

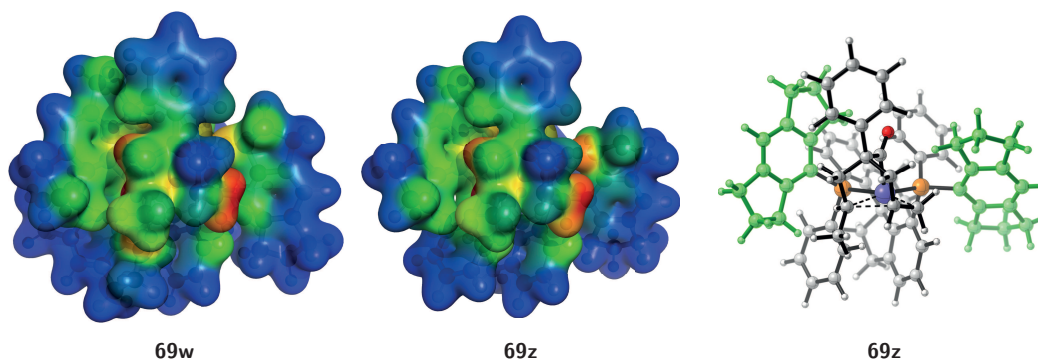
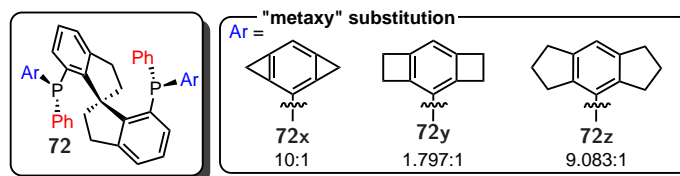


Figure 3.16. Dispersion interaction density plot with **72w** and **72z**

Going back to transition state **69w**, the key contacts between ligand and substrate have been visualized in a dispersion interaction density plot (Figure 3.16). Only two out of the four *s*-hydrindacenes of the ligand are in contact with the substrate. In the next iteration of *in-silico* designs, the new ligands bear now asymmetric phosphines. Where one aryl group carries a *metaxy* isosteric substitution and the other remains as phenyl group (Table 3.3).

Table 3.3. Predicted *rr* for P-chiral ligand designs



The predicted *rr* did not change significantly for ligand **72x**, bearing the cyclopropyl-fused

benzenes. Surprisingly, the rr changed dramatically for ligand **72y** and **72z** with 1.797:1 and 9.083:1 rr , respectively. To better understand the surge in rr , ligand **72w** (ω -SDP, four s -hydrindacenes) and **72z** (ω^* -SDP, two s -hydrindacenes) have been studied, using the distortion/interaction-activation strain model (Figure 3.17).^{203–209}

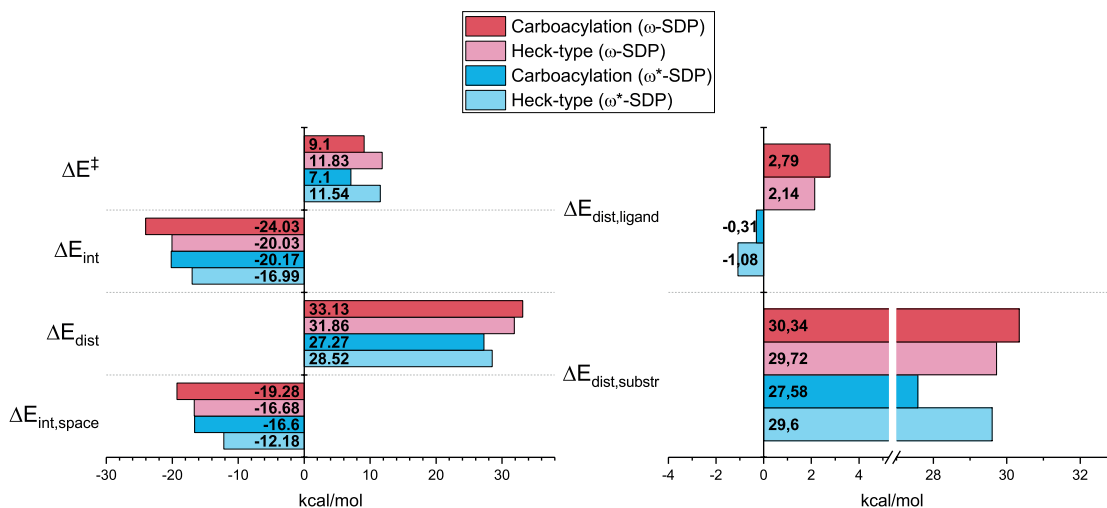


Figure 3.17. Distortion-Interaction analysis for new SDP-ligands

Overall, ΔE^\ddagger is reduced by around 2 kcal/mol for the carboacylation pathway, when going from ω -SDP to ω^* -SDP. While ΔE^\ddagger remains similar for the Heck-type pathway. Going into more detail, ΔE_{int} gets weaker for both pathways by a similar magnitude when comparing ω -SDP to ω^* -SDP. This trend is also observed for $\Delta E_{int,space/bond}$, which is part of ΔE_{int} (Eq. 3.2). As a side note, $\Delta E_{int,space/bond}$ increased significantly, in both ω -SDP and ω^* -SDP when compared to Ph-SDP and DTB-SDP. The surge in rr for ω^* -SDP stems from ΔE_{dist} which decreases by around 6 kcal/mol for the carboacylation pathway, compared to a decrease of 3 kcal/mol for the Heck-type pathway. Looking at the individual contributors (Eq. 3.3), $\Delta E_{dist,ligand}$ decreases for both pathways. The increase in the predicted selectivity stems from $\Delta E_{dist,substr}$, which decreases for the carboacylation pathway by around 3 kcal/mol, while staying similar for the Heck-type pathway. The greater conformational freedom within in the ligand allows for a lower $\Delta E_{dist,substr}$.

After synthesizing (*R*)-**80**, the key cross-coupling was tested again. With the less bulky

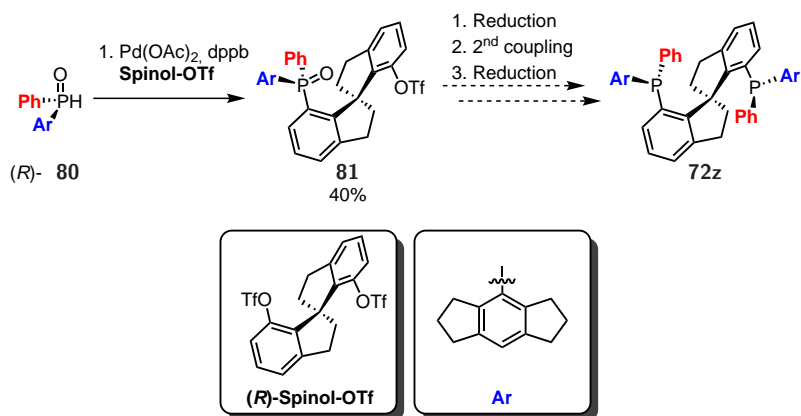


Figure 3.18. Coupling of **80** to the SDP backbone

phosphine oxide (*R*)-**80**, the desired coupling product was obtained in about 40% yield.

3.2.3 Conclusion and Future Work

In summary, several new ligands have been designed *in silico*, with promising predicted selectivities. The insights gained from the computations allowed us to establish a structure-selectivity relationship, resulting in the design of new dispersion energy donors, that fit the unique requirements of transition metal catalysis. Current experimental efforts are guided by the computational results and future work will involve the case studies of other transformations.

3.3 Experimental and Computational Data

3.3.1 Computational Details

Orca 3.0.3 was used to optimize the relaxed potential energy surfaces (PES) using “Grid4” and “TightSCF” as settings.²³⁸ Turbomole 7.0 with grid m_4 ²³⁹ was used in other computations. The TPSS²⁴⁰ functional and def2-SVP or def2-TZVP basis sets²⁴¹ were used to

compute single point energies and to optimize structures. Additionally, the BJ-damped D3-dispersion correction (-D3)^{242,243} was used, as well as resolution-of-the-identity approximation for Coulomb term (RI-J)²⁴⁴ or multipole-accelerated RI-J (MARI-J).²⁴⁵ In the later cases, the corresponding auxiliary basis set²⁴⁶ was used. Structures were illustrated using Cylview*.

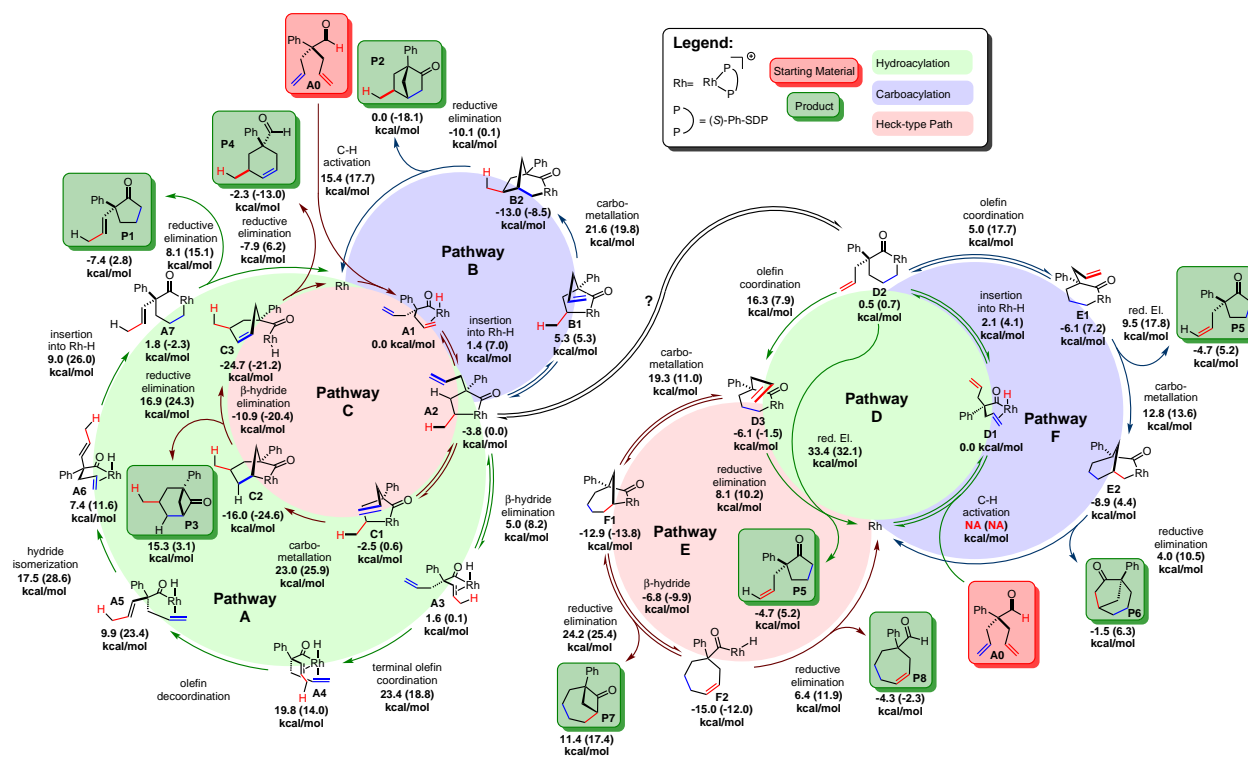
TPPS was chosen over other functionals due to its reliable performance with a variety of different elements, including transition metals.[†]

TPSS-D3/def2-TZVP was used to compute the numerical harmonic vibrational frequencies for all studied transition states (TS). The standard rigid-rotor harmonic-oscillator approximation was used to calculate the chemical potential (c.p.) which was used to study the Gibbs free energies ($G = E(0) + \text{c.p.}$).

It was found experimentally that non-polar solvents with different dielectric constants do not influence the reaction. All calculations were therefore performed *in vacuo*.

Protocol for Transition State Identification

The PES of a reaction step was modeled through ORCA by using 0.1 Å increments. The obtained transition state structure was then optimized in Turbomole.



Computed Reaction Pathways

Protocol for Distortion/Interaction-activation strain model

A similar protocol to a previously reported unimolecular reaction has been applied.^{249–251} The distortion energies for the substrate portion and the ligand portion were determined by fragmenting at the indicated position in Figure 3.19. The ends of the fragments were capped with hydrogen atoms.

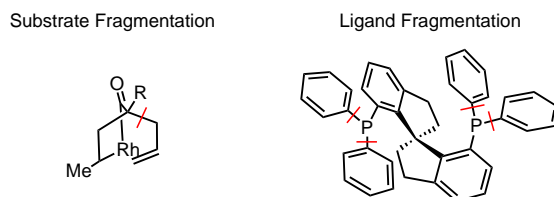


Figure 3.19. Fragmentation of substrate and ligand fragment

*CYLview, 1.0b, C.Y., Legault. Université de Sherbrooke, 2009.

†Goerigk, L.; Grimme, S. *Phys. Chem. Chem. Phys.* **2011**, *13*, 6670–6688.

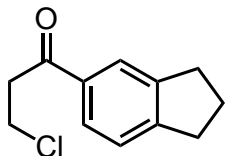
Coordinates

All coordinates can be found in the digitally appended text file.

3.3.2 Experimental Details

Commercial reagents were purchased from Strem, Sigma Aldrich, Alfa Aesar, Acros, Combi-Blocks and Chem-Impex and used without further purification. All reactions were carried out under an atmosphere of nitrogen unless otherwise indicated. Solvents used in cobalt-catalyzed reactions were first distilled and then degassed by three freeze-pump-thaw cycles before being taken into a glove box. Other solvents were dried through two column of activated alumina. Reactions were monitored using GC/MS, GC/FID or thin-layer chromatography (TLC) on EMD Silica Gel 60 F254. Visualization of the developed plates was performed under UV light (254 nm), KMnO_4 , cerium molybdate, and phosphomolybdic acid stain. Column chromatography was performed with Silicycle Silia-P Flash Silica Gel using glass columns. Organic solutions were concentrated under reduced pressure on a Büchi rotary evaporator. ^1H and ^{13}C NMR spectra were recorded on a DRX 400, GN 500, CRYO 500, or CRYO 600 spectrometer. NMR spectra were internally referenced to the residual solvent signal. Data for ^1H NMR are reported as follows: chemical shift (δ ppm), multiplicity (s = singlet, d = doublet, t = triplet, q = quartet, m = multiplet, br = broad), coupling constant (Hz), integration. Data for ^{13}C NMR are reported in chemical shift (δ ppm). High resolution mass spectra (HRMS) were obtained on a micromass 70S-250 spectrometer (EI) or an ABI/Sciex QStar Mass Spectrometer (ESI). Infrared (IR) spectra were obtained on a Perkin-Elmer Spectrum 1000 FT-IR Systems and are reported in terms of frequency of absorption (cm^{-1}). Enantiomeric excess (ee) was ascertained on an Agilent 1100 Series HPLC or Agilent 1200 Series/Aurora SFC. Optical rotations were measured on a Rudolph Research Analytical Autopol IV Automatic Polarimeter.

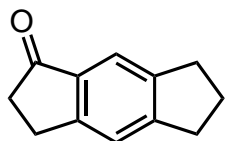
3-chloro-1-(2,3-dihydro-1H-inden-5-yl)propan-1-one **75**



In a 500 ml schlenk flask was added aluminum trichloride (27.0 g, 0.20 mol) in DCM (142 ml) to give a yellow suspension. 3-Chloropropionyl chloride (17.7 ml, 0.18 mol) was added dropwise over 30 minutes. Afterwards, indan (22.6 ml, 0.18 mol) was added dropwise.

The yellow suspension turned into a dark red solution. The reaction mixture was quenched after 1 hour with 1 M HCl (100 ml) solution. The aqueous layer was extracted with DCM (50 ml) four times. The organic layers were washed with sat. NaCl (aq) (100 ml) combined, and dried over MgSO₄, filtered, and concentrated. The unpurified reaction mixture was then purified by recrystallization from hexanes, to afford 32.7 g of (**75**) as a crystalline solid, 85% yield. ¹H-NMR: δ (600 MHz, CDCl₃) 7.82 (s, 1H), 7.75 (d, $J = 7.8$ Hz, 1H), 7.31 (d, $J = 7.8$ Hz, 1H), 3.92 (t, $J = 6.7$ Hz, 2H), 3.44 (t, $J = 6.7$ Hz, 2H), 2.96 (t, $J = 7.3$ Hz, 4H), 2.12 (p, $J = 8.1, 7.6$ Hz, 2H). ¹³C-NMR: δ (151 MHz, CDCl₃) 196.83, 150.98, 145.13, 135.07, 126.74, 124.63, 124.12, 41.48, 39.12, 33.20, 32.70, 25.50. HRMS (ESI-TOF) m/z calc'd for C₁₂H₁₃ClO [M+Na]⁺: 231.0553, found 231.0547. IR (ATR): 2953, 1674, 1603, 1415, 1349, 1274, 1219, 1142, 996, 914, 825, 777, 690, 618 cm⁻¹.

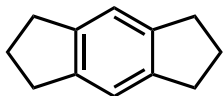
3,5,6,7-tetrahydro-s-indacen-1(2H)-one **76a**



In a 125 ml round-bottom flask was added sulfuric acid (97 ml, 1.83 mol). Indan **75** (25.4 g, 0.12 mol) was added in 3 g portions. The colorless solution turned dark red and was heated at 70 °C. The reaction mixture was quenched after 3 hours by pouring the reaction mixture into ice water. The aqueous layer was extracted with DCM (25 ml) three times. The organic layers were washed with sat. NaCl (aq) (50 ml) combined, and dried over MgSO₄, filtered, and concentrated. The unpurified reaction mixture was then purified by recrystallization from

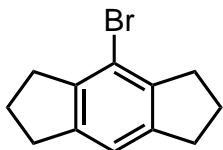
hexanes with a minimal amount of ethyl acetate, to afford 9.5 g of (**76a**) as a crystalline solid, 45% yield. $^1\text{H-NMR}$: δ (499 MHz, CDCl_3) 7.57 (s, 1H), 7.29 (s, 1H), 3.15 – 3.02 (m, 2H), 2.93 (dt, $J = 14.6, 7.4$ Hz, 4H), 2.77 – 2.62 (m, 2H), 2.12 (p, $J = 7.5$ Hz, 2H). $^{13}\text{C-NMR}$: δ (151 MHz, CDCl_3) 206.86, 154.55, 153.10, 144.29, 136.08, 122.30, 119.10, 36.93, 33.23, 32.18, 25.98, 25.68. HRMS (ESI-TOF) m/z calculated for $\text{C}_{12}\text{H}_{12}\text{O}$ $[\text{M}+\text{Na}]^+$: 195.0786, found 195.0794. IR (ATR): 2954, 2920, 1691, 1614, 1433, 1300, 1270, 1249, 1149, 1085, 986, 876, 862, 821, 612 cm^{-1} .

1,2,3,5,6,7-hexahydro-*s*-indacene **77**



In a 300 ml beaker was ketone **76a** (2.7 g, 15.62 mmol), and palladium on carbon (3.3 g, 5 wt%, 1.56 mmol). Ethanol (156 ml) was carefully added under a stream of nitrogen. The beaker was placed into a 600 ml a series 4760 parr reactor and pressurized with hydrogen gas to 200 psi. After 24 hours, the pressure was released, and the palladium catalyst removed by filtration through a pad of silica. The crude reaction product was eluted with diethyl ether. The unpurified reaction mixture was concentrated, to afford 2.2 g of (**77**) as a crystalline solid, 91% yield. $^1\text{H-NMR}$: δ (500 MHz, CDCl_3) 7.10 (s, 2H), 2.87 (t, $J = 7.4$ Hz, 8H), 2.08 (p, $J = 7.4$ Hz, 4H). $^{13}\text{C-NMR}$: δ (126 MHz, CDCl_3) 142.35, 120.43, 32.68, 26.12. HRMS (ESI-TOF) m/z calculated for $\text{C}_{12}\text{H}_{14}$ $[\text{M}]^+$: 158.1095, found 158.1091. IR (ATR): 2935, 2841, 1481, 1439, 1319, 1254, 1211, 1037, 863 cm^{-1} .

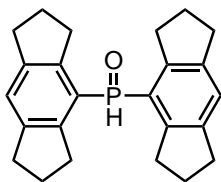
4-bromo-1,2,3,5,6,7-hexahydro-*s*-indacene **78**



In a 100 ml schlenk flask was hydroindacene **77** (2.0 g, 12.64 mmol) in MeCN (25.3 ml) to give colorless solution. The reaction was cooled to 0° and the reaction flask wrapped in aluminum foil, to avoid external

light. *N*-bromosuccinimide (2.5 g, 13.90 mmol) was added and the reaction stirred at 0 °. The reaction mixture was quenched after 3 hours by pouring the reaction into a 250 ml erlenmeyer flask, filled with 2.5 M NaOH solution (100 ml). The aqueous layer was extracted with ethyl acetate (20 ml) three times. The organic layers were washed with 2.5 M NaOH solution (50 ml), sat. NaCl (aq) (50 ml) combined and dried over MgSO₄, filtered, and concentrated. The unpurified reaction mixture was used in the next reaction without further purification.

bis(1,2,3,5,6,7-hexahydro-*s*-indacen-4-yl)phosphine oxide **79**



In a 25 ml schlenk tube was added magnesium (170 mg, 6.95 mmol) in THF (1 ml) to colorless suspension. A few grains of Iodine were added. Bromohydroindacene **78** (0.5 ml, 12 M in THF, 5.90 mmol) was added dropwise. The reaction mixture was stirred at room temperature for 1 hour, then heated to 40 ° for 30 minutes. Diethylphosphite (0.45 ml, 3.47 mmol) was added and the reaction heated to 60 ° for 2 hours and then stirred at room temperature. The reaction mixture was quenched after 24 hours with 1 M HCl solution (2 ml). The aqueous layer was extracted with diethyl ether (5 ml) three times. The organic layers were washed with 1 M HCl solution (5 ml), sat. NaCl (aq) (5 ml) combined and dried over MgSO₄, filtered, and concentrated. The unpurified reaction mixture was then purified by column chromatography (50% Ethyl acetate in Hexanes), to afford 245 mg of (**79**) as a crystalline solid, 19% yield. ¹H-NMR: δ (500 MHz, CDCl₃) 8.32 (d, *J* = 470.6 Hz, 1H), 7.24 (s, 2H), 2.99 – 2.76 (m, 16H), 2.04 (p, *J* = 7.2 Hz, 8H). ¹³C-NMR: δ (126 MHz, CDCl₃) 145.28 (d, *J* = 10.2 Hz), 143.79 (d, *J* = 10.1 Hz), 124.45 (d, *J* = 2.8 Hz), 31.64 (d, *J* = 4.6 Hz). HRMS (ESI-TOF) *m/z* calculated for C₂₄H₂₇OP [M+Na]⁺: 385.1697, found 385.1698.

Chapter 4

Copper Catalyzed Synthesis of γ, δ -Unsaturated Nitriles*

*Reproduced in part with permission from Wu, X.; Riedel, J.; Dong, V. M. *Angew. Chem. Int. Ed.* **2017**, *56*, 11589. Copyright 2017 Wiley

4.1 Introduction

Although radicals play a key role in biochemistry,^{252–255} their potential for use in organic synthesis is vast, with new concepts continually emerging,^{256–266} including applications in cross-coupling.^{267–275} By combining Cu catalysis with radicals, Heck-type transformations have been achieved, including allylic trifluoromethylation,^{276–280} arylation,²⁸¹ and alkylation.^{282–287} These radical transformations enable bond construction patterns that were previously impossible, and provide an attractive approach for olefin synthesis (Figure 4.1). Inspired by the versatility of nitriles,^{288–290} we designed a strategy for transforming simple olefins into γ,δ -unsaturated nitriles by taming the reactivity of the cyanoalkyl radical. Rather than requiring functionalized halides and toxic cyanide reagents, this transformation enables olefin feedstocks to be coupled with alkyl nitriles to generate homoallylic nitriles in a single step, using an earth-abundant metal catalyst (Figure 4.1).^{291,292}

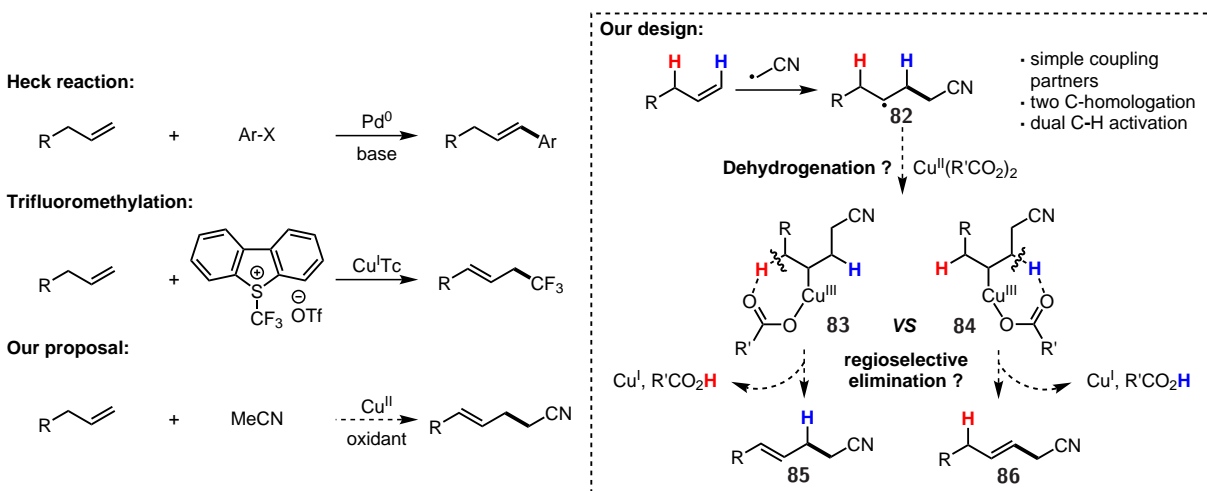


Figure 4.1. Allylic cyanoalkylation

The nitrile functional group is common in both materials²⁹³ and medicines,^{294,295} and is also a useful handle for elaboration.^{288–290} As shown in Figure 4.1, we proposed a cross-dehydrogenative coupling (CDC)^{296–301} between an olefin and acetonitrile.^{302,303} Initial oxidation of an alkyl nitrile forms the corresponding cyanoalkyl radical, which can add to an olefin to give the alkyl radical **82**.^{304–316} Radicals such as **82** have been implicated in olefin

hydrocyanoalkylations^{304–307} and bifunctionalizations.^{308–316} In the presence of a copper(II) catalyst, Koichi showed that radicals can be trapped to generate the alkylcopper(III) intermediate **83** with rate constants in excess of $10^6 \text{M}^{-1}\text{s}^{-1}$.^{317–321} Theoretical studies on the CF_3 allylic functionalization invoke a triflate-counterion-assisted elimination.²⁷⁸ On the basis of these studies, we reasoned that the appropriate counterion would be critical for controlling regio- and stereochemistry in the final elimination.^{322,323}

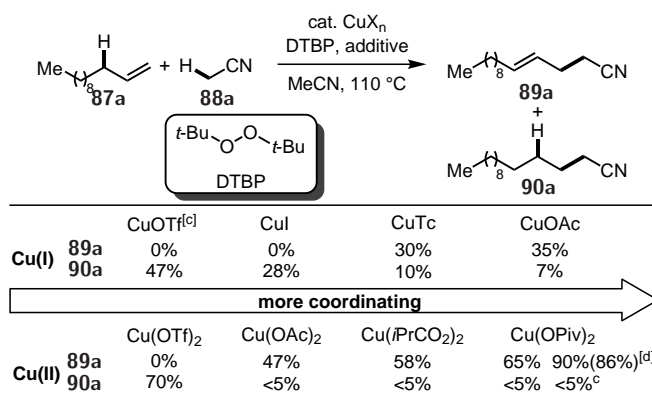
With this mechanistic hypothesis in mind, we focused on the Cu-catalyzed allylic cyanoalkylation of 1-dodecene in acetonitrile, using di-tert-butyl peroxide (DTBP) as the oxidant. DTBP is a convenient and inexpensive radical initiator in synthetic and polymer chemistry, and is commonly used for generating radicals from acetonitrile.^{304–316} Zhu and co-workers demonstrated that Cu/peroxide can generate cyanoalkyl radicals from alkylnitriles, which can then add to alkenes through an intermolecular process.^{308–310,314,315} In Zhu’s work, the generated alkyl radicals are typically trapped to afford bifunctionalizations, such as oxycyanoalkylations^{309,310,314,315} and arylocyanoalkylation.³⁰⁸ Rather than addition reactions across the olefin, we envisaged diverting **82** to achieve dehydrogenative olefin functionalization.

4.2 Results and Discussion

In the absence of copper, treatment of 1-dodecene with DTBP afforded the known hydrocyanoalkylation product **90a** in 25% yield, with no desired cyanoalkene **89a**. Copper(I) and copper(II) complexes bearing weak counterions provided **90a** as the major product (28–70% yields; Table 4.1), in accordance with reported studies on hydrocyanoalkylation.^{304–307} The catalysts used by Zhu and co-workers were not effective in our proposed allylic cyanoalkylation.^{308–310,314,315} In contrast, (thiophene-2-carboxyloxy)copper(I) (CuTc , previously used as a catalyst in allylic trifluoromethylation²⁷⁸) provided cyanoalkene **89a** as the major product

in 30% yield. In comparison to copper(I) acetate, we found that copper(II) acetate showed higher efficiency and chemoselectivity, providing **89a** in 47% yield with >20:1 regioselectivity. By replacing acetate with the more basic pivalate, the desired alkene was obtained in 65% yield, >20:1 regioselectivity. Other oxidants such as tertbutyl hydroperoxide (TBHP) and dicumyl peroxide (DCP) were ineffective. Using an electron-rich benzonitrile derivative as an additive further improved efficiency, presumably by improving catalyst solubility. In the presence of one equivalent of veratronitrile, **89a** was obtained in 90% yield, greater than 20:1 *rr*, and 4:1 *E/Z*. Only trace amounts of **90a** were observed (<5% yield). These results support the notion that a carboxylate counterion facilitates the elimination and enables >20:1 regioselectivity to provide the γ,δ -unsaturated nitrile. A syn elimination affords the *E* isomer as the major product.[19]

Table 4.1. Counter effects on Cu-catalyzed allylic cyanoalkylation



With this method, we elaborated a wide range of terminal olefins (Table 4.1). Unactivated linear terminal olefins gave the corresponding γ,δ -unsaturated nitriles (**89a–c**) in 80–86% yields with >20:1 *rr* and 4:1 *E/Z*. For the substrates bearing ester (**89d**, **89e**), amide (**89f**), cyano (**89g**), and ether (**89h**) groups, regioselective CDC reactions with acetonitrile provided the corresponding products in 75–82% yields. Increasing the steric hindrance at the 4-position of the olefins slightly decreased the yields but increased the *E/Z* ratios of the products (**89i** 7:1 *E/Z*; **89j** 11:1 *E/Z*; **89k** >20:1 *E/Z*). With a tertbutyl group at the 3-position, we observed >20:1 regioselectivity and >20:1 *E/Z* selectivity (**89k**). The regioselectivity was

unaffected by increased steric hindrance at the 4-position of the olefins. 3-Aryl-substituted substrates gave the corresponding nitriles (**89l–n**) in 40–46% yields with >20:1 *E/Z* selectivity. A substrate with an electron-withdrawing group on the phenyl ring (**89n**) showed slightly higher reactivity than one with an electron-donating group (**89m**). Trisubstituted alkenyl nitriles were synthesized in 50–77% yields from 3,3- and 1,1-disubstituted olefins (**89o–r** and **89t**). A series of nitriles were also tested as coupling partners. Propionitrile and butyronitrile showed decreased reactivity compared to acetonitrile, most likely due to steric effects and the lower solubility of the copper catalyst in these nitriles (**89w**, **89x**). Transformation with styrene, which has no allylic C–H bond, gave β,γ -unsaturated nitrile **89y** in 10% yield. Only trace amounts of the hydrocyanoalkylation product **90** were observed with the olefins shown in Figure 4.2. Having established facile access to various nitriles, we next focused on applying them as building blocks.

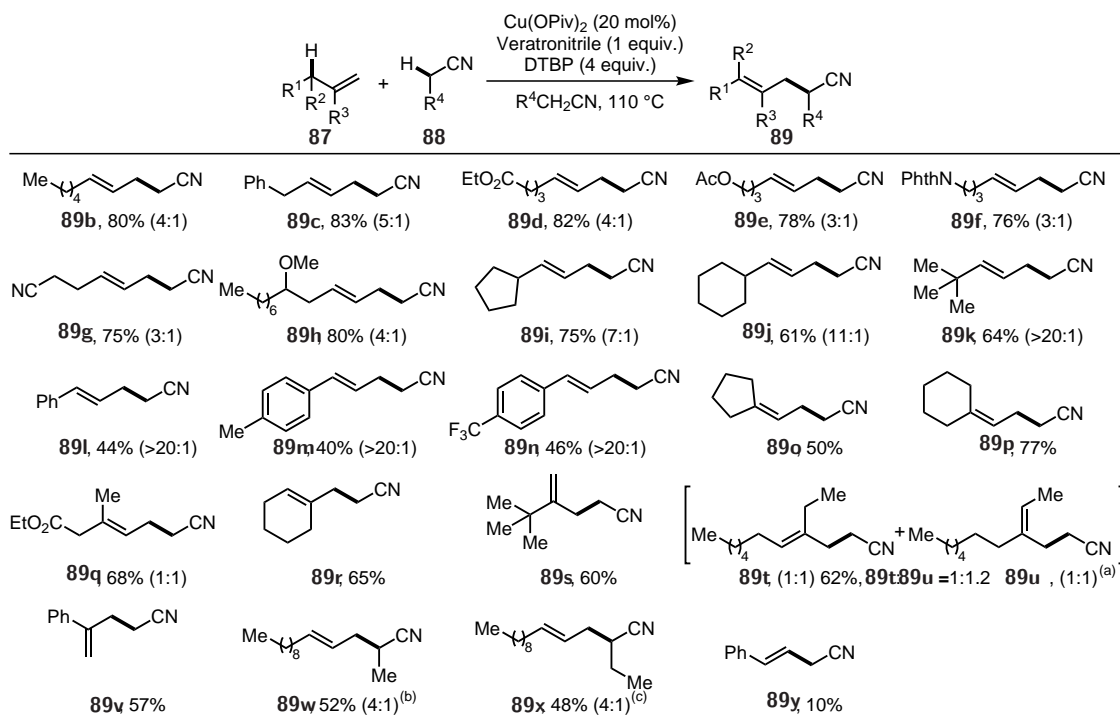


Figure 4.2. Allylic cyanoalkylation of terminal olefins

Owing to the versatility of the cyano group, we were able to use simple olefins to access a range of valuable products, including an industrial flavor agent, a natural product, and

a polymer precursor (Figure 4.3). For example, treatment of **89b** with TMSCl in ethanol provided the pear flavoring ethyl 4-decenoate (**91**) in 85% yield.³²⁴ The 4-alkyl γ -lactones are members of a large family of natural flavors that are widely used in food industry.^{325,326} From the same compound **89b**, γ -decalactone (**92**) was obtained in 73% yield through a one-pot, hydrolysis and intramolecular hydroacyloxylation. Our strategy provides an efficient route to fatty acids. For example, lyngbic acid, which is isolated from the marine cyanophyte *Lyngbya majuscula*,³²⁷ exhibits antimicrobial activity.³²⁸ Through hydrolysis of the cyano group in compound **89h**, lyngbic acid (**93**) can be obtained in 87% yield. Ru-catalyzed hydrogenation of **89d** provided the nylon-9 precursor **94** in 75% yield.³²⁹

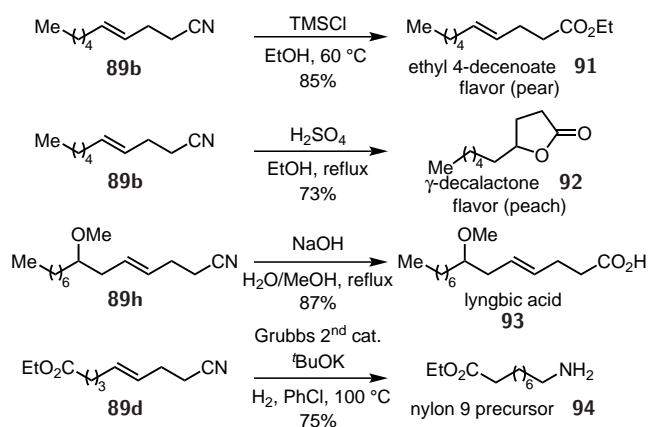


Figure 4.3. Application of the γ,δ -unsaturated nitriles

Next, we examined internal olefins (Figure 4.4). With (*E*)-5-decene, the transformation gave cyanoalkene **89y** in 62% yield with >20:1 *rr* and 11:1 *E/Z* after 24 h (Figure 4.4a). With (*Z*)-5-decene, the *E* isomer **89y** was obtained as the major product in a similar yield and *E/Z* selectivity as the *E*-olefin substrate (60% yield, 12:1 *E/Z*) (Figure 4.4b). The C–C bonds were formed at the 5-position of the substrates. No 3-propylnon-4-enenitrile (**97**) was observed from either the potential allylic radical **95** or π -allylcopper intermediate **96** through allylic C–H bond activation (Figure 4.4c). We observed no carbocation-rearrangement-type products (**100**), which would arise from the carbocation intermediate **98** (Figure 4.4d).³³⁰ Nor were these 1,2-hydride shift products detected in experiments yielding compounds **89o–q** (Figure 4.2). These observations suggest that allylic radicals or carbocations are most likely

not key intermediates in our cross-coupling.

On the basis of further experiments and previous reports,^{307–311,313–316} we propose the mechanism shown in Figure 4.5. Pivalate-assisted deprotonation of alkylnitrile with copper(II) pivalate produces the cyanoalkylcopper(II) species **32** (pathway a). Homolytic cleavage of **32** gives the cyanoalkyl radical and copper(I) species. Addition of the cyanoalkyl radical to the olefin generates the radical intermediate **82**. Concerted carboxylate elimination of **82** provides the γ,δ -unsaturated nitrile product and a copper(I) species. To explain the regioselectivity, we propose that π -bonding of the cyano group to copper(III)^{331,332} shields the H at the β position to direct the pivalate to abstract the H at the δ position. The copper(I) species decomposes DTBP through a single-electron-transfer redox reaction to regenerate copper(II) and a methyl radical. The methyl radical could also abstract hydrogen from alkylnitrile to produce the cyanoalkyl radical (pathway b).

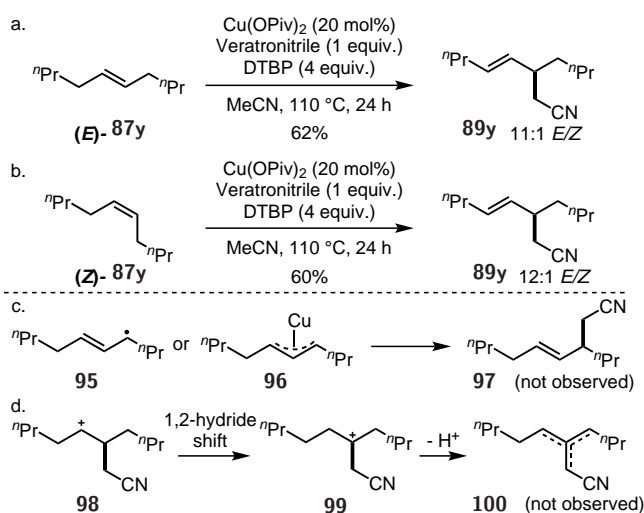


Figure 4.4. Allylic cyanoalkylation of internal olefins

The following radical-trapping and radical-clock experiments support the proposed mechanism (Figure 4.6). Formation of the allylic cyanoalkylation product was suppressed in the presence of TEMPO, a known radical inhibitor. Instead, the products of cyanomethyl radical trapping (**101**) and methyl trapping (**102**) were both observed in 14% and 27% yields, respectively. These results support the notion that cyanomethyl radical and methyl radical

intermediates are involved in the transformation. In the absence of $\text{Cu}(\text{OPiv})_2$, the products **101** and **102** were also observed (in 5% and 39% yields, respectively). However, in the absence of DTBP, only **101** was observed (12% yield). These results support the idea that pathways a and b are responsible for the activation of acetonitrile. Next, we found that the compound **104** was obtained in 60% yield from (1-cyclopropylvinyl)benzene (**103**) through sequential ring opening of cyclopropylmethyl radical intermediate and cyclization (Figure 4.6b).^[6e,13b, 18] This radical-clock experiment supports the generation of **82**.

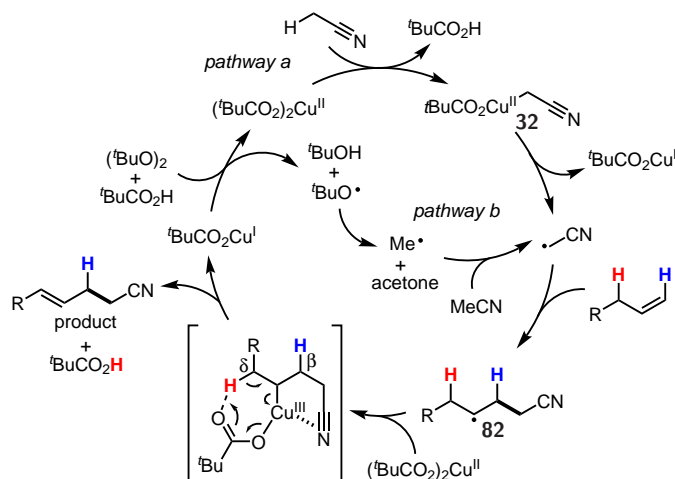


Figure 4.5. Proposed mechanism and rationale for the regioselectivity

In summary, we have developed a copper-catalyzed crossdehydrogenative coupling of unactivated olefins with alkylnitriles through dual sp^3 C–H bond cleavage. High chemo- and regioselectivity for E_2 -type elimination is conferred by 1) the pivalate counterion and 2) the directing effect of cyano groups. By using a catalyst derived from earth-abundant salts, we can access 4-alkenylnitriles from simple olefins. Both terminal and internal olefins can be transformed into γ,δ -unsaturated nitriles, which are versatile synthetic building blocks. These studies contribute to the emerging use of radicals for catalytic cross-coupling.

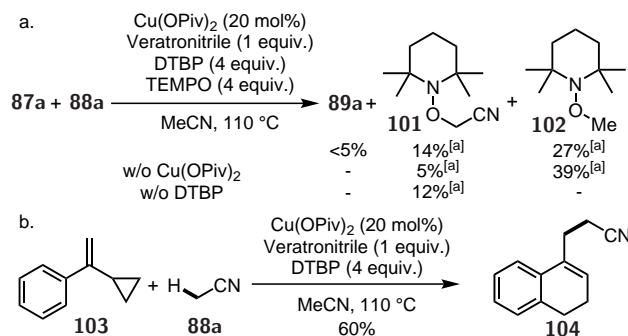


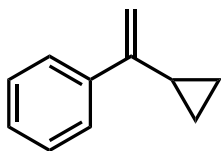
Figure 4.6. Intermediate-trapping and radical-clock experiment

4.3 Experimental Data

The details of the studies described in this chapter can be found in the Supporting Information of the published manuscript.³³³ My contributions to the project are detailed in this section.

4.3.1 Experimental Details

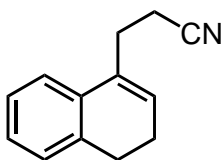
(1-cyclopropylvinyl)benzene 103



To a 100 ml schlenk flask equipped with a stir bar was added methyltriphenylphosphonium bromide (9.1 g, 32.6 mmol) in THF (44 ml) to give a white suspension. The reaction mixture was cooled to 0 °C and *n*-BuLi (14.2 ml, 2.3 M, 32.6 mmol) was added dropwise to give a bright red solution and was stirred for 1 hour at room temperature. Cyclopropyl(phenyl)methanone (3.0 ml, 21.8 mmol) was added dropwise to give an orange solution. The reaction mixture was heated to 65 °C and stirred for 24 hours. After complete conversion, the reaction was diluted with pentane (40 ml) and aq. NH₄Cl (30 ml) was added. The layers were separated and the organic layer was washed with brine (30 ml) three times. The organic layer was then dried over MgSO₄ and concentrated under reduced pressure. Purification of the crude

residue by column chromatography (pentane) afforded (1-cyclopropylvinyl)benzene (**103**) as a colorless oil (2.0 g, 64% yield). $^1\text{H-NMR}$: δ (400 MHz, CDCl_3) 7.64 (dd, $J = 8.3, 1.2$ Hz, 2H), 7.41 – 7.35 (m, 2H), 7.34 – 7.29(m, 1H), 5.32 (s, 1H), 4.98 (s, 1H), 1.74 – 1.65(m, 1H), 0.90 – 0.84(m, 2H), 0.66 – 0.60 (m, 2H). $^{13}\text{C-NMR}$: δ (101 MHz, CDCl_3) 149.5, 141.8, 128.3, 127.6, 126.3, 109.1, 15.8, 6.8. This compound is known.³³⁴

3-(3,4-dihydronaphthalen-1-yl)propanenitrile **104**



In a N_2 -filled glovebox, veratronitrile (32.6 mg, 0.20 mmol) and dry acetonitrile (1.5 ml) were added to a 1 dram vial (diameter 1.4 cm/height 4.3 cm) containing $\text{Cu}(\text{OPiv})_2$ (10.6 mg, 0.040 mmol). After stirring for 3 minutes, **103** (29.0 mg, 0.20 mmol) and di-*tert*-butyl peroxide (0.15 ml, 117 mg, 0.80 mmol) were added. The vial was sealed completely by a screw cap with a Teflon septum. Then the reaction mixture was stirred at 110 °C for 6 hours. Upon completion, the reaction mixture was filtered through a short silica gel pad and washed with 50% ethyl acetate in hexanes. The filtrate was concentrated in vacuo. The selectivity was determined by NMR analysis of the unpurified reaction mixture. Purification of the crude residue by preparatory TLC (10% ethyl acetate in hexanes) afforded 3-(3,4-dihydronaphthalen-1-yl)propanenitrile (**104**) as a colorless oil (22.0 mg, 60% yield). $^1\text{H-NMR}$: δ (400 MHz, CDCl_3) 7.25 – 7.12 (m, 4H), 6.01 (t, $J = 4.6$ Hz, 1H), 2.84 – 2.74 (m, 4H), 2.57 (t, $J = 7.4$ Hz, 2H), 2.33 – 2.27 (m, 2H). $^{13}\text{C-NMR}$: δ (101 MHz, CDCl_3) 137.0, 133.3, 133.2, 128.2, 127.6, 127.4, 126.7, 121.9, 119.5, 28.7, 28.2, 23.1, 16.9. This compound is known.³³⁵

References

- (1) Miller, S., J.; Blackwell, H., E.; Grubbs, R., H. *J. Am. Chem. Soc.* **1996**, *118*, 9606–9614.
- (2) White, C. J.; Hickey, J. L.; Scully, Conor C. G.; Yudin, A. K. *J. Am. Chem. Soc.* **2014**, *136*, 3728–3731.
- (3) Illesinghe, J.; Guo, C. X.; Garland, R.; Ahmed, A.; van Lierop, B.; Elaridi, J.; Jackson, W. R.; Robinson, A. J. *Chem. Commun.* **2009**, 295–297.
- (4) Hili, R.; Rai, V.; Yudin, A. K. *J. Am. Chem. Soc.* **2010**, *132*, 2889–2891.
- (5) White, C. J.; Yudin, A. K. *Nat. Chem.* **2011**, *3*, 509–524.
- (6) Tang, Y.-Q.; Yuan, J.; Ösapay, G.; Ösapay, K.; Tran, D.; Miller, C., J.; Ouellette, A., J.; Selsted, M., E. *Science* **1999**, *286*, 498–502.
- (7) Fernandez-Lopez, S.; Kim, H.-S.; Choi, E., C.; Delgado, M.; Granja, J., R.; Khasanov, A.; Kraehenbuehl, K.; Long, G.; Weinberger, D., A.; Wilcoxon, K., M.; Ghadiri, M., R. *Nat. Chem.* **2001**, *412*, 452–455.
- (8) Levine, D. P. *Clin. Infect. Dis.* **2006**, *42*, S5–12.
- (9) Laupacis, A.; Keown, P., A.; Ulan, R., A.; McKenzie, N.; Stiller, C., R. *Can. Med. Assoc. J.* **1982**, *126*, 1042–1046.
- (10) Craik, D. J. *Science* **2006**, *311*, 1563–1564.

- (11) Fairlie, D. P.; Abbenante, G.; March, Darren, R. *Curr. Med. Chem.* **1995**, *2*, 654–686.
- (12) Mas-Moruno, C.; Rechenmacher, F.; Kessler, H. *Anticancer Agents Med. Chem.* **2010**, *10*, 753–768.
- (13) Kathrina, H.; Werner, P.; Heinrich, N.; Wolfgang Beck *Angew. Chem. Int. Ed.* **1998**, *37*, 1086–1089.
- (14) Meutermans, W. D. F.; Bourne, G. T.; Golding, S. W.; Horton, D. A.; Campitelli, M. R.; Craik, D.; Scanlon, M.; Smythe, M. L. *Org. Lett.* **2003**, *5*, 2711–2714.
- (15) Yun-hua, Y.; Xing-ming, G.; Mian, L.; Yan-chun, T.; Gui-ling, T. *Lett. Pept. Sci.* **2003**, *10*, 571–579.
- (16) Bock, V. D.; Perciaccante, R.; Jansen, T. P.; Hiemstra, H.; van Maarseveen, J. H. *Org. Lett.* **2006**, *8*, 919–922.
- (17) Thakkar, A.; Trinh, T. B.; Pei, D. *ACS Comb. Sci.* **2013**, *15*, 120–129.
- (18) Bray, B. L. *Nat. Rev. Drug Discovery* **2003**, *2*, 587–593.
- (19) Mulder, K. C. L.; Viana, A. A. B.; Xavier, M.; Parachin, N. S. *Curr. Protein Pept. Sci.* **2013**, *14*, 556–567.
- (20) Skropeta, D.; Jolliffe, K. A.; Turner, P. *J. Org. Chem.* **2004**, *69*, 8804–8809.
- (21) Robinson, J. A. *Acc. Chem. Res.* **2008**, *41*, 1278–1288.
- (22) Fairweather, K. A.; Sayyadi, N.; Luck, I. J.; Clegg, J. K.; Jolliffe, K. A. *Org. Lett.* **2010**, *12*, 3136–3139.
- (23) Ehrlich, A.; Heyne, H.-U.; Winter, R.; Beyermann, M.; Haber, H.; Carpino, L., A.; Bienert, M. *J. Org. Chem.* **1996**, *61*, 8831–8838.
- (24) Schmidt, U.; Langer, J. *J. Pept. Res.* **1997**, *49*, 67–73.
- (25) Busetti, V.; Crisma, M.; Toniolo, C.; Salvadori, S.; Balboni, G. *Int. J. Biol. Macromol.* **1992**, *14*, 23–28.

- (26) Bhandary, Krishna, K.; Chauhan, V. S. *Biopolymers* **1993**, *33*, 209–217.
- (27) Broda, M. A.; Siodlak, D.; Rzeszotarska, B. *J. Peptide Sci.* **2005**, *11*, 546–555.
- (28) Tang, W.; Jiménez-Osés, G.; Houk, K. N.; van der Donk, Wilfred A. *Nat. Chem.* **2014**, *7*, 57–64.
- (29) Rajashankar, K., R.; Ramakumar, S.; Chauhan, V. S. *J. Am. Chem. Soc.* **1992**, *114*, 9225–9226.
- (30) Ramagopal, U., A.; Ramakumar, S.; Joshi, R., M.; Chauhan, V. S. *J. Pept. Res.* **1998**, *52*, 208–215.
- (31) Mathur, P.; Ramakumar, S.; Chauhan, V. S. *Biopolymers* **2004**, *76*, 150–161.
- (32) Gupta, M.; Chauhan, V. S. *Biopolymers* **2011**, *95*, 161–173.
- (33) Jiang, J.; Ma, Z.; Castle, S. L. *Tetrahedron* **2015**, *71*, 5431–5451.
- (34) Somvanshi, R. K.; Goel, V. K.; Dey, S.; Singh, T. P. *J. Chem. Crystallogr.* **2005**, *35*, 761–768.
- (35) Bonauer, C.; Walenzyk, T.; König, B. *Synthesis* **2006**, *1*, 1–20.
- (36) Holder, J. R.; Haskell-Luevano, C. *Med. Res. Rev.* **2004**, *24*, 325–356.
- (37) Hill, T. A.; Shepherd, N. E.; Diness, F.; Fairlie, D. P. *Angew. Chem. Int. Ed.* **2014**, *53*, 13020–13041.
- (38) Morita, H.; Kayashita, T.; Shishido, A.; Takeya, K.; Itokawa, H.; Shiro, M. *Tetrahedron* **1996**, *52*, 1165–1176.
- (39) Nitz, T. J.; Holt, E. M.; Rubin, B.; Stammer, C. H. *J. Org. Chem.* **1981**, *46*, 2667–2671.
- (40) Patel, H., C.; Singh, T. P.; Chauhan, V. S.; Kaur, P. *Biopolymers* **1990**, *29*, 509–515.
- (41) Zhang, L.; Tam, J. P. *J. Am. Chem. Soc.* **1999**, *121*, 3311–3320.
- (42) Kenneth D., K. *J. Pharm. Sci.* **1972**, *61*, 1345–1356.

- (43) Monteiro, L. S.; Andrade, J. J.; Suárez, A. C. *Eur. J. Org. Chem.* **2011**, *2011*, 6764–6772.
- (44) Shultz, C. S.; Krska, S. W. *Acc. Chem. Res.* **2007**, *40*, 1320–1326.
- (45) Liu, D.; Zhang, X. *Eur. J. Org. Chem.* **2005**, *2005*, 646–649.
- (46) Robert W., W. *Meth. Enzymol.* **1995**, *246*, 34–71.
- (47) Mutzenhardt, P., et al. *J. Magn. Reson.* **1999**, *141*, 312–321.
- (48) Karplus, M. *J. Am. Chem. Soc.* **1963**, *85*, 2870–2871.
- (49) Kessler, H. *Angew. Chem. Int. Ed.* **1982**, *21*, 512.
- (50) Hong, J.; Jing, Q.; Yao, L. *J. Biomol. NMR* **2013**, *55*, 71–78.
- (51) Menting, J. G. et al. *Proc. Natl. Acad. Sci. U.S.A.* **2014**, *111*, E3395–E3404.
- (52) Crisma, M.; Formaggio, F.; Toniolo, C.; Yoshikawa, T.; Wakamiya, T. *J. Am. Chem. Soc.* **1999**, *121*, 3272–3278.
- (53) Merrifield, R. B. *J. Am. Chem. Soc.* **1963**, *85*, 2149–2154.
- (54) Le, D. N.; Riedel, J.; Kozlyuk, N.; Martin, R. W.; Dong, V. M. *Org. Lett.* **2017**, *19*, 114–117.
- (55) P. M. Dewick, *Medicinal Natural Products: A Biosynthetic Approach*; Wiley: West Sussex, 2002.
- (56) Baran, P. S.; Maimone, T. J.; Richter, J. M. *Nature* **2007**, *446*, 404–408.
- (57) Park, J.-W.; Kou, K. G. M.; Kim, D. K.; Dong, V. M. *Chem. Sci.* **2015**, *6*, 4479–4483.
- (58) Park, J.-W.; Chen, Z.; Dong, V. M. *J. Am. Chem. Soc.* **2016**, *138*, 3310–3313.
- (59) Jiang, G.; List, B. *Adv. Synth. Catal.* **2011**, *353*, 1667–1670.
- (60) Willis, M. C. *Chem. Rev.* **2010**, *110*, 725–748.
- (61) Barry M. Trost *Science* **1991**, *254*, 1471–1477.

- (62) Newhouse, T.; Baran, P. S.; Hoffmann, R. W. *Chem. Soc. Rev.* **2009**, *38*, 3010–3021.
- (63) Yip, S. Y. Y.; Aïssa, C. *Angew. Chem. Int. Ed.* **2015**, *54*, 6870–6873.
- (64) Christian P. Lenges; Maurice Brookhart* *J. Am. Chem. Soc.* **1997**, *119*, 3165–3166.
- (65) Murphy, S. K.; Park, J.-W.; Cruz, F. A.; Dong, V. M. *Science* **2015**, *347*, 56–60.
- (66) Yang, J.; Seto, Y. W.; Yoshikai, N. *ACS Catal.* **2015**, *5*, 3054–3057.
- (67) M. G., V.; A. B., T.; G. I. Nikishin; B. N., S.; V. B., K. *J. Organomet. Chem.* **1988**, *348*, 123–134.
- (68) Yang, J.; Yoshikai, N. *J. Am. Chem. Soc.* **2014**, *136*, 16748–16751.
- (69) Hyatt, I. F. D.; Anderson, H. K.; Morehead, A. T.; Sargent, A. L. *Organometallics* **2008**, *27*, 135–147.
- (70) R. H. Grubbs and A. Miyashita *J. Am. Chem. Soc.* **1978**, *100*, 1300–1302.
- (71) Schmidt, V. A.; Hoyt, J. M.; Margulieux, G. W.; Chirik, P. J. *J. Am. Chem. Soc.* **2015**, *137*, 7903–7914.
- (72) Paul, B.; Michael J., D. *J. Organomet. Chem.* **1978**, *162*, 195–207.
- (73) Klaus H. Theopold; Paul N. Becker; Robert G. Bergman *J. Am. Chem. Soc.* **1982**, *104*, 5250–5252.
- (74) Masahiro Murakami, Hideki Amii, Yoshihiko Ito *Nature* **1994**, *370*, 540–541.
- (75) Chao, K. C.; Rayabarapu, D. K.; Wang, C.-C.; Cheng, C.-H. *J. Org. Chem.* **2001**, *66*, 8804–8810.
- (76) Treutwein, J.; Hilt, G. *Angew. Chem. Int. Ed.* **2008**, *47*, 6811–6813.
- (77) Hilt, G.; Paul, A.; Treutwein, J. *Org. Lett.* **2010**, *12*, 1536–1539.
- (78) Abulimiti, A.; Nishimura, A.; Ohashi, M.; Ogoshi, S. *Chem. Lett.* **2013**, *42*, 904–905.
- (79) Hu, J.; Yang, Q.; Yu, L.; Xu, J.; Liu, S.; Huang, C.; Wang, L.; Zhou, Y.; Fan, B. *Org. Biomol. Chem.* **2013**, *11*, 2294–2301.

- (80) McNally, A.; Haffemayer, B.; Collins, B. S. L.; Gaunt, M. J. *Nature* **2014**, *510*, 129–133.
- (81) Nishimura, A.; Tamai, E.; Ohashi, M.; Ogoshi, S. *Chemistry* **2014**, *20*, 6613–6617.
- (82) Camasso, N. M.; Sanford, M. S. *Science* **2015**, *347*, 1218–1220.
- (83) Hoyt, J. M.; Schmidt, V. A.; Tondreau, A. M.; Chirik, P. J. *Science* **2015**, *349*, 960–963.
- (84) Darren Willcox, Ben G. N. Chappell, Kirsten F. Hogg, Jonas Calleja, Adam P. Smalley, Matthew J. Gaunt *Science* **2016**, *354*, 851–857.
- (85) Ravindra Kumar, Eri Tamai, Akira Ohnishi, Akira Nishimura, Yoichi Hoshimoto, Masato Ohashi, Sensuke Ogoshi *Synthesis* **2016**, *48*, 2789–2794.
- (86) Ohashi, M.; Ueda, Y.; Ogoshi, S. *Angew. Chem. Int. Ed.* **2017**, *56*, 2435–2439.
- (87) Friedfeld, M. R.; Shevlin, M.; Hoyt, J. M.; Krska, S. W.; Tudge, M. T.; Chirik, P. J. *Science* **2013**, *342*, 1076–1080.
- (88) Friedfeld, M. R.; Margulieux, G. W.; Schaefer, B. A.; Chirik, P. J. *J. Am. Chem. Soc.* **2014**, *136*, 13178–13181.
- (89) Collins, K. D.; Glorius, F. *Nat. Chem.* **2013**, *5*, 597–601.
- (90) Collins, K. D.; Rühling, A.; Glorius, F. *Nat. Protoc.* **2014**, *9*, 1348–1353.
- (91) Collins, K. D.; Glorius, F. *Acc. Chem. Res.* **2015**, *48*, 619–627.
- (92) Janssen-Müller, D.; Schedler, M.; Fleige, M.; Daniliuc, C. G.; Glorius, F. *Angew. Chem. Int. Ed.* **2015**, *54*, 12492–12496.
- (93) Schmidt, J.; Choi, J.; Liu, A. T.; Slusarczyk, M.; Fu, G. C. *Science* **2016**, *354*, 1265–1269.
- (94) Yetra, S. R.; Mondal, S.; Mukherjee, S.; Gonnade, R. G.; Biju, A. T. *Angew. Chem. Int. Ed.* **2016**, *55*, 268–272.

- (95) L., R.; C., B.; M. R., V., *PATAI'S Chemistry of Functional Groups*; Wiley: Hoboken, NJ, 2009.
- (96) K. C., B., *Organic Syntheses*; Wiley: Hoboken, NJ, 2003.
- (97) Semproni, S. P.; Milsmann, C.; Chirik, P. J. *J. Am. Chem. Soc.* **2014**, *136*, 9211–9224.
- (98) E. V., A.; D. A., D., *Modern Physical Organic Chemistry*; University Science Books: Sausalito, CA, 2006.
- (99) J. F., H., *Organotransition Metal Chemistry: From Bonding to Catalysis*; University Science Books: Sausalito, 2010.
- (100) Seiser, T.; Saget, T.; Tran, D. N.; Cramer, N. *Angew. Chem. Int. Ed.* **2011**, *50*, 7740–7752.
- (101) Christopher J. Douglas; Larry E. Overman *Proc. Natl. Acad. Sci. U.S.A.* **2004**, *101*, 5363–5367.
- (102) Du, J.; Skubi, K. L.; Schultz, D. M.; Yoon, T. P. *Science* **2014**, *344*, 392–396.
- (103) Quasdorf, K. W.; Overman, L. E. *Nature* **2014**, *516*, 181–191.
- (104) Xu, Y.; Conner, M. L.; Brown, M. K. *Angew. Chem. Int. Ed.* **2015**, *54*, 11918–11928.
- (105) Michael C. Willis *J. Chem. Soc., Perkin Trans. 1* **1999**, *13*, 1765–1784.
- (106) Jafarpour, F.; Biancalani, T.; Goldenfeld, N. *Phys. Rev. E* **2017**, *95*, 032407.
- (107) Daniel S. La; John B. Alexander; Dustin R. Cefalo; David D. Graf; Amir H. Hoveyda; Richard R. Schrock *J. Am. Chem. Soc.* **1998**, *120*, 9720–9721.
- (108) Liu, Q.; Rovis, T. *J. Am. Chem. Soc.* **2006**, *128*, 2552–2553.
- (109) Rowland, E. B.; Rowland, G. B.; Rivera-Otero, E.; Antilla, J. C. *J. Am. Chem. Soc.* **2007**, *129*, 12084–12085.
- (110) Wadamoto, M.; Phillips, E. M.; Reynolds, T. E.; Scheidt, K. A. *J. Am. Chem. Soc.* **2007**, *129*, 10098–10099.

- (111) Gu, Q.; Rong, Z.-Q.; Zheng, C.; You, S.-L. *J. Am. Chem. Soc.* **2010**, *132*, 4056–4057.
- (112) Phan, D. H. T.; Kou, K. G. M.; Dong, V. M. *J. Am. Chem. Soc.* **2010**, *132*, 16354–16355.
- (113) Zeng, X.-P.; Cao, Z.-Y.; Wang, Y.-H.; Zhou, F.; Zhou, J. *Chem. Rev.* **2016**, *116*, 7330–7396.
- (114) Kelley, A. M.; Minerali, E.; Wilent, J. E.; Chambers, N. J.; Stingley, K. J.; Wilson, G. T.; Petersen, K. S. *Tetrahedron Lett.* **2019**, *60*, 1262–1264.
- (115) Enquist, J. A.; Stoltz, B. M. *Nature* **2008**, *453*, 1228–1231.
- (116) Anastas, P.; Eghbali, N. *Chem. Soc. Rev.* **2010**, *39*, 301–312.
- (117) Sheldon, R. A. *Chem. Soc. Rev.* **2012**, *41*, 1437–1451.
- (118) Kim, D. K.; Riedel, J.; Kim, R. S.; Dong, V. M. *J. Am. Chem. Soc.* **2017**, *139*, 10208–10211.
- (119) Benito Fernandez; Jose A. Martinez Perez; Juan R. Granja; Luis Castedo; and Antonio Mourino *J. Org. Chem.* **1992**, *57*, 3173–3178.
- (120) Garcia-Fandiño, R.; Codesido, E. M.; Sobarzo-Sánchez, E.; Castedo, L.; Granja, J. R. *Org. Lett.* **2004**, *6*, 193–196.
- (121) Canham, S. M.; France, D. J.; Overman, L. E. *J. Am. Chem. Soc.* **2010**, *132*, 7876–7877.
- (122) Jung, M. E.; Chang, J. J. *Org. Lett.* **2010**, *12*, 2962–2965.
- (123) Hartrampf, F. W. W.; Furukawa, T.; Trauner, D. *Angew. Chem. Int. Ed.* **2017**, *56*, 893–896.
- (124) Murphy, S. K.; Zeng, M.; Herzon, S. B. *Science* **2017**, *356*, 956–959.
- (125) Zeng, M.; Murphy, S. K.; Herzon, S. B. *J. Am. Chem. Soc.* **2017**, *139*, 16377–16388.
- (126) Reddy, T. J.; Bordeau, G.; Trimble, L. *Org. Lett.* **2006**, *8*, 5585–5588.

- (127) Frie, J. L.; Jeffrey, C. S.; Sorensen, E. J. *Org. Lett.* **2009**, *11*, 5394–5397.
- (128) Yamashita, D.; Murata, Y.; Hikage, N.; Takao, K.-I.; Nakazaki, A.; Kobayashi, S. *Angew. Chem. Int. Ed.* **2009**, *48*, 1404–1406.
- (129) Murphy, R. A.; Sarpong, R. *Org. Lett.* **2012**, *14*, 632–635.
- (130) Zeng, C.; Zheng, C.; Zhao, J.; Zhao, G. *Org. Lett.* **2013**, *15*, 5846–5849.
- (131) Tang, Y.; Liu, J.-t.; Chen, P.; Lv, M.-c.; Wang, Z.-z.; Huang, Y.-k. *J. Org. Chem.* **2014**, *79*, 11729–11734.
- (132) Eagan, J. M.; Hori, M.; Wu, J.; Kanyiva, K. S.; Snyder, S. A. *Angew. Chem. Int. Ed.* **2015**, *54*, 7842–7846.
- (133) Cheong, P. H.-Y.; Houk, K. N.; Warrier, J. S.; Hanessian, S. *Adv. Synth. Catal.* **2004**, *346*, 1111–1115.
- (134) Davies, S. G.; Sheppard, R. L.; Smith, A. D.; Thomson, J. E. *Chem. Commun.* **2005**, 3802–3804.
- (135) Zhou, P.; Zhang, L.; Luo, S.; Cheng, J.-P. *J. Org. Chem.* **2012**, *77*, 2526–2530.
- (136) Robert A. Micheli; Zoltan G. Hojos; Noal Cohen; David R. Parrish; Louis A. Portland; Werner Sciamanna; Melinda A. Scott; and Pius A. Wehrli *J. Org. Chem.* **1975**, *40*, 675–681.
- (137) Deukjoon Kim; Young Kyoung Lee *Tetrahedron Lett.* **1991**, *32*, 6885–6886.
- (138) Gilbert Stork; Choon Sup Ra *Bull. Korean Chem. Soc.* **1997**, *18*, 137–139.
- (139) Michiel Van Gool; Maurits Vandewalle *Eur. J. Org. Chem.* **2000**, 3427–3431.
- (140) Gándara, Z.; Rivadulla, M. L.; Pérez, M.; Gómez, G.; Fall, Y. *Eur. J. Org. Chem.* **2013**, *2013*, 5678–5682.
- (141) Hog, D. T.; Huber, F. M. E.; Mayer, P.; Trauner, D. *Angew. Chem. Int. Ed.* **2014**, *53*, 8513–8517.

- (142) Ballio, A.; Castiglione Morelli, M. A.; Evidente, A.; Graniti, A.; Randazzo, G.; Sparapano, L. *Phytochemistry* **1991**, *30*, 131–136.
- (143) Evidente, A.; Motta, A.; Sparapano, L. *Phytochemistry* **1993**, *33*, 69–78.
- (144) Ramachary, D. B.; Kishor, M. *J. Org. Chem.* **2007**, *72*, 5056–5068.
- (145) Tanaka, M.; Imai, M.; Fujio, M.; Sakamoto, E.; Takahashi, M.; Eto-Kato, Y.; Wu, X. M.; Funakoshi, K.; Sakai, K.; Suemune, H. *J. Org. Chem.* **2000**, *65*, 5806–5816.
- (146) Chen, Q.-A.; Kim, D. K.; Dong, V. M. *J. Am. Chem. Soc.* **2014**, *136*, 3772–3775.
- (147) Xu, W.; Pek, J. H.; Yoshikai, N. *Adv. Synth. Catal.* **2016**, *358*, 2564–2568.
- (148) Xu, W.; Yoshikai, N. *Angew. Chem. Int. Ed.* **2016**, *55*, 12731–12735.
- (149) Yan, J.; Yoshikai, N. *ACS Catal.* **2016**, *6*, 3738–3742.
- (150) Yang, J.; Rérat, A.; Lim, Y. J.; Gosmini, C.; Yoshikai, N. *Angew. Chem. Int. Ed.* **2017**, *56*, 2449–2453.
- (151) Graniti, A. *Annu. Rev. Phytopathol.* **1998**, *36*, 91–114.
- (152) James C. Sacchettini, C. Dale Poulter *Science* **1997**, *277*, 1788–1789.
- (153) Thomas J. Maimone; Phil S. Baran *Nat. Chem. Biol.* **2007**, *3*, 396–407.
- (154) Zhang, Q.; Catti, L.; Pleiss, J.; Tiefenbacher, K. *J. Am. Chem. Soc.* **2017**, *139*, 11482–11492.
- (155) Christianson, D. W. *Chem. Rev.* **2017**, *117*, 11570–11648.
- (156) Cane, D. E. *Chem. Rev.* **1990**, *90*, 1089–1103.
- (157) Sunahara, R. K.; Dessauer, C. W.; Gilman, A. G. *Annu. Rev. Pharmacol. Toxicol.* **1996**, *36*, 461–480.
- (158) Kimberly A. Lucas; Giovanni M. Pitari; Shiva Kazerounian; Inez Ruiz-Stewart; Jason Park; Stephanie Schulz; Kenneth P. Chepenik; Scott A. Waldman *Pharmacol. Rev.* **2000**, *52*, 375–413.

- (159) Bryan Greenhagen, J. C. *Proc. Natl. Acad. Sci. U.S.A.* **2001**, *98*, 13479–13481.
- (160) Xiong, W.; Fu, J.; Köllner, T. G.; Chen, X.; Jia, Q.; Guo, H.; Qian, P.; Guo, H.; Wu, G.; Chen, F. *Phytochemistry* **2018**, *149*, 116–122.
- (161) Corkey, B. K.; Toste, F. D. *J. Am. Chem. Soc.* **2005**, *127*, 17168–17169.
- (162) Johansson, M. J.; Gorin, D. J.; Staben, S. T.; Toste, F. D. *J. Am. Chem. Soc.* **2005**, *127*, 18002–18003.
- (163) Luzung, M. R.; Mauleón, P.; Toste, F. D. *J. Am. Chem. Soc.* **2007**, *129*, 12402–12403.
- (164) Melhado, A. D.; Luparia, M.; Toste, F. D. *J. Am. Chem. Soc.* **2007**, *129*, 12638–12639.
- (165) Watson, I. D. G.; Ritter, S.; Toste, F. D. *J. Am. Chem. Soc.* **2009**, *131*, 2056–2057.
- (166) Hatakeyama, T.; Hashimoto, T.; Kondo, Y.; Fujiwara, Y.; Seike, H.; Takaya, H.; Tamada, Y.; Ono, T.; Nakamura, M. *J. Am. Chem. Soc.* **2010**, *132*, 10674–10676.
- (167) Zhu, S.; Niljianskul, N.; Buchwald, S. L. *J. Am. Chem. Soc.* **2013**, *135*, 15746–15749.
- (168) Cooper, P.; Crisenza, G. E. M.; Feron, L. J.; Bower, J. F. *Angew. Chem. Int. Ed.* **2018**, *57*, 14198–14202.
- (169) Cheng, L.; Li, M.-M.; Xiao, L.-J.; Xie, J.-H.; Zhou, Q.-L. *J. Am. Chem. Soc.* **2018**, *140*, 11627–11630.
- (170) Ling, F.; Nian, S.; Chen, J.; Luo, W.; Wang, Z.; Lv, Y.; Zhong, W. *J. Org. Chem.* **2018**, *83*, 10749–10761.
- (171) Liu, Y.; Fiorito, D.; Mazet, C. *Chem. Sci.* **2018**, *9*, 5284–5288.
- (172) You, C.; Li, S.; Li, X.; Lan, J.; Yang, Y.; Chung, L. W.; Lv, H.; Zhang, X. *J. Am. Chem. Soc.* **2018**, *140*, 4977–4981.
- (173) Che, W.; Li, Y.-Z.; Liu, J.-C.; Zhu, S.-F.; Xie, J.-H.; Zhou, Q.-L. *Org. Lett.* **2019**, *21*, 2369–2373.

- (174) Che, W.; Wen, D. C.; Zhu, S.-.-F.; Zhou, Q.-.-L. *HCA* **2019**, *102*, e1900023.
- (175) Dai, X.-J.; Engl, O. D.; León, T.; Buchwald, S. L. *Angew. Chem. Int. Ed.* **2019**, *58*, 3407–3411.
- (176) Kennington, S. C. D.; Taylor, A. J.; Romea, P.; Urpí, F.; Aullón, G.; Font-Bardia, M.; Ferré, L.; Rodrialvarez, J. *Org. Lett.* **2019**, *21*, 305–309.
- (177) Csermely, P.; Palotai, R.; Nussinov, R. *Trends Biochem. Sci.* **2010**, *35*, 539–546.
- (178) Vogt, A. D.; Di Cera, E. *Biochemistry* **2012**, *51*, 5894–5902.
- (179) Gianni, S.; Dogan, J.; Jemth, P. *Biophys. Chem.* **2014**, *189*, 33–39.
- (180) Stank, A.; Kokh, D. B.; Fuller, J. C.; Wade, R. C. *Acc. Chem. Res.* **2016**, *49*, 809–815.
- (181) Baer, P.; Rabe, P.; Fischer, K.; Citron, C. A.; Klapschinski, T. A.; Groll, M.; Dickschat, J. S. *Angew. Chem. Int. Ed.* **2014**, *53*, 7652–7656.
- (182) Mustard, T. J. L.; Wender, P. A.; Cheong, P. H.-Y. *ACS Catal.* **2015**, *5*, 1758–1763.
- (183) Jack Halpern *Science* **1982**, *217*, 401–407.
- (184) Clark R. Landis; Jack Halpern *J. Am. Chem. Soc.* **1987**, *109*, 1746–1754.
- (185) Clark R. Landis; Steven Feldgus *Angew. Chem. Int. Ed.* **2000**, *39*, 2863–2866.
- (186) Mori, S.; Vreven, T.; Morokuma, K. *Chem. Asian J.* **2006**, *1*, 391–403.
- (187) Robles, V. M.; Dürrenberger, M.; Heinisch, T.; Lledós, A.; Schirmer, T.; Ward, T. R.; Maréchal, J.-D. *J. Am. Chem. Soc.* **2014**, *136*, 15676–15683.
- (188) Zhang, X.; Chung, L. W.; Wu, Y.-D. *Acc. Chem. Res.* **2016**, *49*, 1302–1310.
- (189) Sakai, K.; Ide, J.; Oda, O.; Nakamura, N. *Tetrahedron Lett.* **1972**, *13*, 1287–1290.
- (190) Larock, R., C.; Oertle, K.; Potter, G., F. *J. Am. Chem. Soc.* **1980**, *102*, 190–197.
- (191) Milstein, D. *J. Chem. Soc. Chem. Commun.* **1982**, 1357.
- (192) Fairlie, D.; Bosnich, B. *Organometallics* **1988**, *7*, 936–945.

- (193) Fairlie, D.; Bosnich, B. *Organometallics* **1988**, *7*, 946–954.
- (194) McPherson, K. E.; Bartolotti, L. J.; Morehead, A. T.; Sargent, A. L. *Organometallics* **2016**, *35*, 1861–1865.
- (195) Nishio, M.; Hirota, M. *Tetrahedron* **1989**, *45*, 7201–7245.
- (196) Nishio, M.; Umezawa, Y.; Hirota, M.; Takeuchi, Y. *Tetrahedron* **1995**, *51*, 8665–8701.
- (197) Nishio, M. *CrystEngComm* **2004**, *6*, 130.
- (198) Nishio, M. *Tetrahedron* **2005**, *61*, 6923–6950.
- (199) Hobza, P. *Phys. Chem. Chem. Phys.* **2008**, *10*, 2581–2583.
- (200) Nishio, M.; Umezawa, Y.; Honda, K.; Tsuboyama, S.; Suezawa, H. *CrystEngComm* **2009**, *11*, 1757.
- (201) Nishio, M. *Phys. Chem. Chem. Phys.* **2011**, *13*, 13873–13900.
- (202) Nishio, M.; Umezawa, Y.; Fantini, J.; Weiss, M. S.; Chakrabarti, P. *Phys. Chem. Chem. Phys.* **2014**, *16*, 12648–12683.
- (203) Morokuma, K. *J. Chem. Phys.* **1971**, *55*, 1236–1244.
- (204) Bickelhaupt, F. M. *J. Comput. Chem.* **1999**, *20*, 114–128.
- (205) Ess, D. H.; Houk, K. N. *J. Am. Chem. Soc.* **2007**, *129*, 10646–10647.
- (206) Ess, D. H.; Houk, K. N. *J. Am. Chem. Soc.* **2008**, *130*, 10187–10198.
- (207) Fernández, I.; Bickelhaupt, F. M. *Chem. Soc. Rev.* **2014**, *43*, 4953–4967.
- (208) Wolters, L. P.; Bickelhaupt, F. M. *WIREs Comput Mol Sci* **2015**, *5*, 324–343.
- (209) Bickelhaupt, F. M.; Houk, K. N. *Angew. Chem. Int. Ed.* **2017**, *56*, 10070–10086.
- (210) Krenske, E. H.; Houk, K. N. *Acc. Chem. Res.* **2013**, *46*, 979–989.
- (211) Sandro Mecozzi; Anthony P. West, Jr., Dennis A. Dougherty *Proc. Natl. Acad. Sci. U.S.A.* **1996**, *93*, 10566–10571.
- (212) Zondlo, N. J. *Acc. Chem. Res.* **2013**, *46*, 1039–1049.

- (213) Vladimir B. Birman, Arnold L. Rheingold and Kin-Chung Lam *Tetrahedron: Asymmetry* **1999**, *10*, 125–131.
- (214) Xie, J.-H.; Wang, L.-X.; Fu, Y.; Zhu, S.-F.; Fan, B.-M.; Duan, H.-F.; Zhou, Q.-L. *J. Am. Chem. Soc.* **2003**, *125*, 4404–4405.
- (215) Zheng, Z.; Cao, Y.; Chong, Q.; Han, Z.; Ding, J.; Luo, C.; Wang, Z.; Zhu, D.; Zhou, Q.-L.; Ding, K. *J. Am. Chem. Soc.* **2018**, *140*, 10374–10381.
- (216) *Phosphorus(III) Ligands in Homogeneous Catalysis: Design and Synthesis*; Paul C. J. Kamer, Piet W. N. M. van Leeuwen, Eds.; Wiley: West Sussex, 2012.
- (217) G. I. Mackay; H. I. Schiff; D. K. Bohme *Can. J. Chem.* **1981**, *59*, 1771–1778.
- (218) L. I. Yeh; J. M. Price; and Yuan T. Lee *J. Am. Chem. Soc.* **1989**, *111*, 5597–5604.
- (219) Margaret French; Paul Kebarle *Can. J. Chem.* **1975**, *53*, 2268–2267.
- (220) Shigeki Obata; Kimihiko Hirao *Bull. Chem. Soc. Jpn.* **1993**, *66*, 3271–3282.
- (221) Shuang-Ling Chong and J. L. Franklin *J. Am. Chem. Soc.* **1972**, *94*, 6347–6351.
- (222) Knowles, R. R.; Jacobsen, E. N. *Proc. Natl. Acad. Sci. U.S.A.* **2010**, *107*, 20678–20685.
- (223) Lin, S.; Jacobsen, E. N. *Nat. Chem.* **2012**, *4*, 817–824.
- (224) Lu, G.; Liu, R. Y.; Yang, Y.; Fang, C.; Lambrecht, D. S.; Buchwald, S. L.; Liu, P. *J. Am. Chem. Soc.* **2017**, *139*, 16548–16555.
- (225) Neel, A. J.; Hilton, M. J.; Sigman, M. S.; Toste, F. D. *Nature* **2017**, *543*, 637–646.
- (226) Wheeler, S. E.; Seguin, T. J.; Guan, Y.; Doney, A. C. *Acc. Chem. Res.* **2016**, *49*, 1061–1069.
- (227) Halton, B. *Chem. Rev.* **1989**, *89*, 1161–1185.
- (228) Halton, B. *Chem. Rev.* **2003**, *103*, 1327–1369.
- (229) Halton, B. *Chem. Rec.* **2014**, *14*, 726–739.

- (230) Bradsher, C. K.; Hunt, D. A. *J. Org. Chem.* **1981**, *46*, 4608–4610.
- (231) Yoshinori, K.; Masahiko, I.; Masaji, O. *Tetrahedron Lett.* **1983**, *24*, 1727–1730.
- (232) Masahiko, I.; Tetsuhiro, Y.; Masaji, O. *J. Chem. Soc. Chem. Commun.* **1986**, 303–304.
- (233) Buchwald, S. L.; Lucas, E. A.; Dewan, J. C. *J. Am. Chem. Soc.* **1987**, *109*, 4396–4397.
- (234) Sadana, A. K.; Saini, R. K.; Billups, W. E. *Chem. Rev.* **2003**, *103*, 1539–1602.
- (235) Arisawa, T.; Hamura, T.; Uekusa, H.; Matsumoto, T.; Suzuki, K. *Synlett* **2008**, *2008*, 1179–1184.
- (236) Horst K., N. *Monatsh. Chem.* **1987**, *118*, 627–657.
- (237) Zysman-Colman, E.; Arias, K.; Siegel, J. S. *Can. J. Chem.* **2009**, *87*, 440–447.
- (238) Neese, F. *WIREs Comput Mol Sci* **2012**, *2*, 73–78.
- (239) TURBOMOLE V7.2 2017, a development of University of Karlsruhe and Forschungszentrum Karlsruhe GmbH, 1989-2007, TURBOMOLE GmbH, since 2007; available from <http://www.turbomole.com>.
- (240) Tao, J.; Perdew, J. P.; Staroverov, V. N.; Scuseria, G. E. *Phys. Rev. Lett.* **2003**, *91*, 146401.
- (241) Weigend, F.; Ahlrichs, R. *Phys. Chem. Chem. Phys.* **2005**, *7*, 3297–3305.
- (242) Grimme, S.; Ehrlich, S.; Goerigk, L. *J. Comput. Chem.* **2011**, *32*, 1456–1465.
- (243) Grimme, S.; Antony, J.; Ehrlich, S.; Krieg, H. *J. Chem. Phys.* **2010**, *132*, 154104.
- (244) Karin Eichkorn; Oliver Treutler; Holger Öhm; Marco Häser; Reinhart Ahlrichs *Chem. Phys. Lett.* **1995**, *240*, 283–290.
- (245) Sierka, M.; Hogekamp, A.; Ahlrichs, R. *J. Chem. Phys.* **2003**, *118*, 9136–9148.
- (246) Weigend, F. *Phys. Chem. Chem. Phys.* **2006**, *8*, 1057–1065.

- (247) CYLview, 1.0b, C.Y., Legault. Université de Sherbrooke, 2009.
- (248) Goerigk, L.; Grimme, S. *Phys. Chem. Chem. Phys.* **2011**, *13*, 6670–6688.
- (249) Fernández, I.; Bickelhaupt, F. M.; Cossío, F. P. *Chemistry* **2012**, *18*, 12395–12403.
- (250) Fernández, I.; Bickelhaupt, F. M.; Cossío, F. P. *Chemistry* **2014**, *20*, 10791–10801.
- (251) Fernández, I.; Cossío, F. P.; Sierra, M. A. *Chem. Rev.* **2009**, *109*, 6687–6711.
- (252) Halliwell, B.; Gutteridge, J. M. *Meth. Enzymol.* **1990**, *186*, 1–85.
- (253) Cadenas, E.; Davies, K. J. *Free Radical Biol. Med.* **2000**, *29*, 222–230.
- (254) Dröge, W. *Physiol. Rev.* **2002**, *82*, 47–95.
- (255) Valko, M.; Leibfritz, D.; Moncol, J.; Cronin, M. T. D.; Mazur, M.; Telser, J. *Int. J. Biochem. Cell Biol.* **2007**, *39*, 44–84.
- (256) Ghosh, I.; Ghosh, T.; Bardagi, J. I.; König, B. *Science* **2014**, *346*, 725–728.
- (257) Lo, J. C.; Gui, J.; Yabe, Y.; Pan, C.-M.; Baran, P. S. *Nature* **2014**, *516*, 343–348.
- (258) Gui, J.; Pan, C.-M.; Jin, Y.; Qin, T.; Lo, J. C.; Lee, B. J.; Spergel, S. H.; Mertzman, M. E.; Pitts, W. J.; La Cruz, T. E.; Schmidt, M. A.; Darvatkar, N.; Natarajan, S. R.; Baran, P. S. *Science* **2015**, *348*, 886–891.
- (259) Jeffrey, J. L.; Terrett, J. A.; MacMillan, D. W. C. *Science* **2015**, *349*, 1532–1536.
- (260) Müller, D. S.; Untiedt, N. L.; Dieskau, A. P.; Lackner, G. L.; Overman, L. E. *J. Am. Chem. Soc.* **2015**, *137*, 660–663.
- (261) Nawrat, C. C.; Jamison, C. R.; Slutsky, Y.; MacMillan, D. W. C.; Overman, L. E. *J. Am. Chem. Soc.* **2015**, *137*, 11270–11273.
- (262) Brill, Z. G.; Grover, H. K.; Maimone, T. J. *Science* **2016**, *352*, 1078–1082.
- (263) Choi, G. J.; Zhu, Q.; Miller, D. C.; Gu, C. J.; Knowles, R. R. *Nature* **2016**, *539*, 268–271.

- (264) Murphy, J. J.; Bastida, D.; Paria, S.; Fagnoni, M.; Melchiorre, P. *Nature* **2016**, *532*, 218–222.
- (265) Yan, M.; Lo, J. C.; Edwards, J. T.; Baran, P. S. *J. Am. Chem. Soc.* **2016**, *138*, 12692–12714.
- (266) Musacchio, A. J.; Lainhart, B. C.; Zhang, X.; Naguib, S. G.; Sherwood, T. C.; Knowles, R. R. *Science* **2017**, *355*, 727–730.
- (267) Kalyani, D.; McMurtrey, K. B.; Neufeldt, S. R.; Sanford, M. S. *J. Am. Chem. Soc.* **2011**, *133*, 18566–18569.
- (268) Biswas, S.; Weix, D. J. *J. Am. Chem. Soc.* **2013**, *135*, 16192–16197.
- (269) Tellis, J. C.; Primer, D. N.; Molander, G. A. *Science* **2014**, *345*, 433–436.
- (270) Zuo, Z.; Ahneman, D. T.; Chu, L.; Terrett, J. A.; Doyle, A. G.; MacMillan, D. W. C. *Science* **2014**, *345*, 437–440.
- (271) Green, S. A.; Matos, J. L. M.; Yagi, A.; Shenvi, R. A. *J. Am. Chem. Soc.* **2016**, *138*, 12779–12782.
- (272) Johnston, C. P.; Smith, R. T.; Allmendinger, S.; MacMillan, D. W. C. *Nature* **2016**, *536*, 322–325.
- (273) Shaw, M. H.; Shurtleff, V. W.; Terrett, J. A.; Cuthbertson, J. D.; MacMillan, D. W. C. *Science* **2016**, *352*, 1304–1308.
- (274) Shields, B. J.; Doyle, A. G. *J. Am. Chem. Soc.* **2016**, *138*, 12719–12722.
- (275) Zhang, W.; Wang, F.; McCann, S. D.; Wang, D.; Chen, P.; Stahl, S. S.; Liu, G. *Science* **2016**, *353*, 1014–1018.
- (276) Parsons, A. T.; Buchwald, S. L. *Angew. Chem. Int. Ed.* **2011**, *50*, 9120–9123.
- (277) Wang, X.; Ye, Y.; Zhang, S.; Feng, J.; Xu, Y.; Zhang, Y.; Wang, J. *J. Am. Chem. Soc.* **2011**, *133*, 16410–16413.

- (278) Xu, J.; Fu, Y.; Luo, D.-F.; Jiang, Y.-Y.; Xiao, B.; Liu, Z.-J.; Gong, T.-J.; Liu, L. *J. Am. Chem. Soc.* **2011**, *133*, 15300–15303.
- (279) Chu, L.; Qing, F.-L. *Org. Lett.* **2012**, *14*, 2106–2109.
- (280) Beniazza, R.; Molton, F.; Duboc, C.; Tron, A.; McClenaghan, N. D.; Lastécouères, D.; Vincent, J.-M. *Chem. Commun.* **2015**, *51*, 9571–9574.
- (281) Phipps, R. J.; McMurray, L.; Ritter, S.; Duong, H. A.; Gaunt, M. J. *J. Am. Chem. Soc.* **2012**, *134*, 10773–10776.
- (282) Liwosz, T. W.; Chemler, S. R. *J. Am. Chem. Soc.* **2012**, *134*, 2020–2023.
- (283) Liwosz, T. W.; Chemler, S. R. *Org. Lett.* **2013**, *15*, 3034–3037.
- (284) Bao, H.; Bayeh, L.; Tambar, U. K. *Angew. Chem. Int. Ed.* **2014**, *53*, 1664–1668.
- (285) Bovino, M. T.; Liwosz, T. W.; Kendel, N. E.; Miller, Y.; Tyminska, N.; Zurek, E.; Chemler, S. R. *Angew. Chem. Int. Ed.* **2014**, *53*, 6383–6387.
- (286) Liu, D.; Liu, C.; Li, H.; Lei, A. *Chem. Commun.* **2014**, *50*, 3623–3626.
- (287) Zhu, Y.; Wei, Y. *Chem. Sci.* **2014**, *5*, 2379.
- (288) Z. Rappoport, *The Chemistry of the Cyano Group*; Wiley: London, 1970.
- (289) Fleming, F. F.; Wang, Q. *Chem. Rev.* **2003**, *103*, 2035–2077.
- (290) López, R.; Palomo, C. *Angew. Chem. Int. Ed.* **2015**, *54*, 13170–13184.
- (291) Guo, X.-X.; Gu, D.-W.; Wu, Z.; Zhang, W. *Chem. Rev.* **2015**, *115*, 1622–1651.
- (292) Miao, J.; Ge, H. *Eur. J. Org. Chem.* **2015**, *2015*, 7859–7868.
- (293) Hu, P.; Chai, J.; Duan, Y.; Liu, Z.; Cui, G.; Chen, L. *J. Mater. Chem. A* **2016**, *4*, 10070–10083.
- (294) Fleming, F. F. *Nat. Prod. Rep.* **1999**, *16*, 597–606.
- (295) Fleming, F. F.; Yao, L.; Ravikumar, P. C.; Funk, L.; Shook, B. C. *J. Med. Chem.* **2010**, *53*, 7902–7917.

- (296) Li, C.-J. *Acc. Chem. Res.* **2009**, *42*, 335–344.
- (297) Scheuermann, C. J. *Chem. Asian J.* **2010**, *5*, 436–451.
- (298) Liu, C.; Zhang, H.; Shi, W.; Lei, A. *Chem. Rev.* **2011**, *111*, 1780–1824.
- (299) Yeung, C. S.; Dong, V. M. *Chem. Rev.* **2011**, *111*, 1215–1292.
- (300) Li, B.-J.; Shi, Z.-J. *Chem. Soc. Rev.* **2012**, *41*, 5588–5598.
- (301) Girard, S. A.; Knauber, T.; Li, C.-J. *Angew. Chem. Int. Ed.* **2014**, *53*, 74–100.
- (302) Liu, Y.; Yang, K.; Ge, H. *Chem. Sci.* **2016**, *7*, 2804–2808.
- (303) Zhang, W.; Yang, S.; Shen, Z. *Adv. Synth. Catal.* **2016**, *358*, 2392–2397.
- (304) Bruno, J. W.; Marks, T. J.; Lewis, F. D. *J. Am. Chem. Soc.* **1981**, *103*, 3608–3609.
- (305) Bruno, J. W.; Marks, T. J.; Lewis, F. D. *J. Am. Chem. Soc.* **1982**, *104*, 5580–5585.
- (306) Sonawane, H. R.; Bellur, N. S.; Shah, V. G. *J. Chem. Soc. Chem. Commun.* **1990**, 1603.
- (307) Li, J.; Wang, Z.; Wu, N.; Gao, G.; You, J. *Chem. Commun.* **2014**, *50*, 15049–15051.
- (308) Bunescu, A.; Wang, Q.; Zhu, J. *Angew. Chem. Int. Ed.* **2015**, *54*, 3132–3135.
- (309) Bunescu, A.; Wang, Q.; Zhu, J. *Org. Lett.* **2015**, *17*, 1890–1893.
- (310) Chatalova-Sazepin, C.; Wang, Q.; Sammis, G. M.; Zhu, J. *Angew. Chem. Int. Ed.* **2015**, *54*, 5443–5446.
- (311) Chu, X.-Q.; Xu, X.-P.; Meng, H.; Ji, S.-J. *RSC Adv.* **2015**, *5*, 67829–67832.
- (312) Li, Z.; Xiao, Y.; Liu, Z.-Q. *Chem. Commun.* **2015**, *51*, 9969–9971.
- (313) Tang, S.; Zhou, D.; Li, Z.-H.; Fu, M.-J.; Jie, L.; Sheng, R.-L.; Li, S.-H. *Synthesis* **2015**, *47*, 1567–1580.
- (314) Ha, T. M.; Chatalova-Sazepin, C.; Wang, Q.; Zhu, J. *Angew. Chem. Int. Ed.* **2016**, *55*, 9249–9252.
- (315) Ha, T. M.; Wang, Q.; Zhu, J. *Chem. Commun.* **2016**, *52*, 11100–11103.

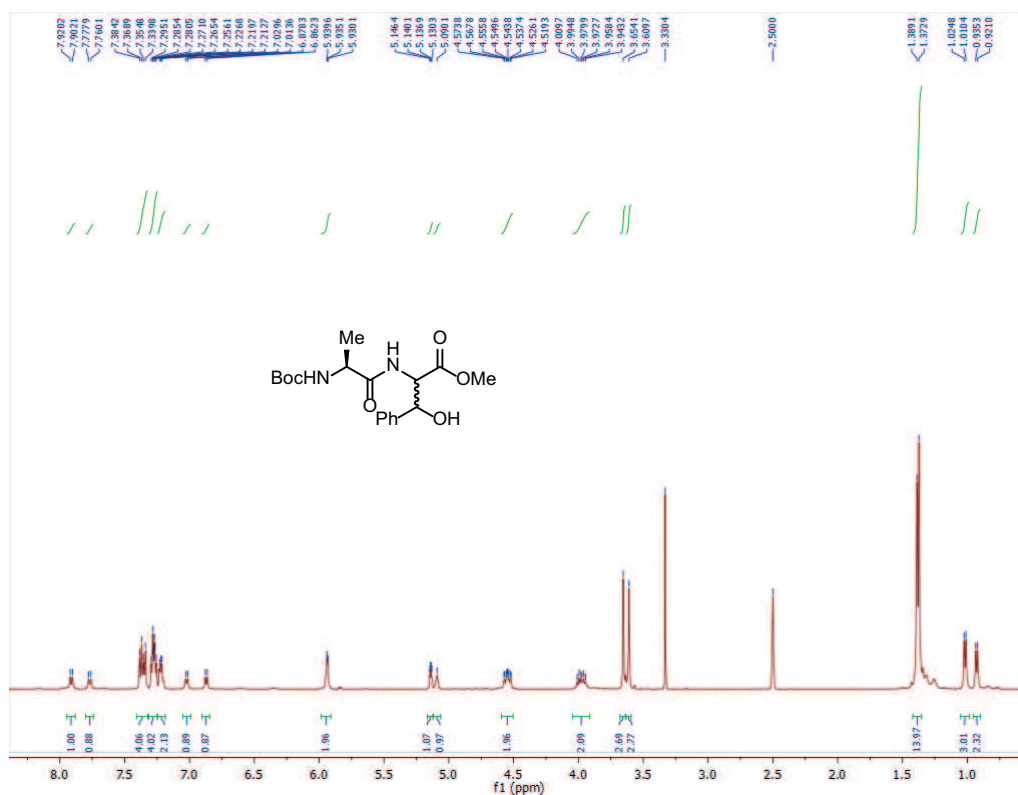
- (316) Liu, Y.-Y.; Yang, X.-H.; Song, R.-J.; Luo, S.; Li, J.-H. *Nat. Commun.* **2017**, *8*, 14720.
- (317) Kochi, J. K. *J. Am. Chem. Soc.* **1962**, *84*, 3271–3277.
- (318) Kochi, J. K.; Bemis, A.; Jenkins, C. L. *J. Am. Chem. Soc.* **1968**, *90*, 4616–4625.
- (319) Jenkins, C. L.; Kochi, J. K. *J. Am. Chem. Soc.* **1972**, *94*, 856–865.
- (320) Jenkins, C. L.; Kochi, J. K. *J. Am. Chem. Soc.* **1972**, *94*, 843–855.
- (321) Kochi, J. K. *Acc. Chem. Res.* **1974**, *7*, 351–360.
- (322) Liwosz, T. W.; Chemler, S. R. *Chemistry* **2013**, *19*, 12771–12777.
- (323) Xiong, P.; Xu, F.; Qian, X.-Y.; Yohannes, Y.; Song, J.; Lu, X.; Xu, H.-C. *Chemistry* **2016**, *22*, 4379–4383.
- (324) S. McDonald; M. Schulze; M. Peltz; D. Bolliet; L. Burroughs *Perfum. Flavor.* **2011**, *36*, 24.
- (325) Peter Schreier; Friedrich Drawer; Zolàn Kerènyi; Albrecht Junker *Z. Lebensm. Unters. Forsch.* **1974**, *155*, 342–347.
- (326) Lübke, M.; Guichard, E.; Tromelin, A.; Le Quéré, J. L. *J. Agric. Food Chem.* **2002**, *50*, 7094–7099.
- (327) Cardellina, J. H.; Dalietos, D.; Marner, F.-J.; Mynderse, J. S.; Moore, R. E. *Phytochemistry* **1978**, *17*, 2091–2095.
- (328) Gekwick, W. H.; Reyes, S.; Alvarado, B. *Phytochemistry* **1987**, *26*, 1701–1704.
- (329) Ameh Abel, G.; Oliver Nguyen, K.; Viamajala, S.; Varanasi, S.; Yamamoto, K. *RSC Adv.* **2014**, *4*, 55622–55628.
- (330) Whitmore, F. C. *J. Am. Chem. Soc.* **1932**, *54*, 3274–3283.
- (331) Bullock, R. M.; Headford, C. E. L.; Kegley, S. E.; Norton, J. R. *J. Am. Chem. Soc.* **1985**, *107*, 727–729.
- (332) Michelin, R. A.; Mozzon, M.; Bertani, R. *Coord. Chem. Rev.* **1996**, *147*, 299–338.

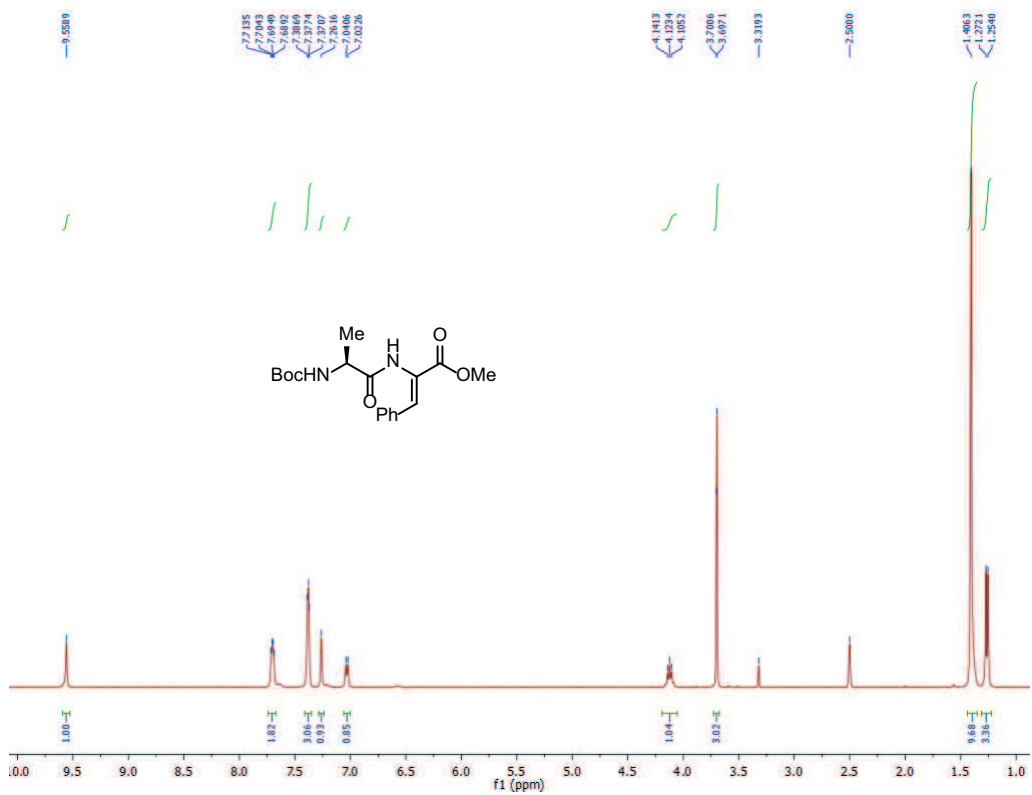
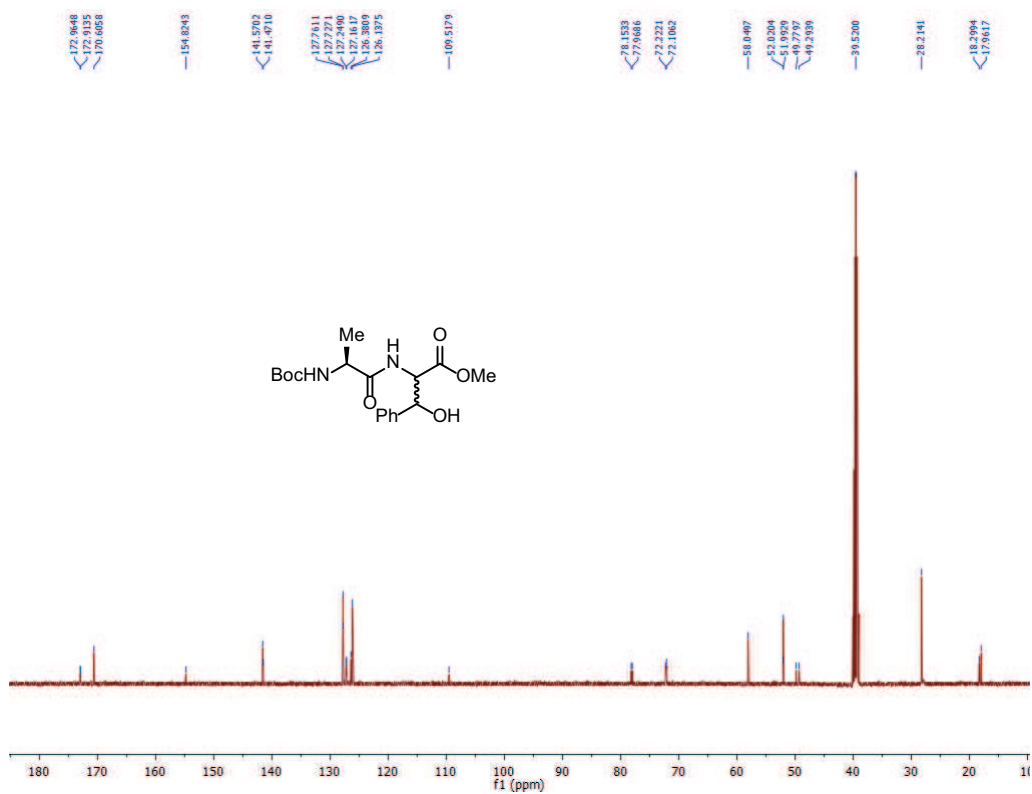
- (333) Wu, X.; Riedel, J.; Dong, V. M. *Angew. Chem. Int. Ed.* **2017**, *56*, 11589–11593.
- (334) Elsinghorst, P. W.; Tanarro, C. M. G.; Gütschow, M. *J. Med. Chem.* **2006**, *49*, 7540–7544.
- (335) Wang, Y.; Zhang, L.; Yang, Y.; Zhang, P.; Du, Z.; Wang, C. *J. Am. Chem. Soc.* **2013**, *135*, 18048–18051.

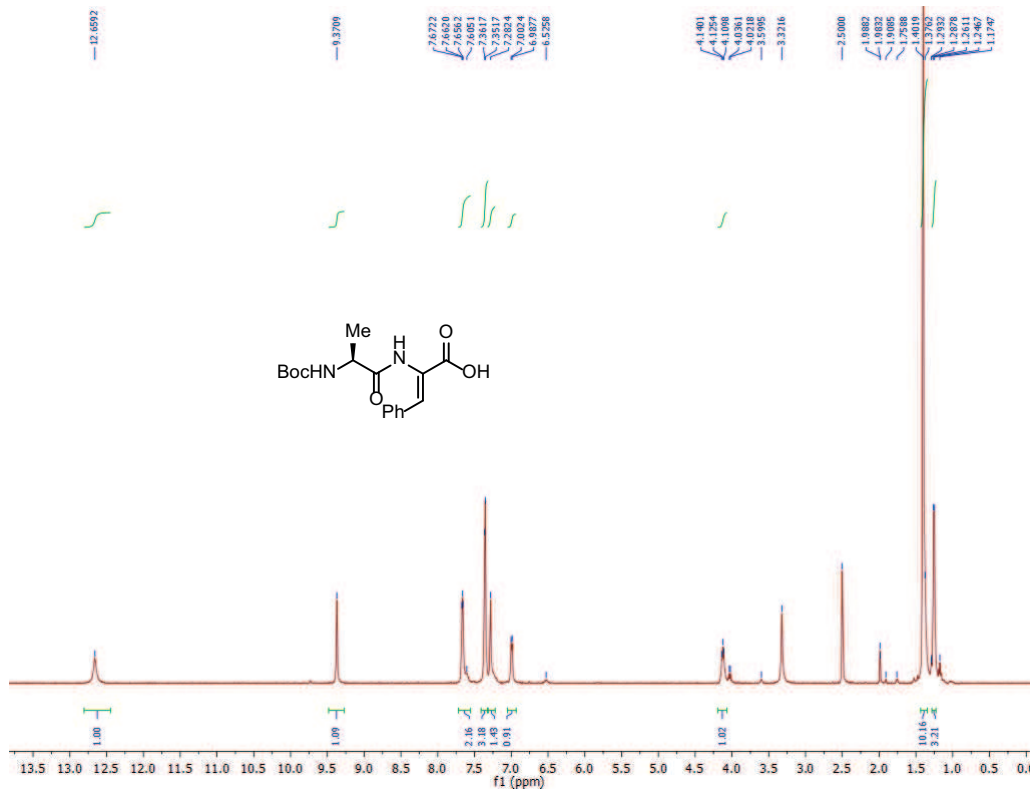
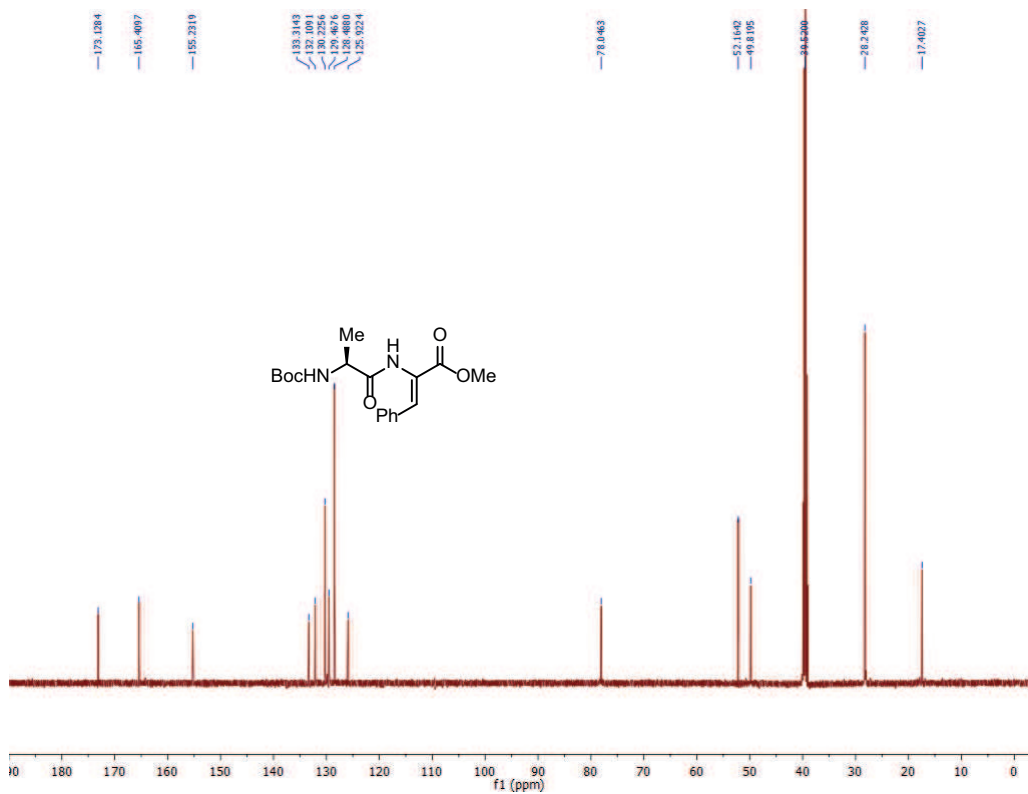
Appendix A

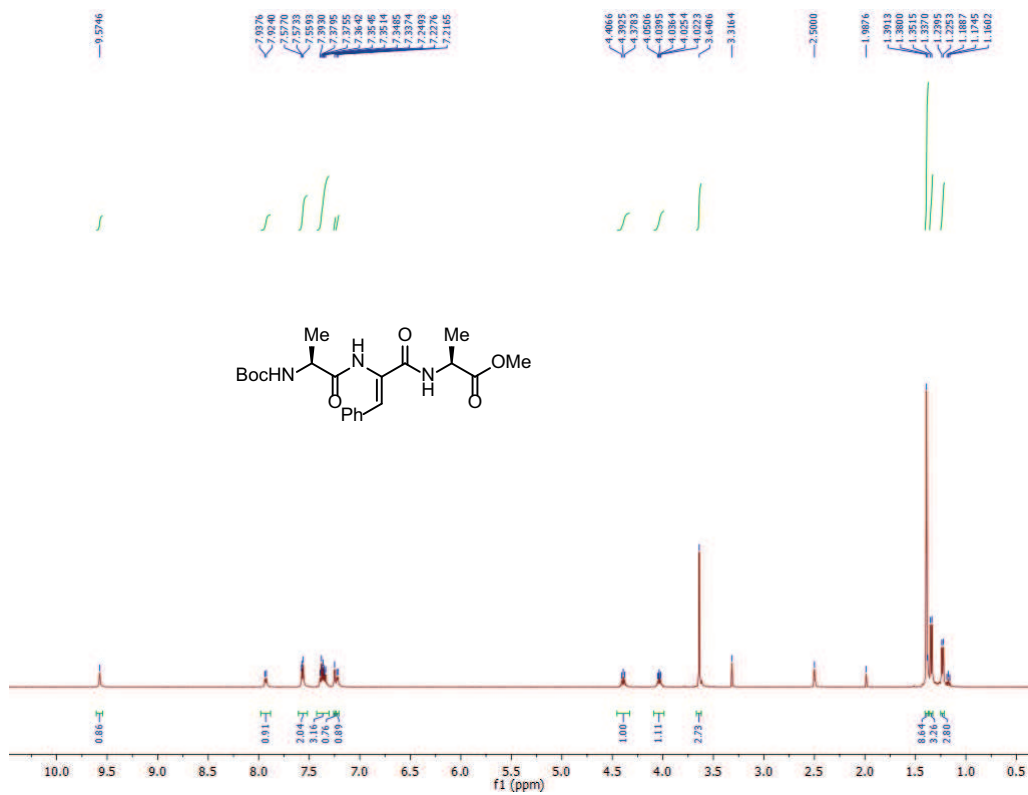
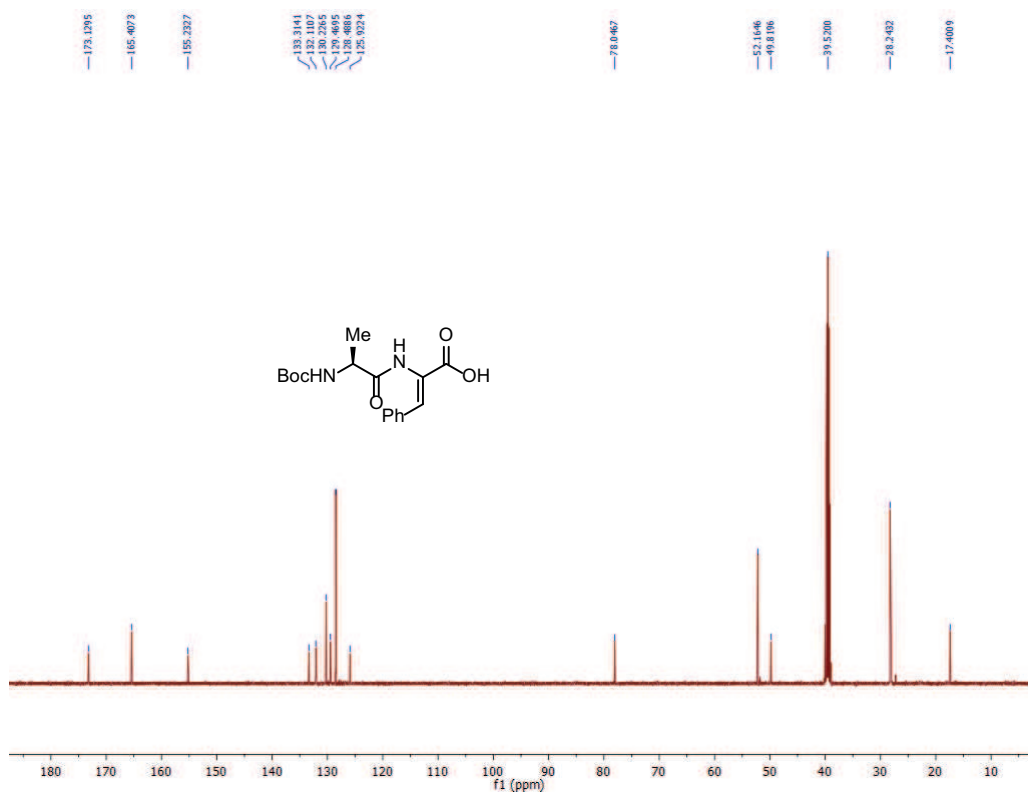
Supporting Information for Chapter 1

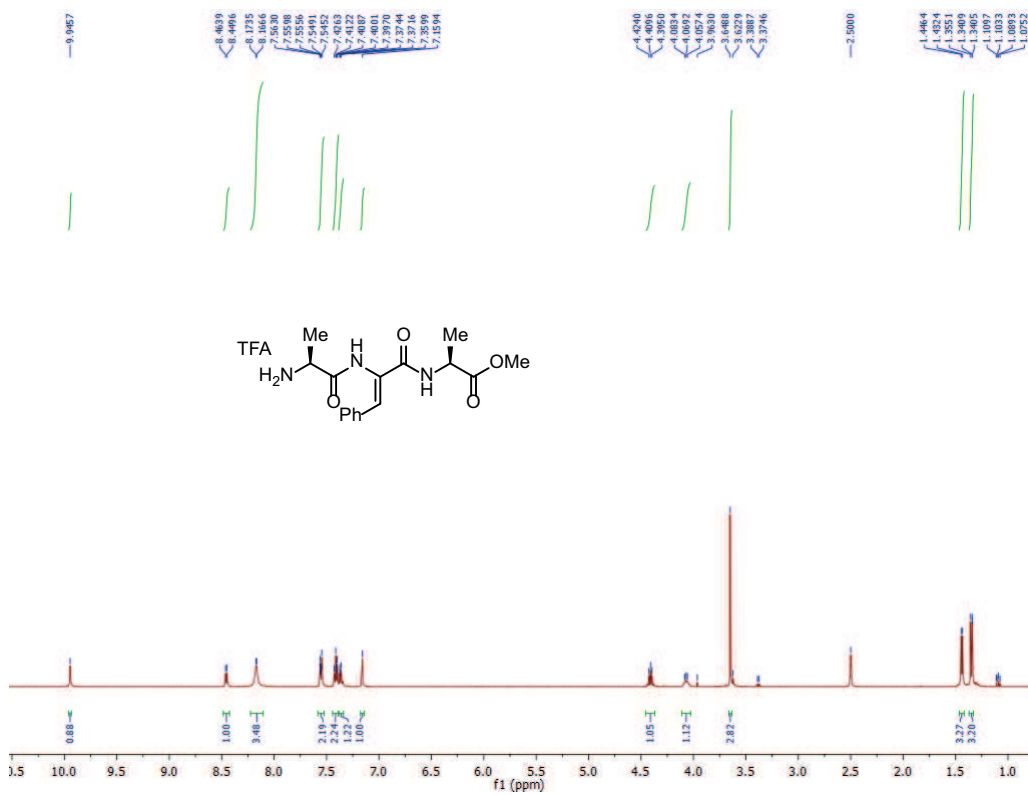
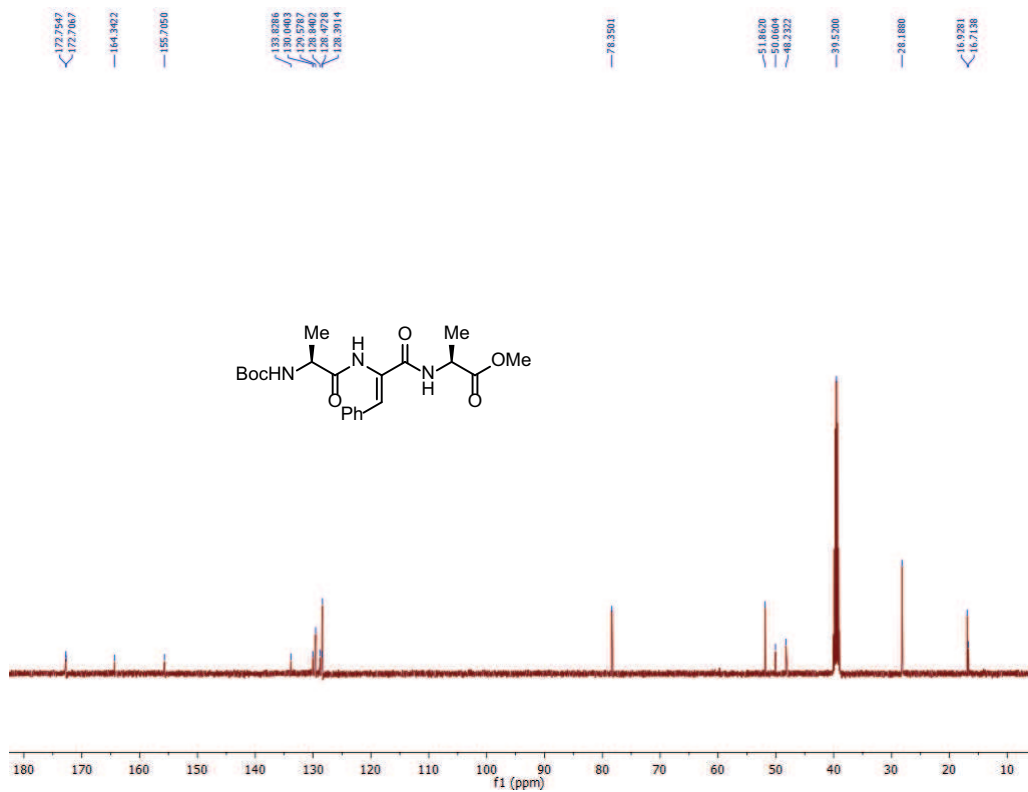
A.1 NMR Spectra

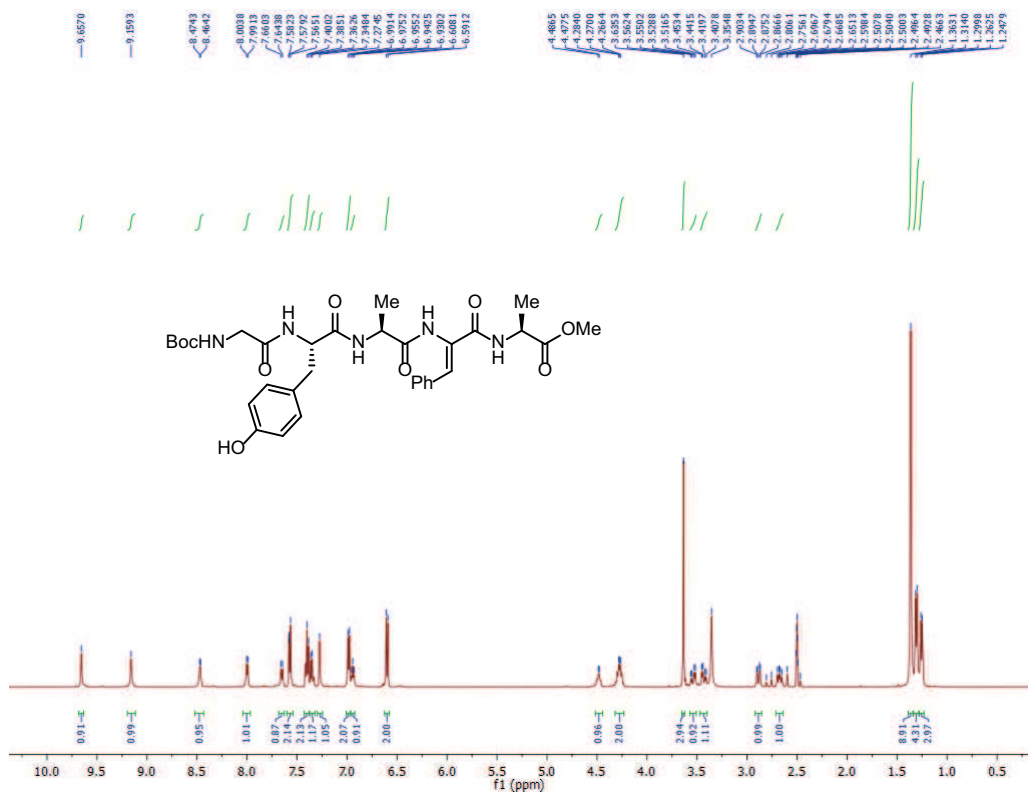
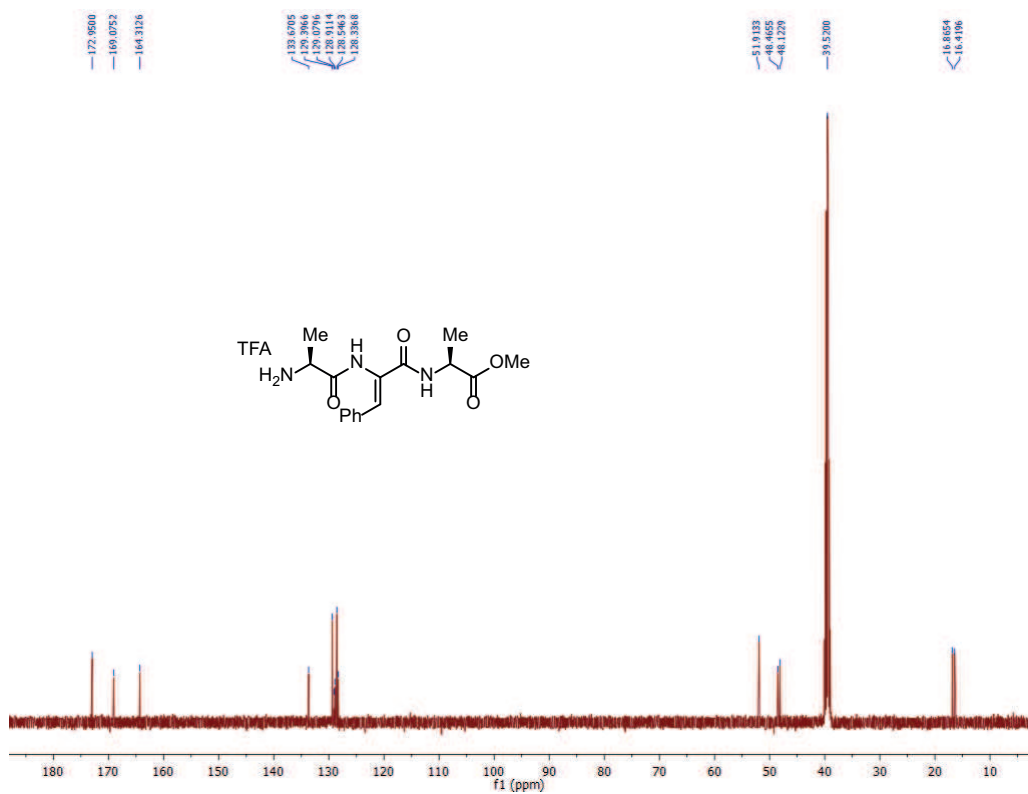


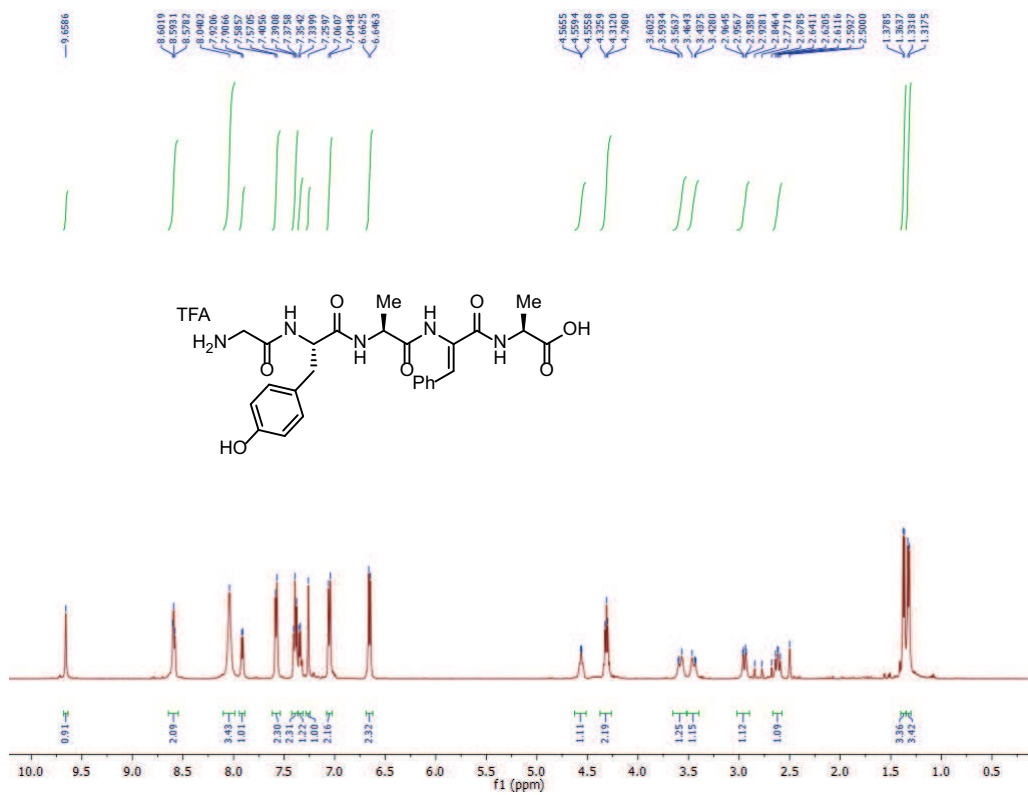
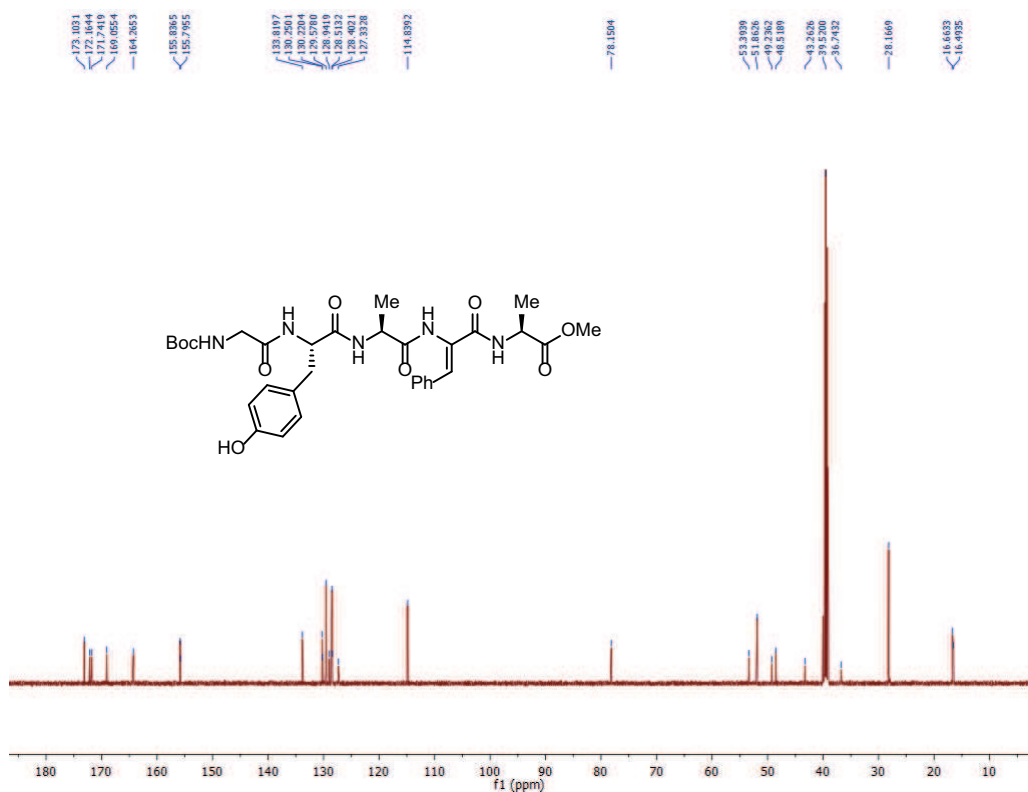


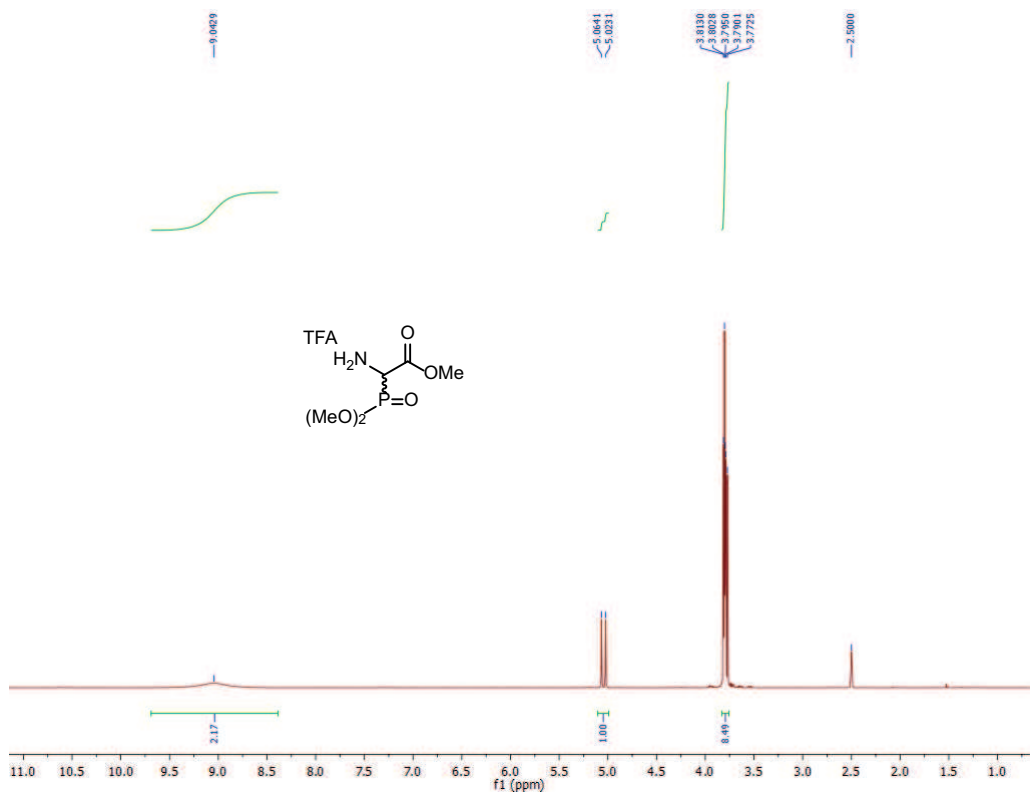
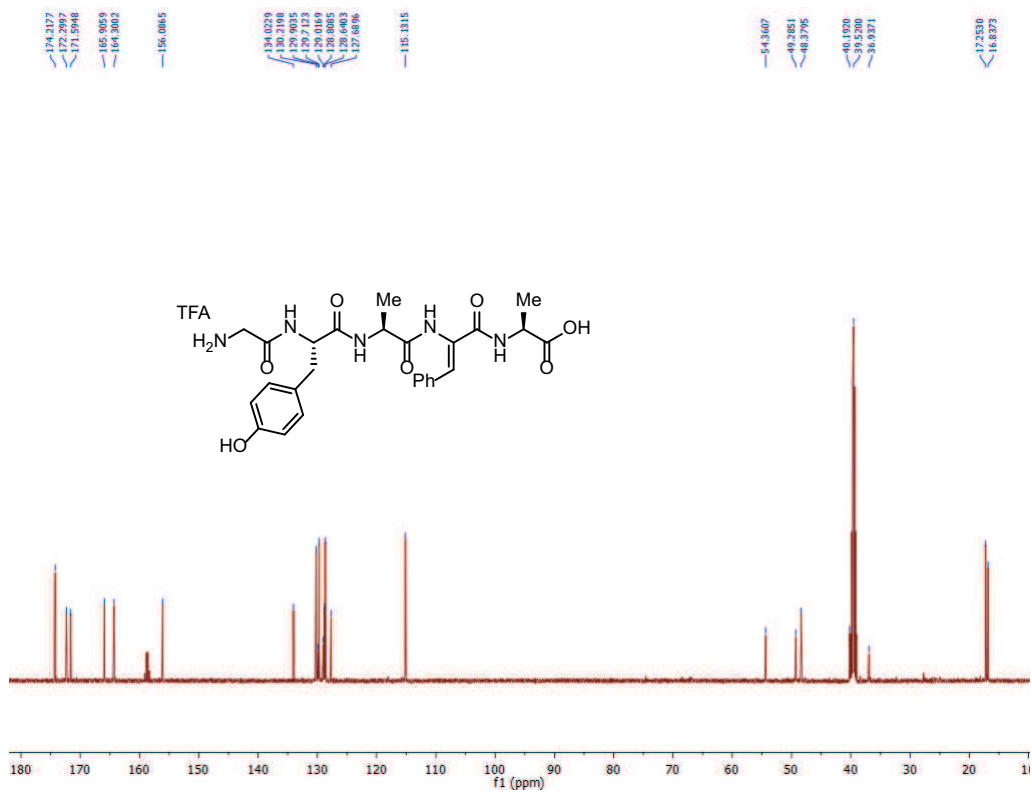


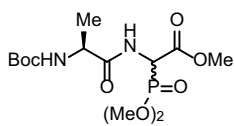
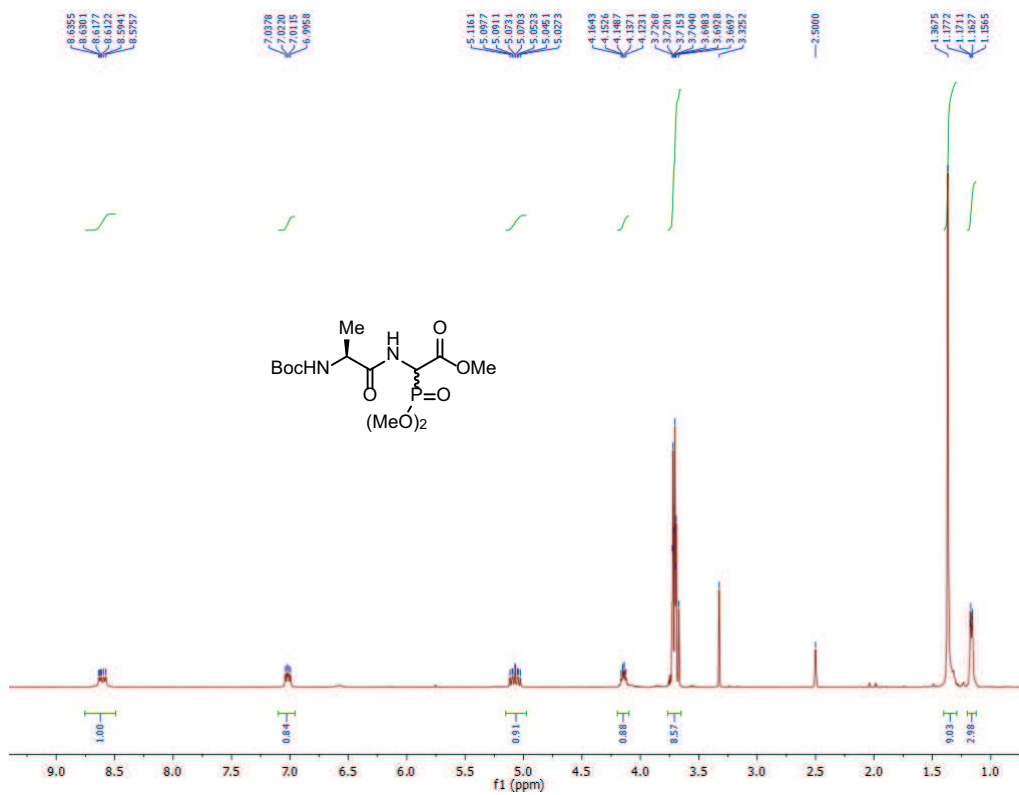
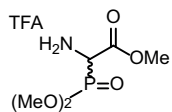
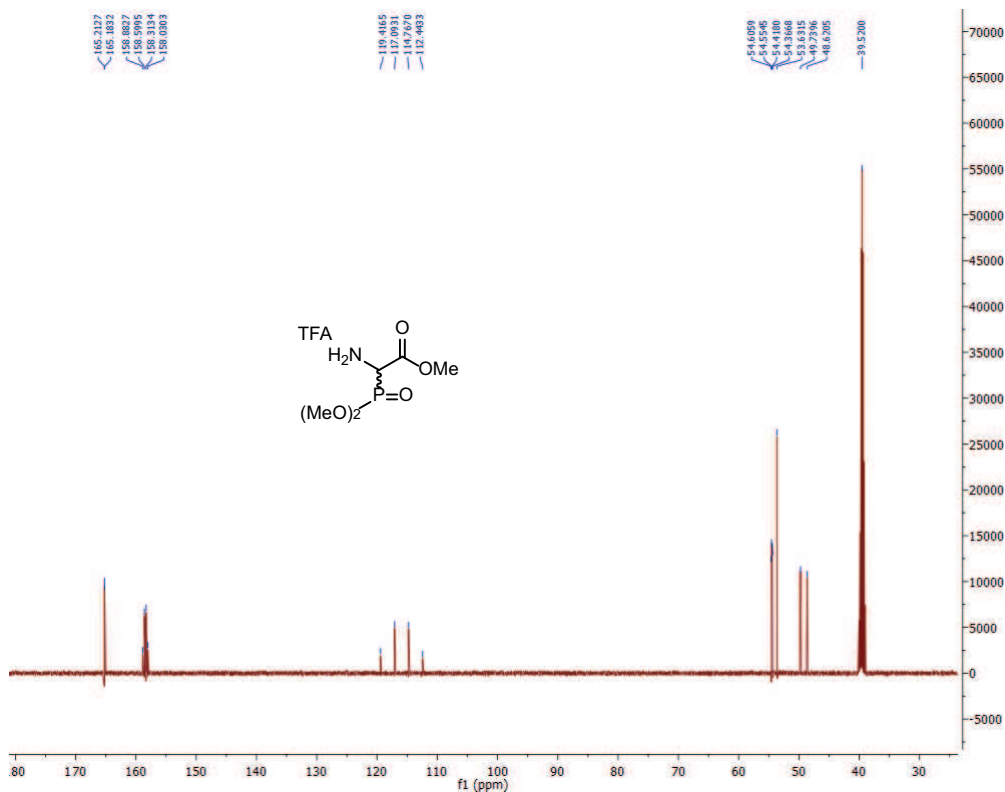


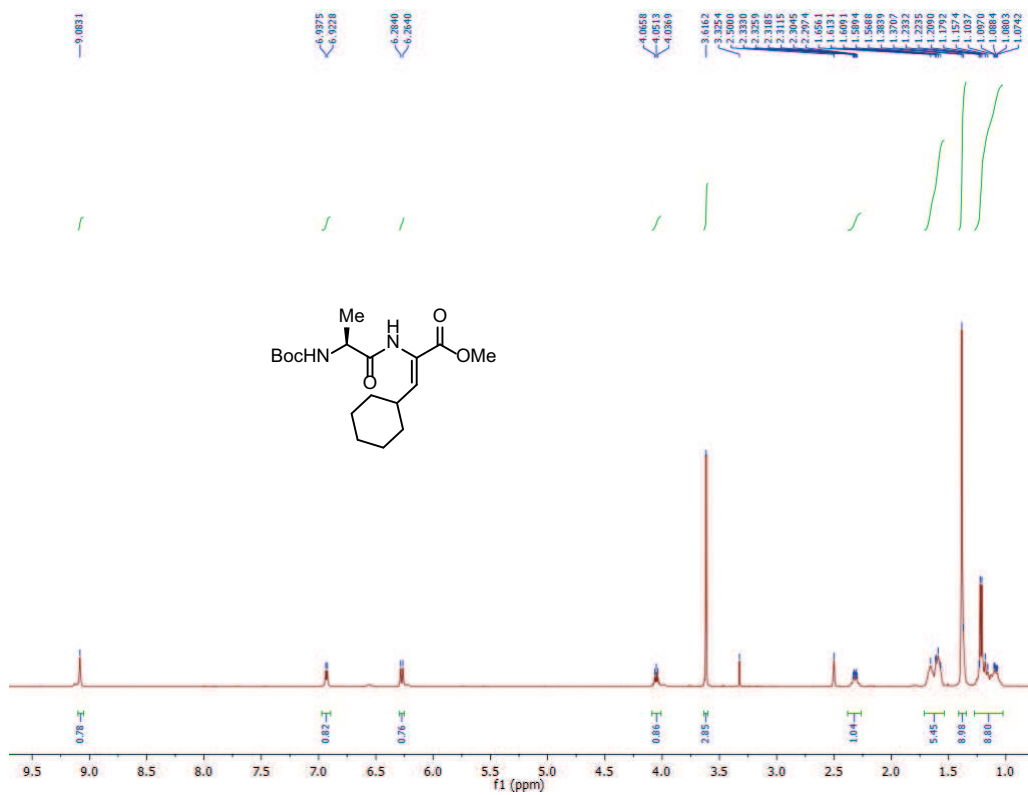
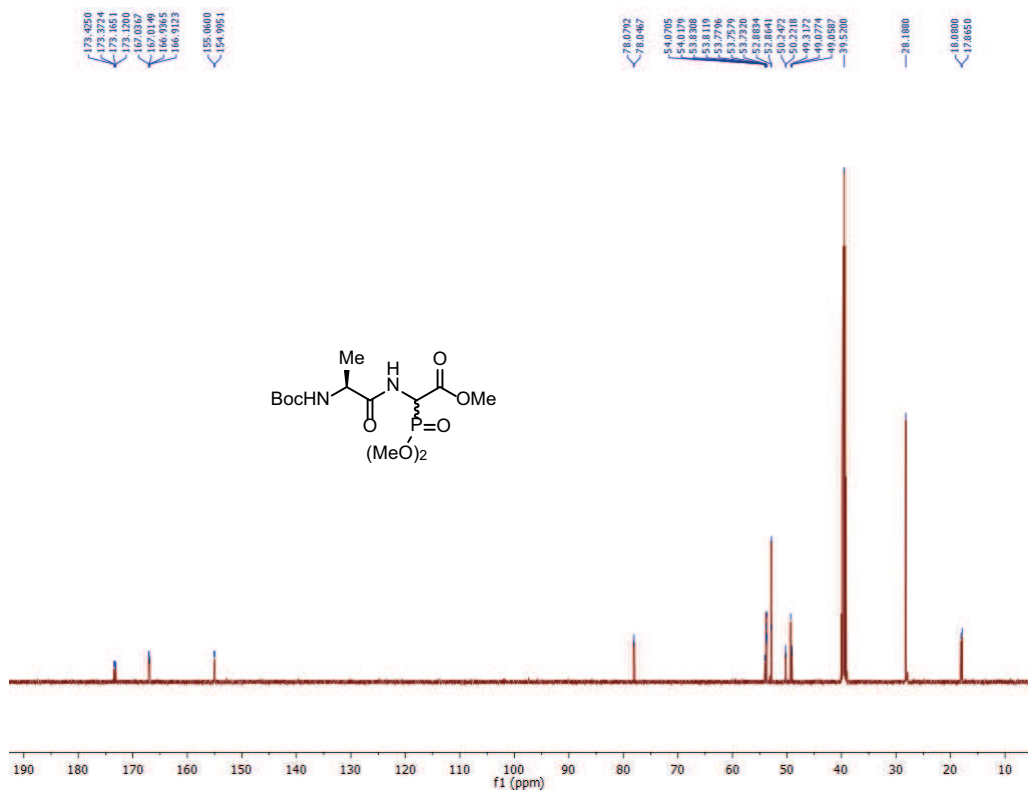


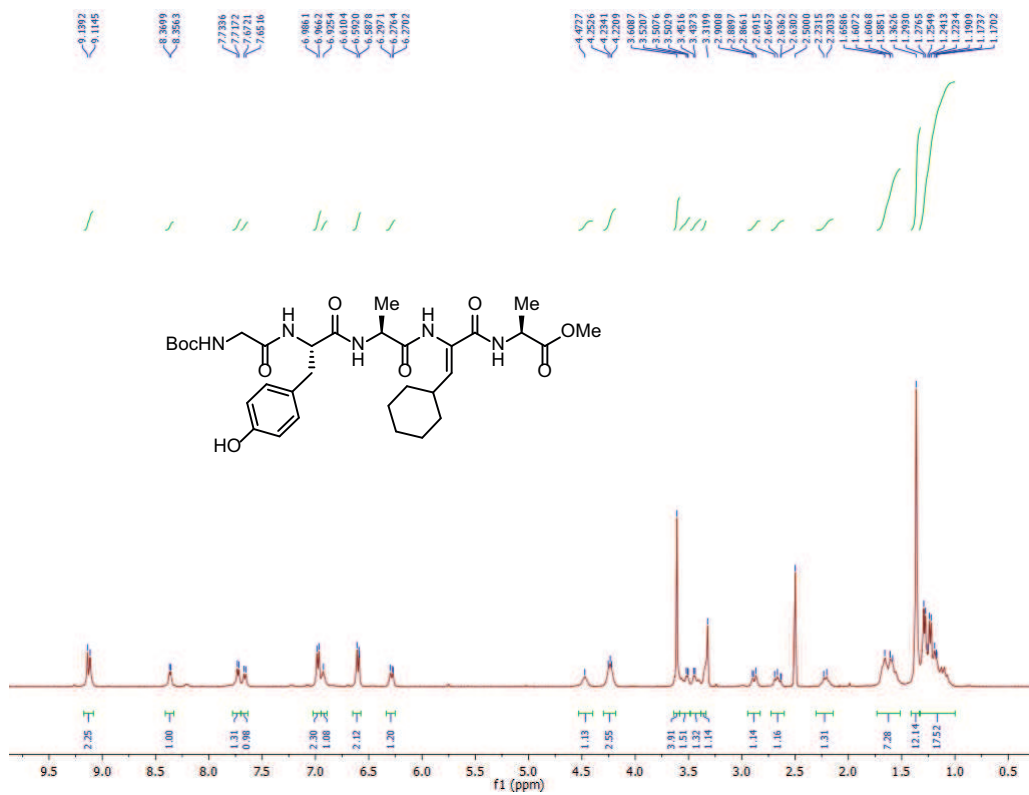
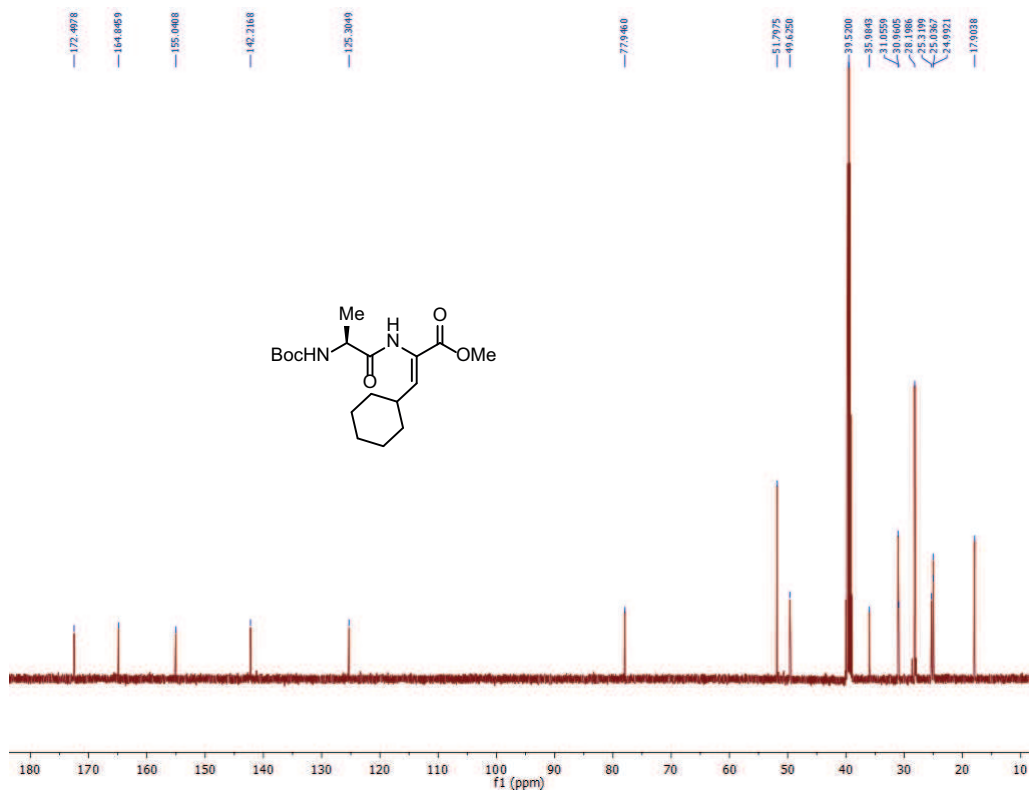








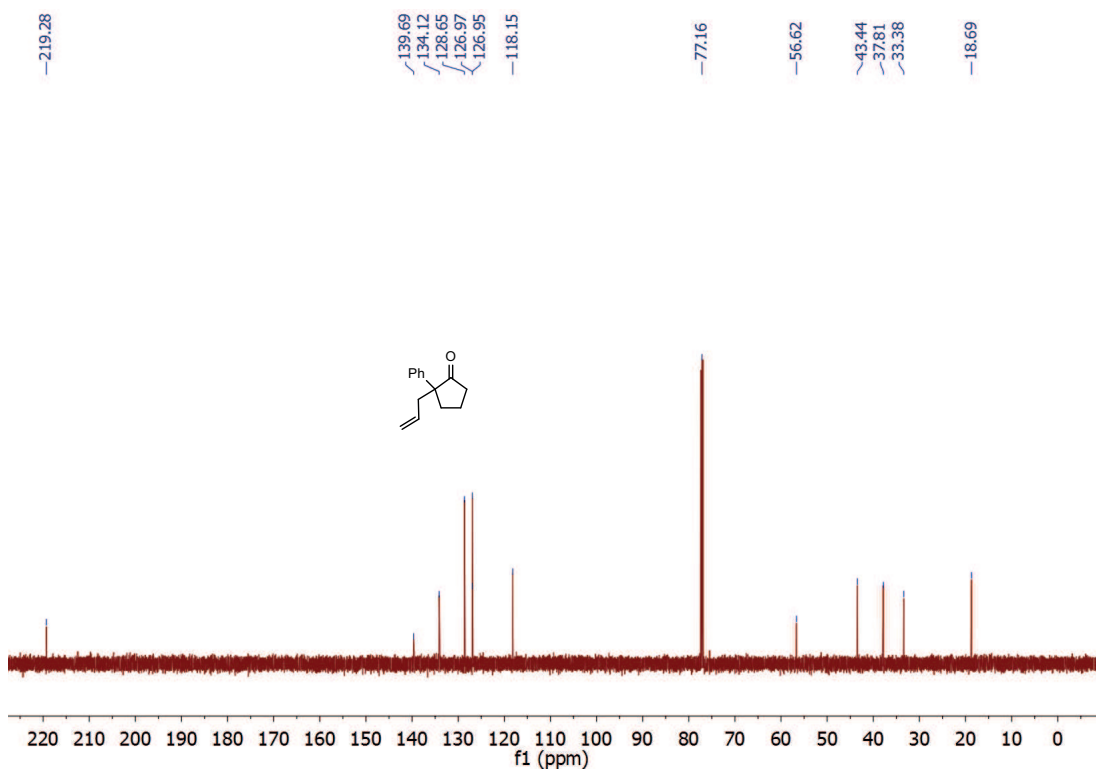
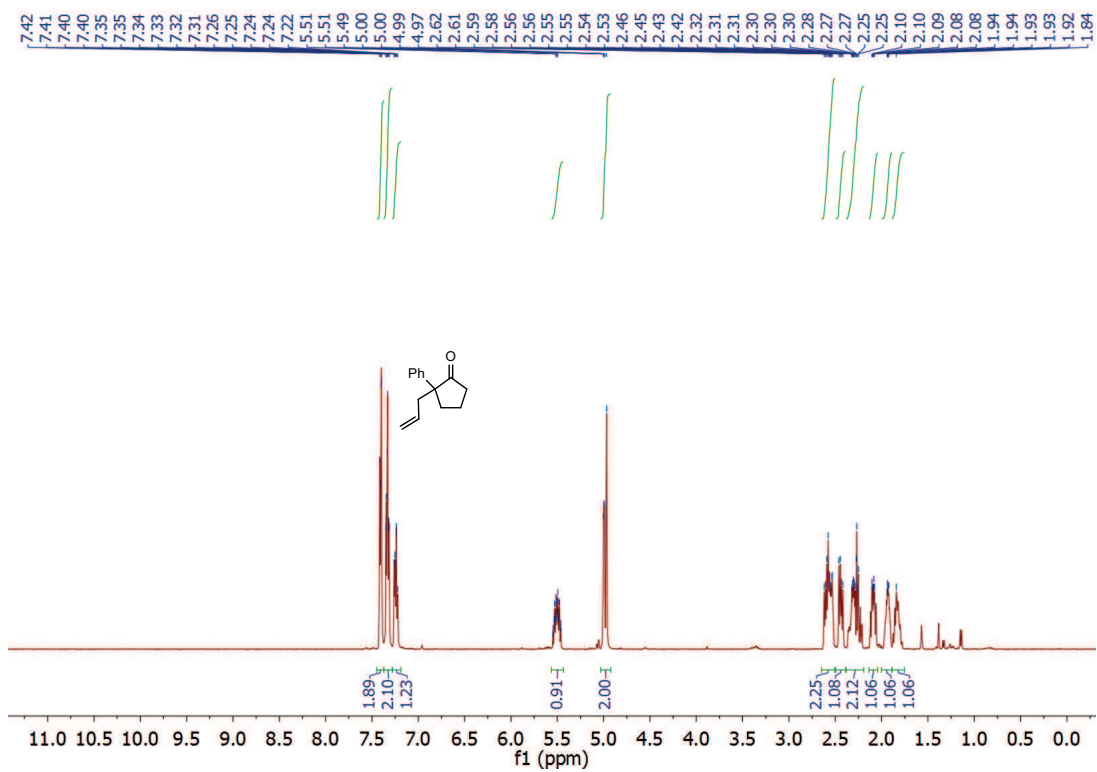


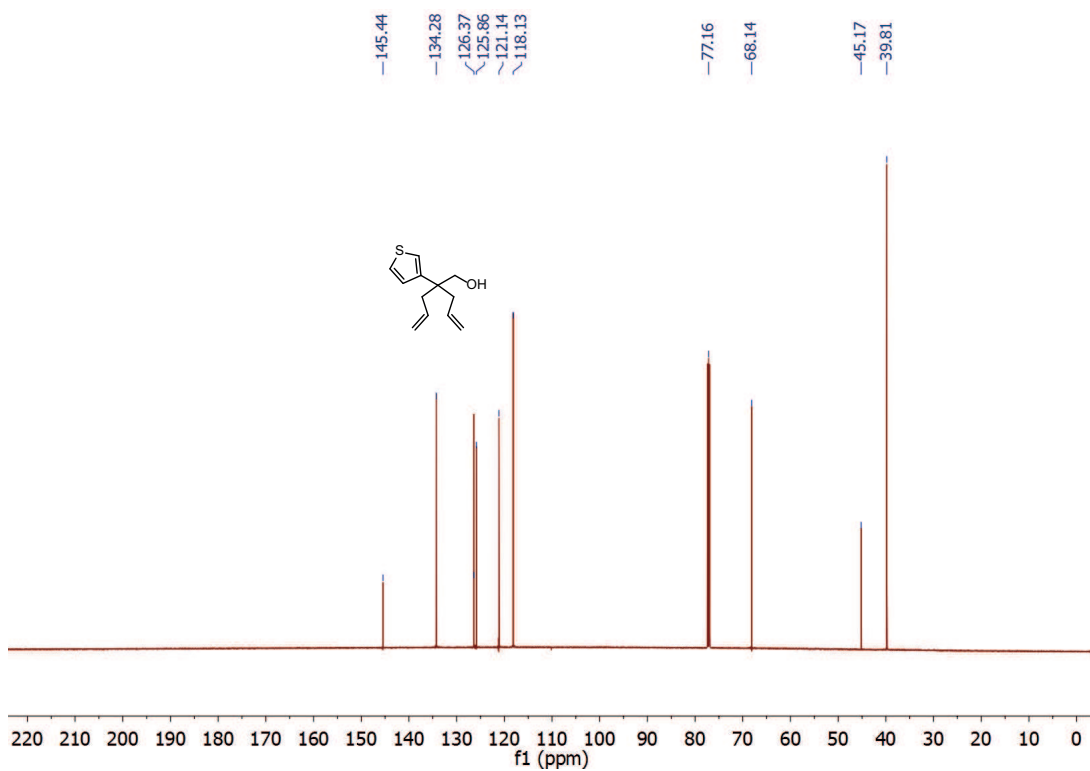
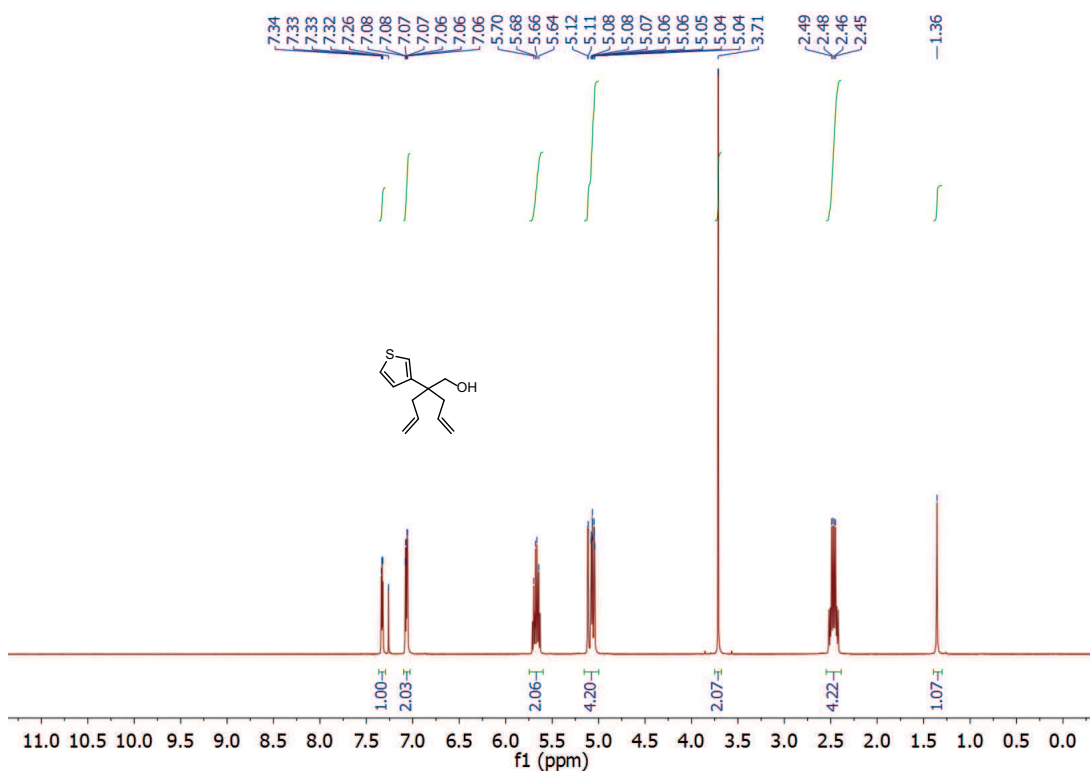


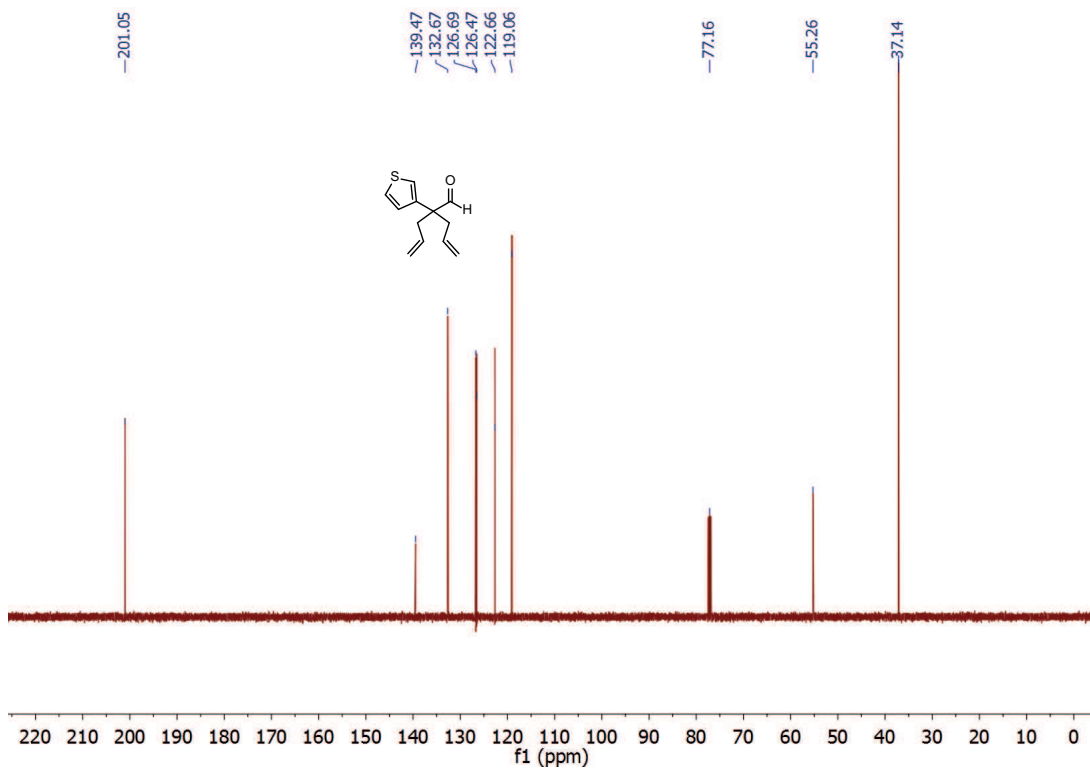
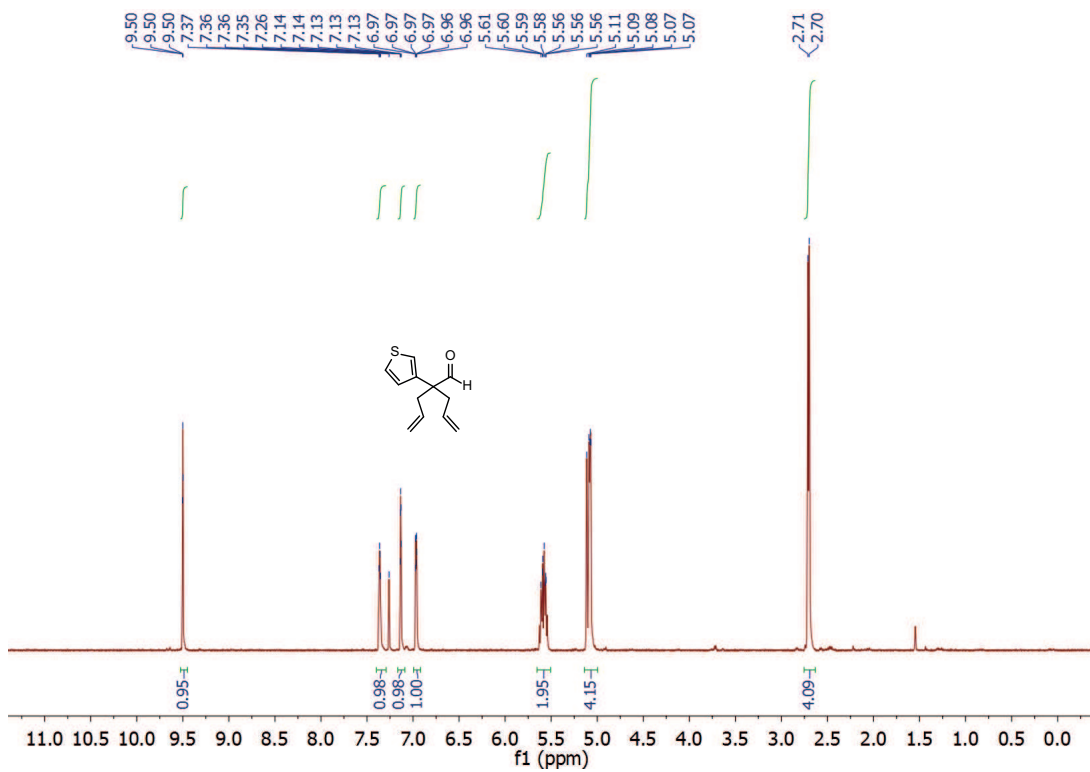
Appendix B

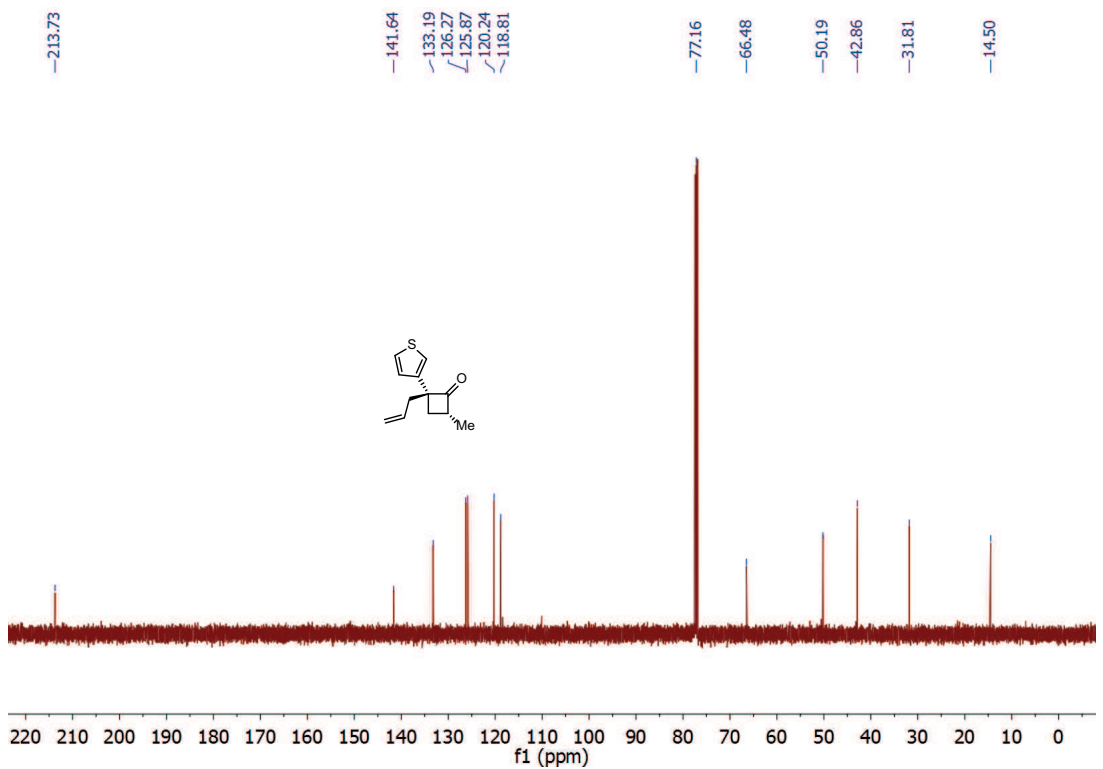
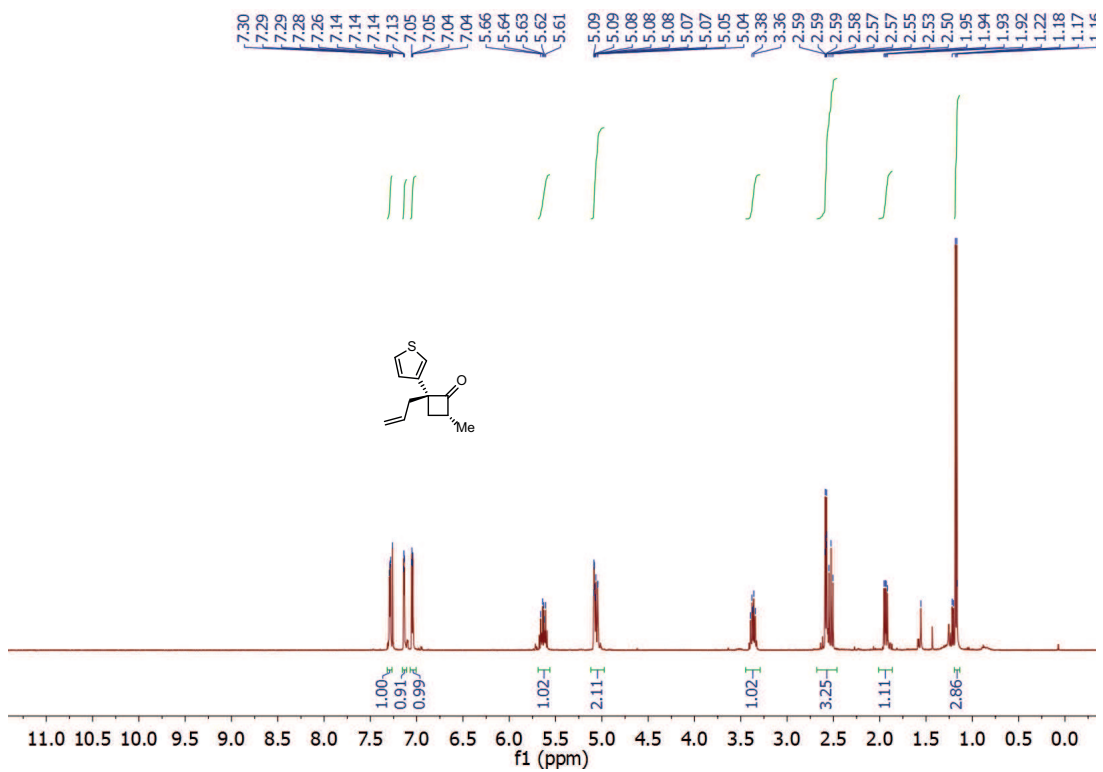
Supporting Information for Chapter 2.1

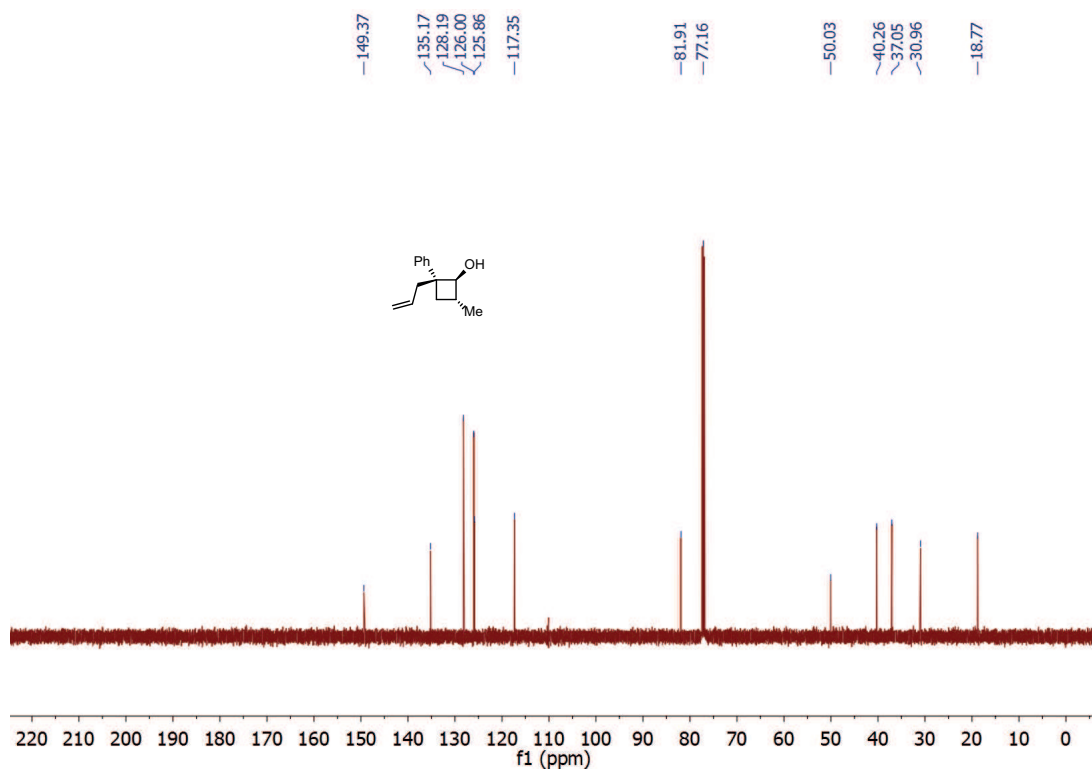
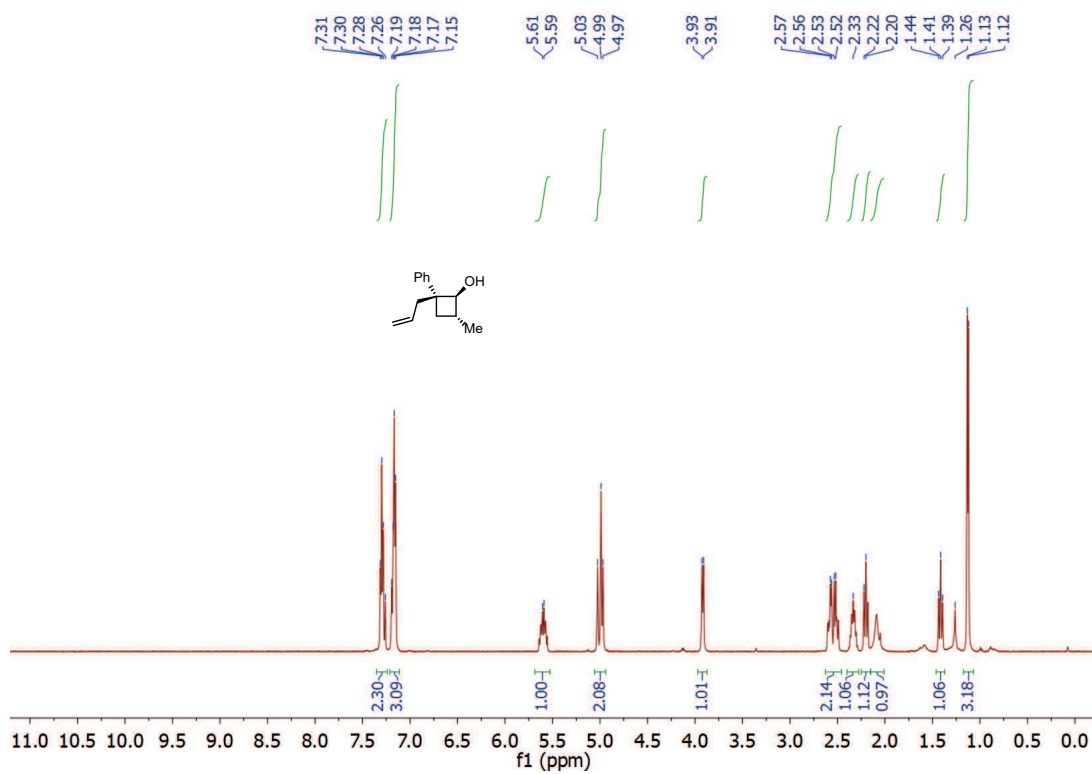
B.1 NMR Spectra

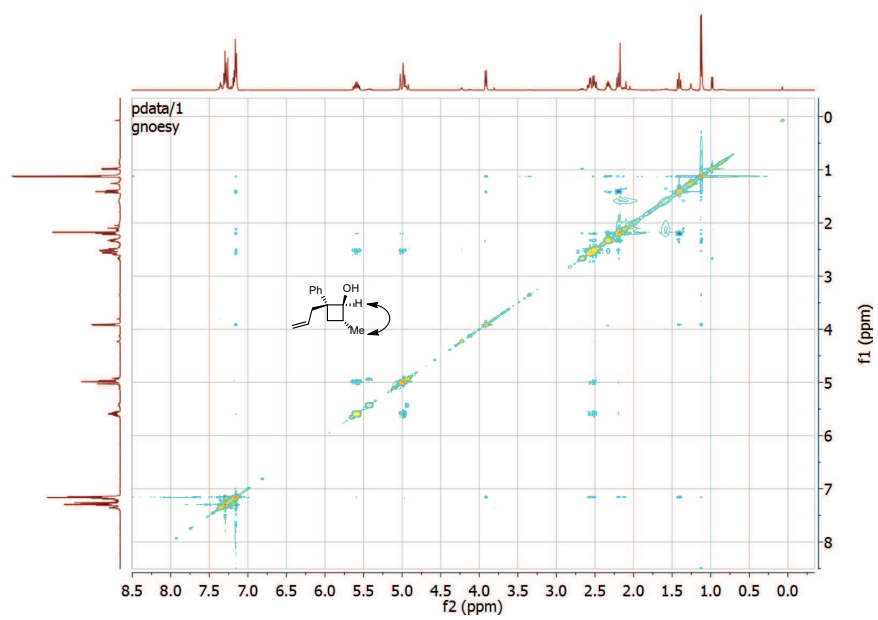
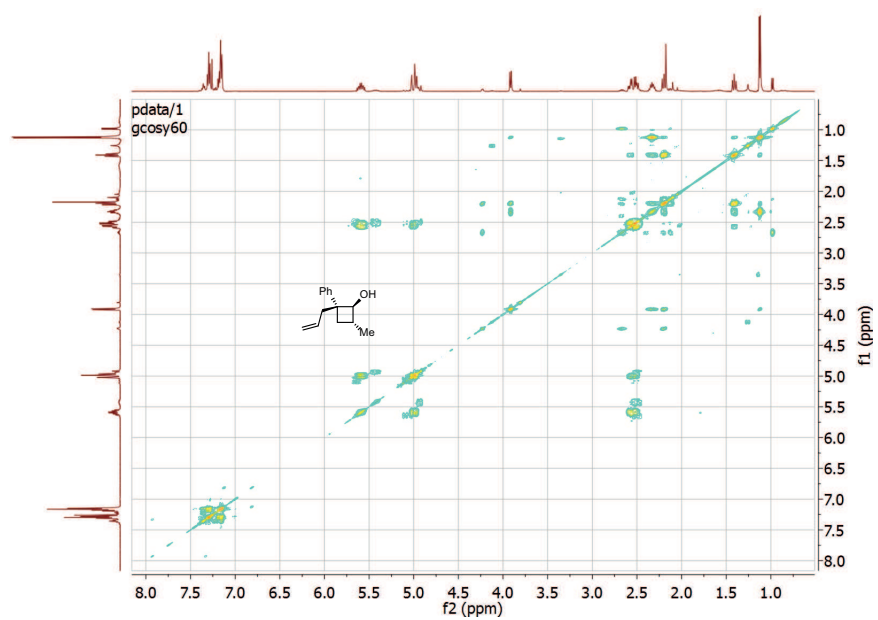


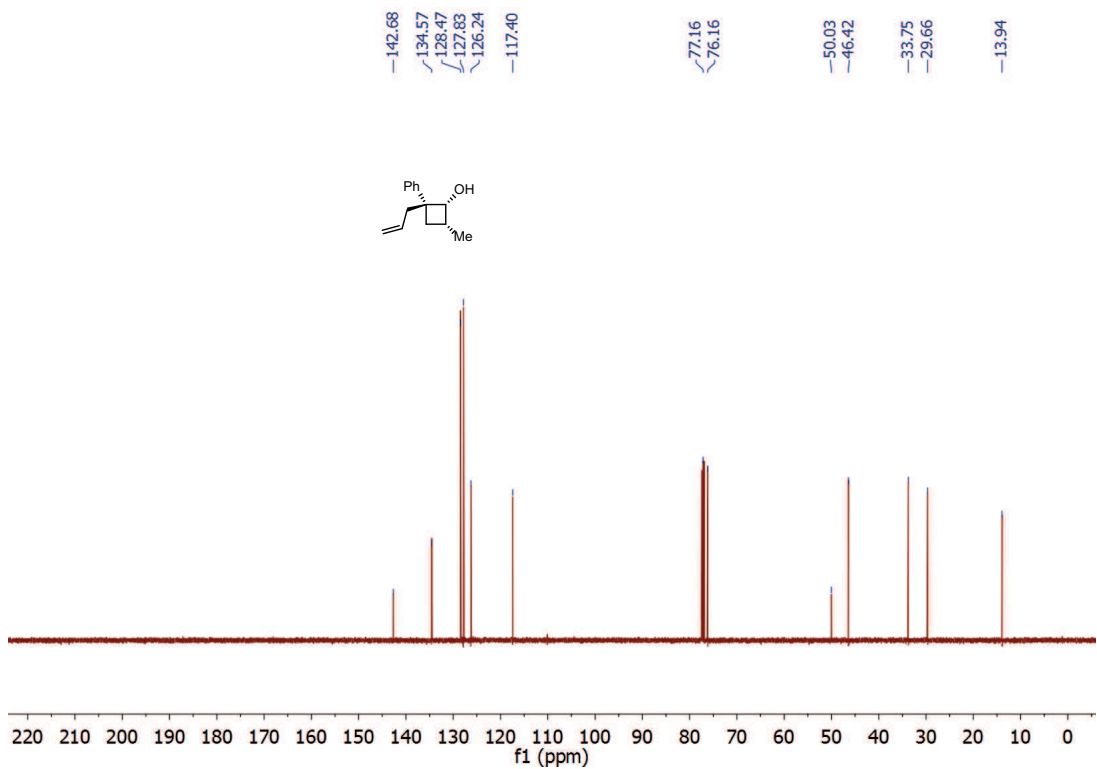
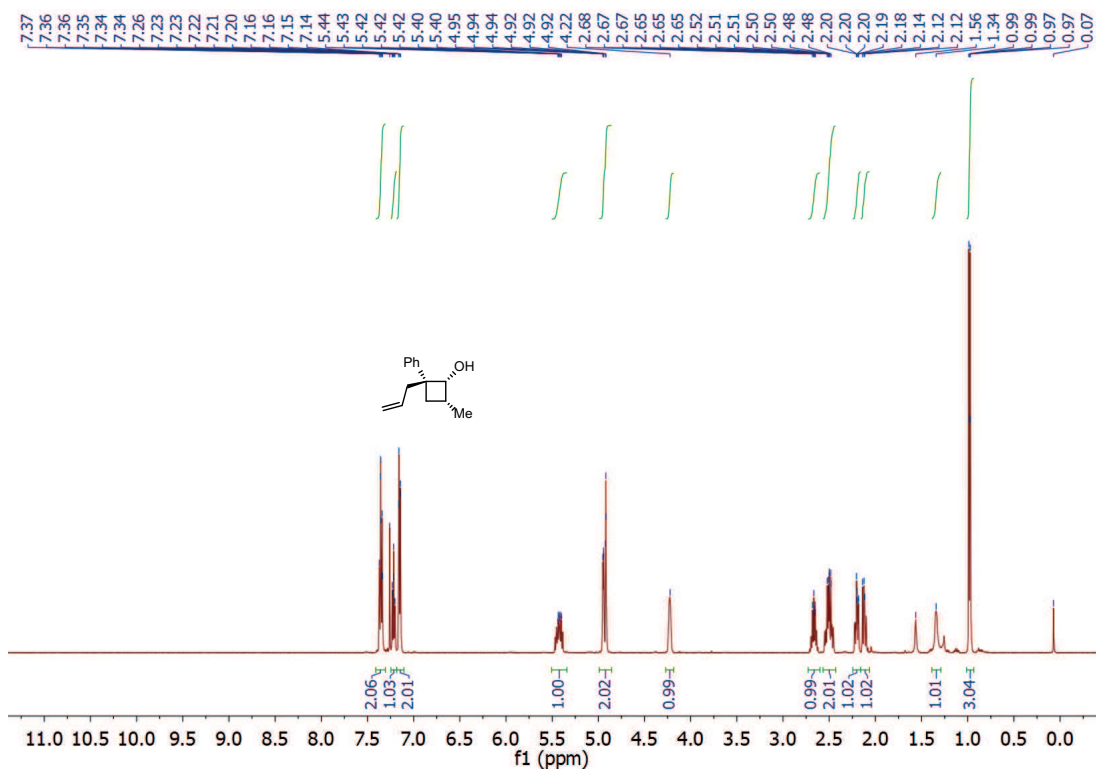


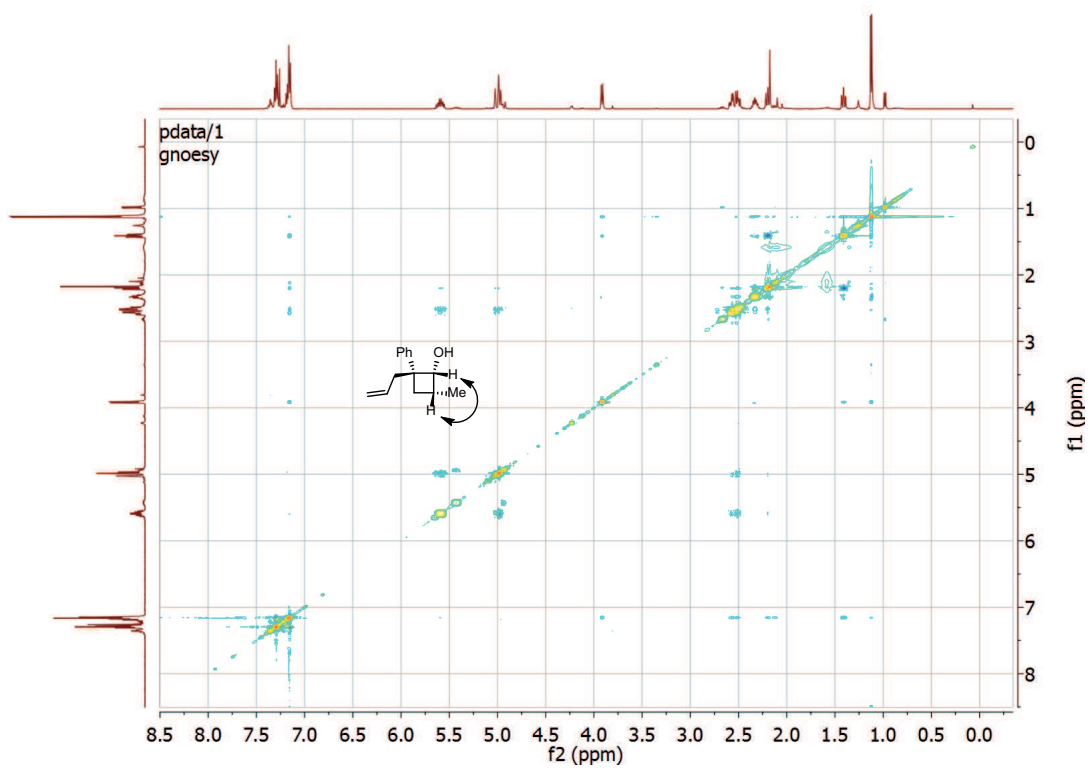
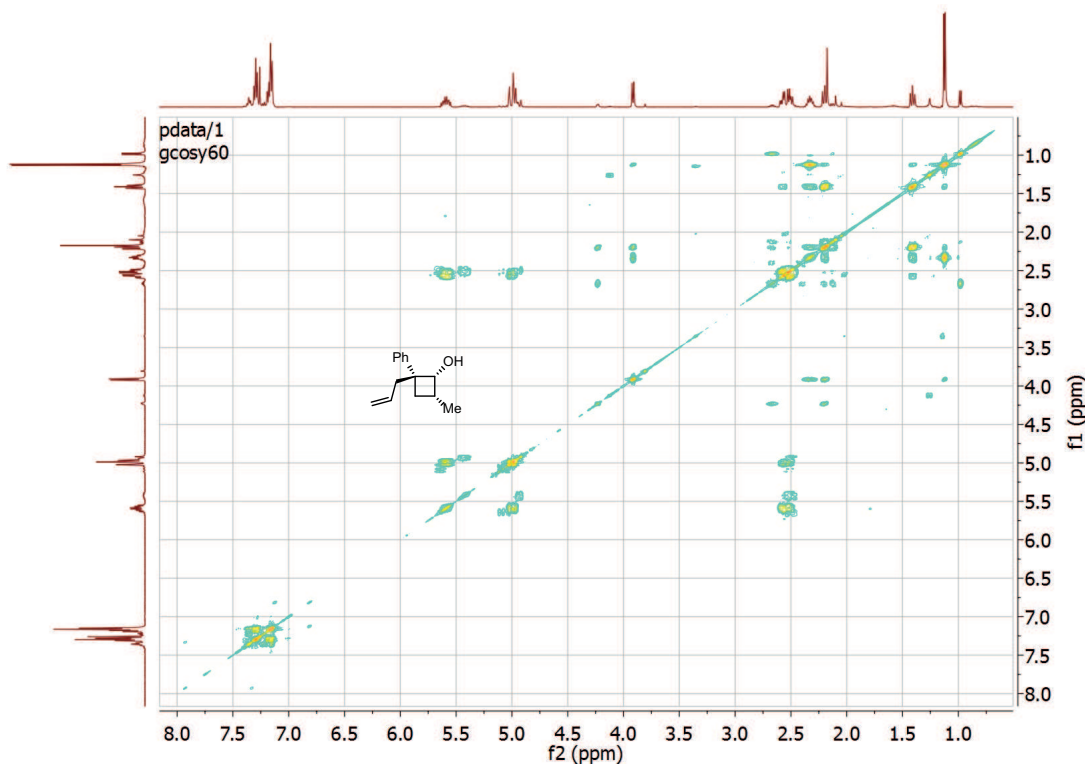


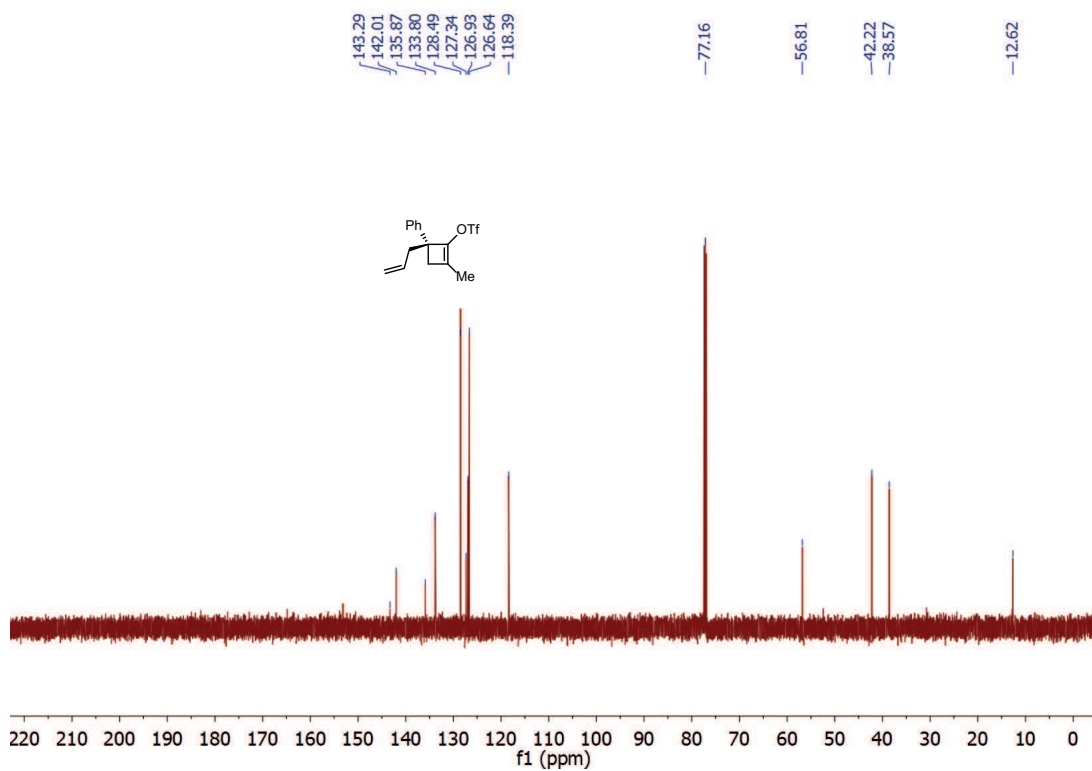
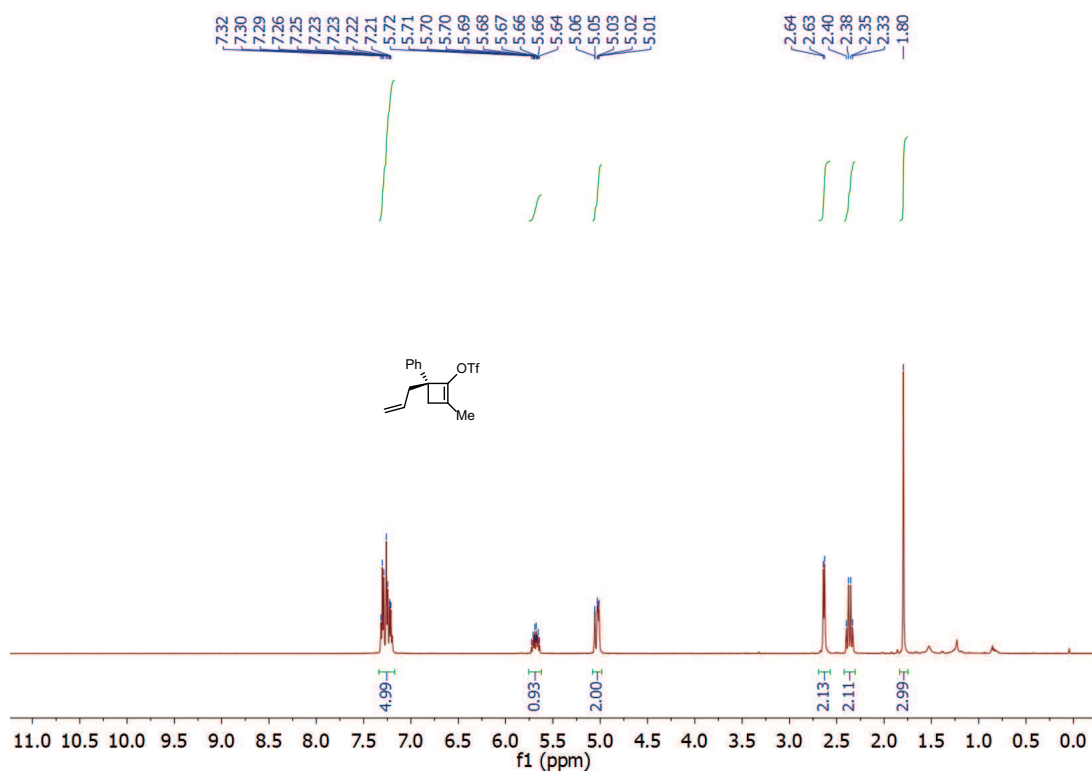


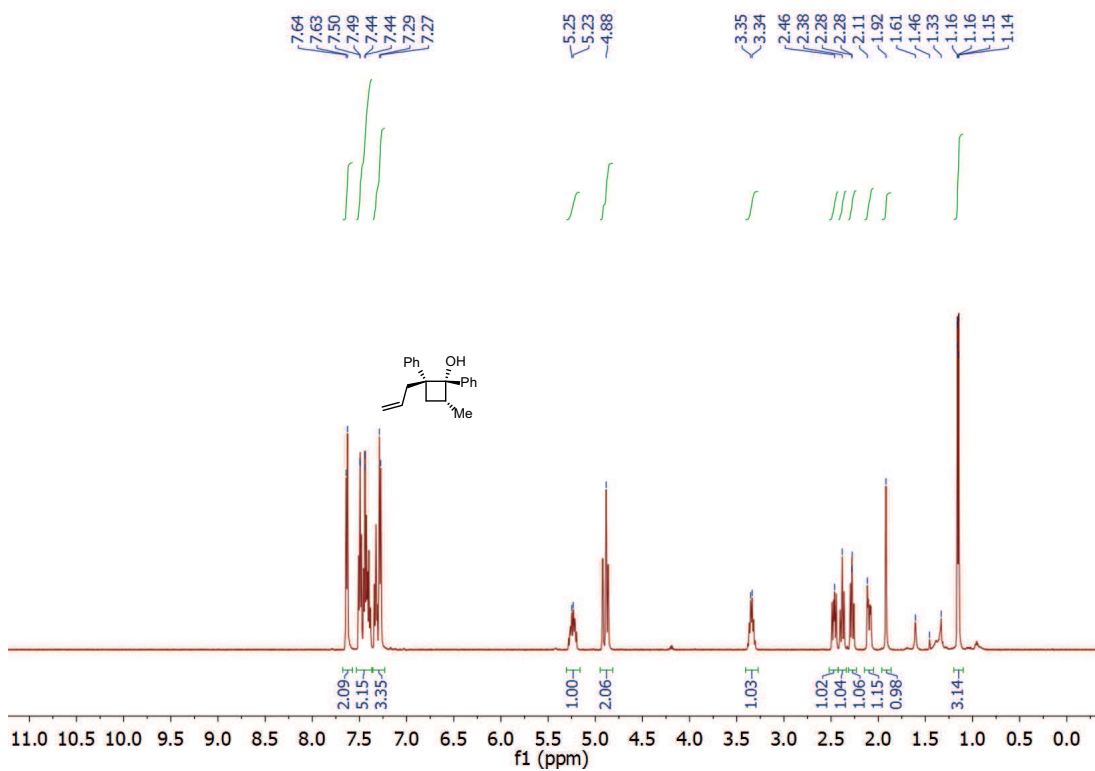
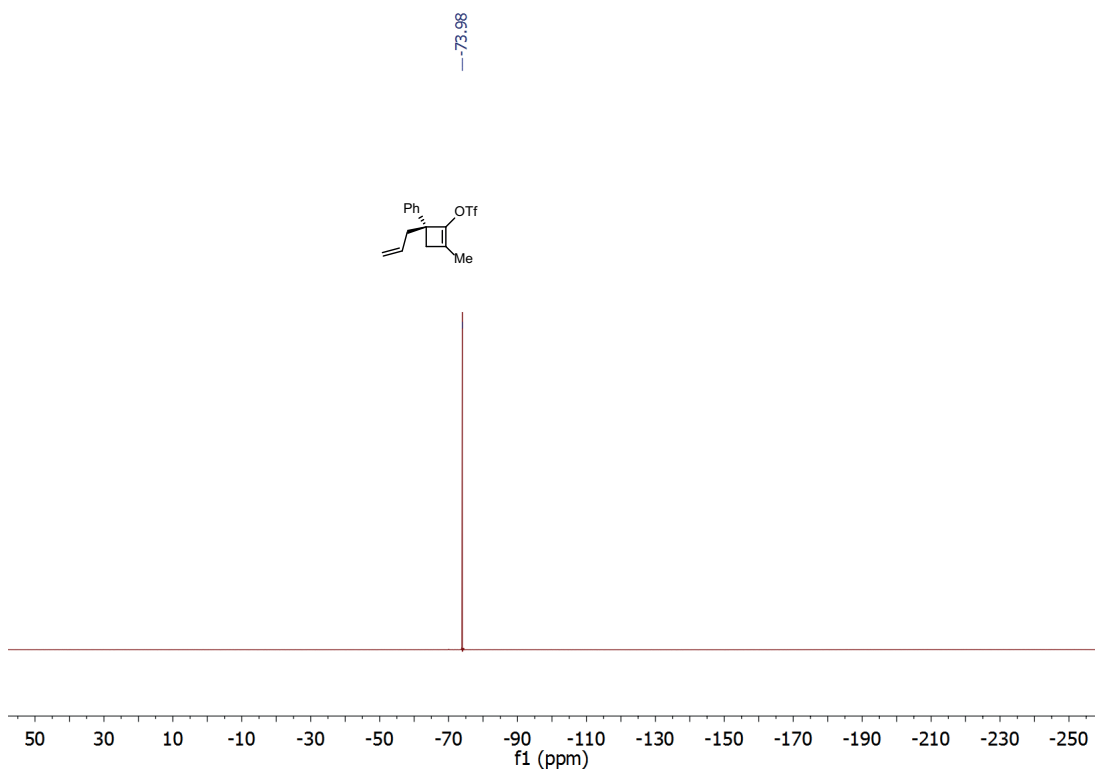


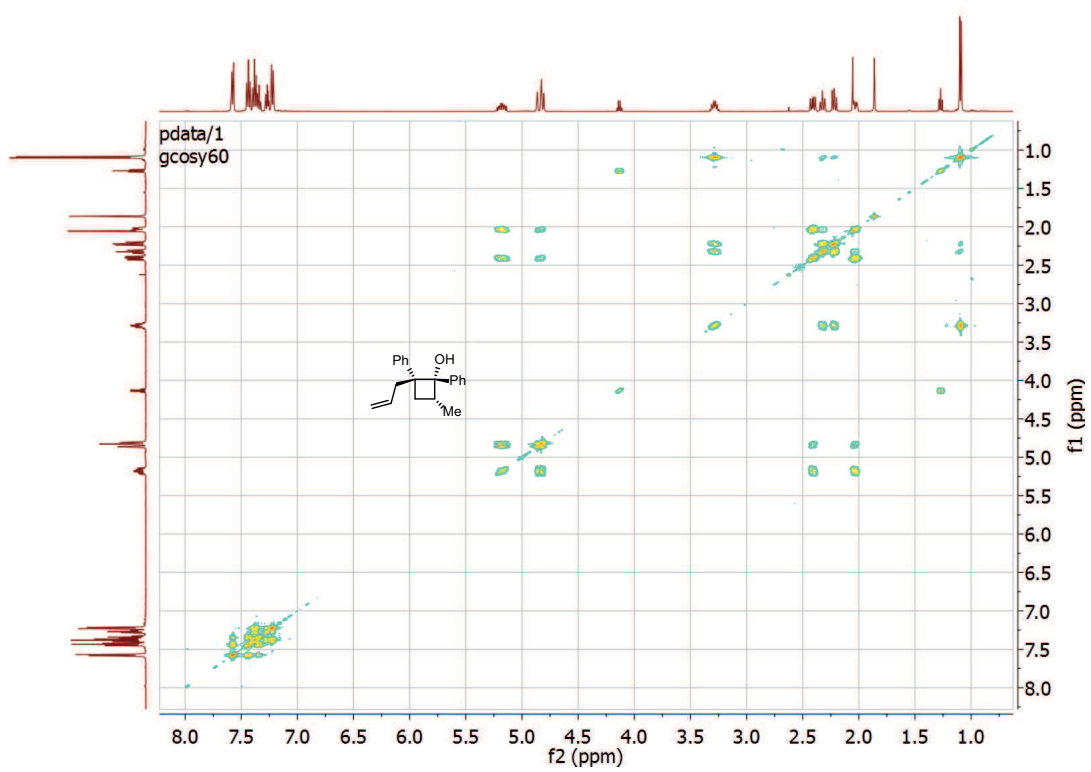
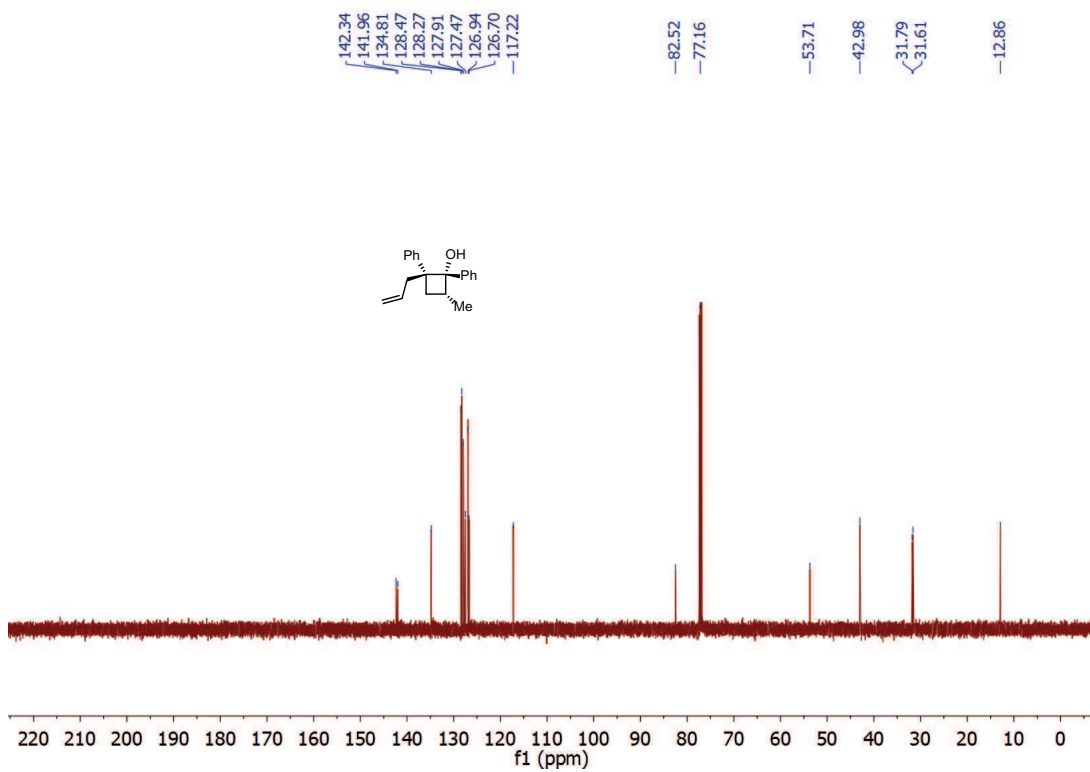


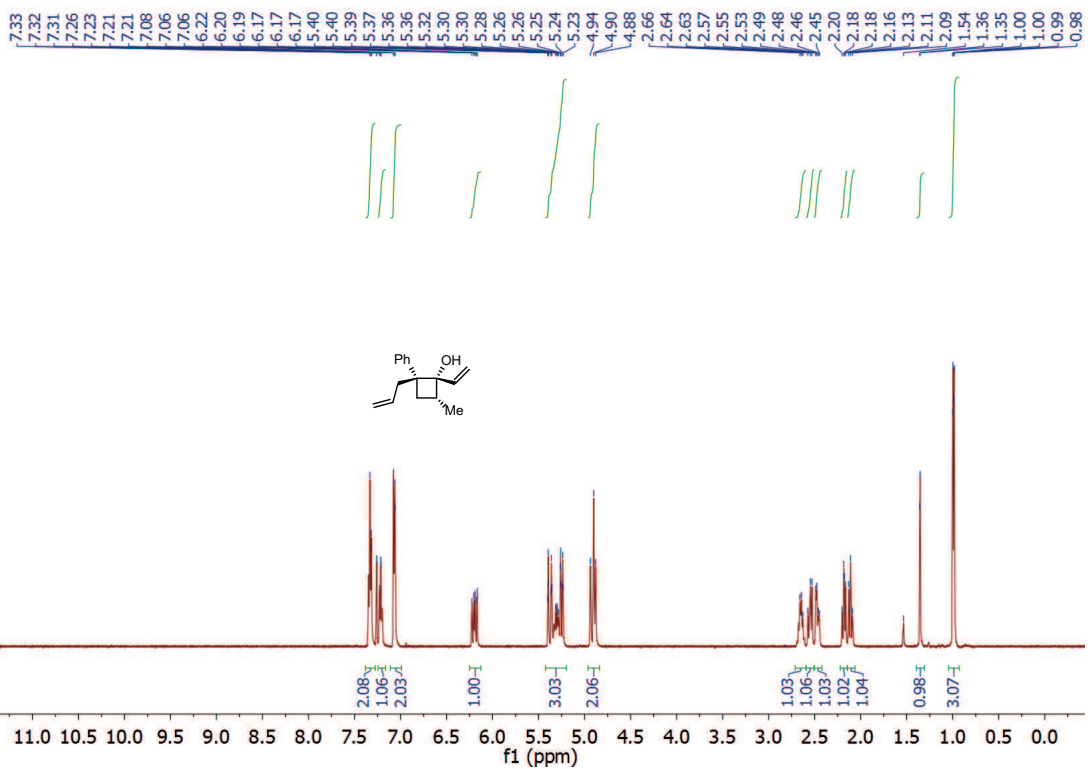
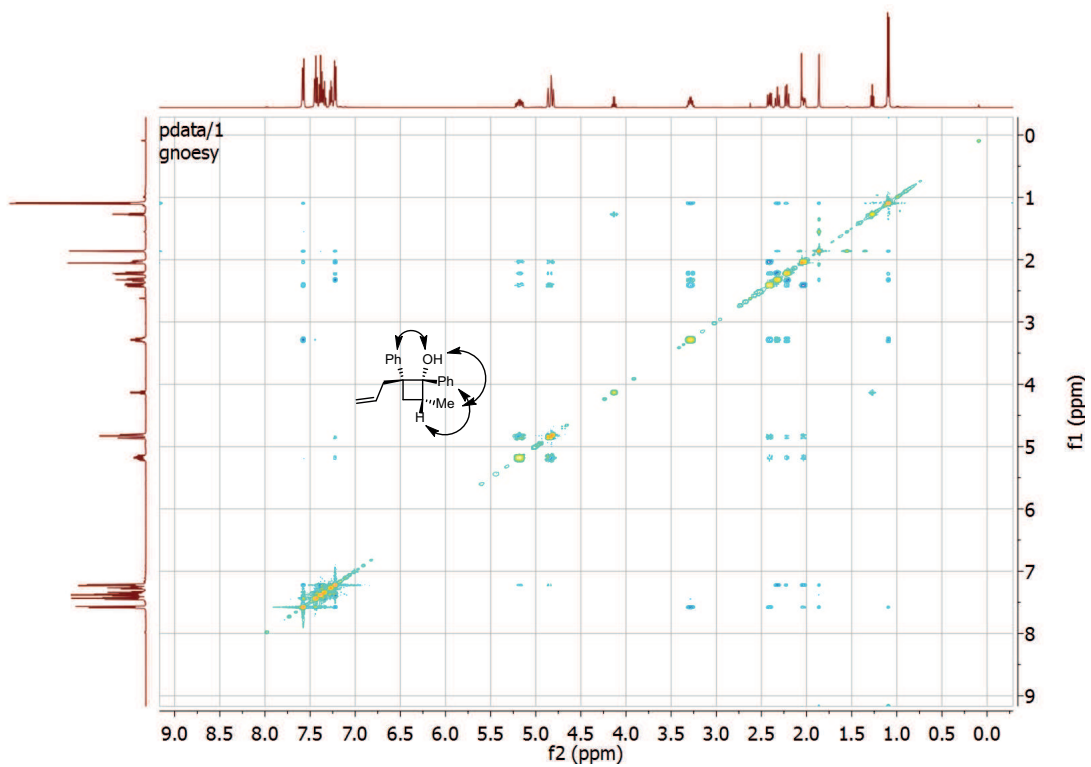


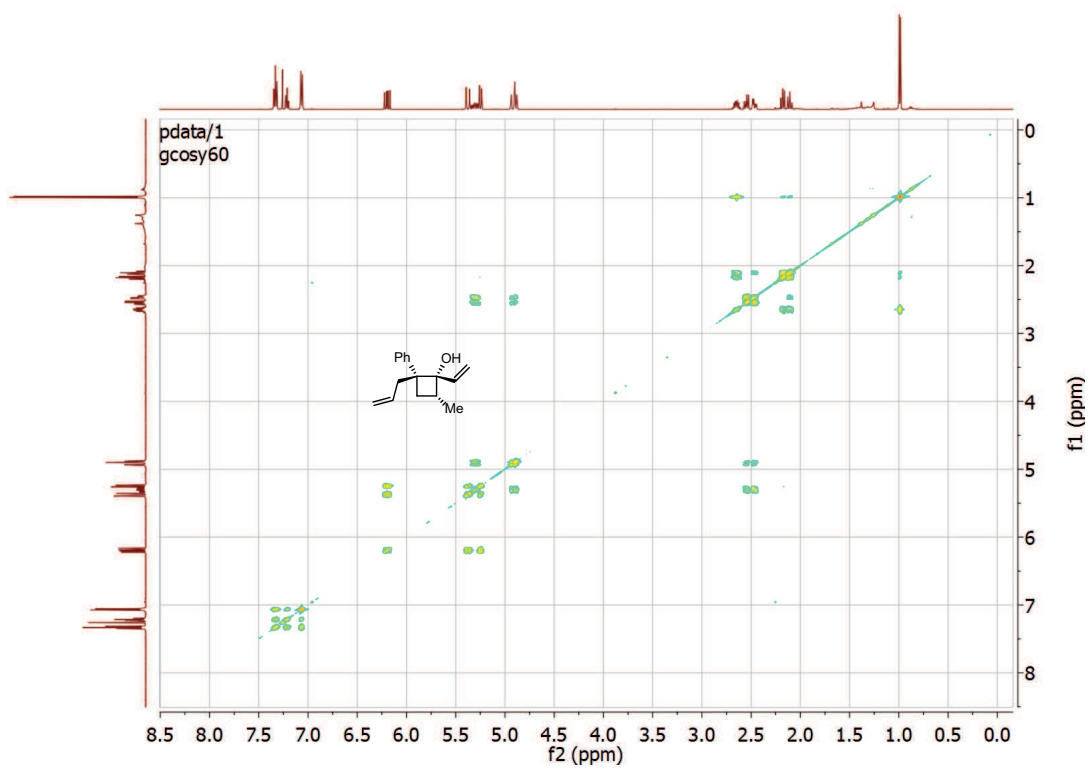
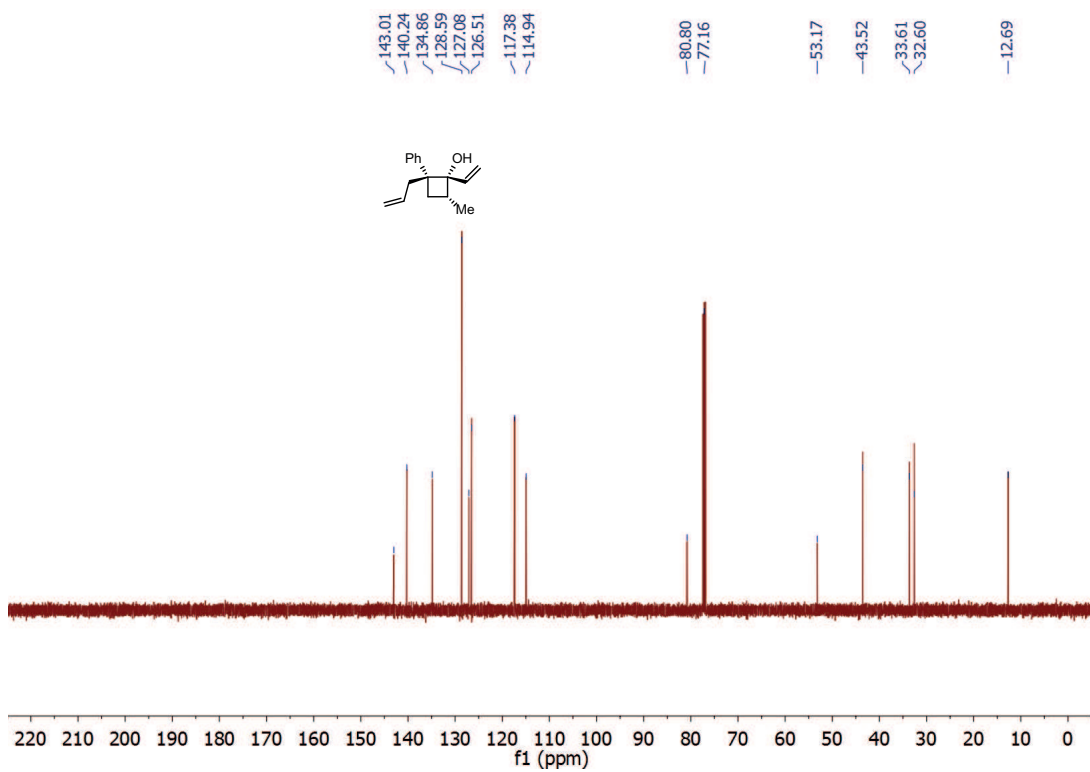


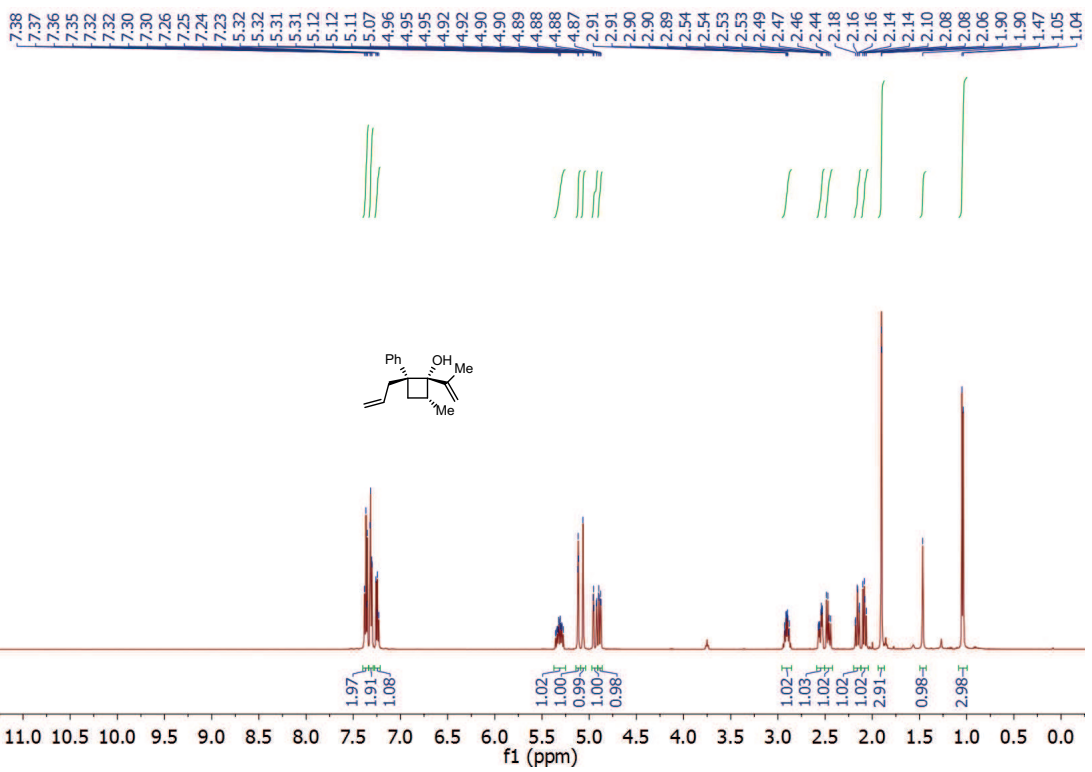
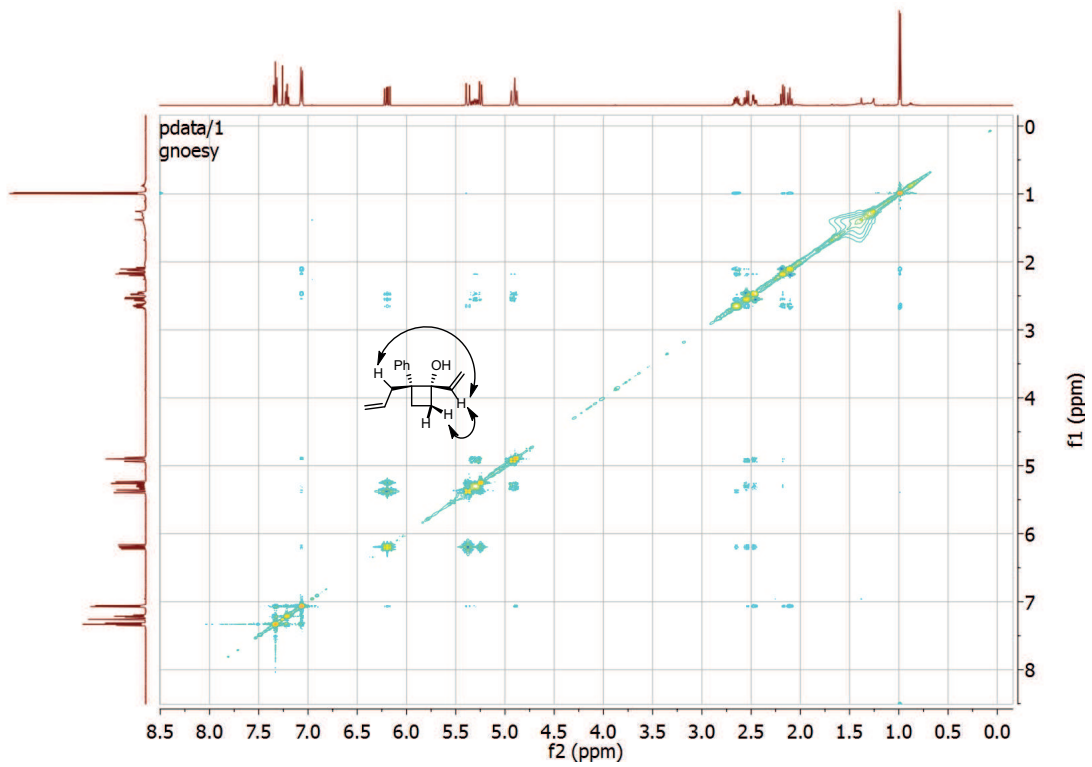


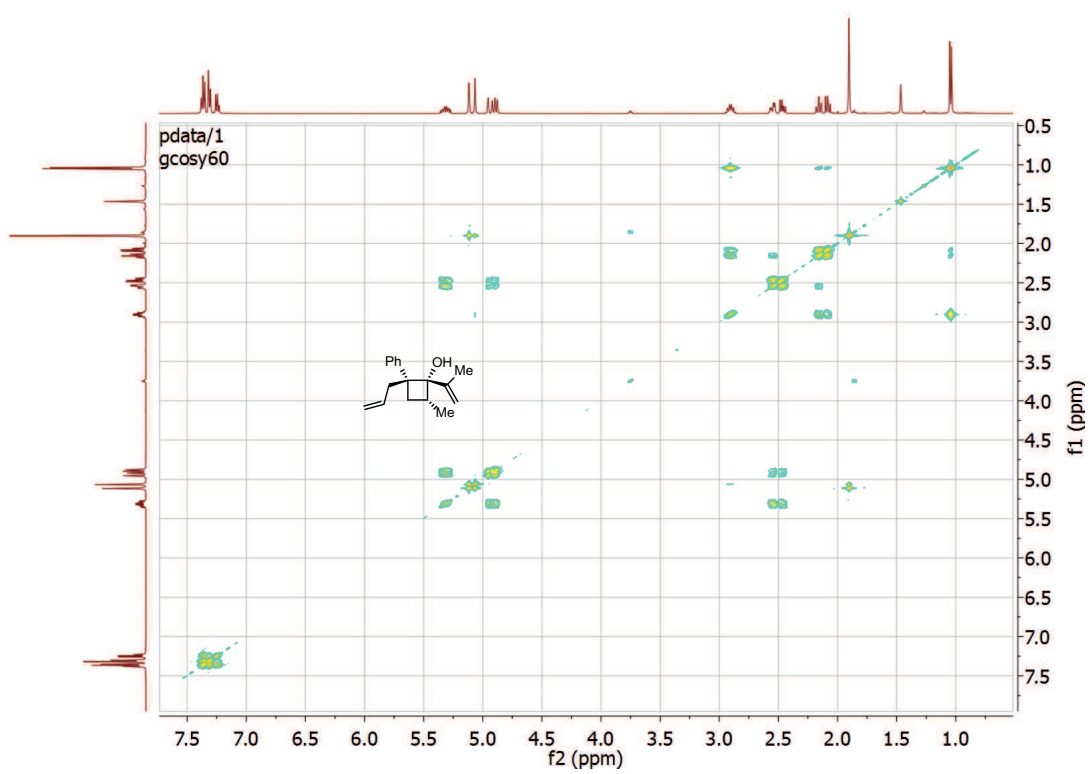
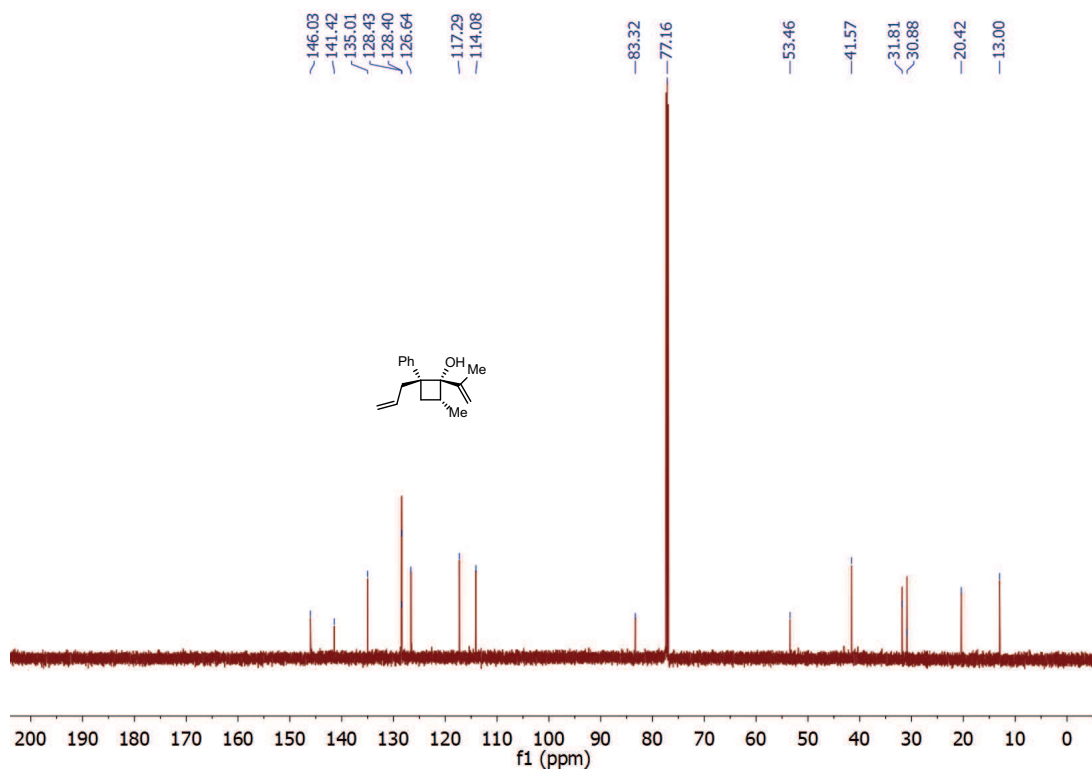


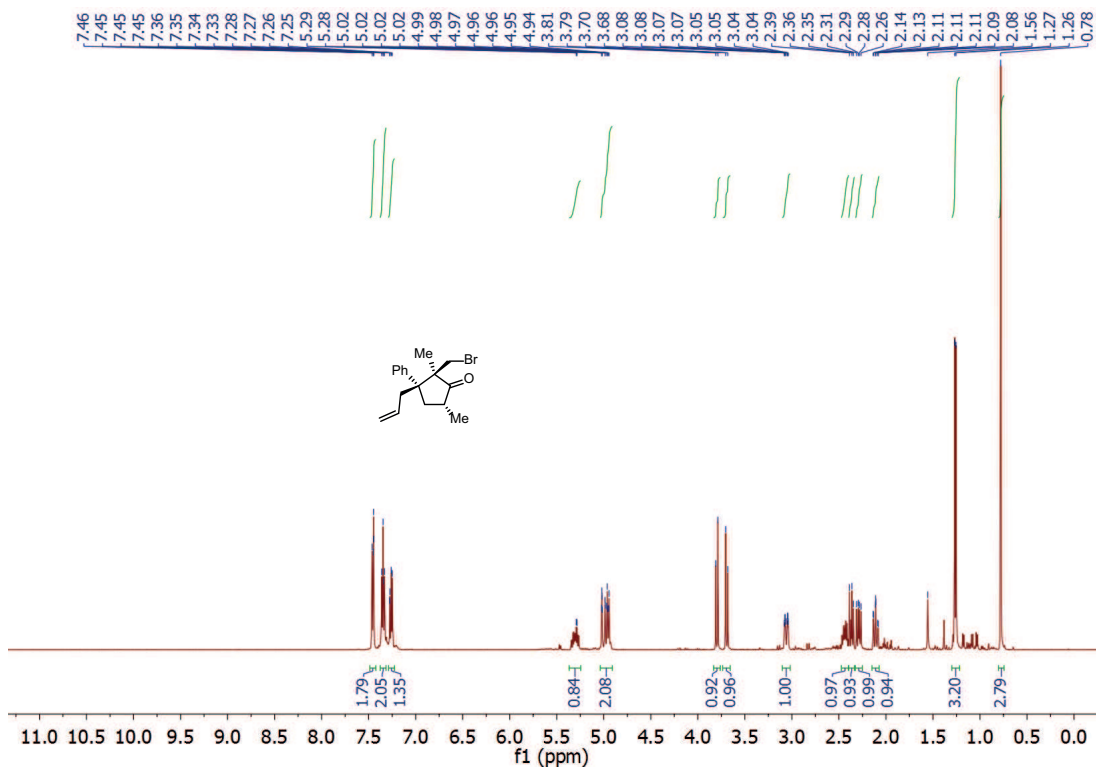
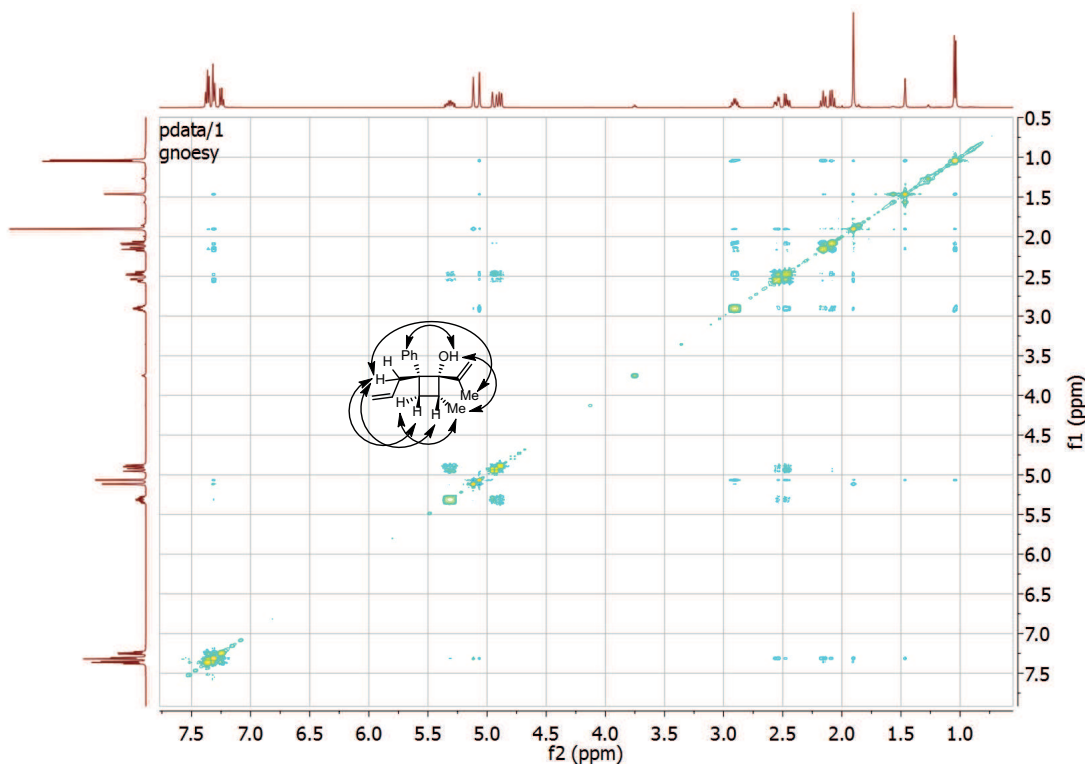


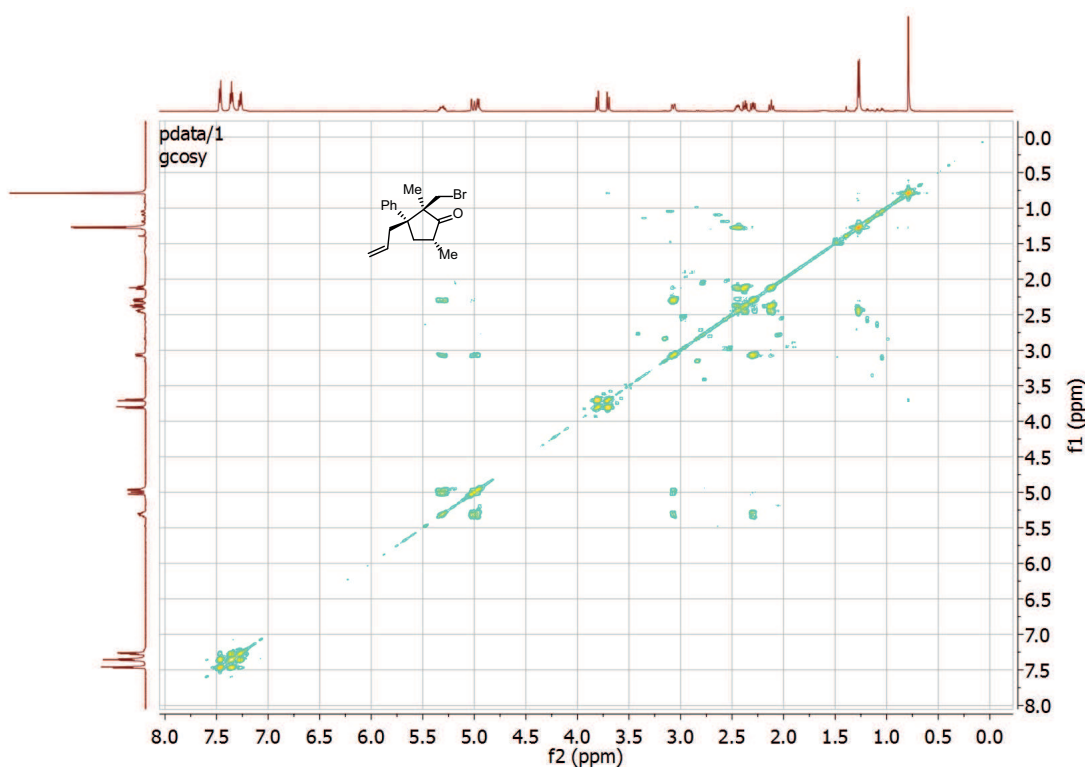
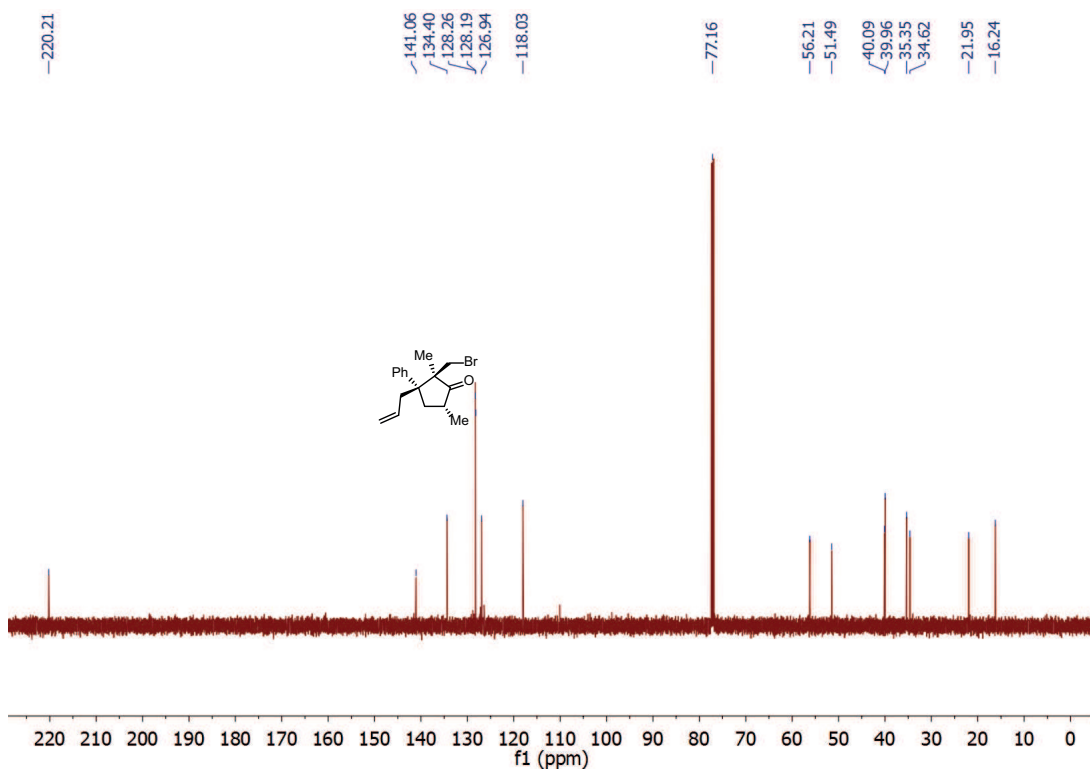


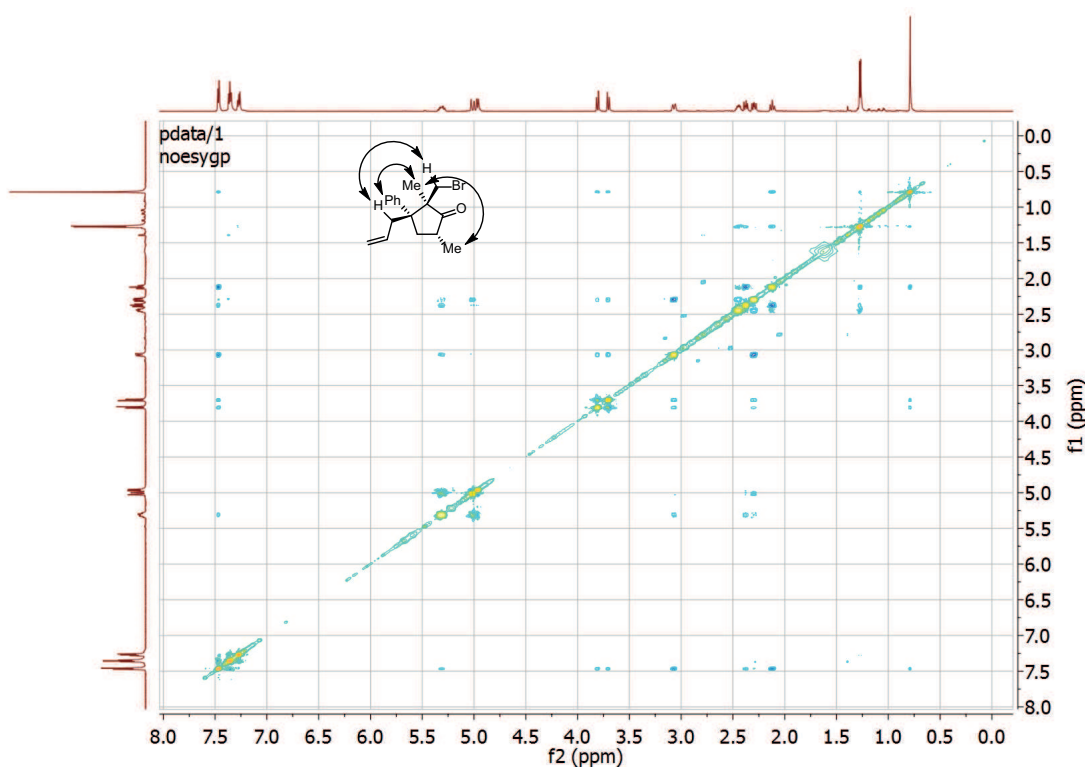
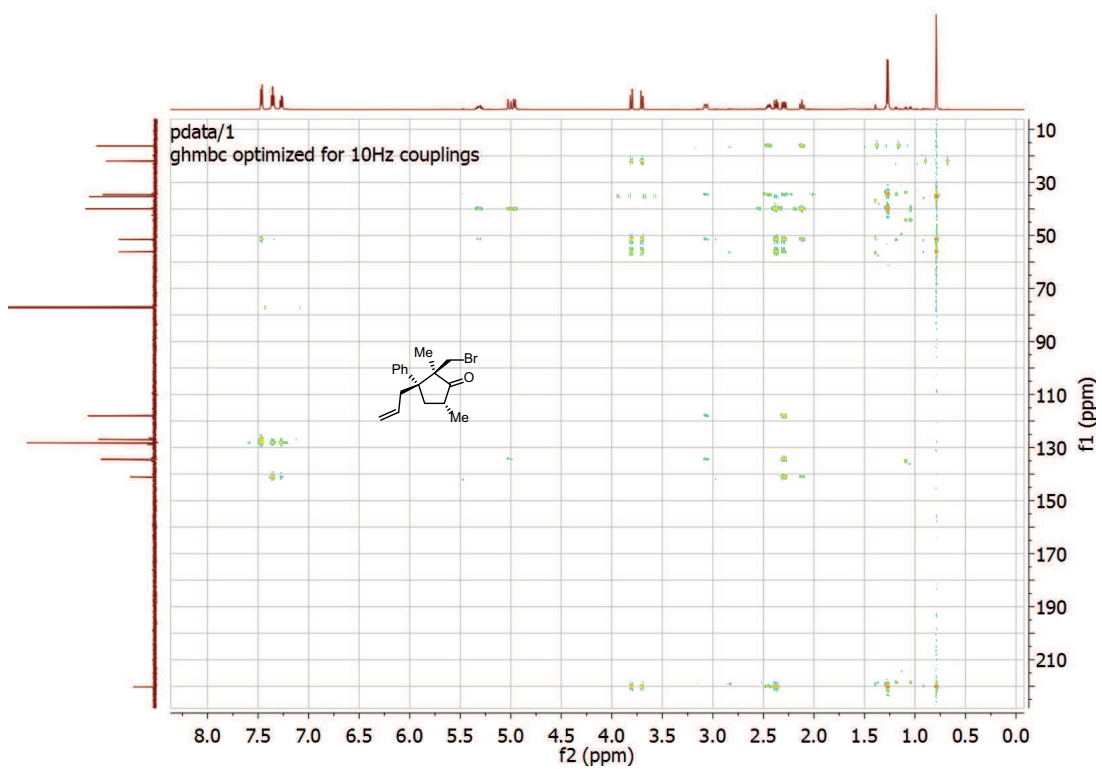


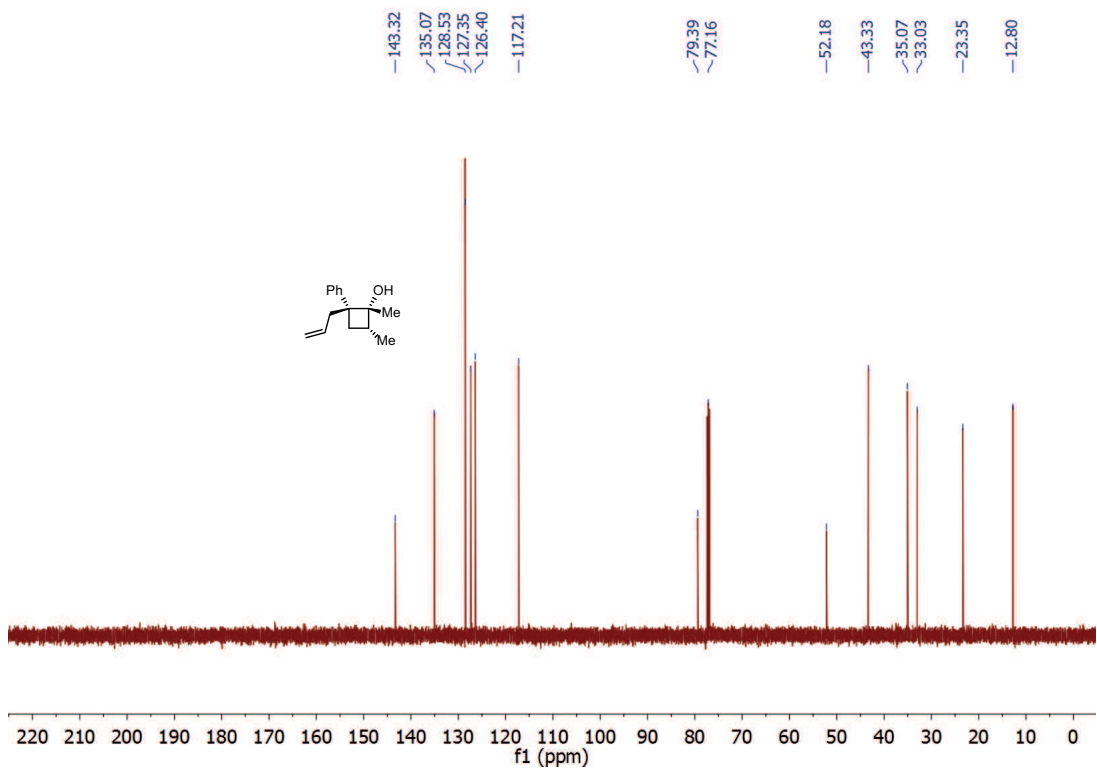
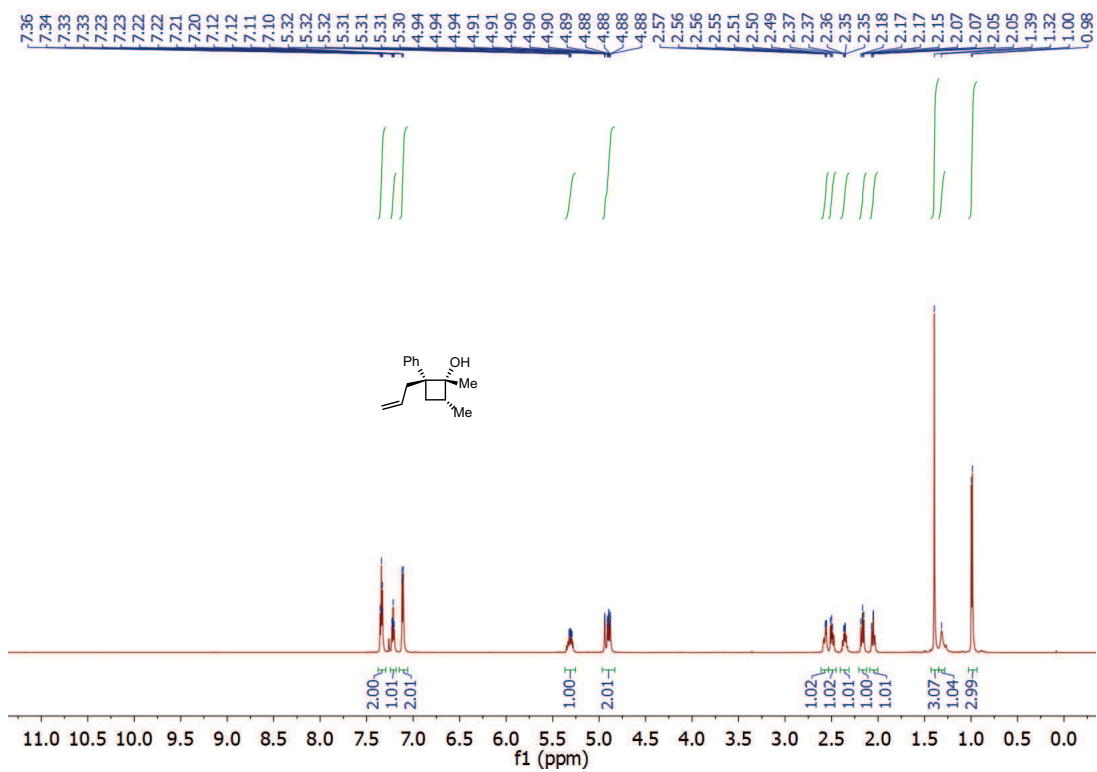


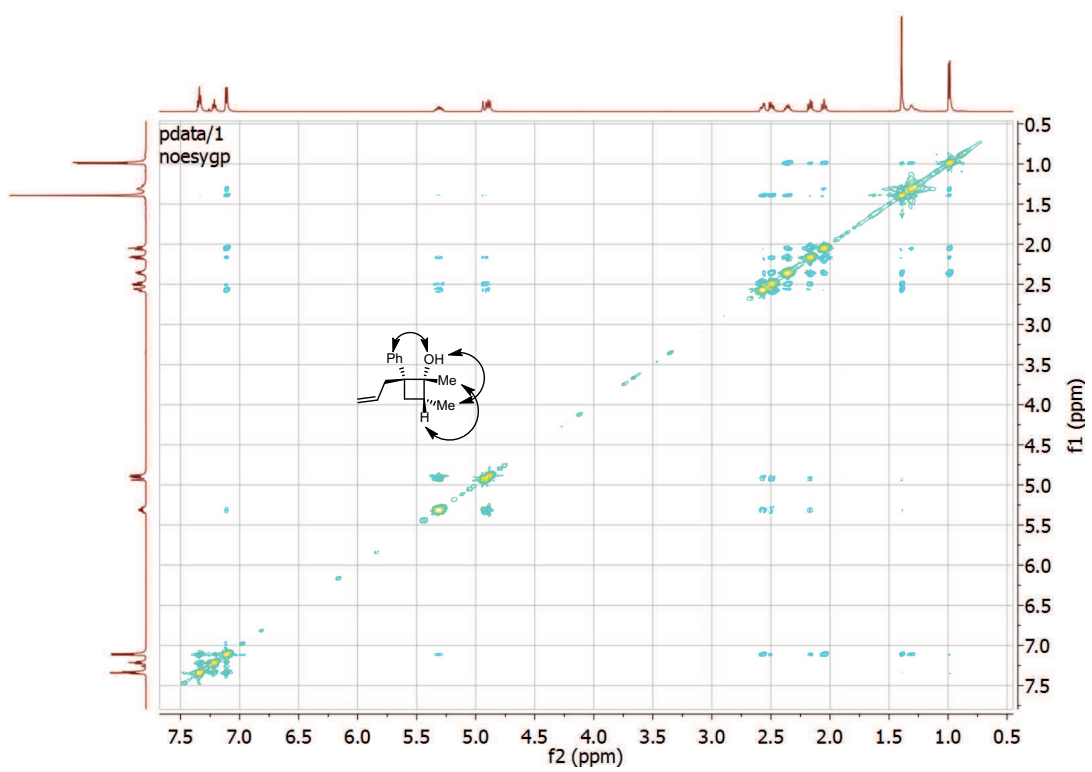
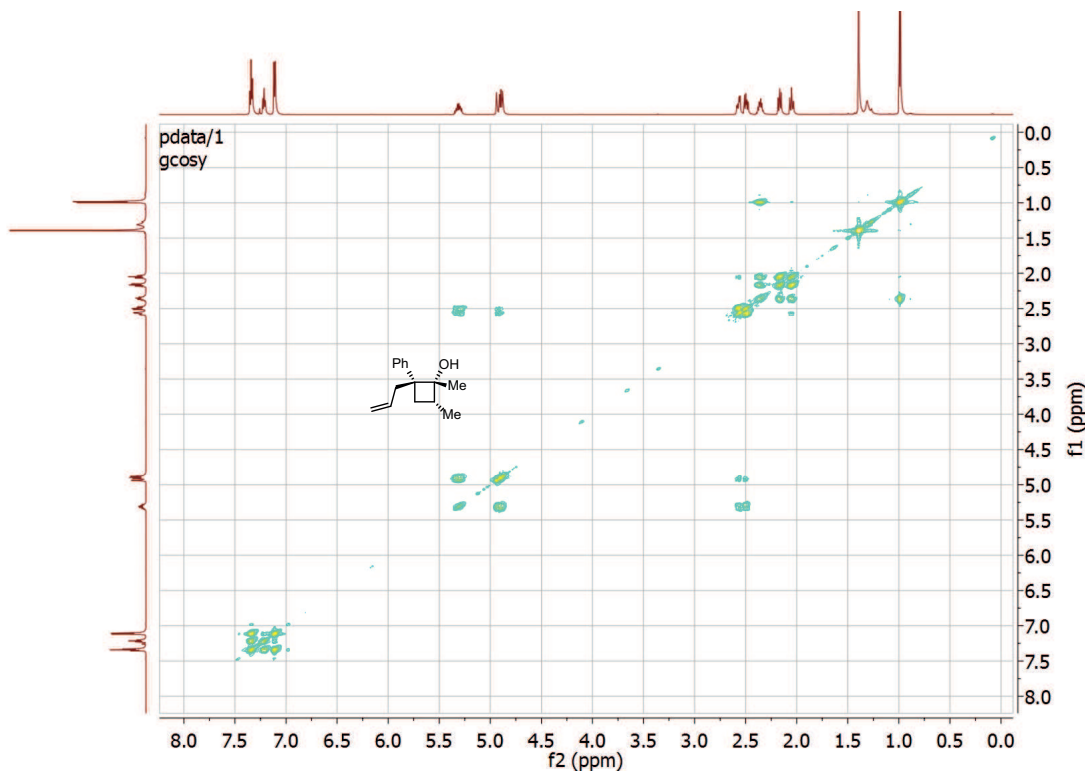


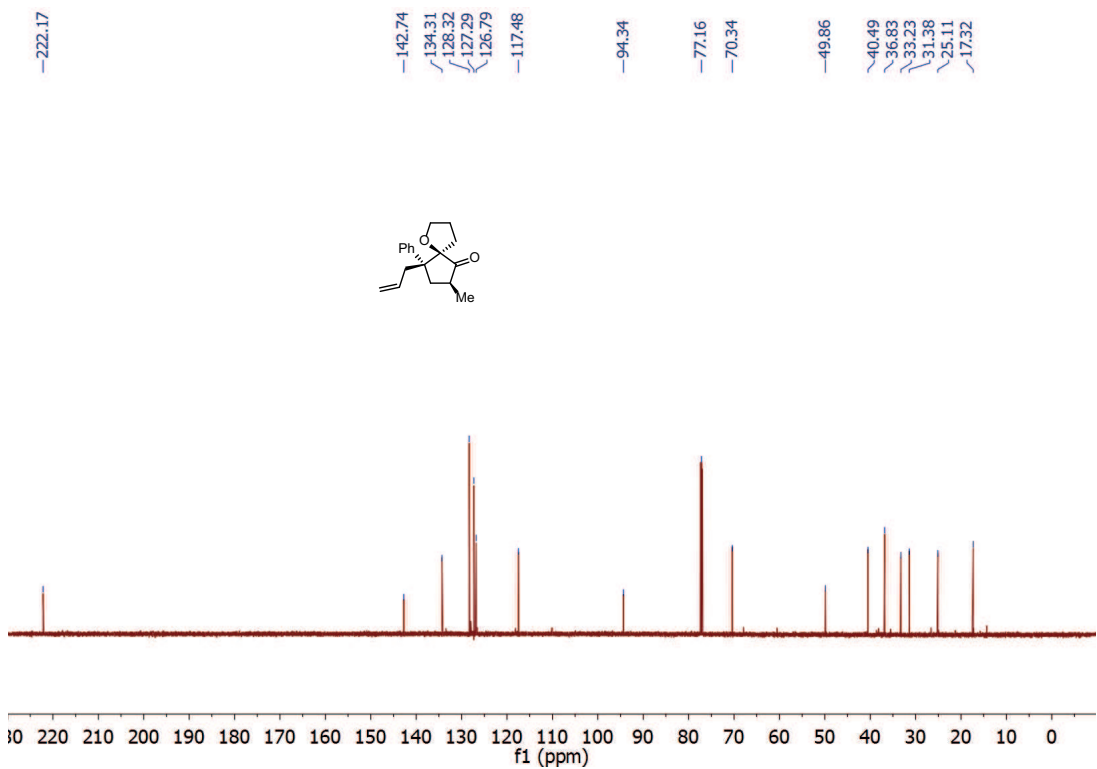
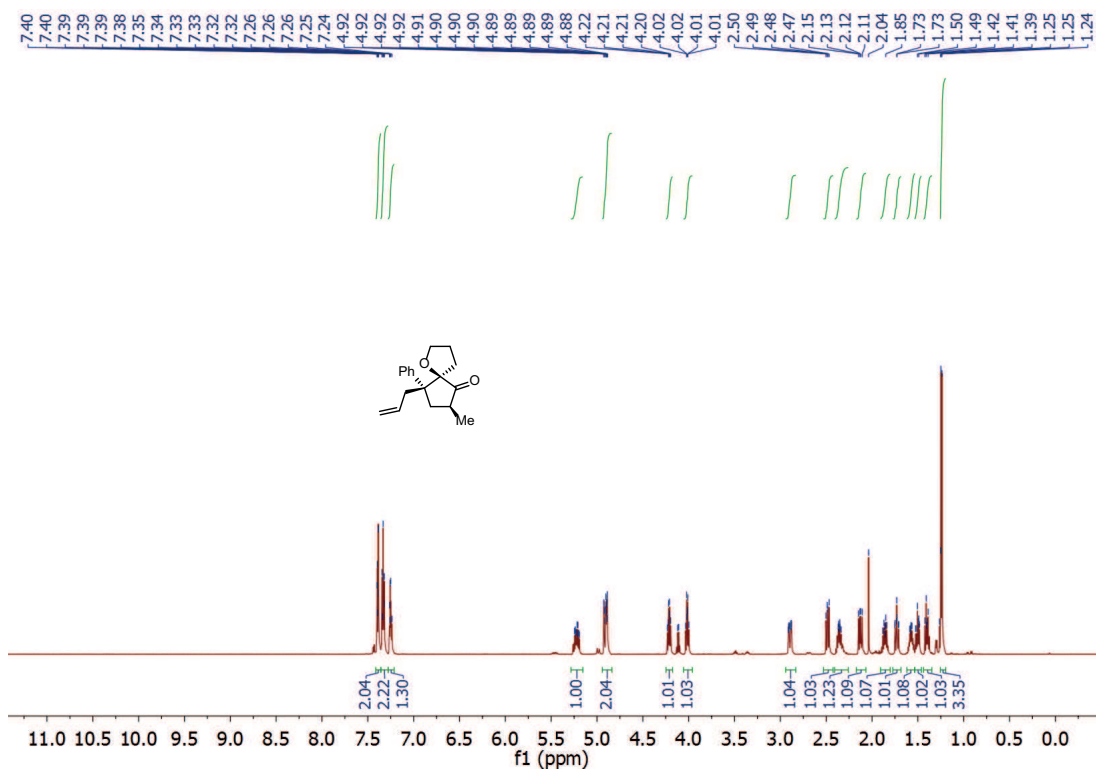


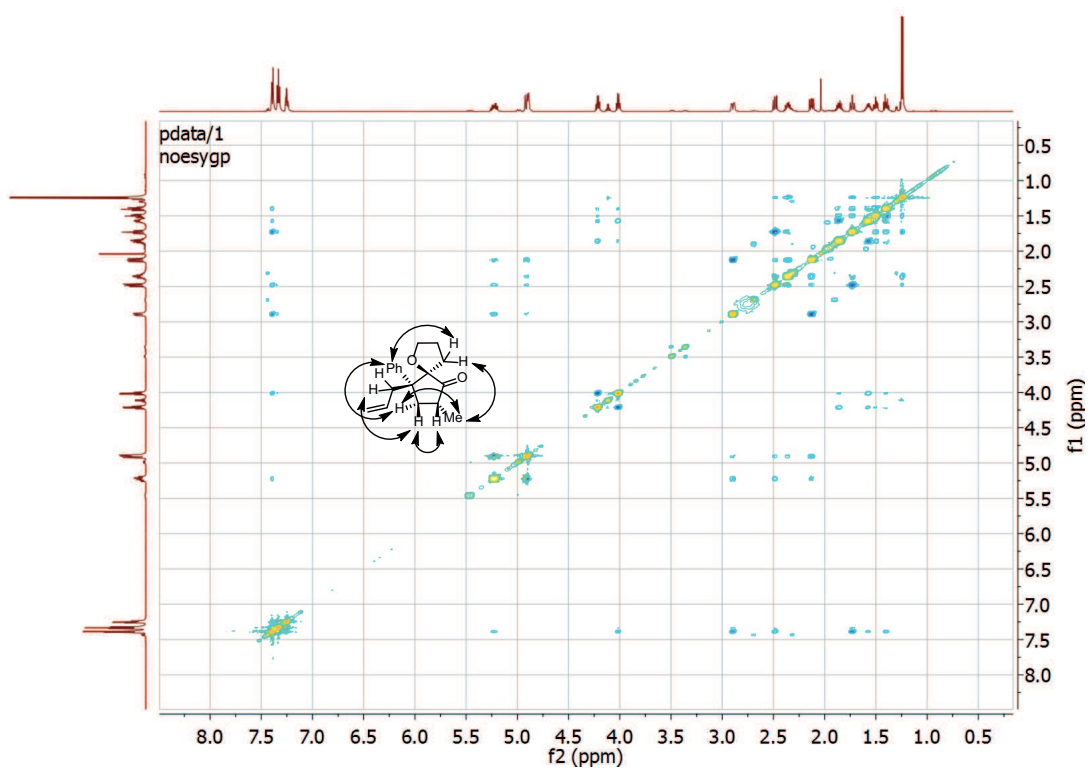
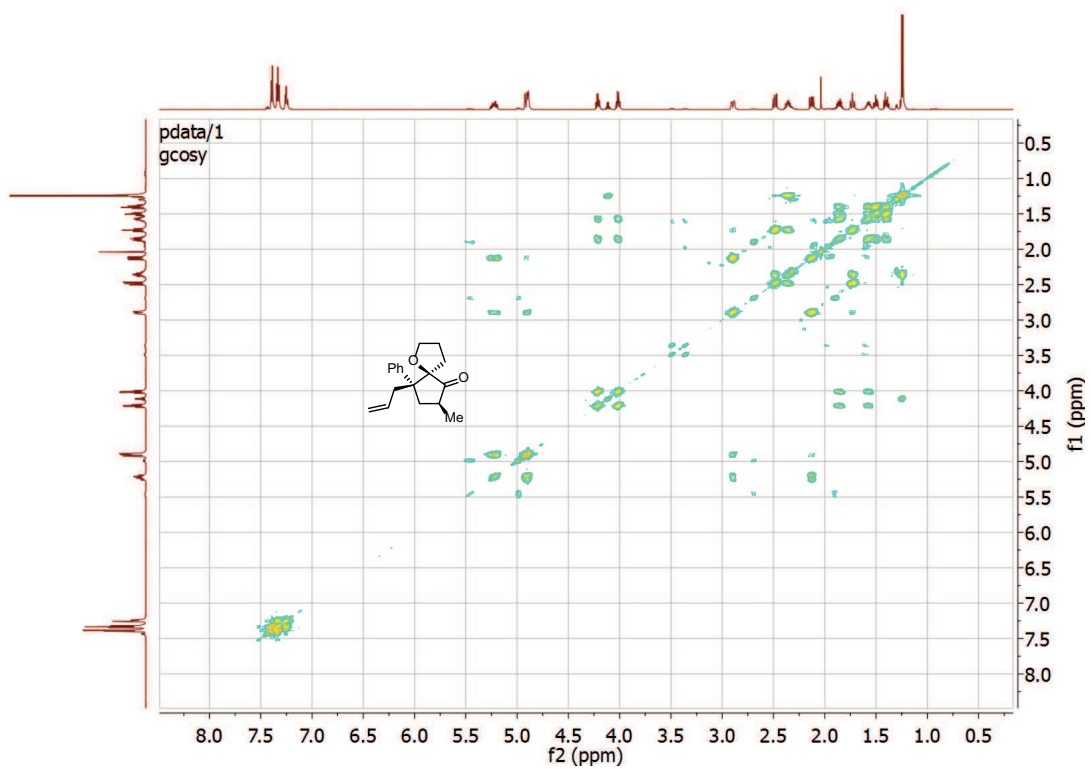








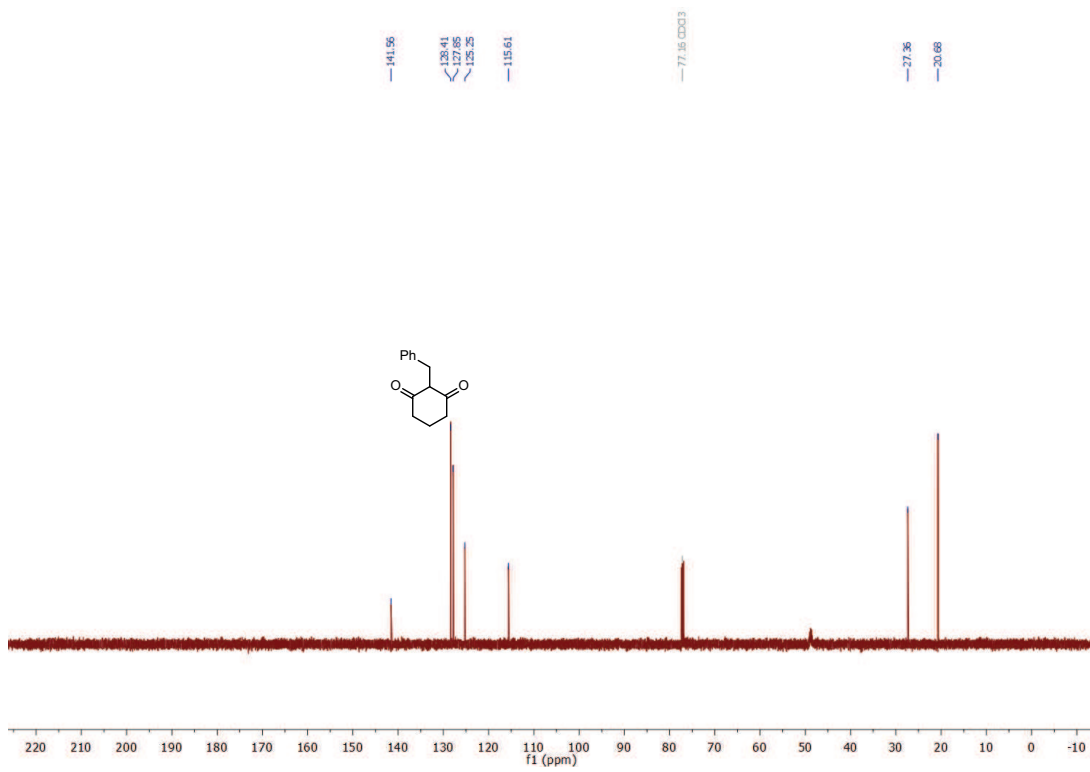
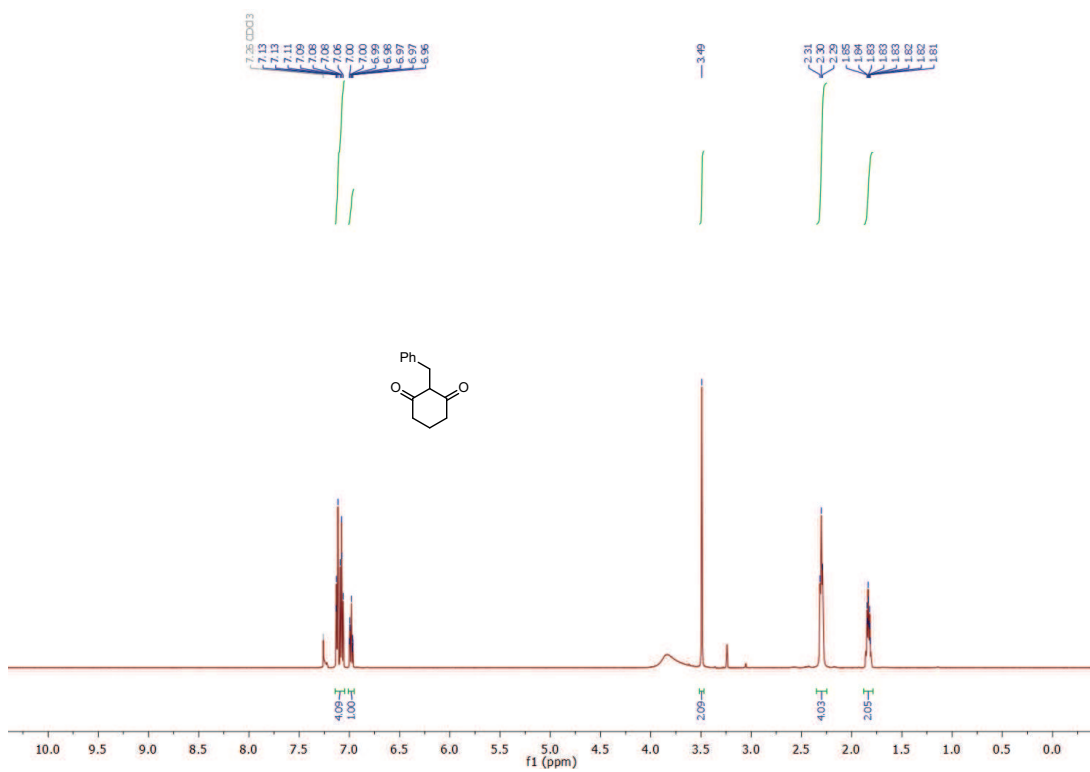


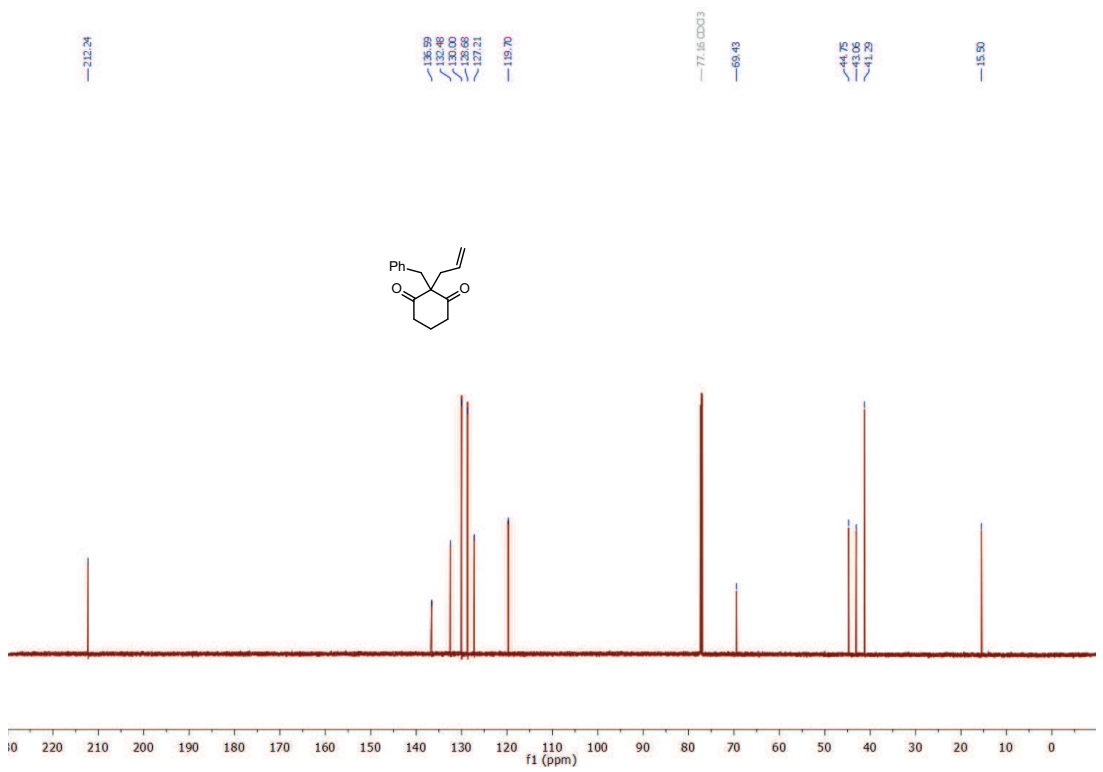
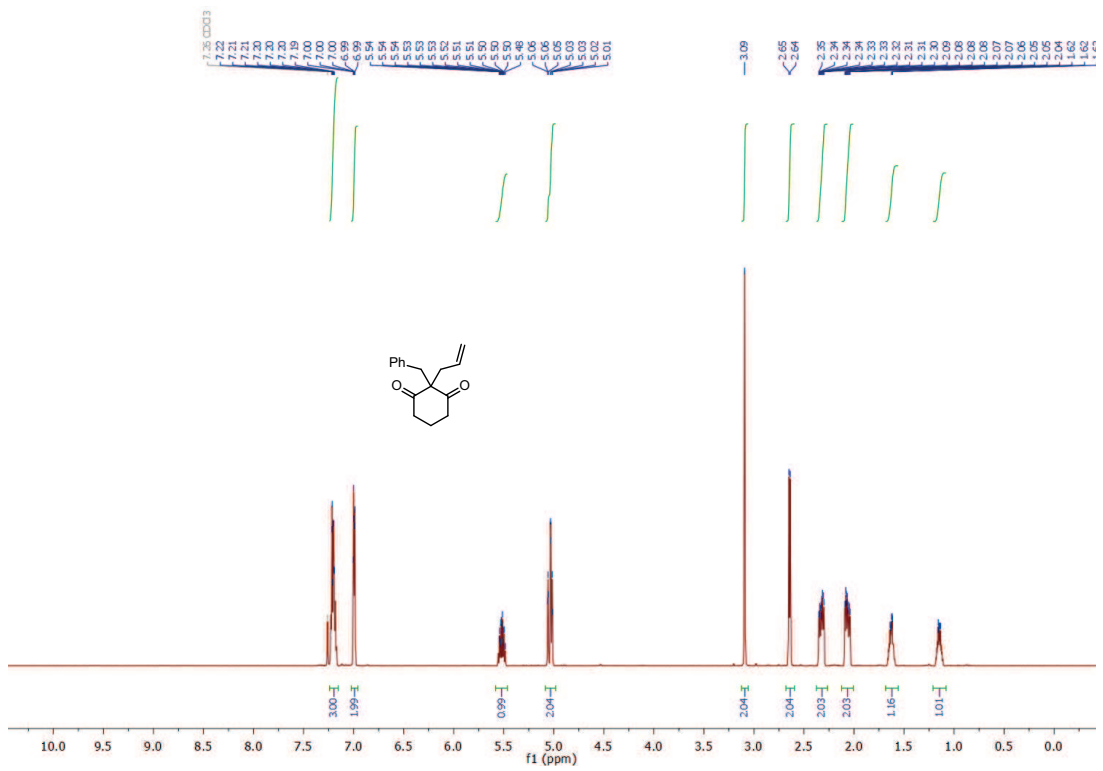


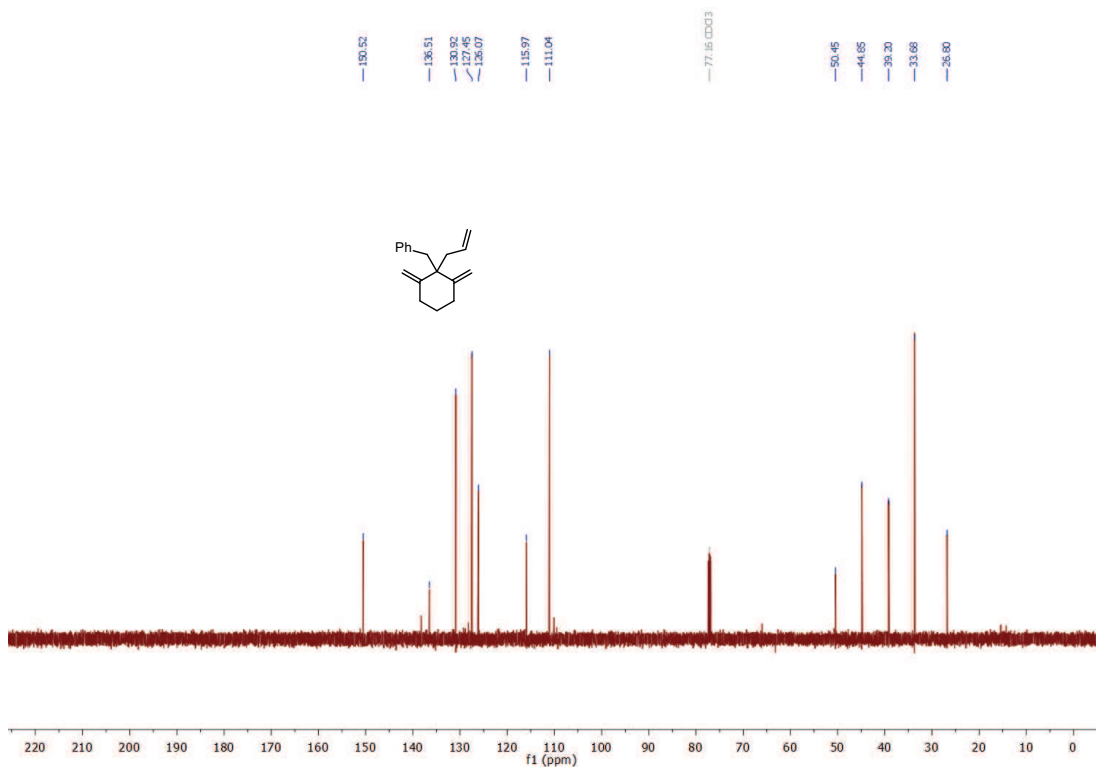
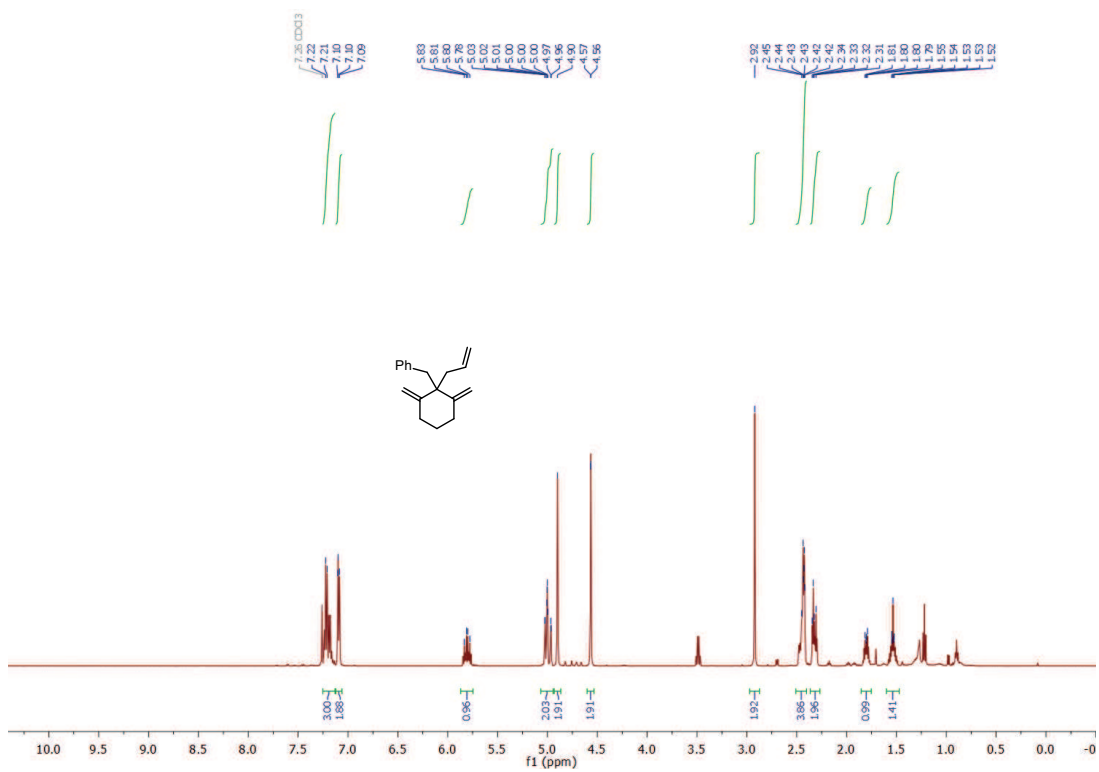
Appendix C

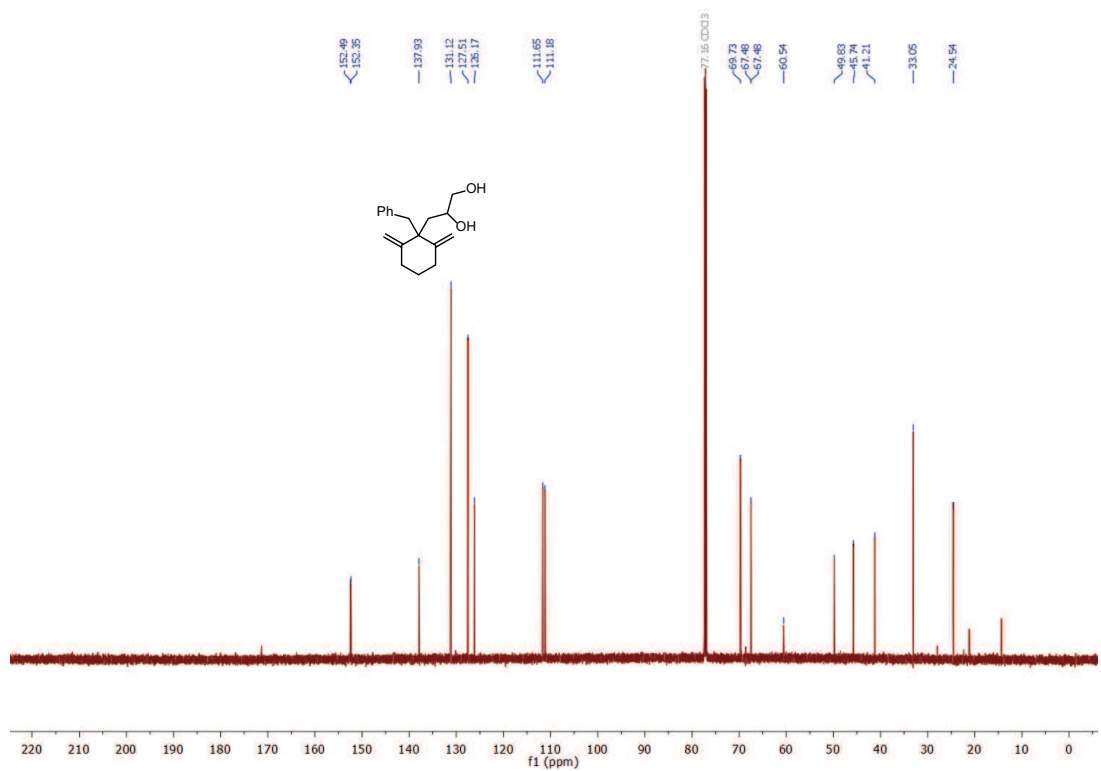
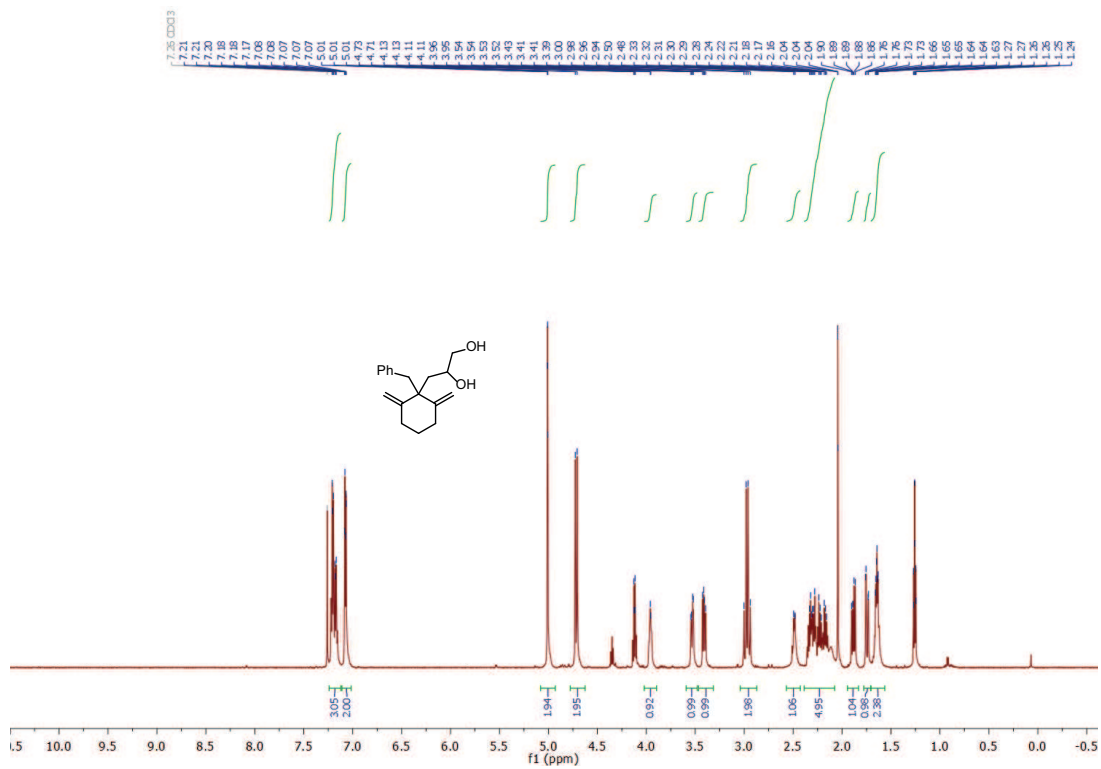
Supporting Information for Chapter 2.2

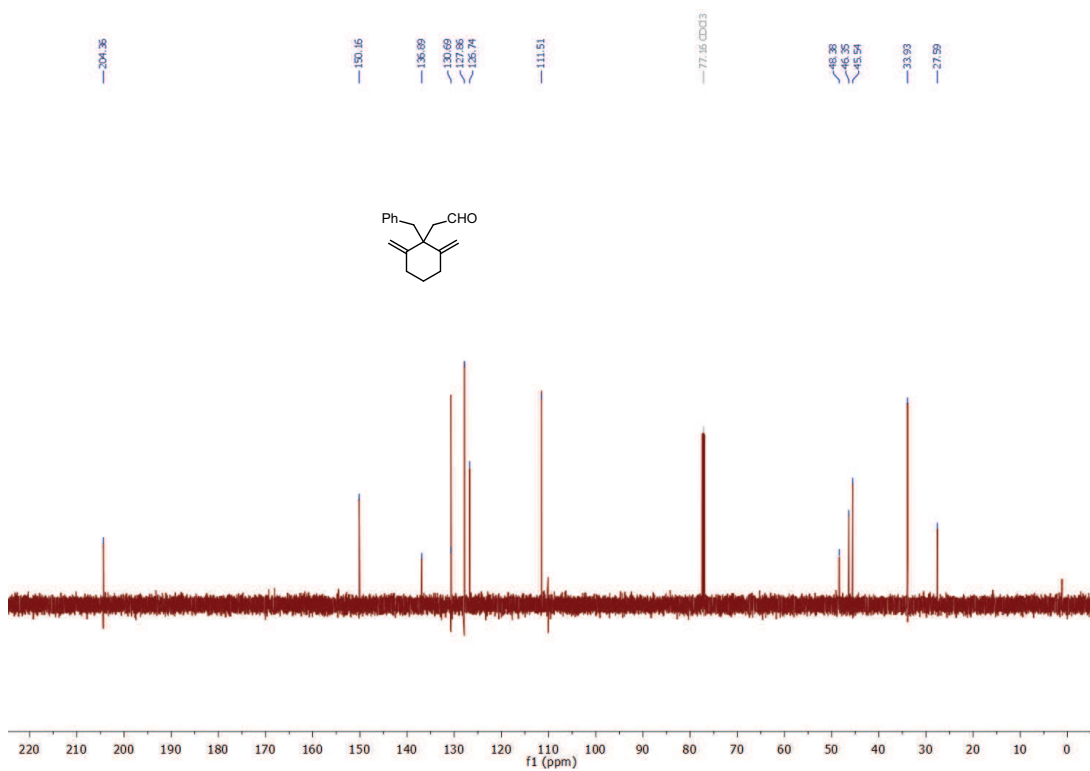
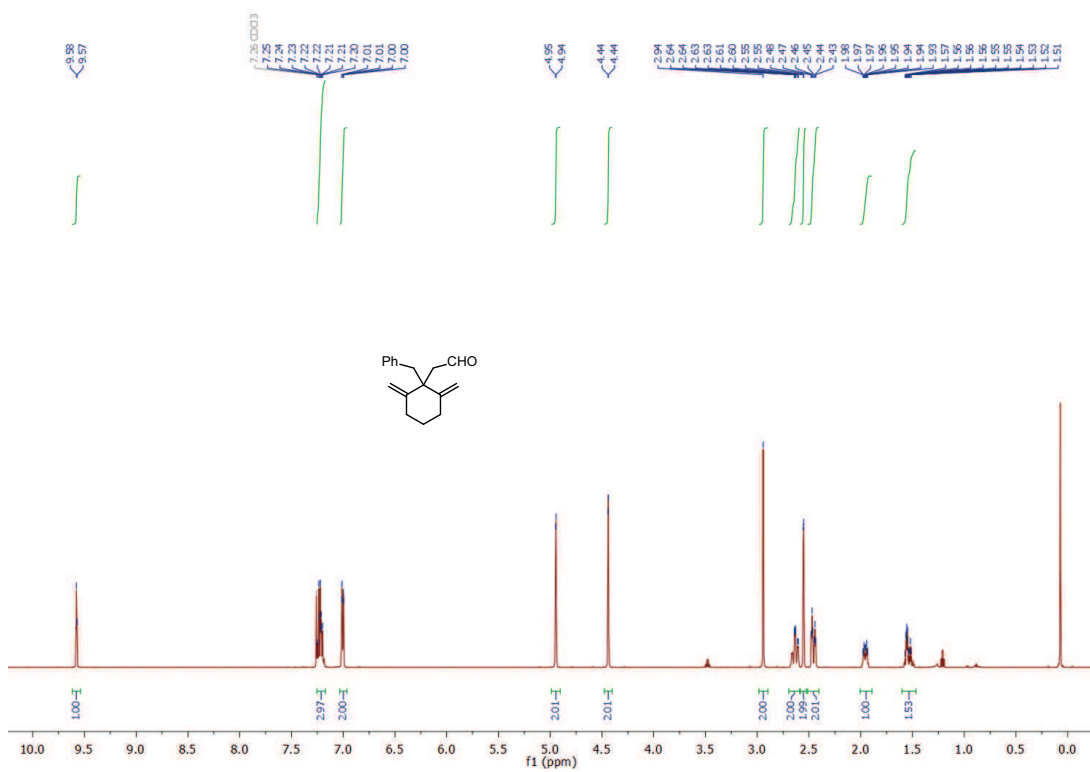
C.1 NMR Spectra

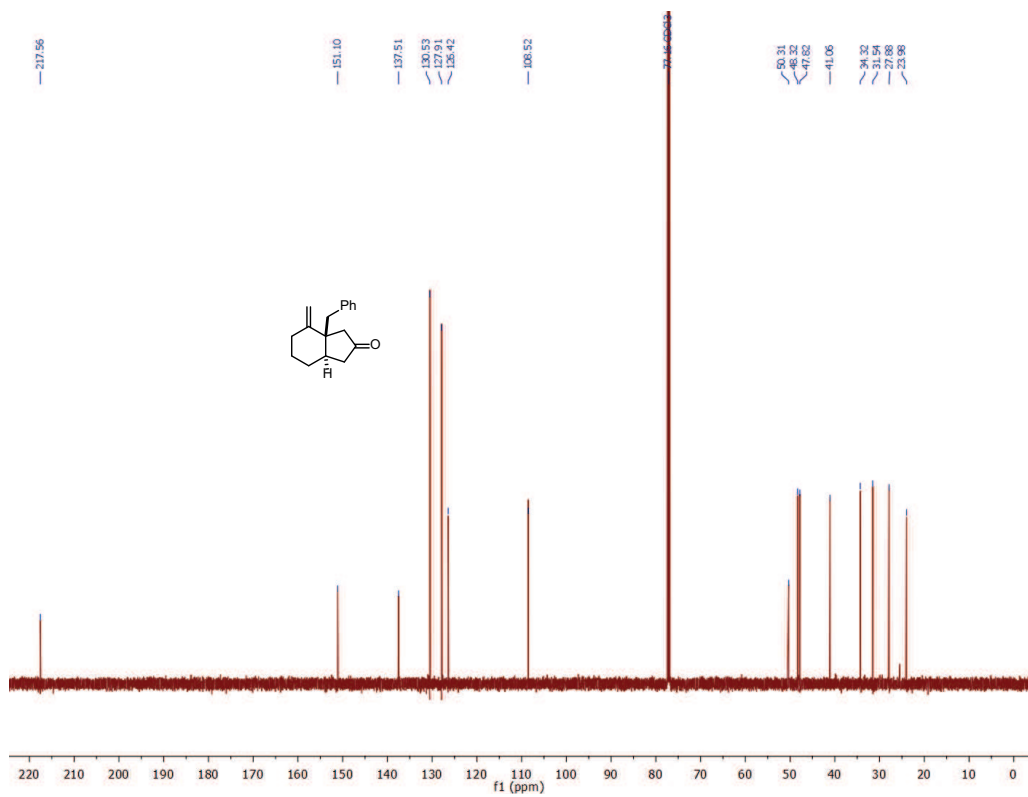
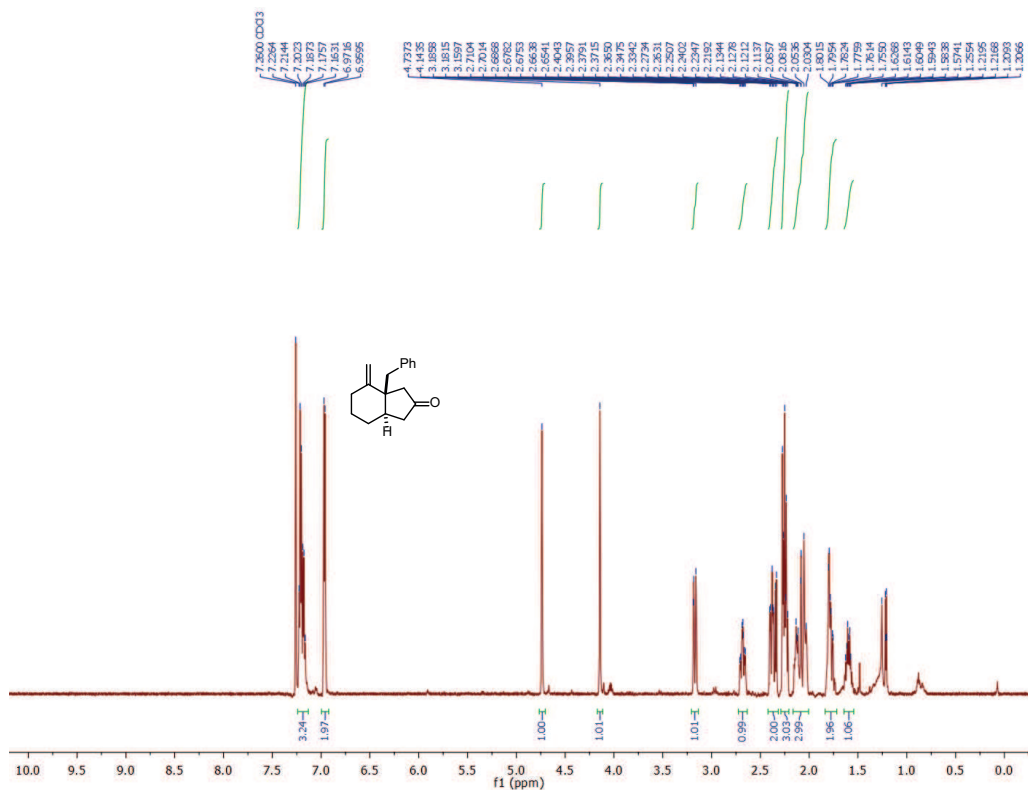








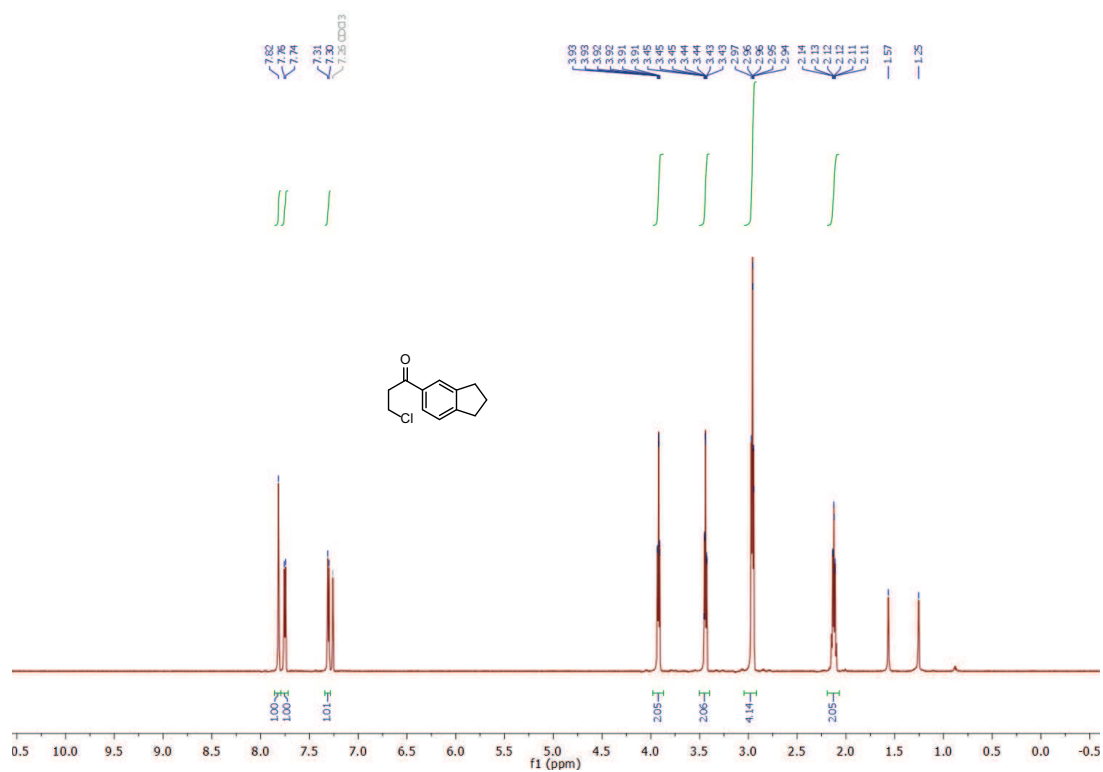


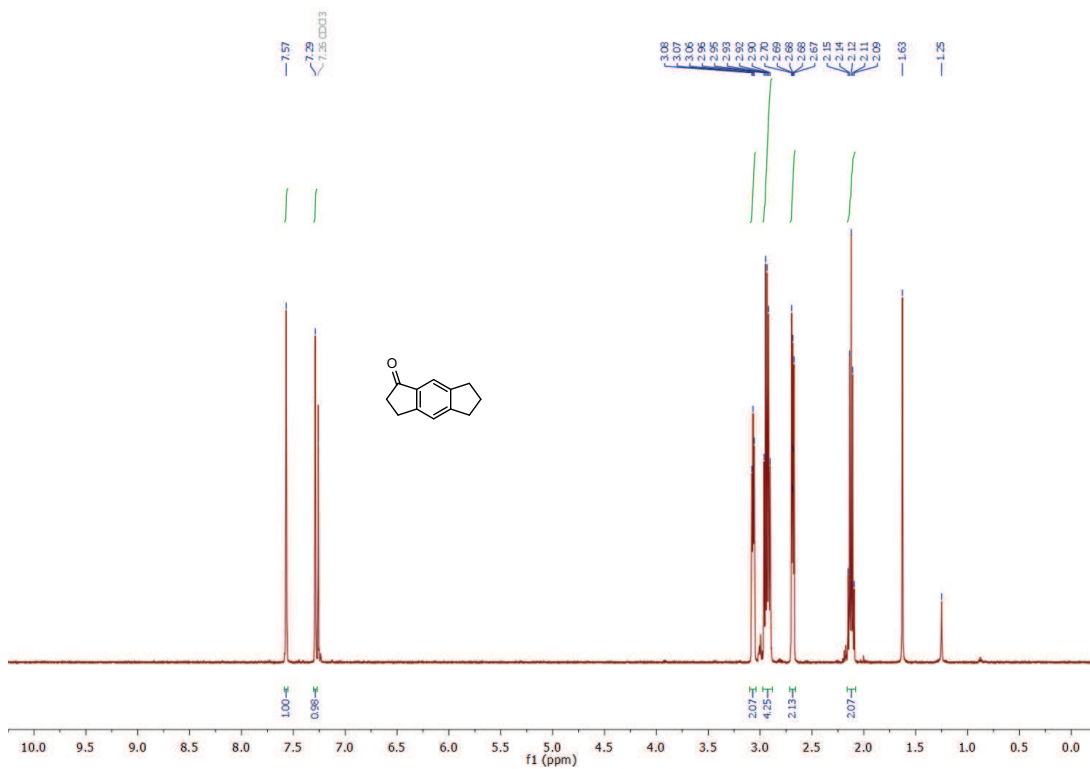
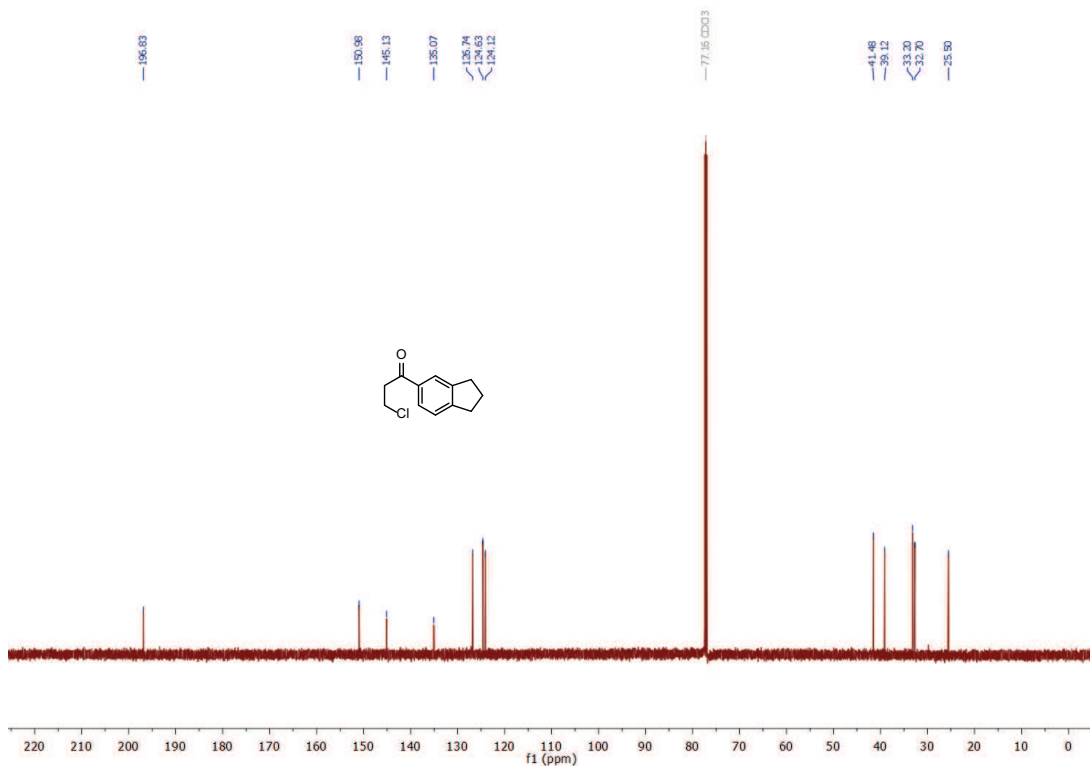


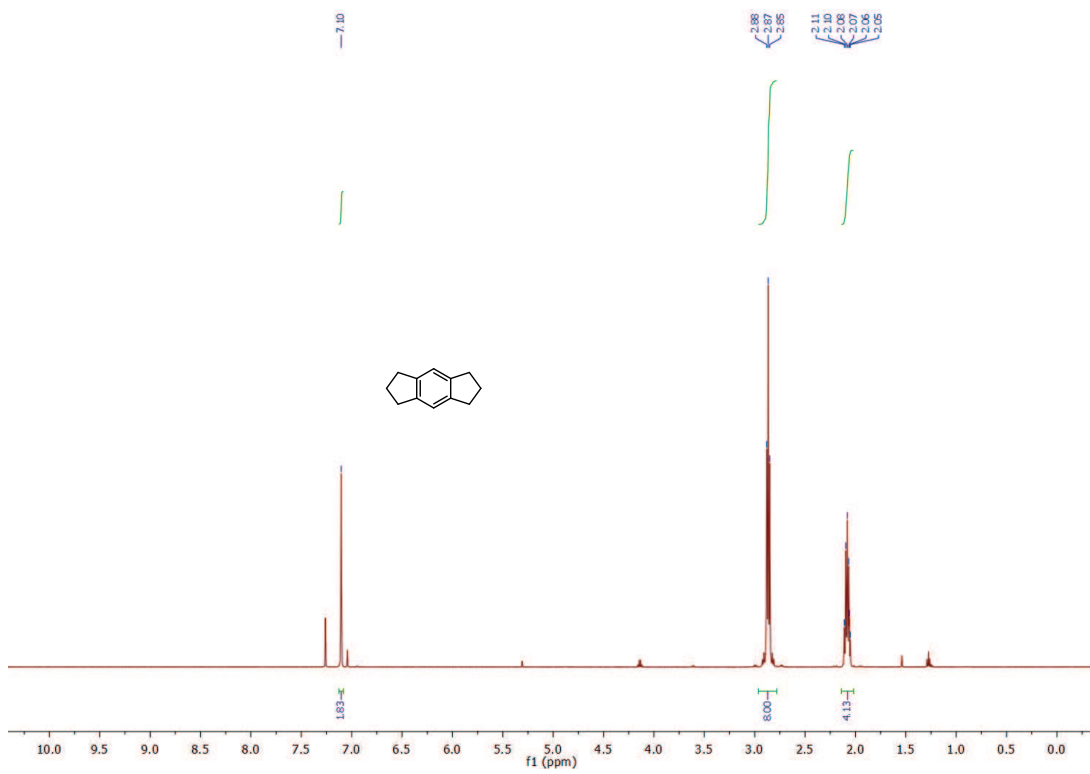
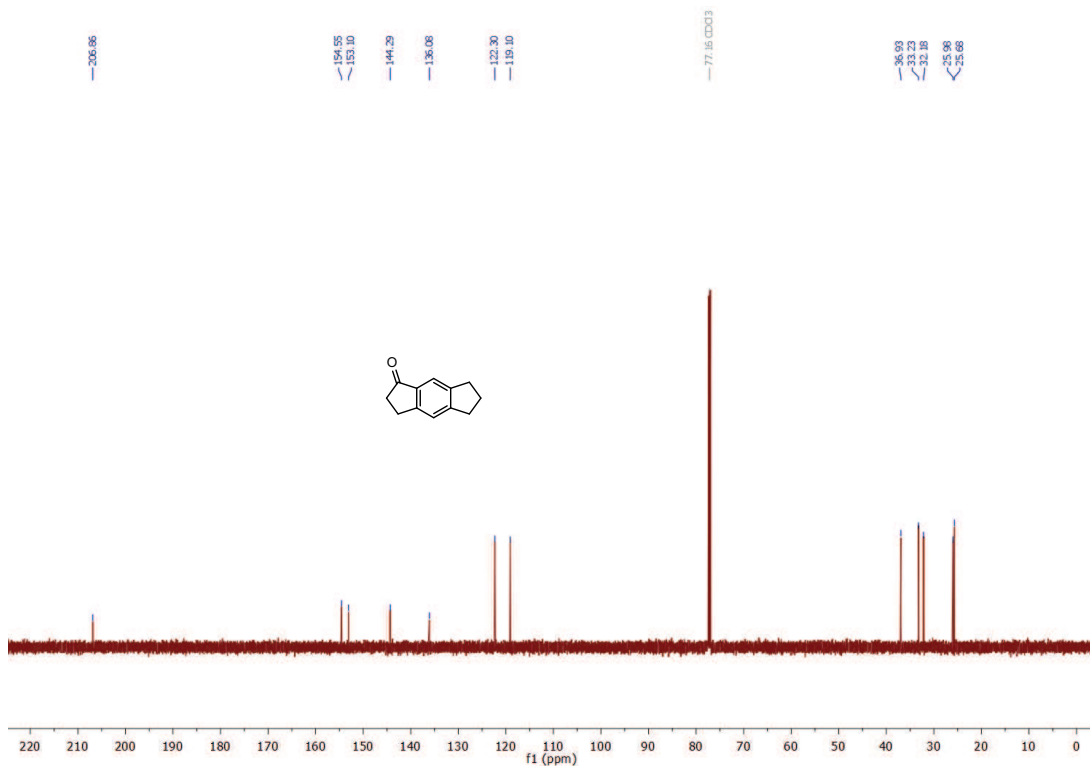
Appendix D

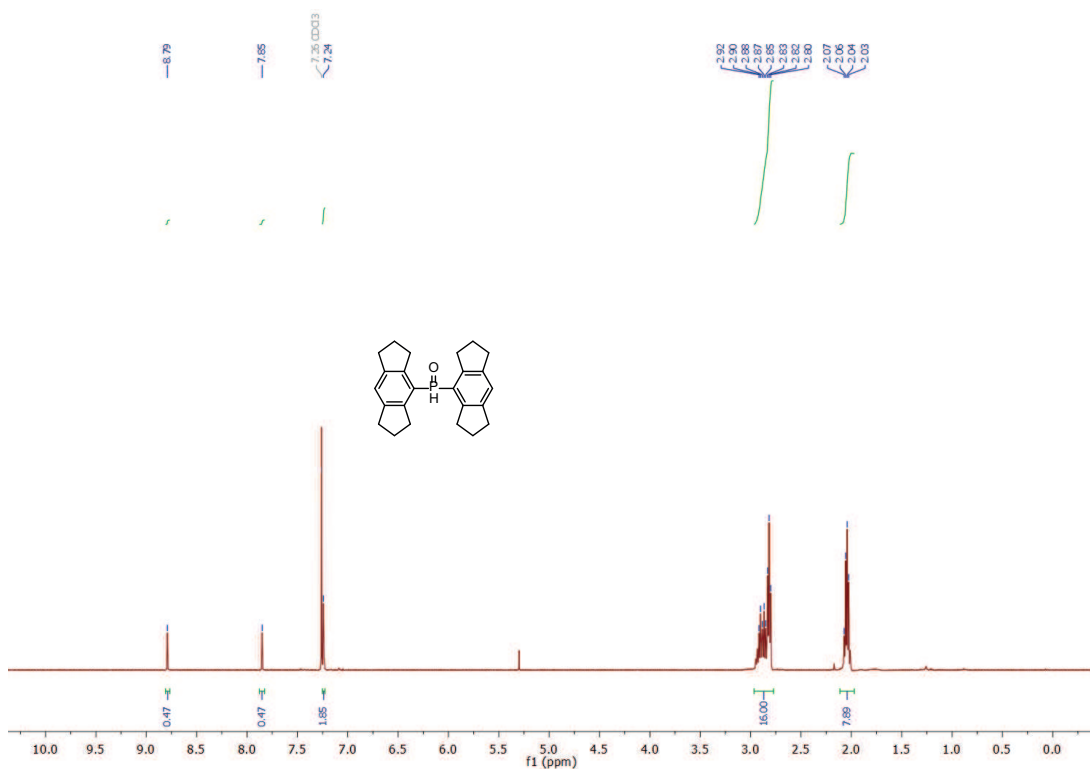
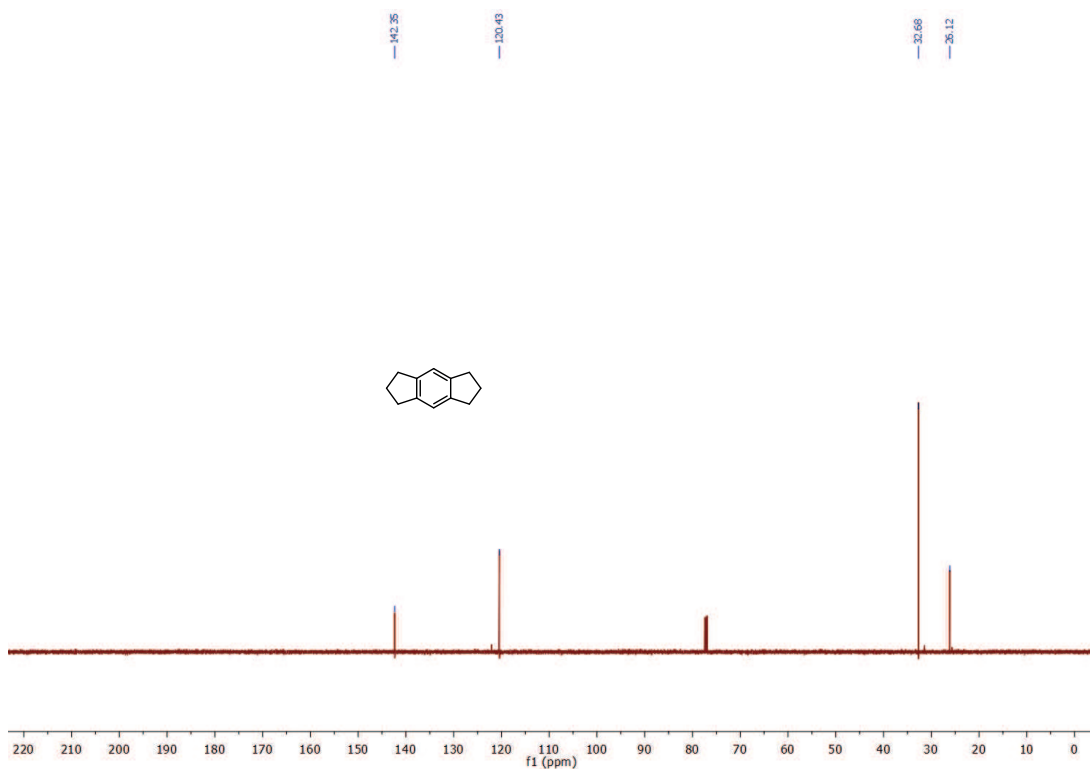
Supporting Information for Chapter 3

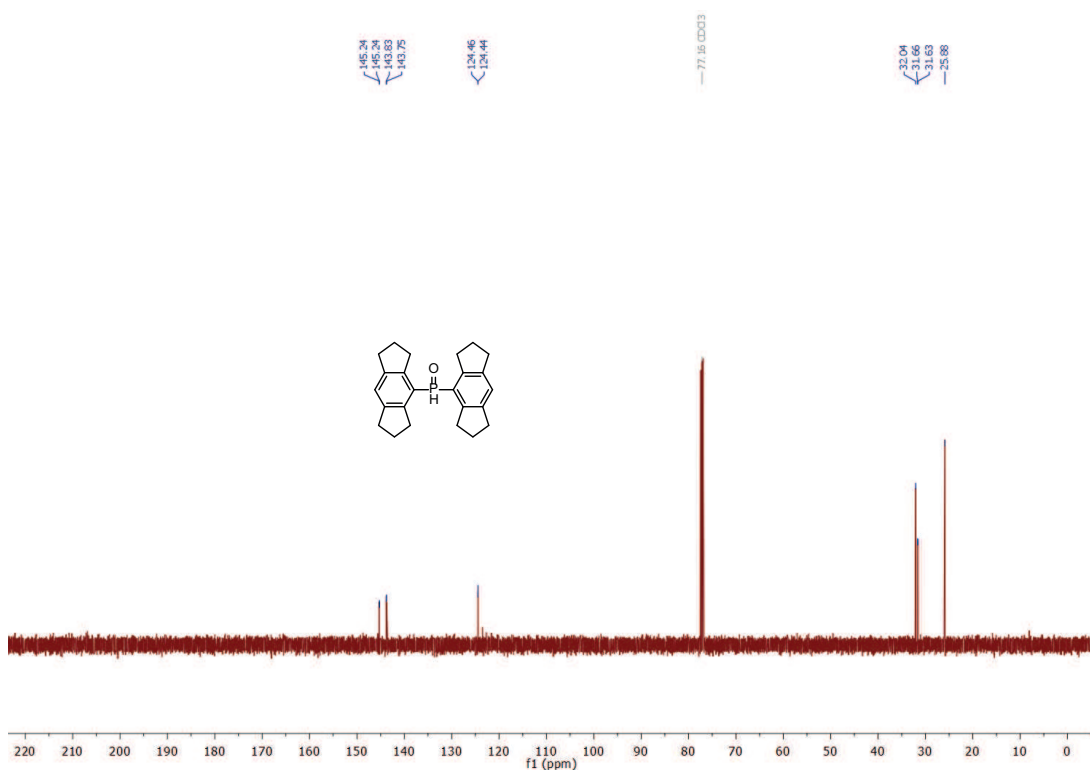
D.1 NMR Spectra











Appendix E

Supporting Information for Chapter 4

E.1 NMR Spectra

